Carbon and nitrogen transport across the legume symbiosome membrane

By

Nicholas Booth
Bachelor of Science (Honours) (Biotechnology)

Thesis
Submitted to Flinders University
for the degree of

Doctor of Philosophy

College of Science and Engineering
12th July 2023

Table of Contents

Abstract

Nitrogen is one of the most limiting factors for plant growth. The application of synthetic nitrogen fertilisers can alleviate this issue, but they are expensive and can leach into the surrounding environment. Legumes have developed a symbiotic relationship with soil bacteria known collectively as rhizobia, which fix atmospheric nitrogen into a form usable by the plant. During this symbiosis, legumes develop highly specialised organs on their roots, called nodules, which are infected by the rhizobia. Inside the infected nodule cells, the rhizobia differentiate into nitrogen fixing bacteroids that are excluded from the plant cytosol by a membrane of plant origin to form an organelle-like structure. This is the functioning unit of symbiotic nitrogen fixation and is referred to as the symbiosome. The Symbiosome Membrane (SM) regulates metabolite exchange between the symbionts via transport proteins synthesised by the plant. While the bacteroids are dependent on the plant for many nutrients, the principal exchange of nutrients across the SM is the uptake of reduced carbon to support nitrogen fixation in the bacteroids and the efflux of fixed nitrogen that is supplied to the plant. However, the identity of the transporters involved in this exchange remains elusive.

Previous studies have implicated a non-selective cation channel in the efflux of fixed nitrogen from the symbiosome, which is inwardly rectified by cytosolic Mg^{2+} and has a preference for ammonium. The present work has shown that when the aquaporin Nodulin 26 (NOD26), an abundant protein on the soybean symbiosome membrane, is heterologously expressed in *Xenopus laevis* oocytes, monovalent cation induced currents are observed. These currents are selective for ammonium and inhibited by divalent cations. GmNOD26 is regulated by phosphorylation of a specific serine residue, S262. Using phosphomimetics I demonstrate a switch in the permeability of GmNOD26 to water and cations. Through expression in *X. laevis* oocytes and complementation of mutant *Saccharomyces cerevisiae* strains, ammonia and ammonium are confirmed as the only nitrogen species transported through GmNOD26. This study provides strong evidence that GmNOD26 is a multifunctional channel that facilitates both ammonia and ammonium efflux from nitrogen-fixing nodules and that this transport is regulated by phosphorylation of S262.

Previous work has established that uptake of reduced carbon, in the form of organic acids like malate, by symbiosomes occurs through a dicarboxylate carrier energised by the electrochemical potential across the SM and inhibited by phthalonic acid. However, proteomic studies of isolated SM have failed to identify typical plant dicarboxylate transporters. Transcriptomic studies have shown that Aluminium activated Malate Transporters (ALMT) are highly expressed in nodules. I identified 13 ALMT genes in the *Lotus japonicus* genome, but only LjALMT1 was highly expressed in nodules, but it appears to localise to the root and nodule vascular tissues, rather than the infected region of nodules. I therefore turned to other possible candidates in the proteome of isolated soybean SM, in particular eight members of the Nitrate Peptide

transporter Family (NPF) of proteins. I analysed the dicarboxylate transport activity of these proteins in *X. laevis* oocytes and identified GmNPF1.2 as a dicarboxylate carrier. In GmNPF1.2-expressing *X. laevis* oocytes, ionic currents were activated by both malate and succinate. The transport of malate by GmNPF1.2 was confirmed through [^{14}C] measurements and shown to be inhibited by phthalonic acid.

These data suggest that ammonium/malate exchange across the soybean SM is facilitated by GmNPF1.2, as the SM dicarboxylate carrier, and GmNOD26, as the SM non-selective monovalent cation channel. However, confirmation requires further experimentation with soybean, using mutagenesis techniques to investigate symbiotic phenotypes.

Declaration

I certify that this thesis:

1. does not incorporate without acknowledgment any material previously submitted for a degree or diploma in any university

2. and the research within will not be submitted for any other future degree or diploma without the permission of Flinders University; and

3. to the best of my knowledge and belief, does not contain any material previously published or written by another person except where due reference is made in the text.

X

Nicholas Booth

11th July 2023

Acknowledgements

Firstly, thank you to my supervisors; Prof. Kathleen Soole, Prof. David Day and Dr Sunita Ramesh, without your dedication it would not have been possible to complete this thesis. The expertise provided throughout the duration of my candidature pushed me to develop all areas of my research, from critical analysis and method development to communication and publishing. I cannot thank you enough for guiding me through this process.

I would also like to express my appreciation to the collaborators of my research. To Prof. Steve Tyerman, Dr Jiaen Qiu and Wendy Sullivan of Adelaide University, thank you for all of the time you have taken away from your own research to teach me electrophysiology, and how to appropriately study *X. laevis* oocytes. To Assoc. Prof. Penelope Smith and Dr Frank Bedon of La Trobe University, your expertise in the legume symbiosis and Gateway Cloning has not gone unnoticed, I cannot thank you enough for all of the troubleshooting zoom calls and for sharing your findings and constructs with me.

To the entire Flinders Plant Molecular Physiology Research Group, you have made my time at Flinders University far more enjoyable than I would have imagined! Thank you to the lab heads not directly involved in my thesis; Assoc. Prof. Colin Jenkins, Assoc. Prof. Peter Anderson, Dr Crystal Sweetman and Dr Yuri Shavrukov, you always made time for constructive feedback and to just check in on how things were going. To my fellow PhD students; Troy Miller, Lauren Philp-Dutton, Barry Rainbird, Kathryn Schleyer and Shayne Faulkner; along with past students Dr Thanh Hai Tran, Dr Christopher Waterman and Carly Schramm, thank you for all of your advice over the years, whether that be in the lab or at the Flinders tavern. Thank you to all past and present lab members including Alexandra Cunningham, Antonio Pupulin, Gulmira Khassanova, Mitchell Eglinton and Sholpan Khalbayeva for always being ready for a chat.

I would also like to thank all of those who have taught undergraduate topics alongside me over the years, in particular thank you to Dr James Herbert and Carly Schramm for making my time in the Biodiscovery Centre (mostly) enjoyable. Thank you to Dominic Reppucci for the time he has spent training me on almost all of the equipment in the Biology building, and for allowing me to work and learn alongside you.

To my friends and family, thank you for all of your support they have given me during my candidature. In particular I would like to thank my parents for always supporting me during my academic pursuit. Finally, I must thank my wife, Maddy, who I have been ever so lucky to marry during an extremely stressful time of my life, you and Emmy make it all the better.

I must also acknowledge the financial support I received from the Australian Government Research Training Program Scholarship and Playford Trust PhD Scholarship.

Abbreviations

ABC - ATP-binding cassette
ADP - Adenosine di-phosphate
AGRF - Australian genome research facility
ALMT - Aluminium activated malate transporter
AMT - Ammonium transport protein
AQP – Aquaporin
AS - Air space
At - *Arabidopsis thaliana*
ATP - Adenosine triphosphate
B&D - Broughton and Dilworth
bHLH - basic helix-loop-helix
BNF - Biological nitrogen fixation
cDNA - complementary DNA
Cds - Coding sequence
cRNA - complementary ribonucleic acid
Ct - Threshold cycle
DAI - Days after inoculation
DCAT1 - Dicarboxylate transporter 1
DMT - Divalent metal transporter
DNS - Data not shown
dNTP - Deoxynucleotide triphosphate
DsRED - *Discosoma sp.* red fluorescent protein
ESTs - Expressed sequence tags
F - Forward
gDNA - genomic DNA
GFP - Green fluorescent protein
Gm – *Glycine max*
GS - Glutamine synthetase
GUS - β-glucuronidase
I - Inflorescence
IC - Infected cell
L - Leaf
LB - Luria-Bertani
LiAc - Lithium acetate
Lj - *Lotus japonicus*
LORE1 - Lotus retrotransposon 1
MeA$^+$ - Methylammonium
MIP – Major intrinsic protein
mRNA - messenger ribonucleic acid
Mt - *Medicago truncatula*
N - Nodule
N70 - Nodulin 70
NAXT - Nitrate excretion transporter
NCBI - National center for biotechnology information
NEB - New England biolabs
NOD26 – Nodulin 26
NPF - Nitrate peptide transporter family
ns - Non-stop
NSCC - Non-selective cation channel
P - pod
PBU - Peribacteroid units
PCR - Polymerase chain reaction
PIP - Plasma membrane intrinsic protein
PM - Plasma membrane
PTR - Proton-dependent oligopeptide transporter
r - Root
R - Reverse
RE - Regulatory element
S - Stem
SAT – Symbiotic ammonium transporter
Se - Seed
SLAC - Slow anion channel
SLAH – SLAC homolog
SM – Symbiosome membrane
SST - Symbiotic sulphate transporter
TAE - TRIS acetic acid EDTA
TCA - Tricarboxylic acid
tDT - tonoplast dicarboxylate transporters
TE – Tris EDTA
TIP - Tonoplast intrinsic protein
TMH - Transmembrane helix
TSS - Transformation and storage solution
UC - Uninfected cell
VDAC - Voltage-dependent anion channels
VTL - Vacuolar iron transporter like
Wt - Wild type
X-Gluc - 5-bromo-4-chloro-3-indolyl-β-Dglucuronide cyclohexylammonium salt
YMB - Yeast mannitol broth
YNB - Yeast nitrogen base
YPD - Yeast extract peptone dextrose
ZIP - Zinc transporter
Zone I - Meristematic zone
Zone II - Invasion zone
Zone III - Nitrogen-fixing zone
Zone II-III - Interzone
Zone IV - Senescence zone
882 - LjALMT1 LORE line 30085822

List of Figures

List of Tables

1 Introduction

1.1 Agricultural nitrogen use

Nitrogen is essential for plant growth, being required for the synthesis of amino acids in proteins and as a building block for chlorophyll (Varinderpal et al. 2012). It is usually obtained from the soil as nitrate or ammonium, but its supply can often be limiting to maximal plant growth, considered the second greatest restriction behind water deficiency (Lea and Morot-Gaudry 2000). The Green Revolution refers to a period of time in the 20th century were advancements in technologies accelerated global agricultural production and adverted the global food crisis (Ruttan and Conway 1998). These technologies included breeding of high-yielding varieties, irrigation, pesticides and the production of synthetic nitrogen fertilisers, the latter of these technologies has been attributed to feeding ~48% of the global population (Stein and Klotz 2016). Although application of synthetic nitrogen fertilisers does improve growth and yield (Ingestad and Lund 1979; Walker et al. 2001), uptake efficiency of nitrogen does not necessarily increase with increasing availability (Ingestad and Lund 1979). As a result, nitrogen runoff is a major environmental concern, due to adverse effects on human and animal health, and its potential to cause eutrophication of waterways (Keeney 1982; Weil et al. 1990). Additionally, synthetic nitrogen fertilisers are expensive, making their use limited in many developing countries and unfavourable in sustainable agricultural models.

1.2 Biological nitrogen fixation

An alternative to synthetic nitrogen fertilisers is the employment of biofetilisers, which refers to the application of microorganisms that colonise the rhizosphere of a plant and increases the availability of particular nutrients (González-Andrés and James 2016). Biological Nitrogen Fixation (BNF) is a process by which nitrogen gas is fixed (converted) to a form readily accessible to the plant, such as ammonium (Postgate 1998). The earth's atmosphere consists of ~78% nitrogen gas, however in this form nitrogen is inaccessible to the plant, making the ability to obtain nitrogen through BNF a great competitive advantage, particularly when gown under low soil nitrogen availability (Vessey 2003; Ferguson et al. 2010). However, BNF is limited to a group of prokaryotes containing the enzyme nitrogenase, these bacteria are known collectively as diazotrophs and it is thought that they supply up to 40% of available soil nitrogen (Postgate 1998). Associations between diazotrophs and plants in the rhizosphere are common (Postgate 1998; Vessey 2003), although the transfer efficiency of fixed nitrogen to the plant is often low (Vessey et al. 2005). In some cases, specialised organs called nodules form on the host plant, usually on the root (see Figure 1.1), and house the diazotrophic bacteria and provide optimal conditions for BNF (Soltis et al. 1995; Gordon et al. 2001). This

symbiotic interaction allows direct transfer of assimilated fixed nitrogen to the plant, but it is limited to a few plant groups. These include legumes, actinorhizal plants, *Parasponia sp.* and cycads (Vessey et al. 2005), although the symbiosis formed in legumes is of the most economical importance.

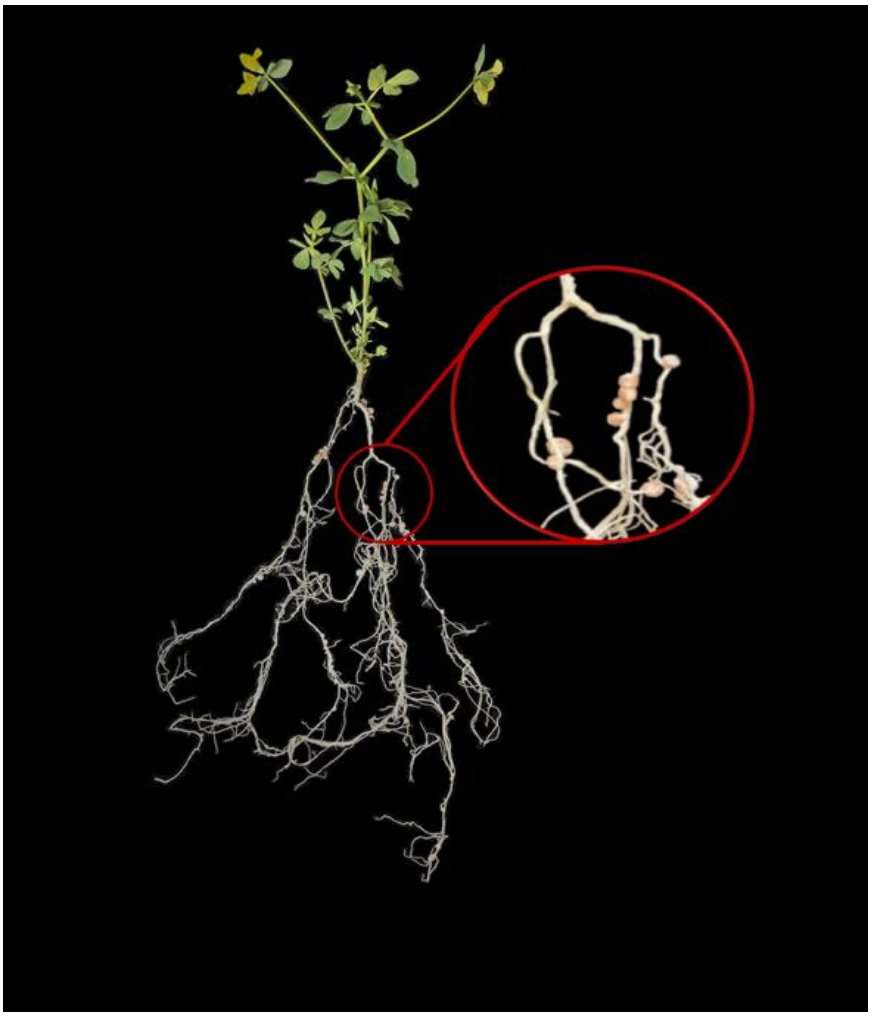

Figure 1.1 *Mesorhizobium loti* induced nodulation of *Lotus japonicus* root system.

1.3 Legumes in agriculture

Legumes belong to the large Fabaceae family, with more than 750 genera and 19,000 species (Christenhusz and Byng 2016). With such a large family, legumes are usually divided into two groups according to their favourable growing season: cool season legumes, with crops including broad bean, lentil and chickpea; and tropical legumes, with crops including pigeon pea, soybean and alfalfa (Miller et al. 2002; Sprent et al. 2017). Legumes are an economically important crop, with their production only exceeded by that of cereals (Ahmad 2015). The nutritional content of legumes has made them favourable in the Mediterranean diet, a staple in many developing countries and important in agricultural feed (Nedumaran et al. 2015). This is largely due to the high protein, calcium, iron and phosphorus content of leguminous crops, and their affordability relative to cereals

(Armstrong et al. 1996; Latham 1997). Between 2008 and 2010 the production of major grain legumes exceeded 300 million tonnes, dominated by soybean, which accounts for ~240 million tonnes or 74% of production (Nedumaran et al. 2015). However, legumes are not only important directly as a cash crop but are also useful in reducing greenhouse gas emissions and improving soil quality, due to their BNF capacity.

The ability to fix biological nitrogen allows legumes to be grown on marginally fertile lands, without the application of synthetic nitrogen fertilisers, as 70-80% of the plants total nitrogen content can be fixed through BNF (Peoples 1995). It has been reported that the BNF capacity of a majority of the important food legumes is in excess of 200 kilograms of nitrogen per hectare (Peoples 1995; Bruning and Rozema 2013), with 40-60% of fixed nitrogen remaining in the soil when grown as green manure (Sullivan 2003). However, since most food legumes are harvested, this net loss of nitrogen must be considered when calculating the input of nitrogen to the soil. Studies have reported a post-harvest soil nitrogen balances of 62 to 157 kilograms of nitrogen per hectare for lupin (Evans et al. 1989), and -134 to 69 kilograms of nitrogen per hectare for soybean (Bergersen et al. 1989; Hughes and Herridge 1989). This level of variation is common and highlights that in some circumstance's legumes require an input of nitrogen, rather than acting to replenish its supply in the soil. This is largely dependent on the harvest index, removal of vegetative nitrogen and rates of BNF of the particular site (Peoples 1995; Blesh and Drinkwater 2013).

According to Myers (1988), cereal crops require 20 to 40 kilograms of nitrogen per hectare over a 3 to 5 month period to support the growth of one tonne of grain, within the post-harvest soil nitrogen balances of many legume crops. Additionally, since soil nitrogen availability is one of the major limitations to the rate of BNF, as nodule growth and nitrogenase activity is strongly inhibited by nitrate (Kennedy et al. 1975; Streeter 1985), it could be expected that when grown in crop rotation, legume crops would be sown in relatively nitrogen deficient soil, helping to maximise BNF rates. Increased BNF has been shown in pea and soybean when grown in rotation with cereal crops (Bergersen et al. 1989; Peoples 1995). Legume-based rotations have existed in agricultural systems long before the mechanisms by which it improved crop yields were understood. Numerous studies have shown that legume-based rotations contribute to increased biomass and help sustain soil nitrogen concentrations when compared with monoculture systems (Norden et al. 1977; Chalk 1997; Gregorich et al. 2001; Ryan et al. 2009; Blesh and Drinkwater 2013; Reckling et al. 2016; Nunes et al. 2018). Through improving soil nitrogen reserves, legumes also contribute to the production of nitrogen-rich humus, a sink for atmospheric carbon (Christopher and Lal 2007). Humus is desirable in

agricultural systems, as it increases the field capacity of the soil, reducing the likelihood of drought (Olness 2005), and chelates cations, making them more readily accessible to the plant (Szalay 1964). The numerous economic and environmental benefits of leguminous crops in agricultural systems, with an emphasis on legume-based rotations, highlights their importance in developing a sustainable agricultural model that can feed the ever-growing human population.

1.4 Nodule formation

The ability of legumes to form nodules is critical to BNF, as nitrogen fixation can only occur when the plants are in the symbiotic state with rhizobia (Cooper 2004). Nodules are specialised organs, approximately 2-5 mm in diameter, that form on the root providing optimal conditions for BNF and supporting the growth of up to 10^9 rhizobia (Downie 2014). This process will be described briefly, but for a detailed review please see Downie (2010) or Ferguson et al. (2010).

1.4.1 Signalling

To initiate the symbiotic interaction that is nodulation, the host legume and infecting rhizobia must exchange signals (Garg and Geetanjali 2009). Under low nitrogen conditions the legume exudes flavonoids, isoflavonoids and related compounds into the rhizosphere, acting as chemoattractants to the rhizobia that then colonise this region (Djordjevic et al. 1987; Peters and Verma 1990; Phillips 1992). These compounds bind the rhizobial transcriptional activator NodD and initiate transcription of nodulation genes (Cooper 2004). As a result, rhizobia produce highly decorated Nod factors that bind to the host specific receptors LysM receptor kinases LYK3/NFR1 and NFP/NFR5 in *M. truncatula* and *L. japonicus*, respectively (Downie 2014). Nod factor recognition leads to nodule organogenesis through Does not Make Infection 2 and 3-Hydroxy-3-Methylglutaryl CoA Reductase 1 interactions resulting in calcium spiking and ultimately activating the nuclear calcium and calmodulin-binding kinase that phosphorylates the transcriptional activator CYCLOPS (Oldroyd and Downie 2004; Moling and Bisseling 2015).

1.4.2 Nodule infection

Following the induction of nodule organogenesis, root infection occurs to allow rhizobia access to the growing nodule. Rhizobia primarily target the tip of emerging root hairs, although they have also been shown to enter the plant through cracks in the root epidermal tissue (Oldroyd and Downie 2008). Attachment of rhizobia to the root hair tip induces deformation and curling that encapsulates the dividing bacteria (Yao and Vincent 1969; Bauer 1981; Rolfe and Gresshoff 1988; Mathews et al. 1989; Ferguson et al. 2010). This leads to formation of the plant cell wall-derived infection thread, providing a passage to the cortical cells of the plant. Here, cell division results in the development of the nodule primordium where in an exocytotic process droplets from the growing tip of the infection thread are released into the host cytoplasm (Ferguson et al. 2010). This 'droplet' functions as a transient organelle and is regarded as the symbiosome, previously termed peribacteroid unit (PBU) (Roth and Stacey 1989; Udvardi and Day 1997). Once encompassed by the plant derived Symbiosome Membrane (SM), transcriptional changes cause the free-living rhizobia to differentiate into N_2 fixing bacteroids that are totally reliant on the host plant for their survival (Figure 1.2) (Roth and Stacey 1989). An infected cell formed in a typical soybean nodule may contain up to 1 x 10^4 symbiosomes (Bergersen and Goodchild 1973), with the SM undergoing enormous proliferation to accommodate the dividing bacteroids (Roth and Stacey 1989).

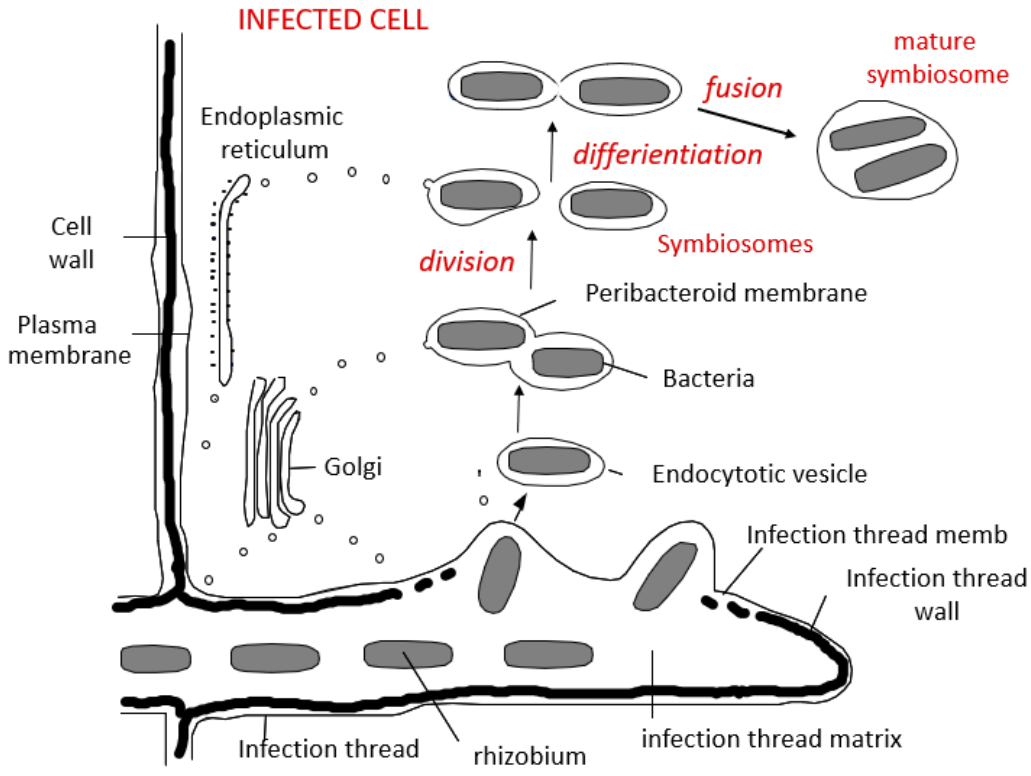

Figure 1.2 Symbiosome formation in determinate type nodules (Whitehead and Day 1997). Reprinted with permission from John Wiley and Sons.

1.4.3 Nodules provide a unique environment for nitrogenase activity

Once in this symbiotic state, the plant must provide a niche that supports nitrogenase activity while ensuring survival of the bacteroid. Inside nitrogen fixing zones of the nodule, plants maintain an extremely low and buffered free oxygen concentration (Appleby 1984; Ott et al. 2005). Nitrogenase is a metalloenzyme composed of both an iron protein, containing a single iron-sulphate cluster and two magnesium-ATP binding sites, and an iron-molybdenum protein, containing two complex metalloclusters and the iron-molybdenum cofactor (Shah and Brill 1973; Hageman and Burris 1978; Rubio and Ludden 2005; Seefeldt et al. 2009). The metallocentres of the nitrogenase complex are extremely oxygen liable, but maintenance of this micro-anaerobic environment prevents their rapid oxidation (Shaw 1983; Fischer 1994; Guasch et al. 2001). While the nodule must provide a micro-anaerobic environment to prevent oxidative damage to this enzyme, the reduction of nitrogen gas to ammonia is a highly energetic process requiring 16 ATP per molecule of N_2 reduced (Day et al. 2001a); see the following reaction:

$$N_2 + 8\ H^+ + 8\ e^- + 16\ MgATP \rightarrow 2\ NH_3 + H_2 + 16\ MgADP + 16\ P_i$$

To maintain high respiration rates in a micro-anaerobic environment the nodules express leghemoglobin to bind free oxygen (Bergersen 1980). These leghemoglobin proteins are extremely abundant in the nodule cytosol, occurring at concentrations of up to 5 mM, but it is estimated that only 20% of these proteins are oxygenated under physiological conditions (Lee et al. 1995; Sainz et al. 2015). Interestingly, oxygen concentrations in excess of 57 nM can reduce nitrogenase activity in soybean nodules (Kuzma et al. 1993), but calculations by Appleby (1984) and Bergersen et al. (1989) estimate that free oxygen at the bacteroid surface would be approximately 10 nM. Furthermore, the concentration of leghemoglobin-bound-oxygen would be 7×10^3 and 7.5×10^5 times greater in the symbiosome space and infected nodule cytoplasm, respectively. This leghemoglobin-bound-oxygen is essential in fuelling the highly energetic conversion of nitrogen gas into ammonia, as this bound oxygen can be 'snatched' by the bacteroid cytochrome oxidase, which has a high affinity for oxygen, during oxidative phosphorylation (Appleby 1984).

1.4.4 Determinate and indeterminate nodules

Legume nodules have evolved in two extremely specialised ways, and are usually regarded as determinate or indeterminate depending on whether a persistent meristem is formed (Figure 1.3) (Hirsch 1992). Determinate nodules lack a persistent meristem and the formation of the nodule primordium synchronises infected cell development to the nitrogen fixing zone. Indeterminant nodules contain a persistent meristem and clear developmental stages are present through the

nodule. These include the meristematic (zone I), the invasion zone (zone II), the interzone (zone II-III), the nitrogen-fixing zone (zone III), and the senescence zone (zone IV) (Figure 1.3) (Kereszt et al. 2011). In addition to the presence of a true meristem, determinate and indeterminate nodules differ in their bacteroid size and composition. Indeterminate nodules contain a singular enlarged bacteroid in each symbiosome due to coordinated SM and bacteroid division, whereas symbiosomes of determinate nodules contain multiple bacteroids as division is not so tightly regulated (Robertson and Lyttleton 1984). Soybean (*Glycine max*) and the model species *Lotus japonicus* are examples of legumes that form determinate nodules, while chickpea (*cicer arietinum*), pea (*Pisum sativum*) and the model species *Medicago truncatula* and *Medicago sativa* form indeterminate nodules. Due to these features, species forming determinate type nodules are generally regarded as simpler models for biochemical assessment, although the distinct developmental stages of indeterminate type nodules can provide an in-depth understanding of the system and are particularly valuable in transcriptomics studies. Interestingly, these bacteroids that infect indeterminant or determinant nodule types may differ significantly in their metabolism. Dicarboxylic acids provided to the bacteroids are metabolised via the tricarboxylic acid (TCA) cycle and used to drive nitrogen fixation (Lodwig and Poole 2003). But in slow growing determinant type nodules such as *Bradyrhizobium japonicum* infection of *G. max*, TCA mutants can still effectively fix nitrogen (Thöny-Meyer and Künzler 1996). However, in the faster-growing indeterminant type nodules, formed by *Sinorhizobium meliloti* or *Rhizobium leguminosarum*, which infect *M. sativa* and *P. sativum*, respectively, require a functional TCA cycle.

1.5 The symbiosome

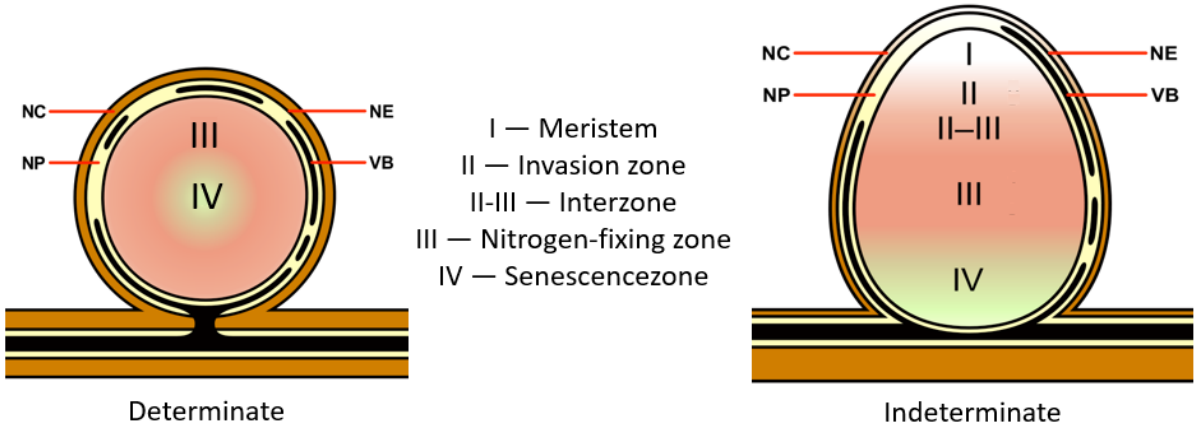

Figure 1.3 Developmental stages of mature determinate and indeterminate nodules. Indeterminate type nodules contain a persistent meristem that determinate type nodules lack, this results in distinct developmental stages occurring during growth. Adapted from Ninjatacoshell under the Creative Commons Attribution-Share Alike 3.0 Unported license.

Inside the infected cells of the root nodules, symbiosomes are the functioning unit of BNF and are sometimes referred to as ammoniaplasts, as they act as moonlighting organelles that produce ammonia (Udvardi and Poole 2013). During symbiosome proliferation the entire infected cell differentiates, becoming abnormally large and altering in carbon and nitrogen metabolism (Streeter 1995). The SM acts to exclude the bacteroids from the plant's cytosol, creating a highly specialised symbiosome space, which exists between the SM and bacteroid (Figure 1.4). The SM is unique in both its protein and lipid content, resembling a mixture of the plasma membrane (PM) and tonoplast (Brewin 1991; Udvardi and Day 1997). The primary metabolic exchange across the SM is the import of carbon and the export of nitrogen, representing export from and import to the plant cell, respectively (Udvardi and Day 1997). It is important to understand that the transport activities of the SM and bacteroid are distinct (Mohd Noor et al. 2015). To aid with its function, the SM contains numerous proteins, encoded by plant genes that allow transport of metabolites between symbionts.

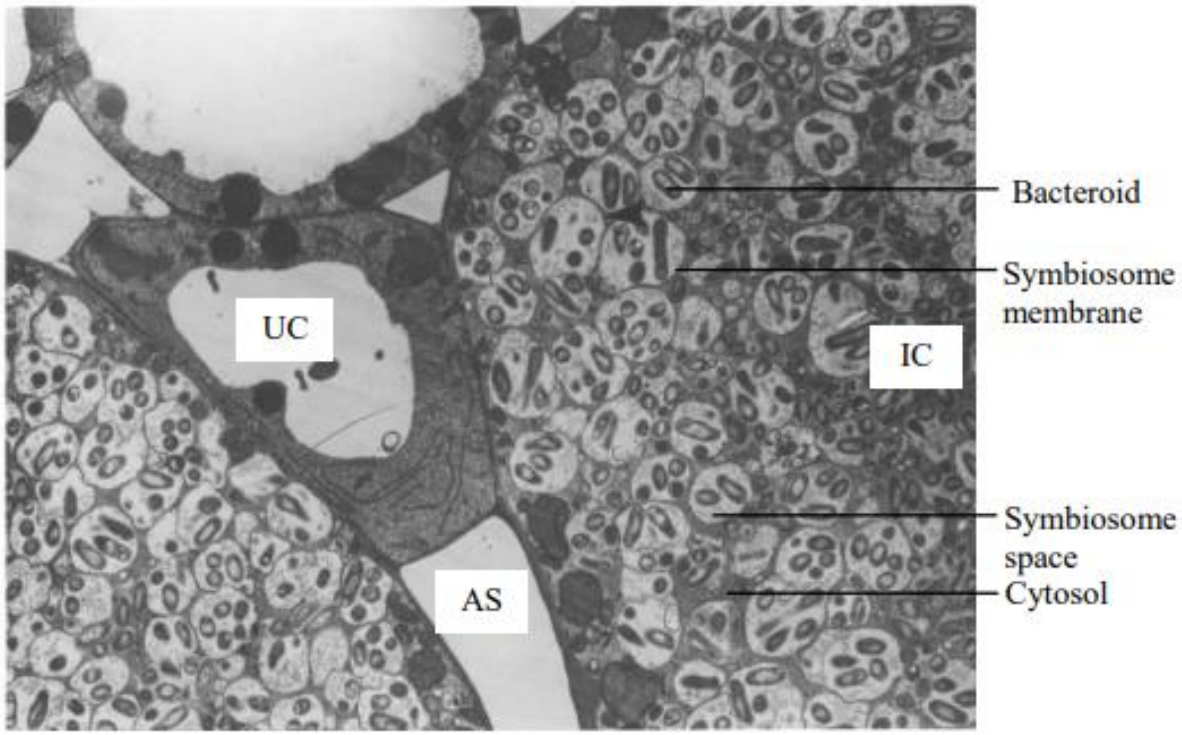

Figure 1.4 Electron micrograph of soybean infected nodule cells containing numerous symbiosomes. Abbreviations: IC – infected cell; UC – uninfected cell; AS – air space. (Udvardi and Day 1997). Reprinted with permission from Annual Reviews.

1.6 Transport across the SM

Reverse genetics have been at the forefront in identifying potential candidates for metabolite transport across the SM. Early work screened rhizobial mutants for nitrogen fixation phenotypes (Udvardi and Poole 2013), however recently mutant lines of the model plant species *L. japonicus* (Fukai et al. 2012) and *M. truncatula* (Tadege et al. 2008) have been utilised to elucidate the protein transporters. It has been well established that the principal exchange of nutrients across the SM is the uptake of reduced carbon and efflux of fixed nitrogen, but other transport process must also be present for successful symbiosis (Day et al. 1989; Udvardi and Day 1997; Clarke et al. 2014). These include the activity of ATPases, transport of metabolites required for bacteroid growth and nitrogenase activity, as well as less well understood secondary transport processes (summarised in Figure 1.5).

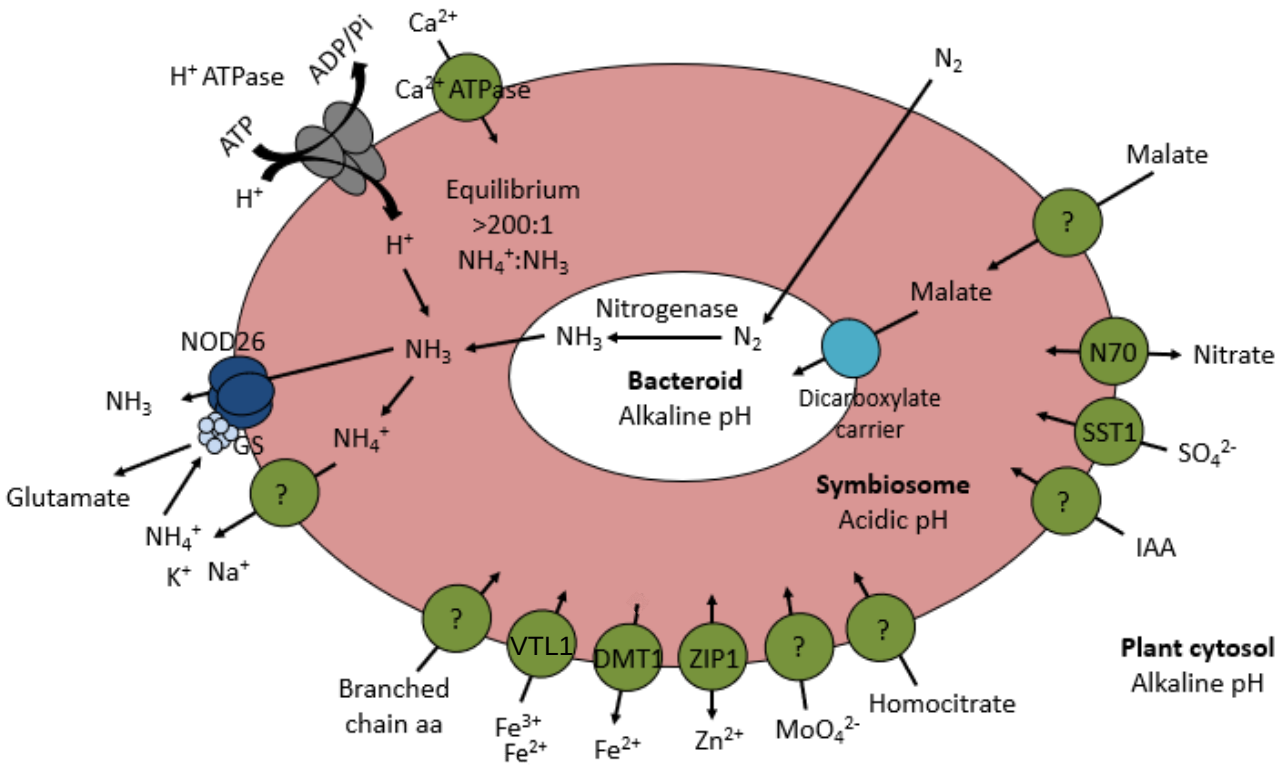

Figure 1.5 Transport processes of the legume SM. Numerous transport processes have been characterised across the legume SM and are summarised in section 1.6, where identified the related protein transporter is indicated, if unknown it is represented by ?. Key: DMT1 – Divalent Metal Transporter 1; GS – Glutamine synthetase; N70 – Nodulin 70; NOD26 – Nodulin 26; SST1 – Symbiotic Sulphate Transporter 1; VTL1 – Vacuolar iron Transporter Like 1; ZIP1 – Zinc Transporter 1.

1.6.1 Reduced carbon

Recently, malate transport and metabolism in nitrogen-fixing legume nodules has been reviewed as part of this thesis (Booth et al. 2021). Carbon is transported to the nodule cells primarily as sucrose, which is rapidly metabolised to glucose, fructose and a number of dicarboxylates (Stumpf and Burris 1979; Streeter 1981; Udvardi et al. 1988). However, the SM is impermeable to most of these carbon sources except a few species of dicarboxylates, which bacteroids can completely oxidise via the tricarboxylic acid cycle. In the soybean nodule cytosol, the dicarboxylates; malonate, malate, fumarate and succinate are present at 5.40, 4.18, 1.27 and 0.72 µmol per gram fresh weight, respectively (Stumpf and Burris 1979). To determine which dicarboxylates are substrates *in vivo*, respiration studies using isolated symbiosomes were used to demonstrate permeability of the SM to malate, fumarate and succinate but not glutamate, malonate, oxoglutarate and pyruvate (Price et al. 1987; Udvardi et al. 1988; Day et al. 1989). This uptake was catalysed by a dicarboxylate carrier (DC) and when malate or succinate were the substrates, uptake rates were sufficient to support estimated nitrogen fixation *in vivo.* Interestingly, however, this was not the case for fumarate (Price et al. 1987; Day et al. 1989).

Udvardi et al. (1988) were first to directly measure dicarboxylate transport across the SM using the silicon oil centrifugation technique with [^{14}C] labelled substrates. This group differentiated between transport activities of the symbiosome and bacteroid membranes through selective inhibition of the membranes with phthalonate and hydroxycyanocinnanic acid. They found these compounds, which are known inhibitors of mitochondrial organic acid transporters, to be potent inhibitors of the SM-DC but not of the bacteroid dicarboxylate system. Additionally, they determined that the true substrate for the SM-DC is monovalent dicarboxylate anions (Udvardi et al. 1988). With this information, they calculated the K_m for malate and succinate to be 2 and 15 µM respectively, suggesting that the SM-DC would be saturated at physiological levels, as malate and succinate concentrations within the nodule cytosol are estimated to be ~ 4.17 and 0.8 mM respectively (Stumpf and Burris 1979; Udvardi et al. 1988).

The SM-DC remains unidentified, although it has been well characterised though biochemical studies. Work by Ou Yang et al. (1990) demonstrated that the rate of bacteroid respiration affected malate uptake, as inhibition with potassium cyanide, an inhibitor of the bacteroid electron transport chain, significantly decreased malate transport across the SM. Through ATP incubation and carbonyl cyanide m-chlorophenylhydrazone inhibition studies, it is thought that regulation of anion uptake by the symbiosome is also, at least partly, mediated by the energisation of the SM through its ATPase activity (Ou Yang et al. 1990; Udvardi et al. 1991). Additionally, the phosphorylation status of the

carrier is correlated with malate uptake across the SM (Ou Yang et al. 1991). Preincubation of isolated SMs with alkaline phosphatase inhibited malate transport across the SM, but this was completely restored through addition of ATP and $CaCl_2$. This suggests phosphorylation of the SM-DC by a calcium dependent protein kinase is essential for malate uptake (Ou Yang et al. 1991). Finally, malate transport by the SM-DC is competitively inhibited by a range of other dicarboxylates, suggesting it also transports these substrates, but with an apparent preference for malate (Ou Yang et al. 1990). To summarise, the SM-DC is likely phosphorylated, requires energisation across the SM and has a preference for the monovalent form of malate (Figure 1.6).

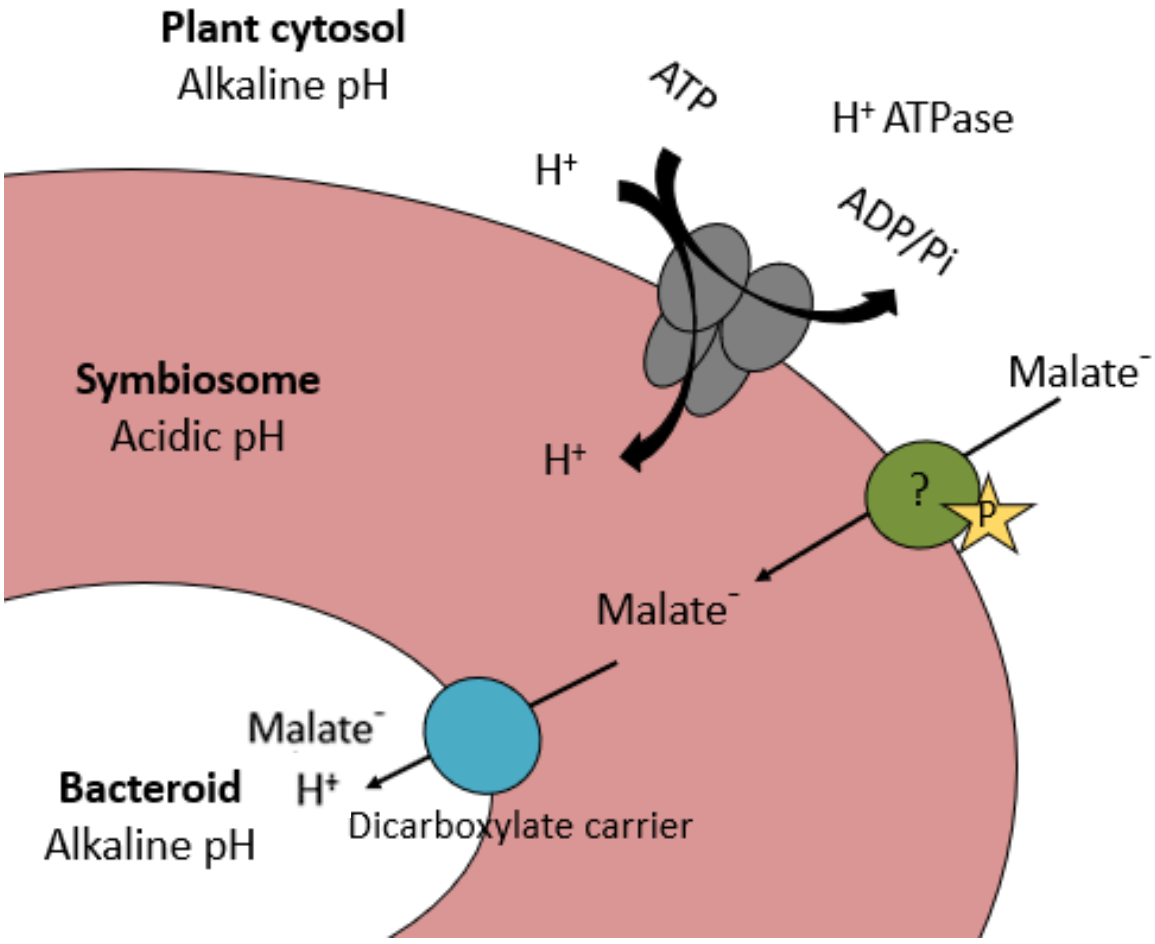

Figure 1.6 Transport of dicarboxylates across the SM. The monovalent form of malate is the primary dicarboxylate transported across the SM by an unidentified dicarboxylate carrier. This movement is energised by the H^+-ATPase activity on the SM. Dicarboxylates in the symbiosome space are readily taken up by the bacteroid expressed dicarboxylates carrier. Key: P – phosphorylation; ? – unknown protein.

Mellor and Werner (1987) suggested that the symbiosome is comparable of the vacuole in normal root cells, making tonoplast dicarboxylate transporters excellent candidates for the SM-DC. Due to the energetics of the system, the SM-DC essentially acts as an efflux protein, transporting malate out of the plants cytosol. This has been one of the major limitations to identifying this carrier, as cDNA library screens are unlikely to rescue the growth of mae1 deficient yeast strains which require complementation with malate influx proteins. However, there are a number of tonoplastic dicarboxylate transporters referenced in the literature, including tonoplast Dicarboxylate Transporters (tDT) and Aluminium Activated Malate Transporters (ALMT), as well as more general anion transport families such as ATP-Binding Cassette (ABC) type transporters, Nitrate Peptide transporter Family (NPF), Slow Anion Channel (SLAC) and Voltage-Dependent Anion Channels (VDAC) providing a range of excellent candidates. Omic studies have aiding in narrowing down the search for the SM-DC. Roux et al. (2014) and Takanashi et al. (2012) have completed tissue–specific transcriptomic analyses of *M. truncatula* and *L. japonicus,* respectively, and recently an integrated single cell and spatial transcriptomics approach has been performed in soybean nodules (Liu et al. 2023). These studies, along with a number of proteomic analyses on isolated SMs (Saalbach et al. 2002; Wienkoop and Saalbach 2003; Clarke et al. 2015; Luo et al. 2023), have revealed a number of putative transporters on the SM, but no definitive candidates for the SM-DC have been identified.

The *Arabidopsis* tDT was the first vacuolar malate carrier identified at the molecular level. It is able to facilitate dicarboxylate import to the vacuole (Emmerlich et al. 2003; Hurth et al. 2005). Through ^{14}C uptake studies into vacuoles isolated from wildtype and *At*tDT knockout plants, it was shown that this carrier can transport both malate and fumarate, observations similar to that of the SM-DC, but distinct as *At*tDT transport is inhibited by carbonyl cyanide m-chlorophenylhydrazone (Emmerlich et al. 2003; Hurth et al. 2005). ALMTs are another candidate for the SM-DC; this family was first implicated in aluminium tolerance as the wheat *Ta*ALMT1 was activated in the presence of high aluminium concentrations leading to an efflux of malate from the roots that chelates and detoxifies the aluminium cations (Sasaki et al. 2004). *At*ALMT1 was the first of 14 ALMT members to be characterised in *Arabidopsis*, with orthologs found in most plant species (Sharma et al. 2016). It is now accepted that the ALMT family mediates organic acid transport across members from a wide range of tissue types with physiological roles extending beyond aluminium tolerance (Pineros et al. 2008; Meyer et al. 2010; De Angeli et al. 2013a).

Kovermann et al. (2007) were first to demonstrate that *At*ALMT9 was a tonoplast malate transporter, through reduced malate currents in *At*almt9 lines, and by functional expression of the channel in *Nicotiana benthamiana* and *Xenopus laevis* oocytes. These channels have been reported

to transport a range of anions, display voltage-dependent gating and are regulated by phosphorylation (Kovermann et al. 2007; Ligaba et al. 2009; Meyer et al. 2010; Meyer et al. 2011; Imes et al. 2013). Takanashi et al. (2016) hypothesised that an ALMT may be the SM-DC and identified seven ALMT proteins in *L. japonicus.* They determined that three ALMTs were expressed in the nodule tissue, and that *Lj*ALMT4 had nodule specific expression. Further characterisation revealed that *Lj*ALMT4 mediated efflux of dicarboxylates in the nodule vascular bundle, rather than across the SM. The two remaining nodule-expressed ALMTs could not generate malate induced currents when expressed in *X. laevis* oocytes. Recent advances to the *L. japonicus* genome (Li et al. 2020) have revealed additional candidates that are yet to be characterised (Booth et al. 2021).

ABC transporters are found in all known organisms and have been shown to transport a range of substrates, although individual members are usually specific to a particular substrate (Gottesman and Ambudkar 2001; Do et al. 2018). ABC transporters are directly energised by ATP and are capable of transporting substrates including ions, sugars, amino acids, lipids and proteins against their concentration gradients (Do et al. 2018). In the plant pathogen defence system, the *Arabidopsis* PEN3 ABC transporter requires phosphorylation at multiple sites to contribute to its antimicrobial action (Underwood and Somerville 2017). The *Arabidopsis* ABCB14 protein has been implemented in malate import to the stomata, through expression in HeLa cells resulting in an 80% increase in [^{14}C] malate transport and complementation of *Escherichia coli* dicarboxylate transport mutants (Lee et al. 2008). Takanashi and Yazaki (2014) analysed laser microdissection transcriptomics data of *L. japonicus* nodule tissue published by Takanashi et al. (2012) and found five ABC transcripts displaying infected zone specific expression. Additionally, proteomics by Clarke et al. (2015) identified five ABC transporters in soybean SM fractions.

NPFs belong to the major facilitator superfamily, and most of the characterisation of this superfamily has been performed in *Arabidopsis*, where 53 members are found (Léran et al. 2014). The substrate preferences of NPFs are extremely broad, with anion, peptide, amino acid, plant hormone and glucosinolate transport characterised in various *Arabidopsis* family members (Corratgé-Faillie and Lacombe 2017). In the non-legume Alder (*Alnus glutinosa*) DCAT1, a member of the NPF family, is the dicarboxylate transporter localised to the symbiotic interface of infected nodule cells (Jeong et al. 2004). This symbiosis is distinct from that of legumes, as Alder forms an actinorhizal symbiosis with the filamentous soil bacterium *Frankia*, whereby the symbiotic interface is invaginated and the PM of the infected cell is not completely enclosed (Mylona et al. 1995). NPFs are generally regarded as proton symporters (Corratgé-Faillie and Lacombe 2017), and since the symbiosome has an acid interior (Bhandari and Nicholas 1985; Blumwald et al. 1985; Udvardi and Day 1989) the energetics

are seemingly not aligned with what is observed in legumes. However, not all NPFs act as symporters; a subfamily of NPFs, the so-called Nitrate excretion transporter (NAXT) proteins, are thought to facilitate the uniport of nitrate out of the plant cell's cytosol, coupled to proton-pumping by the PM H^+-ATPase and driven by the electrochemical gradient across the PM (Segonzac et al. 2007). Biochemically, this is essentially the transport mechanism described for isolated soybean symbiosomes, making the NPF family excellent candidates for the SM dicarboxylate carrier (Booth et al. 2021). There have been eight NPF proteins identified in soybean SM proteomic studies, with *in vivo* localisation to the SM confirmed for a number of these candidates (Clarke et al. 2015; Luo et al. 2023).

SLAC and the homologous SLAH proteins were originally annotated as dicarboxylate carriers due to sequence similarities with MAE1, a dicarboxylate transporter found in yeast (Negi et al. 2008). Negi et al. (2008) first hypothesised that SLAH1 may be the dicarboxylate channel in guard cells due to the important regulatory role of malate in stomatal opening and observed abnormal levels of malate and fumarate accumulation in slac1 mutant phenotypes. SLAC1 complementation of the yeast mae1 or *E. coli* malate up-take mutants could not rescue malate uptake (Negi et al. 2008; Vahisalu et al. 2008), but this is not unexpected as the guard cell anion channel *in vivo* would energetically favour anion efflux and import is required for bacterial complementation. Expression of SLAC1, SLAH2, and SLAH3 in *X. laevis* oocytes only generated anion currents when phosphorylated, but these currents were selective with a preference for NO_3^- and Cl^- and low permeability to malate (Geiger et al. 2009; Scherzer et al. 2012; Maierhofer et al. 2014; Sun et al. 2016; Chen et al. 2019). There is no evidence in the literature that SLAC/SLAH channels are located on the SM, although there is enhanced nodular expression of at least one member of this gene family (Roux et al. 2014).

VDACs are the most prevalent protein on the mitochondrial outer membrane, and facilitate metabolite flux between the cytoplasm and the mitochondrial intermembrane space (Hodge and Colombini 1997). In general, VDACs are gated at both positive (>+20) and negative (<-20) membrane potentials, but in the presence of a salt gradient a shift in gating occurs so that they are open at more negative membrane potentials (between -30 and +10), allowing anion flux (Zizi et al. 1998). In mammalian cells, VDAC proteins are phosphorylated, although the exact effect this has on the protein remains unknown, with some studies suggesting this prevents the apoptotic process, while others suggest it triggers it (Kerner et al. 2012). While no direct measurements of dicarboxylate transport through VDACs have been made, a porin isolated from spinach leaf peroxisomes contains a high affinity dicarboxylate binding site that is likely to increase the permeability of these metabolites

through the channel (Reumann et al. 1998). Wandrey et al. (2004) immunolocalised four VDACs in *L. japonicus* and soybean nodules but found no evidence for their presence on the SM.

Studies with the tonoplast from non-legume cells have provided several candidates for the SM-DC, the ALMT and NPF families provide the strongest candidates, as they share a number of functional similarities with the SM-DC. ALMTs display voltage-dependent gating, regulation by phosphorylation and would likely transport malate out of the cytoplasm and into the symbiosome space. Although Takanashi et al. (2016) did not identify a symbiosome localised ALMT, the scope of the study may have been insufficient in identifying all ALMT sequences in *L. japonicus*. NPFs are an interesting candidate, typical energetics of this family would not fit with the characterised SM-DC, but exceptions within the family are found in the literature. Given that eight NPFs are found on the SM an investigation into their substrate specificity is warranted. SLAC and ABC families are reasonable candidates as they all share some functional characteristics with the SM-DC. It is unlikely that a member of the tDT or VDAC families are the SM-DC, as there is no evidence of either of these proteins on the SM.

1.6.2 Fixed nitrogen

Carbon transported to the bacteroid is used to energise the reaction catalysed by nitrogenase to fix nitrogen gas into ammonia. This results in an accumulation of ammonia within the bacteroid, favouring its diffusion into the symbiosome space (Dilworth and Glenn 1982; Dilworth and Glenn 1984; Day et al. 2001a). This concentration gradient remains favourable for ammonia efflux from the alkaline bacteroid due to H^+-ATPase activity on the SM, creating an acidic symbiosome space that rapidly protonates ammonia into ammonium (Udvardi et al. 1991; Fedorova et al. 1999). This is commonly referred to as the 'acid trap' and by using the Henderson-Hasselbach equation it can be estimated that the ammonium concentration would be 178 times greater than that of ammonia at pH 7.0, with the acidity of the symbiosome space only enhancing this (Brewin 1991; Day et al. 2001b). Reuptake of ammonium by bacteroids is prevented due to the repression of high affinity ammonium transporters during bacteroid differentiation from free living rhizobia (Howitt et al. 1986), resulting in the accumulation of fixed nitrogen products in the symbiosome space that must be exported across the SM to the plant cytosol. There is evidence for efflux of both ammonia (NH_3) and ammonium (NH_4^+) from the symbiosome. A non-selective cation channel (NSCC) was identified on the SM and shown to facilitate the directional transport of NH_4^+ from the symbiosome space to the cytosol (Tyerman et al. 1995; Roberts and Tyerman 2002), while NH_3 has been shown to move through a Nodulin 26 (NOD26) diffusive pathway (Niemietz and Tyerman 2000) (Figure 1.7). This transport is likely to be passive due to the rapid assimilation of ammonium to glutamate by the

cytosolic glutamine synthetase (GS) bound to NOD26 (Robertson et al. 1975; Liaw et al. 1995; Masalkar et al. 2010).

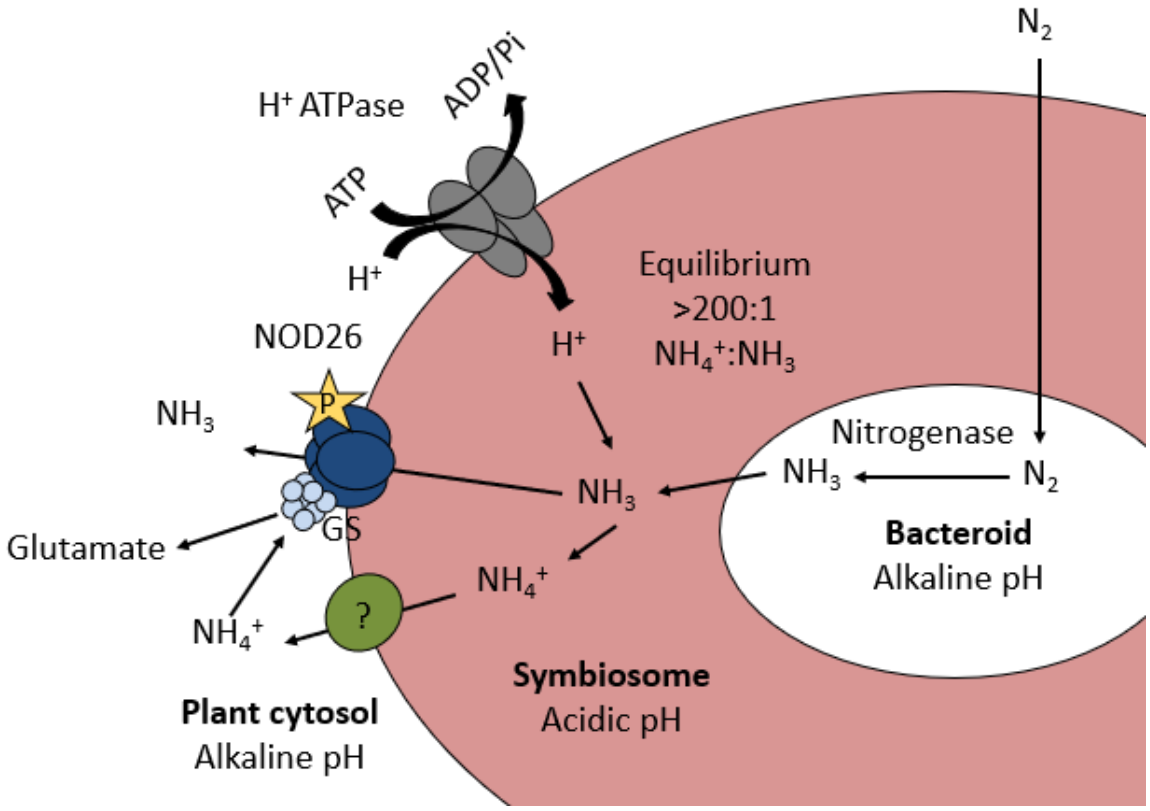

Figure 1.7 Transport of fixed nitrogen products to the plant cytosol. Nitrogen gas diffuses into the bacteroid where the activity of nitrogenase fixes it into ammonia, which diffuses into the symbiosome space. Activity of the SM H^+ ATPase acidifies the symbiosome space and shifts the equilibrium of NH_4^+ to NH_3 ions in excess of 200 to 1. The relatively small amount of NH_3 ions move through NOD26 into the cytosol, while NH_4^+ is transported across the SM through a non-selective cation channel (NSCC). Cytosolic NH_4^+ is rapidly converted to glutamate though the activity of the NOD26-bound GS. Key: GS – Glutamine Synthetase; NOD26 – Nodulin 26; P – phosphorylation; ? – unknown protein.

Early work suggested that the diffusive pathway for NH_3 was likely to be through NOD26 (Tyerman and Niemietz 2000), an aquaporin that constitutes ~10% of the SM total protein mass (Rivers et al. 1997). Rivers et al. (1997) demonstrated that NOD26 was an aquaporin-like channel permeable to water, formamide and glycerol with mercury sensitivity. Building on this knowledge, Niemietz and Tyerman (2000) measured ammonia permeability of isolated soybean symbiosomes and found that it was inhibited by up to 42% by mercury, suggesting it may move through NOD26. It was later

established through expression of soybean NOD26 in *X. laevis* oocytes that NOD26 provides a low energy pathway for ammonia diffusion though the SM (Hwang et al. 2010).

Ammonium transport through the NSCC was first elucidated through the patch-clamping of isolated SMs (Tyerman et al. 1995). Tyerman et al. (1995) demonstrated time and voltage dependent inward currents (in an orientation representing efflux from the symbiosome) in the presence of monovalent cations (NH_4^+, K^+, Na^+), with NH_4^+ generating the largest currents at physiological levels estimated by Streeter (1989). The channel displayed low conductance (SubpicoSiemen in amplitude) but appeared to be present at high density in the patched membrane. Gating of this channel was also observed by the divalent cations, Ca^{2+} and Mg^{2+}, and it was found that this gating was bidirectional dependent on divalent cation concentration on either side of the membrane (Tyerman et al. 1995; Whitehead et al. 1998; Roberts and Tyerman 2002; Obermeyer and Tyerman 2005). Physiological concentrations of Ca^{2+} are reported to be high inside symbiosomes (Udvardi and Day 1997), but it is believed that most of this Ca^{2+} is bound by Ca^{2+} binding proteins (Roberts and Tyerman 2002) or in the bacteroids (Vincent and Humphrey 1963). *In vivo*, free Ca^{2+} concentrations in the symbiosome space would be in a range that allows ammonium efflux to the cytosol (Tyerman et al. 1995). Additionally, cytosolic Mg^{2+} concentrations (~2 mM Mg^{2+}) are sufficient to inwardly rectify ammonium currents and may be responsible for gating of the SM-NSCC *in vivo* (Tyerman 2002).

In an attempt to identify the SM-NSCC, Kaiser et al. (1998) transformed the *Saccharomyces cerevisiae* ammonium transport double mutant 26972c (*mep1-1, mep2-1,* Mep3) with a cDNA library synthesised from soybean nodule tissue. They identified a cDNA, *Gm*SAT1, that complemented the ammonium transport deficiency and localised this protein to fractions of the SM. In the *S. cerevisiae* double mutant (26972c) the activity of the third ammonium carrier Mep3 is inhibited by a mutation in *mep1*-1. Marini et al. (2000) demonstrated that *Gm*SAT1 could not complement the ammonium transport triple mutant 31019b (*mep*1Δ*mep*2Δ*mep*3Δ), suggesting that *Gm*SAT1 interfered with the inhibition of Mep3 rather than acting as a direct transporter of ammonium. This group also highlighted that *Gm*SAT1 contains sequence homologous to a basic helix-loop-helix (bHLH) domain. Further characterisation by Chiasson et al. (2014) revealed that *Gm*SAT1 encoded a bHLH transcription factor, renamed *Gm*bHLHm1, important to nodule function, rather than encoding the SM-NSCC. Molecular characterisation of NSCCs is notoriously difficult, largely due to the low selectivity of the channels (Demidchik et al. 2002). It is not surprising that Kaiser et al. (1998) were unable to identify the cDNA encoding the SM-NSCC through screening in *S. cerevisiae*, as the SubpicoSiemen conductance of this channel may be insufficient to rescue the growth phenotype observed in this mutant. Additionally, Grenson's minimal media was used as the primary testing

media for yeast growth, and this medium contains ~2.7 mM each, Ca^{2+} and Mg^{2+}, which may have gated the channel to block cation influx to the *S. cerevisiae* cytosol, where free cytoplasmic Ca^{2+} and Mg^{2+} are estimated to be at ~0.5 µM and 1 mM, respectively (Beeler et al. 1997; Van Eunen et al. 2010).

The patch-clamp studies indicated that the channel responsible for NH_4^+ flux is present at high density in the SM, suggesting it would make up a significant portion of the SM protein mass. However, no obvious NSCC candidates are apparent in the various proteomics studies with the SM. The most prominent protein detected on the SM is the aquaporin NOD26 (Rivers et al. 1997). Aquaporins are a diverse class of selective membrane channels well characterised to transport water and other neutral solutes and gases across biological membranes (Agre 2004). Yool et al. (1996) first demonstrated that human Aquaporin (AQP) 1 displayed non-selective cation conductance in *X. laevis* oocytes. This protein forms a homotetramer in cellular membranes, with each monomer containing a functional water pore, while the central tetrameric pore transports charged species (see Figure 1.8) (Yu et al. 2006; Campbell et al. 2012). NSCC activity of plant aquaporins has also been reported recently (Jahn et al. 2004; Holm et al. 2005; Kaldenhoff and Fischer 2006; Byrt et al. 2017). This prompts the question: could the SM-NSCC be the aquaporin NOD26? Interestingly Weaver et al. (1994) reconstituted GmNOD26 into liposomes and demonstrated single channel conductance in the nanoSiemen range that was voltage-sensitive. They suggested that the currents were carried by anions although there is no precedent for this in the aquaporins studied to date.

There are several shared characteristics between GmNOD26 and the NSCC found in the SM patches. Firstly, aquaporins are regulated by divalent cations, with time and voltage dependent rectification observed (Byrt et al. 2017; Kourghi et al. 2017). Gating by divalent cations was also reported for the SM-NSCC. Secondly, GmNOD26 accounts for ~10% of the SM total protein mass (Rivers et al. 1997), and the SM-NSCC appeared to be in a high density throughout the SM. Thirdly, phosphorylation of aquaporins can mediate a switch between water or ion conductivity states, and tyrosine dephosphorylation in the *Drosophila* aquaporin BIB has been shown to enhance ion channel conductance (Yanochko and Yool 2002). GmNOD26 phosphorylation at serine 262 leads to increased water permeability of the channel (Guenther et al. 2003) and results in voltage-dependent gating at lower sub conductance states (Lee et al. 1995). Finally, cytosolic GS interacts with the C-terminal domain of GmNOD26 (Masalkar et al. 2010), providing a high affinity ammonium binding site (Liaw et al. 1995) that may act to increase the sink strength of the plant cytosol to ammonium and could explain the ammonium preference of the SM-NSCC.

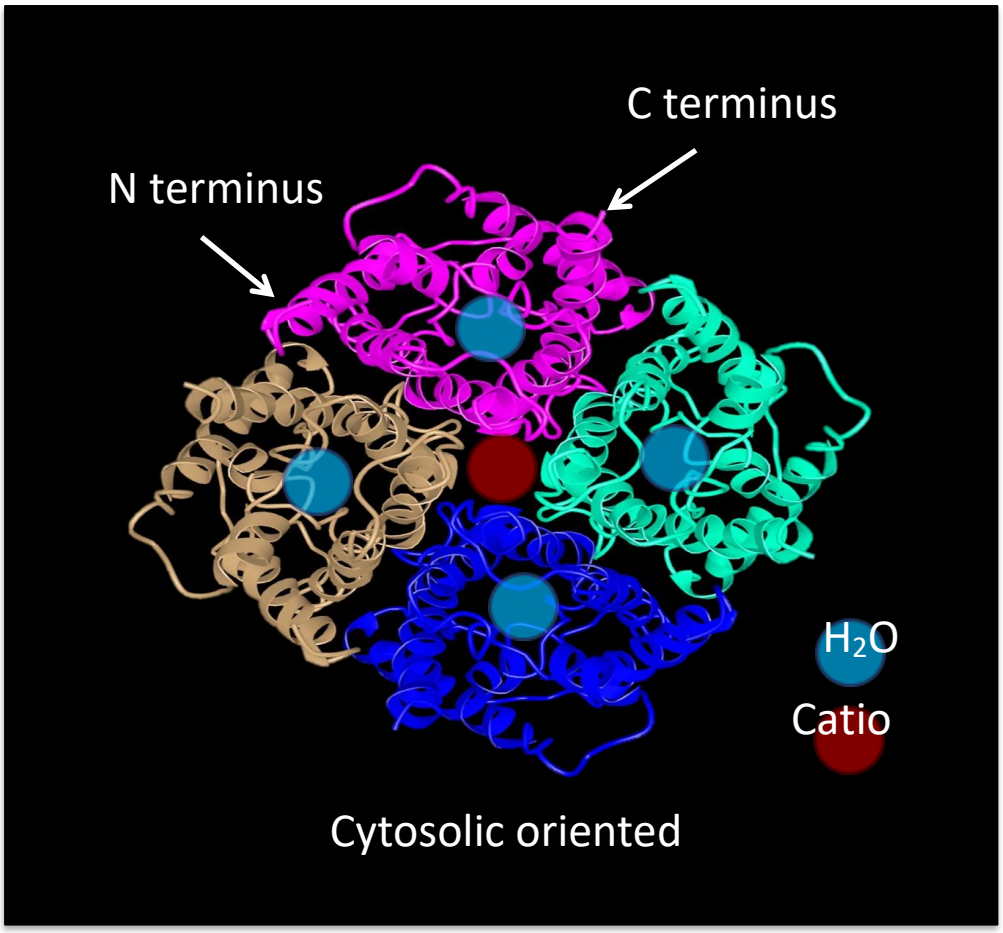

Figure 1.8 Water and cation flux through the aquaporin 1 complex. Ribbon structure of the aquaporin 1 tetramer highlighting the four monomeric water pores, the central tetrameric cation pore and cytosolic exposed N and C terminals (PDB : 1FQY). It is believed that the aquaporin NOD26 shares a similar structure to aquaporin 1.

In addition to NH_3 and NH_4^+ transport, labelling experiments have indicated amino acid pools are synthesised under certain microaerobic conditions (Day et al. 2001a; Day et al. 2001b). In isolated pea bacteroids, alanine production was largely dependent on bacteroid density, with a high bacteroid density activating alanine biosynthesis, attributed to NH_4^+ accumulation (Allaway et al. 2000). Alanine produced by bacteroids is transported to the symbiosome space through general amino acid permeases of the ABC superfamily (Walshaw and Poole 1996; Hosie et al. 2002). However, the mechanism by which alanine crosses the SM is unknown. Swelling assays of isolated soybean symbiosomes revealed asymmetric alanine transport 100 times greater in the direction out of the symbiosome (Tyerman and Niemietz, unpublished data described in Day et al. (2001a)). This transport was strongly inhibited by mercury, and it was suggested that alanine may be transported through GmNOD26 (Day et al. 2001a). Given that water permeability of GmNOD26 is also inhibited by mercury (Rivers et al. 1997; Dean et al. 1999), this may have been an artifact induced by the swelling assay, but further investigation of alanine transport by GmNOD26 is warranted.

1.6.3 ATPase activity

1.6.3.1 H^+-ATPase activity

The SM is energised by the activity of a H^+-ATPase. ATPases, were among the first proteins to be characterised on the SM (Robertson et al. 1978; Verma et al. 1978). This is fundamental to the transport of a range of metabolites across the membrane, as discussed in 1.7.1 and 1.7.2, through acidification of the symbiosome space and subsequent generation of both chemical and electrical potentials across the SM (Udvardi and Day 1989; Udvardi et al. 1991; Udvardi and Day 1997). P-type H^+-ATPases have been identified in fractions of soybean, *L. japonicus* and *M. truncatula* SM (Wienkoop and Saalbach 2003; Catalano et al. 2004; Clarke et al. 2015), and Fedorova et al. (1999) immunolocalised a P-type H^+-ATPase to the soybean SM.

1.6.3.2 Ca^{2+}-ATPase activity

Calcium is an important secondary messenger in plant cells regulating a range of physiological processes. In the symbiosome alone it has been shown to gate the NSCC that facilitates ammonium efflux and is required for calcium dependent protein kinases that stimulate malate uptake. As previously mentioned, the symbiosome may act as a calcium store (Udvardi and Day 1997; Andreev et al. 1999), but most of is bound by Ca^{2+} binding proteins (Roberts and Tyerman 2002) or is located in the bacteroids (Vincent and Humphrey 1963). There are reports of activity of Ca_2^+-ATPases on the SM, hypothesised to actively pump calcium into the symbiosome space (Andreev et al. 1999; Krylova et al. 2013; Andreev et al. 2019), but these have not been substantiated.

1.6.4 Bacteroid metabolites

1.6.4.1 Branch chain amino acids

During bacteroid differentiation repression of AMTB, a high affinity ammonium transporter expressed in free-living *B. japonicum* bacteria, is crucial in preventing re-uptake of fixed nitrogen by the bacteroid (Howitt et al. 1986; Tate et al. 1998; Lodwig et al. 2003). In pea bacteroids, this is accompanied by downregulation of branch chain amino acid biosynthetic enzymes, making bacteroids symbiotic auxotrophs, totally reliant on their plant host to supply branch chain amino acids for their growth (Prell et al. 2009). The identification of the transporter that imports branch chain amino acids into the symbiosome space remains elusive, but the soybean symbiosome proteome identified an amino acid permease and five ABC type transporters (Clarke et al. 2015), which have previously been implicated in amino acid transport (Davidson et al. 2008; Tegeder 2012; Durmort and Brown 2015).

1.6.4.2 Iron

Iron is essential for a stable legume-rhizobia symbiosis, it is an important component of leghemoglobin in the nodule cells, and required for many nitrogen fixing proteins in bacteroids, including cytochromes in the bacteroid electron transport chain and in the metallocentres of nitrogenase (Appleby 1984; Kaiser et al. 2003; Brear et al. 2013). Iron deficiency in peanuts has been shown to lower leghemoglobin concentrations, delay nitrogen fixation and reduce bacteroids by approximately 215 times within the infected cells (O'Hara et al. 1988). Radiolabelled iron uptake measurements with isolated symbiosomes have revealed that both Fe^{2+} and Fe^{3+} are transported into the symbiosome, but bacteroids cannot readily uptake Fe^{3+} (LeVier et al. 1996; Moreau et al. 2002). Fe^{3+} is highly insoluble in the plant cytosol and therefore is transported across the SM in organic acid complexes, where it accumulates in the symbiosome space bound by siderophore-like compounds released by the bacteroid, acting as a major store in the nodule (Wittenberg et al. 1996; Udvardi and Day 1997). LeVier et al. (1996) have reported Fe^{3+} chelate reductase activity on isolated SM and it is believed that this activity is used to reduce Fe^{3+} to Fe^{2+}. This form of iron is much more accessible to bacteroids.

There is also evidence for a Divalent Metal Transporter (DMT), a NRAMP homologue, on the SM from soybean. These transporters act as a H^+-symporters, so GmDMT1 is likely to export stored iron from symbiosomes (Kaiser et al. 2003; Brear et al. 2013; González-Guerrero et al. 2014; González-Guerrero et al. 2016). In soybean, Vacuolar iron Transporter Like (VTL) 1 a/b have been implicated in iron uptake by symbiosomes (Brear et al. 2020; Liu et al. 2020). Both proteins appear to localise to SM, but GmVTL1a is a more effective transporter when expressed in *S. cerevisiae* (Brear et al. 2020; Liu et al. 2020). It is thought that VTLs are the functional ortholog of *L. japonicus* SEN1, as both proteins share sequence homology and *sen*1/*vtl*1-1 mutants display iron deficient phenotypes which ultimately disrupts nitrogen fixation (Suganuma et al. 2003; Hakoyama et al. 2012; Brear et al. 2020; Liu et al. 2020).

1.6.4.3 Sulphate and molybdenum

Similar to iron, sulphate and molybdenum are essential cofactors in several bacteroid enzymes, including the Fe-S cluster and Fe-Mo cofactor of nitrogenase, respectively (Pau and Lawson 2002; Krusell et al. 2005; Rubio and Ludden 2005). Krusell et al. (2005) identified *L. japonicus* Symbiotic Sulphate Transporter (*Lj*SST1) as a candidate for sulphate transport across the SM, with this protein complementing sulphate deficient yeast strains and demonstrating a symbiotic nitrogen fixing phenotype where functioning nodules could not be produced. Proteomics has identified SST1 in SM

fractions of *L. japonicus* and soybean (Wienkoop and Saalbach 2003; Clarke et al. 2015). Recently, Schneider et al. (2019) reported a 20-fold increase in sulphate accumulation in bacteroids relative to the nodule cytosol in Wt *L. japonicus*. This group also provided support for sulphate transport across the SM through SST1, as sulphate accumulation in the symbiosomes of sst1-1 mutants was significantly impeded when compared with Wt plants. Transport of molybdenum has not been directly measured across the SM, but its transport has been inferred through impaired BNF phenotypes in molybdenum deficient plants (Delgado et al. 2006). Some members of the SST family have been characterised to transport molybdenum and it is possible that molybdenum may move through SST1 in addition to sulphate (Tomatsu et al. 2007; Clarke et al. 2014).

1.6.4.4 Homocitrate

Many rhizobial species are unable to synthesise homocitrate, an essential component of the Fe-Mo cofactor of nitrogenase (Hoover et al. 1989; Zheng et al. 1997; Udvardi and Poole 2013). The literature does not describe homocitrate transport into the symbiosome in detail, but *L. japonicus* fen1 mutants, unable to synthesise homocitrate, display impaired BNF phenotypes implying the existence of an unidentified homocitrate transporter on the SM (Imaizumi-Anraku et al. 1997; Hakoyama et al. 2009).

1.6.5 Secondary transport processes

1.6.5.1 Nitrate

Nitrate is one of the major regulators of BNF, shown to inhibit nodule growth and nitrogenase activity, and disperse the membrane potential across the SM (Kennedy et al. 1975; Streeter 1985; Udvardi et al. 1991). Szczyglowski et al. (1998) characterised *L. japonicus* Nodulin 70 (N70) from ESTs associated with late developmental events during nodule organogenesis, initially describing it as a nodule-specific metabolite transporter, proposed to translocate carbon substrates. Later work by Vincill et al. (2005) identified a cDNA from soybean nodules, GmN70, that localised to the SM and demonstrated outward anion currents when expressed in *X. laevis* oocytes with selectivity for nitrate > nitrite ≫ chloride. They also identified that the ortholog LjN70 carried similar currents. N70s were consequently characterised as inorganic anion transporters, with a preference for nitrate, which represents anion influx to the symbiosomes. Nitrate generally inhibits SNF through complex mechanisms, but one such effect could be an uncoupling of the symbiosome and consequent inhibition of metabolite exchange.

1.6.5.2 Zinc

Zinc is an important micronutrient across all kingdoms of life and is an integral component of cellular processes including protein synthesis, carbohydrate and lipid metabolism, and in zinc finger transcription factors (Cakmak 2000; Lin et al. 2005; Palmer and Guerinot 2009). A soybean zinc transporter, GmZIP1, has been identified on the SM and functionally characterised to facilitate bidirectional zinc transport across this membrane (Moreau et al. 2002).

1.6.5.3 Auxin

Auxin is an important plant hormone, it has long been proposed to play a role in nodule development, as nodule cells are known to contain higher levels of auxin than the surrounding root system (Thimann 1936). This hormone acts to control diverse aspects of cell proliferation and differentiation, essential to the formation of nodule cells. Transport of auxin into pea symbiosomes is mediated by an unidentified transporter that is inhibited by the known auxin-transport inhibitor, naphthylphthalamic acid (Rosendahl and Jochimsen 1995). The exact reason why auxin is imported into symbiosomes has not been reported, but perhaps acts to terminate nodule proliferation at maturity through exclusion from the nodule cytosol, or functions in bacteroid proliferation and differentiation.

1.7 Aims

The aims of this thesis are to (1) investigate whether GmNOD26 can transport cations, including NH_4^+, across the SM, and (2) to identify the SM-DC. Firstly, GmNOD26 will be expressed in both *X. laevis* oocytes and in ammonium transport deficient *S. cerevisiae* strains. Two-Electrode Voltage Clamping (TEVC) of whole *X. laevis* oocytes expressing GmNOD26 will be used to elucidate any NSCC activity of this channel as has been demonstrated for both human and plant aquaporins (Yool et al. 1996; Byrt et al. 2017). Experiments will be designed to replicate the conditions of early patch-clamp work by Tyerman et al. (1995) and build on the knowledge of the SM-NSCC. To ensure that the observations are caused by GmNOD26 and not activation of an endogenous *X. laevis* protein, site-directed mutagenesis will be performed to create phosphomimic and non-functional protein phenotypes. GmNOD26 and mutant proteins will also be expressed in ammonium transport deficient *S. cerevisiae* strains to confirm ammonia/ammonium transport through the channel.

To identify the SM-DC, candidates from the ALMT protein family will be identified through publicly available transcriptomic databases. The expression and localisation of these proteins will then be confirmed through a combination of molecular techniques including qRT-PCR, promoter driven GUS

expression and GFP fusion. It is hoped that one of the identified proteins will localise the *L. japonicus* SM. Dicarboxylate transport by these proteins, along with the soybean SM-localised NPF's, will be investigated through expression in *X. laevis* oocytes.

Identification of these proteins on the SM will advance the current understanding of carbon and nitrogen exchanged between symbionts, which could lead to enhanced transfer efficiency, in turn improving legume growth and improve the use of legumes in agricultural systems. There is demand for this improvement, highlighted by the highly variable post-harvest soil nitrogen balances, particularly in soybean, that can often see legumes requiring the application of synthetic nitrogen fertilisers, rather than acting to increase soil nitrogen reserves. This makes this research crucial for developing a sustainable agricultural system using legumes, and possibly extending the symbiosis to other crop species.

2 General methods

2.1 Reagents

All reagents were supplied by Sigma-Aldrich (USA) unless specified. For molecular techniques autoclaved MilliQ water was used unless otherwise stated.

2.2 General lab methods

2.2.1 Agarose gel electrophoresis

Agarose gel electrophoresis was performed according to the methods described by Sambrook and Russell (2001). Typically, 1.0% (w/v) and 1.2% (w/v) agarose (Fisher Biotec, Australia) in 1.0 X TAE buffer containing GelRed (Biotium, USA) were used for DNA and RNA, respectively, submerged in 1.0 X TAE buffer, and run at 100 volts for 60 minutes using the PowerPacTM Basic (BioRad, USA) prior to visualisation via the BioRad EZ Imager (BioRad, USA). For DNA products and extracted RNA, samples were mixed with 5 X Green Go Taq Flexi buffer (Promega, USA) and compared to 1 kB and 100 bp DNA ladders (Promega, USA). For cRNA products, 500 ng of cRNA or single strand RNA ladder (NEB, USA) was mixed with 2 X gel loading buffer (Invitrogen, USA), incubated at 65^{o}C for five minutes and cooled on ice prior to electrophoresis. Horizontal Gel Tanks were treated with hot 0.1 M NaOH and 1 mM EDTA for 30 minutes prior to running RNA samples in autoclaved 1.0 X TAE buffer.

2.2.2 Plasmid purification

Plasmid purification was performed using the Wizard Plus SV miniprep DNA purification system according to the manufacturers protocol (Promega, USA). Bacterial cultures were incubated overnight in 10 ml centrifuge tubes prior to at centrifugation using a Sigma 3-16PK centrifuge (Sigma-Aldrich, USA) at 3893 g for 10 minutes at room temperature. Plasmid DNA was eluted from the spin columns using 40 µl of sterile MilliQ water, quantified using a NanoDrop 1000 spectrophotometer (Thermo Fisher Scientific, USA) and stored at -20°C until required.

2.2.3 PCR clean-up

PCR amplified products were purified using the Wizard® SV Gel and PCR Clean-Up System (Promega, USA). Equal volumes of Membrane Binding Solution (Promega, USA) and PCR amplified product were added to SV minicolumn in a collection tube. For agarose gel purified products, fragments were separated by electrophoresis (2.2.1), sectioned from the gel, and dissolved at 65^{o}C with an equal

volume of Membrane Binding Solution (Promega, USA) prior to binding in an SV minicolumn. Products were purified following manufactures protocol (Promega, USA), eluted in 40 µl of sterile MilliQ water, quantified using a NanoDrop 1000 spectrophotometer (Thermo Fisher Scientific, USA) and stored at -20°C until required.

2.2.4 Restriction digestion

Restriction digests were performed using NEB (USA) restriction digests following manufacturers protocol, and wherever possible high-fidelity enzymes were utilised. Briefly, 100 ng of DNA was incubated with 1.0 X rCutSmart™ Buffer with 1.0 unit of appropriate restriction enzyme overnight at room temperature. Products were visualised through agarose gel electrophoresis (2.2.1) prior to downstream application.

2.2.5 Ammonium acetate precipitation

Ammonium acetate was used to purify plasmid DNA from restriction digests. Briefly, the restriction digest was terminated through addition of 0.5% (v/v) SDS and 10 µg of proteinase K (NEB, USA) for 60 minutes at 50^{o}C. For in vitro transcription, the DNA was further purified though extraction in an equal volume of phenol/chloroform. The aqueous phase was combined with 1/10th volume 5.0 M ammonium acetate and 2 volumes of 100% (v/v) ethanol and incubated overnight at -20^{o}C. Plasmid DNA was pelleted at max speed using an Eppendorf 5425 centrifuge (USA) for 20 minutes at 4^{o}C. The pellet was air dried and resuspended in an appropriate volume of sterile MilliQ water, quantified using a NanoDrop 1000 spectrophotometer (Thermo Fisher Scientific, USA) and stored at -20°C until required.

2.2.6 Genotyping PCR

Genotyping of LORE1 lines was performed as described by Urbanski et al. (2012). Primer sequences were obtained from Lotus Base (Mun et al. 2016), with gene specific forward and reverse primer combinations used to detect Wt allele and the forward and P2 primer combinations for insertion detection. PCR amplification was performed using the Promega (USA) GoTaq® Flexi DNA polymerase kit. Each reaction contained 1.0 X GoTaq Flexi buffer, 2 mM $MgCl_2$, 0.2mM dNTP's, 0.4 µM forward and reverse primer, 1.25 units Taq polymerase and 2 µl of gDNA (2.4.1). Touchdown PCR was performed using the following cycling conditions: initial denaturation at 95°C for 3 minutes; 5 cycles of 95°C for 30 seconds, 72°C for 75 seconds; 10 cycles of 95°C for 30 seconds, 72°C to 68°C for 30 seconds, extension at 72°C for 45 seconds; 20 cycles of 95°C for 30 seconds, 72°C for 45 seconds,

extension at 72°C for 45 seconds; and final extension at 72°C for 10 minutes. Products were visualised though agarose gel electrophoresis (2.2.1).

2.2.7 Colony PCR

Colony PCR amplification was performed using the Promega (USA) GoTaq® Flexi DNA polymerase kit. A pipette tip was used to pick and resuspend a single colony in 10 µl sterile MilliQ water. GoTaq® Flexi reaction was setup containing 1.0 X GoTaq Flexi buffer, 2 mM MgCl, 0.2mM dNTP's, 0.4 µM forward and reverse primer, 1.25 units Taq polymerase and 1 µl of resuspended colony. Cycling conditions were initial denaturation at 95°C for 2 minutes; 25 cycles of 95°C for 30 seconds, annealing at primers specific Tm for 30 seconds, extension at 72°C for 60 seconds/kb; and final extension at 72°C for 5 minutes. Products were visualised though agarose gel electrophoresis (2.2.1).

2.3 Plant materials and growth conditions

2.3.1 Growth conditions

L. japonicus (MG20) plants were grown at 23°C in the Sanyo controlled environment cabinet and exposed to 16 hours light at ~120 µmol m^{-2} s^{-1} and 6 hours of dark. Initial germination was performed by scratching the seeds with 150 grit sandpaper, sterilising in 4% (v/v) bleach for two minutes, washing and incubating the seeds in sterile MilliQ water overnight at 4°C. Imbibed seeds were then place on damp filter paper until cotyledon leaf had emerged. Seedlings were transferred to 50% (v/v) vermiculite perlite containing B&D nutrient solution (Broughton and Dilworth 1971) without a nitrogen source. After seven days, *L. japonicus* plants were either inoculated with *Mesorhizobium loti* (2.3.2) or watered with B&D nutrient solution containing nitrogen. For growth studies B&D nutrient solution contained either limiting (10 µM KNO_3) or sufficient nitrogen (2 mM NH_4NO_3). Plants were maintained in these conditions until maturity (~3 months) when watering was stopped to allow desiccation of seed pods.

2.3.2 Inoculation with *M. loti*

M. loti (NZP2235) cultures were recovered from glycerol stock on YMB media containing 0.04% (w/v) yeast extract, 2.5 mM mannitol, 4 mM K_2HPO_4, 1 mM $MgSO_4$ and 2 mM NaCl. A single colony was used to inoculate 10 ml YMB which was grown shaking at 28°C overnight to OD600 of ~1.0. Cells were pelleted using a Sigma 3-16PK centrifuge (Sigma-Aldrich, USA) at 3893 g for 10 minutes at room temperature and resuspended in B&D nutrient solution without a nitrogen source to a final OD600 of 0.02. The solution containing *M. loti* was used to inoculate each *L. japonicus* plant through 10 ml application to the hypocotyl region.

2.3.3 LORE1 mutants

The ALMT LORE1 mutant (30085822) was obtained from Lotus Base (Malolepszy et al. 2016; Mun et al. 2016) and contained 5 exonic, 4 intronic, 1 intergenic LORE1 mutations. LORE1 mutants were grown under conditions specified in 2.3.1 and gDNA was extracted (2.4.1) for genotyping (2.2.6) of null and mutant segregates.

2.4 Isolation of nucleic acids from *L. japonicus*

2.4.1 gDNA extraction

Genomic DNA was extracted from *L. japonicus* leaf tissue using a modified protocol with an additional RNase treatment included (Márquez et al. 2005). Approximately 100 mg of tissue was collected from three terminal young leaves snap frozen in liquid nitrogen. Tissue was ground in microfuge tubes continuously cooled in liquid nitrogen using ball bearings 5.0 mm in diameter. DNA extraction buffer (500 µl) (pH 8.0) containing 200 mM Tris-HCL, 400 mM LiCl, 25 mM EDTA, 1.0% (v/v) SDS and 10 µg/mL RNase A (Promega, USA) was added, vortexed and incubated at 65°C for five minutes in a Solid-State Dry Block Heater (Ratek Instruments, Australia). Following centrifugation at max speed for five minutes (Eppendorf 5425 centrifuge, Australia) an equal volume of supernatant and isopropanol was combined in a 1.5 mL Eppendorf tube. The solution was centrifugation at max speed for 10 minutes at 4°C, washed with 100% (v/v) ethanol and centrifuged again under the same conditions. The dried DNA pellet was resuspended in 50 µl of sterile MilliQ water and stored at -20°C until required. Concentration and purity of DNA was determined using the NanoDrop™1000 Spectrophotometer (Thermo-Scientific, USA).

2.4.2 RNA extraction

Total RNA was extracted using the modified TRIzol-like reagent as specified by Shavrukov et al. (2013). Approximately 100 mg homogenised frozen tissue was mixed with 1 mL TRIzol-like reagent (38% (v/v) phenol, 1 M guanidine thiocyanate, 1.0 M ammonium thiocyanate, 0.1 M sodium acetate, 5% (v/v) glycerol) and centrifuged using an Eppendorf 5425 centrifuge (Australia) at 12,000 g for 5 minutes at 4°C. The supernatant was collected and combined with 200 µL chloroform prior to three-minute incubation on ice. Following centrifugation at 12,000 g for 15 minutes at 4°C, the aqueous phase was collected, mixed with 500 µL 200-proof isopropanol and allowed to incubate for 10 minutes at room temperature. The mixture was centrifuged at 12,000 g for 10 minutes at 4°C and the supernatant discarded prior to rinsing the pellet with 1 mL ethanol. The RNA pellet was dried in a laminar flow, resuspended in 30 µL sterile MilliQ water, quantified using a NanoDrop 1000 spectrophotometer (Thermo Fisher Scientific, USA) and stored at -80°C until required.

2.5 Gene expression analysis

2.5.1 cDNA synthesis

Isolated total RNA (2.4.1) was treated with Zymo DNase 1 (1 U per 2 µg RNA) (Zymo research, CA) following the manufacturers protocol and inactivated at 65°C prior to cDNA synthesis. The ProtoScript II First Strand cDNA synthesis kit (NEB, USA) was used to transcribe the DNase treated RNA into cDNA. A reaction mix containing 2 µg RNA, 5 µM Oligo $d(T)_{20}$, 0.5 mM dNTP, 1 X ProtoScript II Reaction Buffer, 10 mM DTT, 20 U Murine RNaseOut (Invitrogen, USA) and 100 U ProtoScript II Reverse Transcriptase was prepared. Using a BioRad MyCylcer (BioRad, USA) cDNA was synthesised at 42°C for 45 minutes followed by enzyme inactivation at 80°C for 5 minutes. The cDNA product was diluted 1:10 in sterile MilliQ water and stored at -80°C.

2.5.2 Quantitative Reverse Transcriptase PCR (qRT-PCR)

Gene expression was assessed using qRT-PCR. Each reaction contained 1 X KAPA SYBR (Thermo Fisher Scientific, USA), 0.1 µM forward/reverse primer and 4 µL cDNA (2.5.1). Thermal cycling conditions consisted of 3 minutes of 95°C, followed by 40 cycles of 95°C for 5 seconds and 60°C for 15 seconds. Following amplification, a melt curve consisting of 5 second increments of 0.5°C from 65°C to 95°C was performed to assess if any unintentional products had been produced. Ct values were compared against that of the standard curve (2.5.4) and normalised against two housekeeping genes (LjEiF1a and LjUBQ10) to determine the normalised concentration of cDNA.

2.5.3 qRT-PCR primer design

Primers were designed for qRT-PCR using NCBI Primer-BLAST (Ye et al. 2012) and ordered from Sigma-Aldrich (Australia). Due to the nature of reverse transcription, primers were designed near the 3' end of cDNA sequences. Additionally, it was preferable to design primers that spanned an exon junction and yielded a single 80-150 bp product. The melting temperature and GC content of the designed primers were assessed using NCBI Primer-BLAST, while NetPrimer (http://www.premierbiosoft.com/netprimer/) was used to calculate the probability of primer secondary structure formations. Under these parameters primers were designed for LjALMT1 (Lj3g1v0182300.1) or LjNOD26, previously termed LIMP2, (Lj4g3v2618520.), the primer sequences for LjEF1a and LjUBQ10 were taken from Guether et al. (2009) and used as housekeeping genes (Table 2.1).

Table 2.1 qRT-PCR primers used in this thesis. Primers were synthesised by Sigma-Aldrich, Australia.

	5' primer sequence
LjALMTqPCR-F	GGGAACCTAACACGGTTGTG
LjALMTqPCR-R	CGAAGTTCATATGGGGTCTGGTC
LjNOD26qPCR-F	GGGTTGCCACTGATGATCG
LjNOD26qPCR-R	GGCCCTGCAAACAACAC
LjUBQ10-F	TTCACCTTGTGCTCCGTCTTC
LjUBQ10-R	AACAACAGCACACACAGACAATCC
LjEF1a-F	TGTGAAGGATCTCAAGCGTG
LjEF1a-R	GTATGGCAATCAAGGACTGG

2.5.4 Preparation of qRT-PCR standards

The qRT-PCR products of the selected primer sets, and for the reference genes, were purified (2.2.3) and the concentration of product was determined using a NanoDrop 1000 spectrophotometer Thermo Fisher Scientific, USA). The Promega (USA) BioMath calculator (http://www.promega.com/a/apps/biomath/?calc=tm) was used to convert the concentration of double stranded DNA from µg/µL to pmol/µL, to generate standards between 10^0 and 10^{-8} femtomole/µL.

2.6 Gene cloning

2.6.1 Gateway® vectors

Gateway® vectors were propagated and maintained in ccdB Survival™ 2 *E. coli* strain (F-mcrA Δ(mrr-hsdRMS-mcrBC) Φ80lacZΔM15 ΔlacX74 recA1 araΔ139 Δ(ara-leu)7697 galU galK rpsL (StrR) endA1 nupG fhuA::IS2) which is resistant to the effects of the ccdB gene found in Gateway® donor and destination vectors (Invitrogen, USA). Due to the linear nature of pENTR™/D-TOPO™ the plasmid was order directly from Invitrogen (USA) and was unable to be propagated in the ccdB Survival™ 2 *E. coli* strain. The Gateway® vectors used are listed in Table 2.2 and maintained in LB media (1% (w/v) tryptone, 0.5% (w/v) yeast extract, 1% (w/v) NaCl, pH 7.0) containing appropriate selection.

Table 2.2 List of Gateway® vectors used. Plasmid maps can be found in Appendix 1.

Vector	Recombination site	Selection	Source
pDONR™221	AttP	Kanamycin	Invitrogen, USA
pENTR™/D-TOPO™	AttL	Kanamycin	
pGEMHE-DEST	AttR	Ampicillin	Sunita Ramesh,
pGEMHE-DEST-cYFP	AttR	Ampicillin	Adelaide University,
pYES-DEST52	AttR	Ampicillin	Australia
V33	AttR	Spectinomycin	Penelope Smith, La
V45	AttR	Spectinomycin	Trobe University,
V48	AttR	Spectinomycin	Australia

2.6.2 Preparation of TSS competent DH5a *E. coli*

Overnight culture of DH5a grown in LB media was used to inoculate 50 mL LB at a dilution of 1:100. This culture was growth shaking at 200 RPM at 37°C until at OD600 of ~0.4. Cells were incubated on ice for 10 minutes and harvested using a Sigma 3-16PK centrifuge (Sigma-Aldrich, USA) at 1000 g for 10 minutes at 4°C. The supernatant was discarded, and cells were resuspended TSS buffer (modified LB broth also containing 3 mM PEG 3350, 30 mM $MgCl_2$ and 5% (v/v) DMSO) at a volume 10% (v/v) of the initial culture. Aliquots of TSS competent DH5a were snap frozen in liquid nitrogen and stored at -80°C until required.

2.6.3 Heat-shock transformation of chemically competent cells

Transformation of TSS DH5a or One Shot™ ccdB Survival™ 2 T1R Competent Cells (Invitrogen, USA) was performed according to Sambrook and Russell (2001) with a few modifications. An appropriate volume of reaction mixture or plasmid DNA was added to 50 µl of cells completely thawed on ice and allowed to equilibrate for 30 minutes. Heat shock was performed at 42°C for 30 seconds and

immediately cooled on ice for 2 minutes. Following incubation, 450 µl of S.O.C (2% (w/v) peptone, 0.5% (w/v) yeast extract, 10 mM NaCl, 2.5 mM KCl, 10 mM $MgCl_2$, 10 mM $MgSO_4$, 20 mM glucose) was added and cells were grown for 1 hour at 37°C with shaking at 200 RPM. 50-100 µl of the transformed culture was spread onto a selection plate containing appropriate antibiotic and incubated overnight at 37°C.

2.6.4 Gene synthesis

The full length GmNOD26 (Glyma.08G120100.1) coding sequence (cds) was synthesised into gateway-enabled pUC57 containing Kanamycin resistance (Synbio Technologies, USA). Phosphomimetic mutations were induced to the coding sequence through mutation of serine 262 to alanine (S262A) or aspartic acid (S262D) (Synbio Technologies, USA).

2.6.5 Production of attB products

For recombination of PCR products into pDONR™221, the products must contain attB sites for appropriate activity of BP clonase™ (Invitrogen, USA). For amplification of the 2kb 5' regulatory element (RE) of LjALMT1 (Lj3g1v0182300.1) or LjNOD26 (Lj4g3v2618520) gDNA (2.4.2) was used as the template, while for cds amplification cDNA (2.5.1) was used. Initially, the 2kb 5' RE or cds was amplified using region specific primers specified in Table 2.3. For addition of attB sites, the forward primer was designed to have four guanine (G) residues at the 5' end followed by the 25 bp attB1 site and ~25 bp of region-specific sequence. For coding region primer design two nucleotides, GC, were added to allow the coding region to remain in frame of a N-terminal reporter protein. The reverse primer was designed to contain four guanine residues at the 5' end followed by the 25 bp attB2 site and ~25 bp of region-specific sequence. Region-specific primers were designed using SnapGene (GSL Biotech LLC, USA) at 18-28 bp with an optimal Tm of 60^{o}C and GC content of 50%. NEB (USA) Q5® High-Fidelity DNA Polymerase was used during amplification to minimise miscellaneous mutations. Each reaction contained 1.0 X Q5® Reaction Buffer, 200 µM dNTP's, 0.5 µM forward and reverse primer, 0.5 units of Q5® High-Fidelity DNA Polymerase and 1 µl of template. Thermal cycling conditions consisted of initial denaturation at 98°C for 30 seconds; 35 cycles of denaturation at 98°C for 10 seconds, annealing at primers specific Tm for 30 seconds, extension at 72°C for 90 seconds; and final extension at 72°C for 5 minutes.

Table 2.3 Primers used in the generation of attB products. Primers were synthesised by Sigma-Aldrich, Australia. Key: Regulatory element (RE); Coding sequence (cds); Forward (F); Reverse (R).

Target amplification		5' primer sequence
LjALMT1 2kb RE	F	CTTTAATTTGATTGCTCTCTTTGTGGG
	R	CTGCTACCTATTGCTCCATAGC
LjALMT1 2kb RE attb	F	GGGGACAAGTTTGTACAAAAAAGCAGGCTGCCTTTAATTTGATTGCTCTCTTTGTGGG
	R	GGGGACCACTTTGTACAAGAAAGCTGGGTGCTGCTACCTATTGCTCCATAGC
LjALMT1 cds	F	ATGGCCTCACCAATTGCTGAC
	R	TCACTCGTTAACTGTGATAAC
LjALMT1 cds attb	F	GGGGACAAGTTTGTACAAAAAAGCAGGCTGCATGGCCTCACCAATTGCTGAC
	R	GGGGACCACTTTGTACAAGAAAGCTGGGTGTCACTCGTTAACTGTGATAAC
LjNOD26 2kb RE	F	CACTCACTAGCTAAAACAAGG
	R	TTCCAAATGCTTACCCAAGTGC
LjNOD26 2kb RE attb	F	GGGGACAAGTTTGTACAAAAAAGCAGGCTGCCACTCACTAGCTAAAACAAGG
	R	GGGGACCACTTTGTACAAGAAAGCTGGGTGTTCCAAATGCTTACCCAAGTGC
LjNOD26 cds	F	ATGGGTGAGAGTTCCGCAC
	R	TCATATTCCTTTGAGAAAAGAG
LjNOD26 cds attb	F	GGGGACAAGTTTGTACAAAAAAGCAGGCTGCATGGGTGAGAGTTCCGCAC
	R	GGGGACCACTTTGTACAAGAAAGCTGGGTGTCATATTCCTTTGAGAAAAGAG

2.6.6 Generating entry clones using Gateway™ BP Clonase™

AttB PCR products were recombined with attP- containing pDONR™221 using BP clonase™ (Invitrogen, USA). The quantity of attB PCR product required was calculated by the size of PCR product (bp) * 0.0165. This quantity was combined with 75 ng of pDONR™221 and 0.5 µL of BP clonase™ in a reaction volume of 4.5 µL containing TE buffer (pH 8.0). The reaction was incubated at 25°C overnight and terminated by the addition of 2 µg Proteinase K for 10 min at 37°C. The reaction was transformed into TSS DH5a (2.6.2) using the heat shock protocol (2.6.3) and single colonies containing the PCR product identified through colony PCR (2.2.7) were grown overnight in LB broth containing 50 µg/mL kanamycin. Plasmid DNA was isolated (2.2.3) and sequenced by AGRF (Australia) to confirm no unanticipated mutations had been induced through PCR amplification (Appendix 2). Alignment with the publicly available sequences revealed two Single Nucleotide Polymorphisms (SNPs) in the LjALMT1 RE, while no SNPs were found in the LjALMT1 cds, LjNOD26 RE, or LjNOD26 cds (Appendix 2). Due to the limited coverage of the LjALMT1 genomic sequence, these SNPs (A1138G and A1659C) were preserved in the 2-kb 5' RE of LjALMT1 and used to drive the expression of the GUS reporter and transiently expressed in *L. japonicus* via hairy root transformation (2.9.2/3).

2.6.7 Overlapping PCR for pENTR™/D-TOPO™ cloning

To fuse the 2kb RE with the cds of LjALMT1 and LjNOD26, overlapping PCR primers were developed that incorporated a CACC overhang for the pENTR™/D-TOPO™ cloning system (Invitrogen, USA). RETOPO-F and REcds-R primers were used to clone the 2kb RE and introduce CACC and coding region overhand using V48-promoter as a template (Table 2.4). REcds-F and cdsns-R primers were used to clone the cds while removing the stop codon and introducing 2kb regulatory element overhang (Table 2.4). These products were amplified using Phusion High-Fidelity DNA Polymerase (NEB, USA) and gel purified using the Wizard® SV Gel and PCR Clean-Up System (Promega, USA) (2.2.3). Both purified products were then used as template for a reaction containing RETOPO-F and cdsns-R primer combination and amplified using Phusion High-Fidelity DNA Polymerase (NEB, USA). The resulting LjALMT1-REcds, 3285 bp, and LjNOD26-REcds, 2815 bp, PCR products were gel purified using the Wizard® SV Gel and PCR Clean-Up System (Promega, USA) (2.2.3) and used as template for pENTR™/D-TOPO™ reaction. The reaction contained 30 ng PCR product, 20 ng of pENTR™ TOPO® vector and 20% (w/v) salt solution (1.2 M NaCl and 0.06 M $MgCl_2$) in a total reaction volume of 5.0 µL. Following overnight incubation, the reaction was transformed into TSS DH5a (2.6.2) using the heat shock protocol (2.6.3) and single colonies were grown overnight in LB broth containing 50 µg/mL kanamycin. Plasmid DNA was isolated (2.2.3), directionally of incorporation confirmed through restriction digest (2.2.4) and sequenced by AGRF (Australia) to confirm no unanticipated mutations had been induced through PCR amplification.

Table 2.4 Overlapping PCR primers used in the generation of TOPO cloning. Overhanging primer sequences have been underlined. Primers were synthesised by Sigma-Aldrich, Australia. Key: Regulatory element (RE); Coding sequence (cds); Forward (F); Reverse (R) Non-stop (ns).

	5' primer sequence
LjNOD26 RETOPO-F	CACCTTCCAAATGCTTACCC
LjNOD26 REcds-F	CTAGTGAGTGATGGGTGAGAGTTC
LjNOD26 REcds-R	GAACTCTCACCCATCACTCACTAG
LjNOD26 cdsns-R	TCCTATTCCTTTGAGAAAAGAGAC
LjALMT1 RETOPO-F	CACCCTGCTACCTATTGCTCCATAGC
LjALMT1 REcds-F	GCAATCAAATTAAAGATGGCCTCACC
LjALMT1 REcds-R	GGTGAGGCCATCTTTAATTTGATTGC
LjALMT1 cdsns-R	TCCCTCGTTAACTGTGATAACATGAG

2.6.8 Generating expression clones using Gateway™ LR Clonase™ II

In this thesis, the eight nodule-expressed soybean NPF's were provided by Penelope Smith (La Trobe University, Melbourne) in pDONR™221, GmNOD26 was synthesised into gateway-enabled pUC57 by Synbio Technologies (USA), while LjNOD26 and LjALMT1 sequences were cloned from gDNA or cDNA (2.6.5) into pDONR™221 (2.6.6) or pENTR™/D-TOPO™ (2.6.7). AttL containing entry vectors were recombined with attR-containing destination vectors using LR clonase™ II (Invitrogen, USA). Approximately 5 fmol of both entry and destination vector were combined with 0.5 µL of LR clonase™ II in a reaction volume of 2.5 µL containing TE buffer (pH 8.0). For large destination vectors >10kb, the plasmid was first linearised between the attR sites using BbvCI (NEB, USA) and purified through ammonium acetate precipitation (2.2.5). The reaction was incubated at 25^{o}C overnight and terminated by the addition of 1 µg Proteinase K for 10 min at 37^{o}C. The reaction was transformed into TSS DH5a (2.6.2) using the heat shock protocol (2.6.3) and single colonies were grown overnight in LB broth containing appropriate antibiotic (Table 2.2). Plasmid DNA was isolated (2.2.3) and confirmed through restriction digest (2.2.4).

2.6.9 Site-directed mutagenesis

Primers designed to generate E43N, D177N, R179N, V197H and A206C GmNOD26 mutants can be found in Table 2.5. The molecular weight of each primer was used to calculate the required 125 ng used in each 50 µL reaction. Site-directed mutagenesis was performed using Phusion High-Fidelity DNA Polymerase (NEB, USA) with ~75 ng of plasmid DNA template under thermocycling conditions of 98 °C for 30 s; 18 cycles of 98 °C for 30 s, 55 °C for 60 s, 72 °C for 7 mins; final extension 72 °C for 10 min and followed by Dpn1 digestion. Following transformation into TSS DH5a (2.6.2) using the heat shock protocol (2.6.3) single colonies were grown overnight in LB broth containing appropriate antibiotic. Plasmid DNA was isolated (2.2.3) and sequenced by AGRF (Australia) to confirm mutations had been correctly integrated.

Table 2.5 Primers used in the generation of site-directed mutants. Primers were synthesised by Sigma-Aldrich, Australia.

	5’ primer sequence
GmNOD26$_{D192N}$-F	GGTTGCCACCAATAACAGAGCGGTTGGTGAGTTCG
GmNOD26$_{D192N}$-R	CGAACTCACCAACCGCTCTGTTATTGGTGGCAACC
GmNOD26$_{R194N}$-F	GGTTGCCACCGATAACAATGCGGTTGGTGAGTTCG
GmNOD26$_{R194N}$-R	CGAACTCACCAACCGCATTGTTATCGGTGGCAACC
GmNOD26$_{E43N}$-F	CTTGCAGAAGTTGGTAGCTAACGCGGTGGGAACATATTTCC
GmNOD26$_{E43N}$-R	GGAAATATGTTCCCACCGCGTTAGCTACCAACTTCTGCAAG
GmNOD26$_{V197H}$-F	GGTCGACATTACTGCTGAATCACATTATTGGAGGGCCAGTG
GmNOD26$_{V197H}$-R	CACTGGCCCTCCAATAATGTGATTCAGCAGTAATGTCGACC
GmNOD26$_{A206C}$-F	GAGGGCCAGTGACAGGATGTTCAATGAACCCAGCTAGAAGC
GmNOD26$_{A206C}$-R	GCTTCTAGCTGGGTTCATTGAACATCCTGTCACTGGCCCTC

2.7 Expression in *X. laevis* oocytes

2.7.1 Preparation of *X. laevis* oocytes

Unfertilized *X. laevis* oocytes were harvested according to Byrt et al. (2017) under ethics approval S-2019-024. Oocytes were injected with 46 nL of either nuclease-free water or cRNA using a micro-injector (Nanoinject II, automatic nanolitre injector, Drummond Scientific) and incubated in Ringer's solution (96 mM NaCl, 2 mM KCl, 5 mM $MgCl_2$, 0.6 mM $CaCl_2$, 5 mM HEPES, 5% (v/v) horse serum and antibiotics (0.05 mg/mL tetracycline, 100 units/mL penicillin, 0.1 mg/mL streptomycin) pH 7.6 at 18^{o}C. The quantity of cRNA injected varied dependent on the gene, for: LjALMT1 16 ng; GmNOD26 23 ng; GmNPFs 46 ng. Ringer's solution was replaced daily and for experiments involving sodium testing solutions the oocytes were stored in low sodium Ringer's solution (62 mM NaCl, 36 mM KCl, 5 mM $MgCl_2$, 0.6 mM $CaCl_2$, 5 mM HEPES, 5% (v/v) horse serum and antibiotics (0.05 mg/mL tetracycline, 100 units/mL penicillin, 0.1 mg/mL streptomycin) one day prior to experiments.

2.7.2 cRNA synthesis

For heterologous expression in *X. laevis* oocytes, pGEMHE-DEST or pGEMHE-DEST-cYFP plasmids, containing 5' and 3' *X. laevis* β-globin untranslated regions (Shelden et al. 2009), were linearized (2.2.4) downstream of the 3' *X. laevis* β-globin untranslated regions using appropriate restriction enzyme (Appendix 1). The linearised vector was cleared of any of contaminating proteins and RNA through ammonium acetate precipitation (2.2.5) prior to cRNA synthesis using the mMESSAGE mMACHINE® T7 Transcription kit (Thermo Fisher Scientific, Australia). Following cRNA synthesis for 2 hours at 37^{o}C and plasmid degradation using TURBO DNase (Thermo Fisher Scientific, Australia), cRNA was purified by phenol/chloroform extraction and isopropanol precipitation. Briefly, 115 µL nuclease-free water and 15 µL ammonium acetate stop solution was combined with each 20 µL cRNA reaction and extracted with an equal volume of phenol/chloroform by centrifugation (Eppendorf 5425 centrifuge, Australia) at max speed. The aqueous phase was then combined with an equal volume of chloroform and extracted once again by centrifugation at max speed. The cRNA was precipitated by the addition of 1 volume of isopropanol, chilled overnight at –20°C prior to centrifugation at max speed for 15 minutes at 4°C. The pellet was air dried and resuspended in 10 µL nuclease-free water, quantified using a NanoDrop 1000 spectrophotometer (Thermo Fisher Scientific, USA), integrity checked via agarose gel electrophoresis (2.2.1) and stored at -80°C until required.

2.7.3 Oocyte water permeability

Oocytes incubated for 1 hour in an iso-osmotic solution of 50 mM NaCl, 2 mM KCl, 2 mM $MgSO_4$, 1.8 mM $CaSO_4$, 5 mM HEPES, pH 7.5 with TRIS base and osmolality adjusted to 220 mosmol kg−1 with D-mannitol. Oocytes were transferred to a hypo-osmotic version of this solution (1 in 5 dilution, 44 mosmol kg−1), viewed with a Nikon SMZ800 light microscope (Nikon, Japan) and changes in volume captured every second for 60 seconds following Byrt et al. (2017). Image J software (National Institute of Health, USA) was used to calculate the relative change in volume of the oocytes. Osmotic permeability (P_{os}) was calculated from the increase in volume from 2 to 60 seconds using the equation specified by Byrt et al. (2017).

2.7.4 Voltage-clamp electrophysiology

For Two-Electrode Voltage Clamp (TEVC) recordings, Borosilicate glass pipettes (Harvard Apparatus: GC150F-10, USA) filled with 3 M KCl (0.3-1 MΩ resistance) were used to pierce the oocyte membrane as current and voltage electrodes. The testing solution was continuously perfused during experimentation and a bath clamp system minimized the effect of series resistance. The voltage clamp protocol consisted of a -40 mV holding potential, with the membrane potential decreased from 40 to -120 mV in increments of 20 mV for 0.5 or 1.5 s, followed by -40 mV for 0.5 s. TEVC was performed using the CLAMPEX 9.0 software (Molecular Devices, USA) and recordings analysed using Clampfit 10.2 (Molecular Devices, USA). Conductance was calculated using the slope of the linear portion of the current-voltage curve, from -60 to +20 mV.

2.7.4.1 Cationic testing solutions

Cationic solutions contained 10-, 50- or 100-mM monovalent cations applied as a chloride salt in a base testing solutions of 2 mM KCl, 5 mM HEPES, pH 7.5 with TRIS base and osmolality adjusted to 220 mosmol kg−1 with D-mannitol. The base solution either contained a standard (1 mM $MgSO_4$ and 1.8 mM $CaSO_4$) or low (50 µM $CaSO_4$) concentration of divalent cations.

2.7.4.2 Anionic testing solutions

Anionic solutions contained either: a basal solution of 0.5 mM $CaCl_2$, buffered to pH 5.5 or 7.5 with Bis-tris propane (BTP) and containing 10 mM malic, succinic, α-ketoglutaric, sulphuric, nitric, or hydrochloric acid; or ND88 containing 88 mM NaCl, 1 mM KCl, 2.4 mM $NaHCO_3$, 6.2 mM $Ca(NO_3)_2$, 8.5 mM $CaCl_2$, 0.82 mM $MgCl_2$ and buffered to pH 4.5 with HCl. For all solutions osmolality was adjusted to 220 mosmol kg^{-1} with D-mannitol. In some circumstances the testing solution contain 100 µM aluminium chloride, 100 µM GABA or 5 mM phthalonic acid.

2.7.5 Radiotracer experiments

Experiments were adapted from Gruber et al. (2010). For uptake experiments control, GmNPF1.2 and LjALMT1-expressing oocytes were incubated in basal testing solution (pH 5.5) containing 0.5% (v/v) L-1,4 (2,3) [^{14}C] malic acid (Amersham, USA) at a final malate concentration of 2 mM. Oocytes were then bathed in 100 µL of uptake buffer ± 5 mM phthalonic acid for 15 minutes and washed twice in a solution of equivalent malate concentration without the radiotracer. Following washing, oocytes were digested with 0.1 N HNO_3 and placed in scintillation vials containing Ultima Gold liquid scintillation cocktail (PerkinElmer, USA) for counting in a Tri-Carb 2100 TR Liquid Scintillation Analyser (Packard, USA). For efflux experiments control, GmNPF1.2 and LjALMT1-expressing oocytes were injected with 46 nL of L-1,4 (2,3) [^{14}C] malic acid (Amersham, USA) and placed in 500 µL basal testing solution (pH 5.5). After two and five minutes the efflux buffer was sampled and placed in scintillation vials. Following the efflux experiment the oocytes were digested with 0.1 N HNO_3 and placed in scintillation vials containing Ultima Gold liquid scintillation cocktail (PerkinElmer, USA), all samples were then counted using a Tri-Carb 2100 TR Liquid Scintillation Analyser (Packard, USA).

2.7.6 Confocal microscopy

Oocytes expressing GmNOD26-cYFP fusion were mounted in 100 µl sodium testing solution containing a standard divalent cation concentration and imaged using Nikon A1R Laser Scanning Confocal Microscope (Nikon Instruments, USA). YFP was excited using a 514 nm argon laser and emission recorded from 528 to 603 nm, to minimise variation in signal between samples the gain was kept constant at 28. For contrast the transmitted light channel was also used. Following image capture oocytes were transferred to 30 µl homogenisation buffer for western blot analysis (2.7.8). All images were processed using NIS Elements software (Nikon Instruments, USA).

2.7.7 Oocyte homogenisation

X. laevis oocyte lysates were prepared by homogenising a single oocyte in 30 µL of oocyte homogenization buffer (20 mM Tris-HCl pH 7.4, 5 mM $MgCl_2$, 5 mM NaH_2PO_4, 80 mM sucrose, 1 mM EDTA, 1 mM dithiothreitol, 1 X Protease Inhibitor Cocktail) in a 1.5 ml tube with a Teflon pestle. The samples were centrifuged (Eppendorf 5425 centrifuge, Australia) at 250 g for 10 minutes to remove yolk protein, and the lysate was stored at -80^{o}C.

2.7.8 Protein techniques

2.7.8.1 Estimation of protein concentration

The initial protein concentration of the homogenised oocyte lysate (2.7.7) was estimated using Pierce BCA protein assay kit (Thermo Fisher Scientific). Homogenised oocyte lysate was diluted 10-fold and 10 µL assayed in 200 µL of working reagent containing 20 parts BCA Reagent A and 1 part BCA Reagent B. The absorbance was measured at 562 nm using a CLARIOstar Plate Reader (BMG LABTECH, Australia) and compared to BSA standards.

2.7.8.2 SDS-PAGE

An equal volume of homogenised oocyte lysate (2.7.7) and denaturing sample buffer (125 mM Tris-HCl pH 6.8, 2% (w/v) SDS, 40% (w/v) Glycerol, 0.006% (w/v) Bromophenol Blue, 6 M Urea) were combined and loaded onto a 12.5% (v/v) polyacrylamide resolving and 4% (v/v) stacking SDS-PAGE gel. The gel was run in SDS-PAGE running buffer (192 mM Glycine, 25 mM Trizma-Base, 0.01% (v/v) SDS) for 60 minutes at 170 V using the PowerPac™ Basic Power Supply and Mini-PROTEAN Tetra Vertical Electrophoresis Cell (BioRad). Each gel contained a Precision Plus Protein™ Kaleidoscope™ Prestained Protein Standards (BioRad, USA) and 2 µg of SM.

2.7.8.3 Immunoblotting

Protein was transferred to Amersham™ nitrocellulose membrane (Cytiva, USA) in a typical western blot transfer stack submerged in transfer buffer (152 mM Glycine, 25 mM Trizma-base) using the Mini Trans-Blot® Cell (BioRad, USA) at 60 V at 4°C for 2 hours. Nitrocellulose membranes were then blocked overnight at 4°C on a gyrating platform in blocking buffer (5% (w/v) skim milk powder, 20 mM Trizma-base pH 7.4, 0.1% (v/v) Tween-20, 150 mM NaCl). Following blocking, the membranes were incubated in blocking buffer containing the primary GmNOD26 antibody, kindly provided by Daniel Roberts, at a concentration of 1:7,500 (see 2.7.8.4) for one hour at room temperature prior to three sequential washing steps in blocking buffer for a minimum of 10 minutes. The secondary antibody (anti rabbit-goat) was then applied in blocking buffer (1:10,000) for one hour at room temperature before three sequential washing steps in TBST (25 mM Trizma-base, 0.1% (v/v) Tween-20, 150 mM NaCl) for a minimum of 10 minutes. Protein was then visualised using the Clarity Western ECL Substrate (Bio-Rad, USA) and imaged using the ChemiDoc XRS+ imaging system (Bio-Rad, USA).

2.7.8.4 GmNOD26 antibody optimisation

The GmNOD26 antibody was kindly provided by Dan Roberts (University of Tennessee, USA) and the concentration was first optimised through dot blot. Briefly 10 µg SM was pipetted onto nitrocellulose membrane and incubated in blocking buffer overnight at 4°C. Following blocking, the membranes were incubated in blocking buffer containing various dilutions of GmNOD26 antibody for one hour at room temperature prior to secondary antibody application and visualisation as specified in 2.7.8.3. A dilution of 1:7,500 was sufficient for appropriate quantification of GmNOD26 (Figure 2.1).

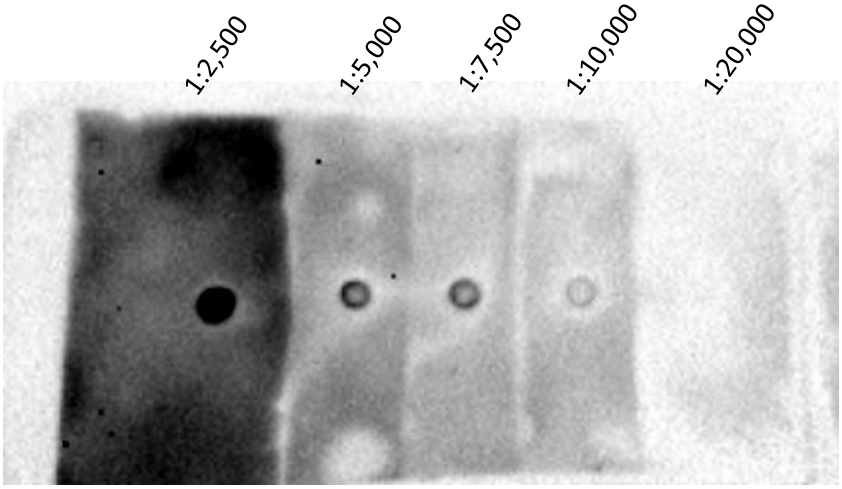

Figure 2.1 GmNOD26 antibody dilutions. Various dilutions of GmNOD26 antibody were incubated with 10 µg SM blotted on nitrocellulose membrane as specified 2.7.8.4.

2.8 Expression in *S. cerevisiae*

2.8.1 *S. cerevisiae* strains

Ammonium transport deficient 26972c (mep1-1, mep2Δ, Mep3, ura-) or 31019b (Δmep1-3, ura-) *S. cerevisiae* strains were kindly provided by Apriadi Situmorang (Adelaide University, Australia). The amino acid transport deficient 22Δ10AA (MATα gap1-1 put4-1 uga4-1 can1::HisG lyp1- alp1::HisG hip1::HisG dip5::HisG gnp1Δ agp1Δ ura-) and parental 23344c (MATα ura-) *S. cerevisiae* strains were kindly provided by Guillaume Pilot (Virginia Tech, USA). All strains were maintained in YPD media containing 2% (w/v) D-glucose, 2% (w/v) peptone and 1% (w/v) yeast extract.

2.8.2 *S. cerevisiae* transformation

S. cerevisiae strains were transformed by lithium acetate (LiAc) method (Gietz and Woods 2002) with pYES-DEST52 plasmids for auxotrophic complementation of ura3. Overnight culture of *S. cerevisiae* grown in YPD media was used to inoculate 50 mL YPD at a dilution of 1:50. This culture was growth shaking at 200 RPM at 28°C until at OD600 of ~0.5. Cells were harvested using a Sigma 3-16PK centrifuge (Sigma-Aldrich, USA) at 3000 g for 5 minutes and resuspended 1.0 ml of 100 mM LiAc. Cells were transferred to a 1.5 ml tube, centrifuged at 8000 rpm using an Eppendorf 5425 centrifuge (Australia) for 15 seconds and resuspended in 100 mM LiAc at a volume 1.0% (v/v) of the initial culture. Transformation mix was assembled containing 50 µL culture, 240 µL PEG 3750 (50% w/v), 36 µL 1.0 M LiAc, 25 µL salmon sperm DNA (2mg/ml) and 1 µg plasmid DNA in a final reaction volume of 400 µL. The transformation mix was incubated at 30°C for 30 minutes, heat shocked at 42°C for 25 minutes and pelted at 8000 rpm. Cells were resuspended in sterile MilliQ water and grown overnight on 1.7% (w/v) Yeast Nitrogen Base (YNB) without ammonium sulphate containing 2% (w/v) D-glucose and 0.192% (w/v) Yeast Synthetic Drop-out Medium Supplements without Uracil at 28°C.

2.8.3 Growth of ammonium transport deficient *S. cerevisiae*

Yeast starter cultures were grown overnight at 28°C with shaking at 180 RPM in Medium M (Ramos and Wiame 1979) containing 0.1% (w/v) proline and 2% (w/v) D-glucose. Cells were pelleted at 3000g using a Sigma 3-16PK centrifuge (Sigma-Aldrich, USA) washed twice with sterile MilliQ water and diluted to an OD600 of 1.0 in Medium M without primary carbon or nitrogen sources. For growth on solid medium, cultures were serially diluted 10-fold with 5 µL spotted onto solid Medium M containing 2% (w/v) agar and grown at 28°C for 5 days. Liquid cultures were grown from an initial OD600 of 0.1 in 200 µL aliquots at 180 RPM for 48 to 72 hours with OD600 recorded every 15 minutes using a CLARIOstar Plate Reader (BMG LABTECH, Australia). Testing media contained 2%

(w/v) D-glucose or 2% (w/v) D-(+)-galactose with either: 0.1% (w/v) proline, 0.1% (w/v) proline and methylamine hydrochloride; or ammonium sulphate.

2.8.4 Growth of amino acid transport deficient *S. cerevisiae*

Overnight cultures were grown at 28°C with shaking (180 RPM) in YNB media containing 5 mM ammonium and 2% (w/v) D-glucose. Cells were pelleted at 3000g using a Sigma 3-16PK centrifuge (Sigma-Aldrich, USA) washed twice with sterile MilliQ water and diluted to an OD600 of 1.0 in YNB without primary carbon or nitrogen sources. Cultures were serially diluted 10-fold with 5 µL grown at 28°C for 5 days on solid YNB without ammonium sulphate and containing either 2% (w/v) D-glucose or 2% (w/v) D-(+)-galactose with 3 mM ammonium or amino acid as the sole nitrogen source.

2.9 Characterisation of transgenic *L. japonicus*

2.9.1 Preparation of electrocompetent *A. rhizogenes*

An overnight culture *A. rhizogenes* (A10) was used to inoculate 250 ml LB liquid medium (1:50 dilution) and incubated at 28°C shaking at 200 RPM until OD600 reached 0.5. Cells were incubated on ice for 30 minutes and harvested using a Sigma 3-16PK centrifuge (Sigma-Aldrich, USA) at 3000 g for 10 minutes at 4°C. The supernatant was discarded, and cells were resuspended in 50 ml of sterile ice-cold MilliQ water. The cells were harvest again and resuspended in 25 ml of sterile ice-cold MilliQ water. Harvesting was again repeated but instead the cells were washed with 10 ml of sterile ice-cold 10% (v/v) glycerol before a final harvest and resuspension in 1.0 ml sterile ice-cold 10% (v/v) glycerol. Aliquots of 50 µL were snap frozen in liquid nitrogen and stored at -80 °C until transformation. Electroporation was performed using 1.0 µg of plasmid DNA and 50 µL of competent cells according to Nagel et al. (1990); a 2 second 2.5 Kv charge dissipation with the capacitor at 25 µF and the resistor at 200 ohms (Gene Pulser® II, Pulse controller plus and Capacitance extender plus BioRad, USA). Following electroporation, the cells were combined with 250 µl LB broth and incubated at 28°C for 1 hour with shaking at 200 RPM shaking. Transformants were selected for on LB agar containing 150 µg/ml spectinomycin and 30 µg/ml rifampicin.

2.9.2 Hairy root transformation

Hairy roots were induced following a modified method from Díaz et al. (2005) and Okamoto et al. (2013). *L. japonicus* seeds were scratched with sandpaper, sterilised in 4% (v/v) bleach, imbibed in sterile MilliQ water, and plated on 0.9% (w/v) agar. After seven days seedlings were sectioned through the middle of the hypocotyl, infected with *A. rhizogenes* containing appropriate vector and placed on co-cultivation media for 24 hours of dark incubation in a growth cabinet at 23°C. Plants were exposed to light (16 hours light/ 8 hours dark) for five days and transferred to root elongation media for 14 days of hairy root induction. Transgenic roots were screened for DsRED expression using ChemiDoc XRS+ imaging system (Bio-Rad, USA) using the 605/50 filter with Green Epi illumination (Appendix 3). Selected plants were transferred to 50% (v/v) vermiculite-perlite and grown as specified in 2.2.3.

2.9.3 GUS staining

Transgenic roots were excised 21 DAI plants and fixed in ice-cold fixative solution containing 3.8% (v/v) formaldehyde. Roots were washed in several changes of ice-cold 0.1 M phosphate buffer (pH 7.4), submerged in X-Gluc substrate solution, containing: 1 µg X-Gluc; 2 mM potassium ferricyanide; 2 mM potassium ferrocyanide; and 0.1% (v/v) Triton-X, and vacuum infiltrated for 30 minutes (Vitha 2007). After one-hour dark incubation distinct blue stain appeared and tissue was fixed in modified tellesnitskill fixative for two hours containing: 70% (v/v) isopropanol; 2% (v/v) formaldehyde; and 5% (v/v) glacial acetic acid. Tissue was stored in 70% (v/v) ethanol and placed in histology cassettes prior to paraffin embedding using the Leica 'HistoPearl' Automated Paraffin Embedding System. Embedded samples were sectioned 10 µm, placed on a microscope slide and cleared using xylene prior to imaging using an Olympus BX53 upright microscope (Oympus LS, Japan).

2.9.4 Fluorescent microscopy

Transgenic nodules were washed in 0.1 M phosphate buffer (pH 7.4), hand sectioned and placed into an ice-cold solution of FM4-64 (30 µg/mL) in 0.1 M phosphate buffer containing 25 mg/mL sucrose (pH 7.4). Following FM4-64 for 60 minutes, sections were mounted on a microscope slide in in 0.1 M sodium phosphate buffer containing 25 mg/mL sucrose (pH 7.4) and imaged using ZEISS LSM 880 Confocal Laser Scanning Microscope (Carl Zeiss, Germany). GFP was excited using a 488 nm argon laser and emission recorded 530 nm. FM4-64 was excited using a 510 nm diode pumped solid state laser and emission recorded at 750 nm. Images were processed using ZEN (black edition) (Carl Zeiss, Germany). Alternatively, the EVOS® FL Auto Imaging System (Thermo Fisher Scientific, USA) was used in the validation of the ChemiDoc XRS+ imaging system (Bio-Rad, USA) for screening successful hairy root transformants (Appendix 3) or to excite GFP (482/25 nm Excitation; 524/24 nm Emission).

2.10 Bioinformatic and statistical analysis

2.10.1 Genome-wide identification of ALMT and tDT-like proteins

Arabidopsis ALMT or tDT protein sequences were obtained from Dreyer et al. (2012) or Emmerlich et al. (2003). These sequences were used as BLAST queries to identify *M. truncatula* proteins using NCBI (https://blast.ncbi.nlm.nih.gov/), and *L. japonicus* proteins using Lotus Base (Mun et al. 2016). ALMT protein sequences were filtered for the presence of Hidden Markov models (Dreyer et al. 2012) using HMMER (http://hmmer.org/). Nomenclature was assigned according to *Arabidopsis* percentage identity which was calculated GenomeNet (https://www.genome.jp/).

2.10.2 Analysis of publicly available transcriptomics data

To determine the tissue specific expression profile of the identified ALMT and tDT transcripts in *L. japonicus* and *M. truncatula,* RNA-seq data was extracted from Lotus Base (Mun et al. 2016) and Genevestigator (Hruz et al. 2008), respectively. *In silico*, ALMT and tDT expression was analysed in five different tissues (nodule, root, stem, leaf and inflorescence) under symbiotic growth conditions and normalised against the total expression of the transcript. The transcript expression across the *M. truncatula* nodule was also analysed through Symbimics (Roux et al. 2014).

2.10.3 Statistical analysis

Statistical analysis was conducted using SPSS V.25 (IBM Corp. 2017). T-Tests and Duncan's Post Hocs were employed to assess differences between control and treated parameters. Figures were created using MATLAB (2022a) or Microsoft excel.

3 GmNOD26 is a non-selective monovalent cation channel

3.1 Introduction

3.1.1 Nitrogen-fixation in symbiosomes

The primary metabolic exchange across the SM is the provision of reduced carbon to the bacteroids and the efflux of fixed nitrogen to the plant (see Udvardi and Poole (2013); Clarke et al. (2014) for reviews). Knowledge of the transporters involved in this exchange, and their regulation, is critical for our understanding of symbiotic nitrogen fixation. Carbon from the plant is provided primarily as malate and a SM-specific malate transporter has been described in symbiosomes from soybean (Udvardi et al. 1988). N_2 is converted to ammonia within the bacteroid and is made available to the plant because the ammonia assimilating enzymes of the rhizobia are down regulated in the symbiotic state (Dilworth and Glenn 1984). Fixed nitrogen may be exported to the plant cytosol as ammonia, ammonium or, under certain conditions, amino acids, principally alanine (Allaway et al. 2000; Day et al. 2001b).

3.1.2 Nitrogen transport across the SM

NH_3 formed in the bacteroid diffuses into the acidic symbiosome space where it is largely protonated to NH_4^+, requiring a channel on the SM for export to the plant cytosol. Patch clamping of soybean SM identified a NSCC of SubpicoSiemen conductance that has a preference for NH_4^+ (Tyerman et al. 1995), but the molecular nature of the channel has not been identified. The described channel was gated by divalent cations and rectified by cytosolic Mg^{2+} (Tyerman et al. 1995; Whitehead et al. 1998; Tyerman 2002; Obermeyer and Tyerman 2005) and was present at high density in the SM patches. However, despite extensive transcriptomic and proteomic studies of nodule tissue and isolated SM from various legumes, including soybean, no candidates have been assigned as NSCCs (Saalbach et al. 2002; Wienkoop and Saalbach 2003; Takanashi et al. 2012; Roux et al. 2014; Clarke et al. 2015; Luo et al. 2023). In the plant cytosol, fixed nitrogen is rapidly assimilated to glutamate via GS, thus maintaining a favourable concentration gradient for NH_4^+ efflux from symbiosomes (Dilworth and Glenn 1984; Day et al. 2001a; Day et al. 2001b).

3.1.3 GmNOD26 is a multifunctional plant aquaporin

The aquaporin NOD26 is a major component of the soybean SM (Fortin et al. 1987), accounting for ~10% of the total protein mass (Rivers et al. 1997). It is a member of the NOD26-like intrinsic proteins subfamily that is permeable to water, formamide, glycerol and ammonia (Rivers et al. 1997;

Dean et al. 1999; Hwang et al. 2010). It is also possible that alanine is transported from symbiosomes through GmNOD26, as mercury has been reported to inhibit alanine movement across vesicles derived from the SM (Day et al. 2001b). When reconstituted into lipid bilayers, GmNOD26 displayed characteristics of an ion channel with an apparent preference for anions (Weaver et al. 1994; Lee et al. 1995). The functional relevance of this ion channel activity remains unclear, although under more physiological conditions its phenotype is likely to be different, particularly *in vivo* where GS is bound to the plant cytosolic side of GmNOD26 (Masalkar et al. 2010) and contains a high affinity binding site for NH_4^+ (Liaw et al. 1995).

3.1.4 Plant aquaporins can function as NSCC

A number of publications have described NSCC activity of aquaporins, with HsAQP1 found to be a cyclic GMP-gated NSCC permeable to a range of monovalent cations when expressed in *X. laevis* oocytes (Yool et al. 1996; Anthony et al. 2000). Similar observations were found for the *Drosophila* Big Brain aquaporin (Yanochko and Yool 2002; Yanochko and Yool 2004), which was also found to be gated by divalent cations, but it was not until more recently that NSCC activity of plant aquaporins was reported (Byrt et al. 2017). In *Arabidopsis*, AtPIP2;1 is a divalent cation, pH gated NSCC that when phosphorylated at the C-terminus increases cation conductance and decreases water permeability (Byrt et al. 2017; Qiu et al. 2020). Divalent cation gating of barley HvPIP2;8 has also been reported (Tran et al. 2020).

In view of these reports, we speculated that the aquaporin GmNOD26 may be responsible for the NSCC activity characterised in patches of soybean SM. Here, NSCC activity of GmNOD26 is characterised in *X. laevis* oocytes.

3.2 Results

3.2.1 GmNOD26 displays characteristics of a monovalent cation channel gated by divalent cations

To determine if GmNOD26 displayed ion conductivity, TEVC was performed on GmNOD26-expressing *X. laevis* oocytes. Control (water injected) and GmNOD26-expressing oocytes were initially bathed in ND50 solution containing a low concentration of divalent cations (50 µM Ca^{2+}), based on the patch-clamp experiments of the SM showing NSCC activity gated by divalent cations (Tyerman et al. 1995; Whitehead et al. 1998), and similar results with other plant aquaporins (Byrt et al. 2017). Oocytes expressing GmNOD26 showed time dependent, Na^{+} induced inward currents that were not observed in control oocytes (Figure 3.1a-b). However, in the presence of high concentrations of divalent cations, GmNOD26-oocyte ionic currents were not significantly different from water injected control oocytes (Figure 3.1c: GmNOD26 I_M at -120 mV = -547 ± 124, Control I_M at -120 mV = -515 ± 100; p = 0.857). When divalent cation concentrations were lowered, currents were significantly larger in GmNOD26-expressing oocytes (mean conductance of 29.6 µS) compared to control oocytes (14.3 µS), and this difference became more pronounced as the membrane was hyperpolarised (Figure 3.1d: GmNOD26 I_M at -120 mV = -1789 ± 409; Control I_M at -120 mV = -783 ± 98; p = 0.014). GmNOD26-expressing oocytes could not be clamped at membrane potentials more negative than -140 mV, as the membrane integrity would be lost due to large inward rectification of the channel (DNS). The reversal potential shifted more positive in GmNOD26-expressing oocytes relative to the control (-28 and -38, respectively), indicating an increased net flow of ions as GmNOD26-expressing oocytes inwardly rectified. The divalent cation gating of monovalent cation currents in GmNOD26-expressing oocytes was dose dependent (Figure 3.1e/f), with conductance of 51.4 µS in divalent cation free testing solution sequentially decreasing to 32.4, 16.3, 8.9, 8.2 and 7.9 µS at magnesium concentrations of 10, 100, 500, 1000 and 2000 µM, respectively. The conductance of control oocyte was substantially less, 20.3, 18.8, 8.5, 5.2, 4.9 and 5.3 µS in 0, 10, 100, 500, 1000 and 2000 µM free magnesium.

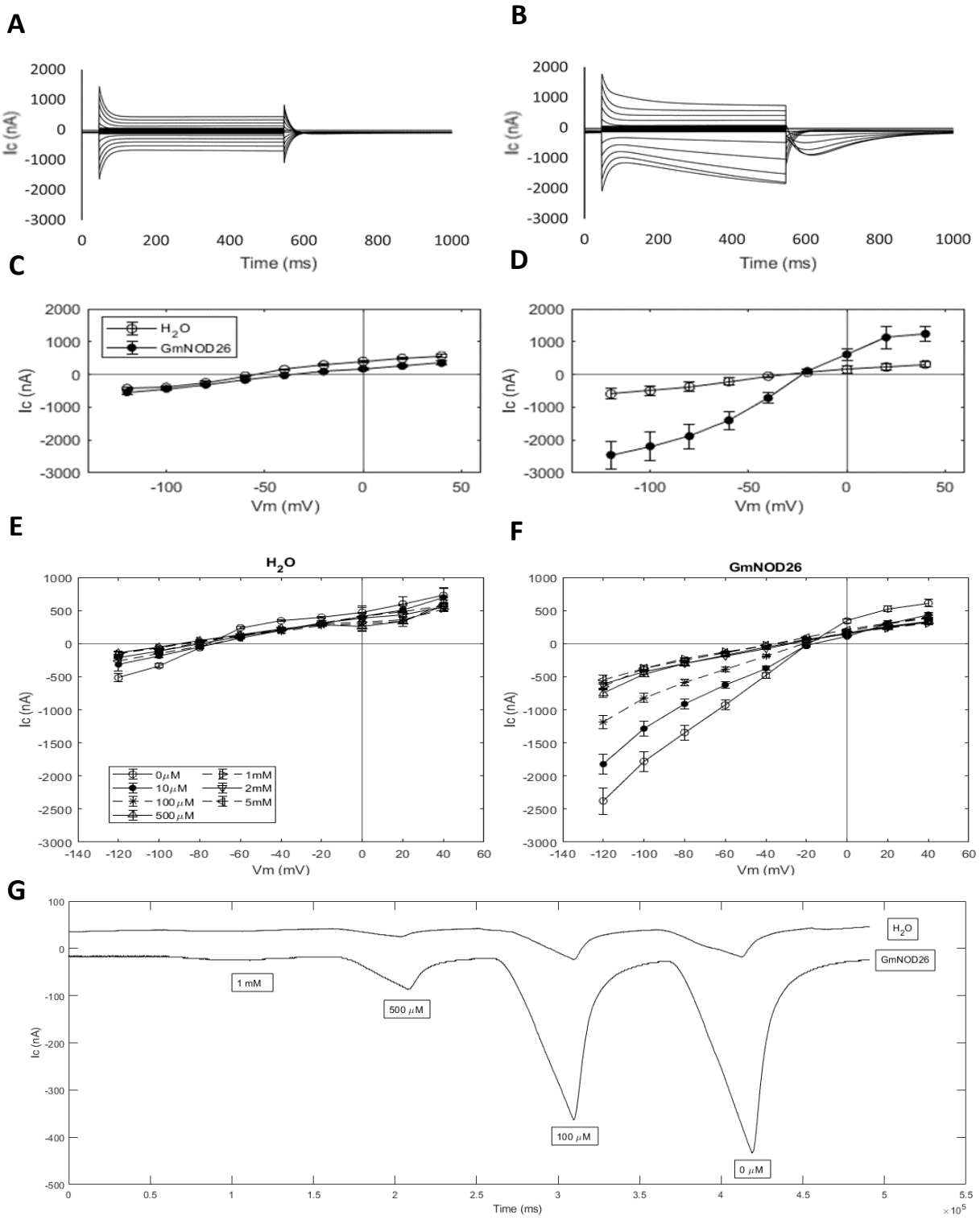

Figure 3.1 NaCl-induced ion currents in GmNOD26-expressing oocytes are gated by magnesium. Current-time traces for control (A) and GmNOD26-expressing oocytes (B), bathed in 50 mM NaCl containing low concentrations of divalent cations (50 µM Ca^{2+}); (C) current-voltage curves of control and GmNOD26-expressing oocytes bathed in 50 mM NaCl solution containing standard concentrations of divalent cations (1 mM Mg^{2+} and 1.8 mM Ca^{2+}); (D) current-voltage curves of control and GmNOD26-expressing oocytes in ND50 solution containing low concentrations of divalent cations (50 µM Ca^{2+}). Magnesium dose response in (E) control oocytes, and (F) GmNOD26 expressing oocytes, or (F) a representative trace of gap-free current recordings at -60 mV. Testing solution contained 50 mM NaCl with osmolarity adjusted to 220 mosmol kg^{-1} with d-mannitol, buffered with HEPES and pH to 7.5 with TRIS base (n=12 for c/d, n=6 for e/f^{-}).

GmNOD26-expresseing oocytes displayed large ion conductivity when bathed in 10 mM NH_4^+ (37.6 µS compared to 7.0 µS in control oocytes) which was inhibited by high divalent cations (14.7 µS for GmNOD26, 8.4 µS for control) (Figure 3.2a/b). GmNOD26 expressing oocytes were permeable to a range of monovalent cations, but the ungated (external divalent cation concentration of 50 µM) inward currents displayed a preference for NH_4^+ and its analogue methylammonium (MeA^+), when applied as 10 mM chloride salts. The relative permeabilities were NH_4^+>MeA^+=K^+>Na^+=choline at -120 mV (Figure 3.2c: GmNOD26 minus control I_C at -120 mV: NH_4^+ = -706; MeA^+ = -425; K^+ = 418; Na^+ = -177; choline = -26). For all investigated monovalent cations, I_C was partially blocked by divalent cations (Figure 3.2). When the large monovalent cation Choline was applied as a chloride salt, no significant change in I_C occurred, suggesting that the currents were not carried by the monovalent anion (Cl^-). Indeed, GmNOD26 expressed in oocytes was not permeable to any anion tested (Cl^-, NO_3^-, SO_4^- or malate), nor were any significant currents elicited in basal testing solution (Figure c: GmNOD26 - control I_C at -120 mV: malate 46; basal -61, DNS for Cl^-, NO_3^-, SO_4^-).

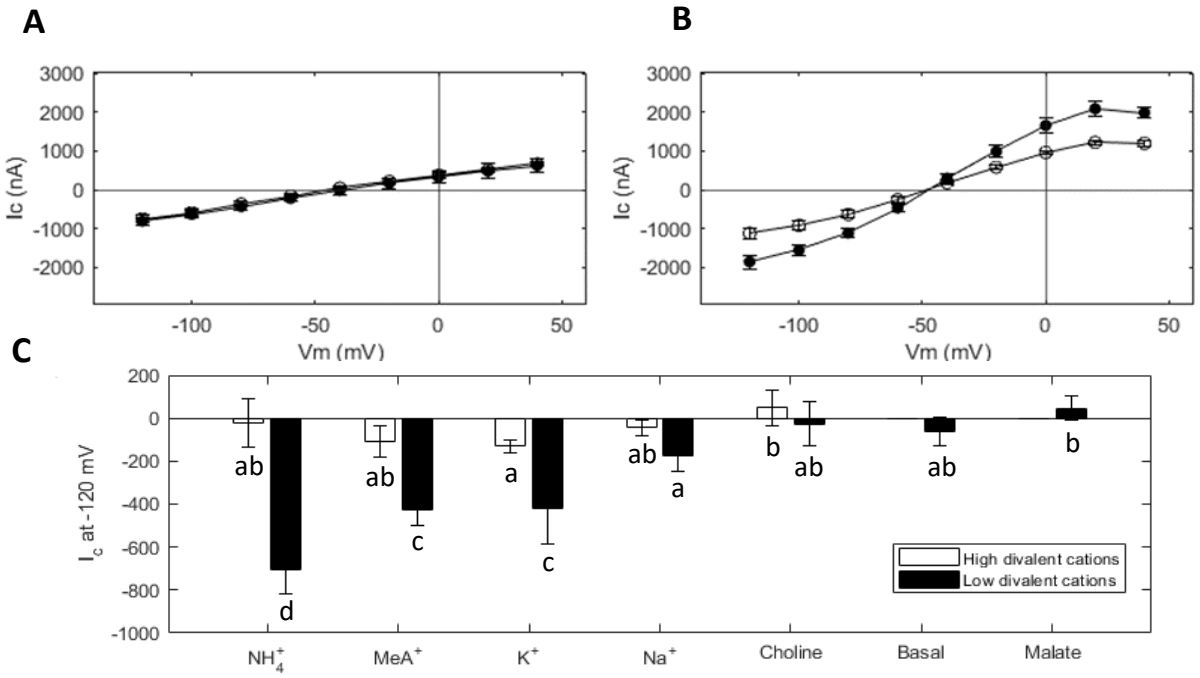

Figure 3.2 GmNOD26 is permeable to a range of monovalent cations when expressed in *X. laevis* oocytes. Current-voltage curves of control and GmNOD26 expressing oocytes bathed in 10 mM NH_4Cl testing solutions containing: (A) standard concentrations of divalent cations (1 mM Mg^{2+} and 1.8 mM Ca^{2+}); or (B) low concentration of divalent cations (50 µM Ca^{2+}). (C) monovalent cation induced clamp currents at -120 mV in GmNOD26 expressing oocytes with control oocyte currents subtracted under high and low concentrations of divalent cations. For all solutions, monovalent cations were applied as 10 mM chloride salts with osmolarity adjusted to 220 mosmol kg^{-1} with d-mannitol, buffered with HEPES and pH to 7.5 with TRIS base (n=22 for NH_4^+; n=8 for MeA^+ and K^+; n=12 Na^+ and choline, n=3 for Basal and $Malate^-$). Subscripts represent significance according to Duncan's Post Hoc.

Oocytes bathed in the presence of 10 mM NH_4Cl at low divalent cation concentrations displayed large outward currents at membrane potentials >40 mV (Figure 3.3a). These currents appear to be independent of GmNOD26 expression and may be carried by an endogenous channel that was activated by injection. However, the magnitude of the inward current was increased by expression of GmNOD26 (Figure 3.3a). Inward currents are representative of external ions moving into the oocyte, and consequently this observation is indicative of GmNOD26 enhancing the membrane permeability to NH_4^+. Conductance for GmNOD26-expressing oocytes was 34.3 µS, while control oocytes had a conductance of 25.4 µS (Figure 3.3a). In the presence of high divalent cations, both GmNOD26-expressing and control oocytes had a similar, lower conductance of 13.5 and 12.4 µS, respectively. Similar observations were made for MeA^+ with a slight increase in ungated conductivity of GmNOD26-expressing oocytes (15.2 µS, compared to the control, 11.6 µS: Figure 3. 3b). The same was true for K^+ (14.5 and 12.0 µS for GmNOD26-expressing and control oocytes, respectively). No significant shift in conductivity was detected in sodium or choline testing solutions when applied as 10 mM chloride salts, nor with malate, but in low divalent cation solutions there was a positive shift in the reversal potential of GmNOD26-expressing oocytes for all ions tested (Figure 3.3).

When bathed in 100 mM chloride salts, GmNOD26-expressing oocytes displayed greater ion conductivity compared to controls (Figure 3.4), but this depended on the divalent cation concentration. The ungated conductance in presence of external potassium was greatest, 124.4 µS compared to 90.2 µS in controls (Figure 3.4a). Similar observations were made for sodium, 75.1 µS in GmNOD26-expressing and 51.6 µS in controls (Figure 3.4b). The ungated conductivity of control oocytes in potassium and sodium testing solutions is large, indicative of endogenous channel activation. Conductivity in choline testing solution was less, 34.1 compared to 22.2 µS, suggesting that it is the monovalent cation inducing the ionic response rather than chloride (Figure 3.4c). These trends are clearer when the I_c at -120 mV of GmNOD26-expressing oocytes is subtracted from the control (Figure 3.4d).

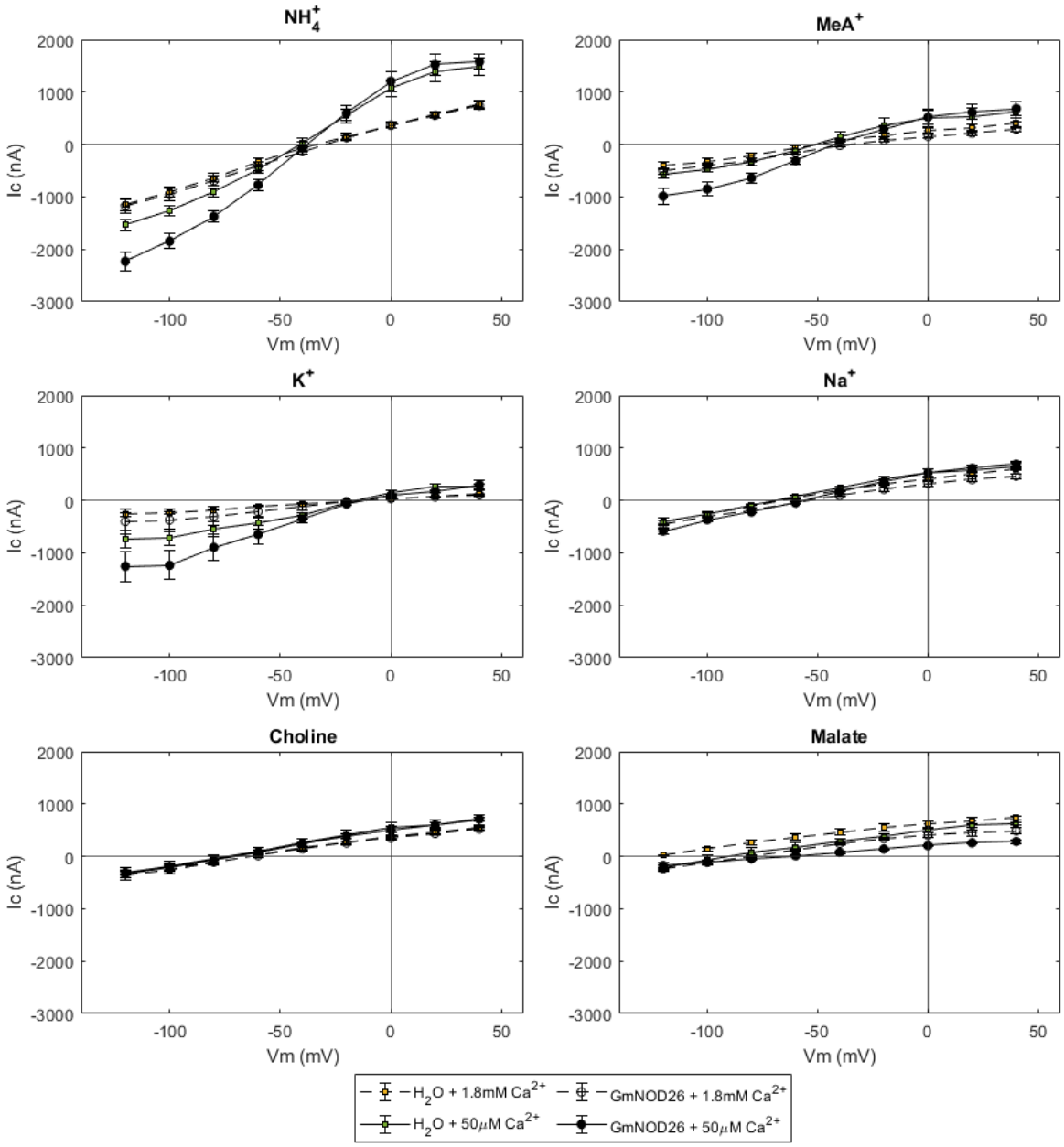

Figure 3.3 Ion-conductance of GmNOD26-expressing oocytes in the presence of 10 mM monovalent ions. Current-voltage curves of control and GmNOD26 expressing oocytes bathed in: (A) NH_4Cl; (B) MeACl; (C) KCl; (D) NaCl; (E) choline chloride; or (F) malic acid (malate). Testing solutions contained either 1.8 mM or 50 µM Ca^{2+}. For all solutions monovalent cations were applied as 10 mM chloride salts with osmolarity adjusted to 220 mosmol kg^{-1} with d-mannitol, buffered with HEPES and pH to 7.5 with TRIS base. Malate was applied as an acid buffered to pH 7.5 with BTP (n=22 for NH_4^+; n=8 for MeA^+ and K^+; n=12 Na^+ and choline, n=3 for malate).

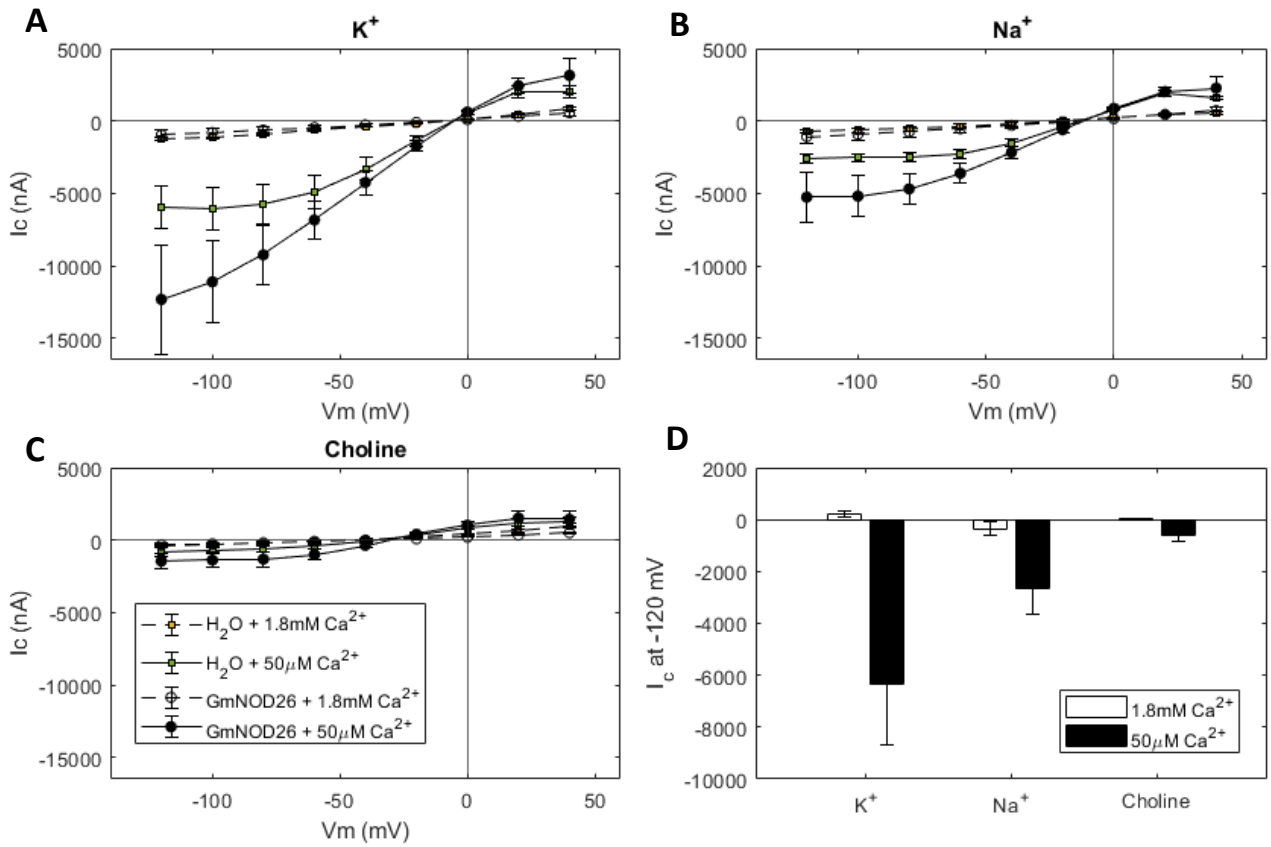

Figure 3.4 Ion-conductance of GmNOD26-expressing oocytes in the presence of 100 mM monovalent cations. Current-voltage curves of control and GmNOD26 expressing oocytes bathed in: (A) KCl; (B) NaCl; (C) choline chloride. Testing solutions contained either 1.8 mM or 50 µM Ca^{2+}. (D) monovalent cation induced clamp currents at -120 mV in GmNOD26-expressing oocytes with control oocyte currents subtracted. For all solutions monovalent cations were applied as 100 mM chloride salts with osmolarity adjusted to 220 mosmol kg^{-1} with d-mannitol, buffered with HEPES and pH to 7.5 with TRIS base (n=8).

3.2.2 GmNOD26 displays pH-sensitive NSCC activity

Under voltage clamp conditions with oocytes, NH_4^+ induced inward currents may be the result of direct transport of NH_4^+ across the oocyte membrane through the heterologously expressed protein, or by NH_3 movement across the membrane stimulating endogenous channel activities (Holm et al. 2005). This must be considered when interpreting NH_4^+ induced currents through GmNOD26, as it has previously been suggested to transport NH_3 (Tyerman and Niemietz 2000; Hwang et al. 2010). In aqueous solutions, the NH_4^+/NH_3 equilibrium is largely dependent on pH and temperature; under our experimental conditions this was calculated to be 9.89 mM NH_4^+ and 0.11 mM NH_3 at pH 7.5. The NH_3 concentration was further reduced to 0.0342 mM and 0.0108 mM by decreasing pH of the testing solution to 7.0 and 6.5, respectively.

X. laevis oocytes display significant endogenous NH_4^+ currents when exposed to concentrations higher than 1 mM, largely carried by an endogenous NSCC (Burckhardt and Frömter 1992; Burckhardt and Burckhardt 1997; Boldt et al. 2003). Since NH_4^+ induced clamp currents in control oocytes decreased as pH, and [NH_3], decreased (Figure 3.5a: I_C at -120 mV = -1531, -1033, -401 for pH 7.5, 7.0, 6.5), it is likely that NH_3 diffusion was also activating endogenous channels. Alternatively, or in addition, the endogenous NSCC may be gated directly by pH, as is the case for other NSCC's (Demidchik et al. 2002; Yu et al. 2001). Similar observations were made with oocytes expressing GmNOD26 (Figure 3.5b: I_C at -120 mV = -2230, -1731, -805 for pH 7.5, 7.0, 6.5). At pH 7.5 and 7.0, the magnitude of GmNOD26 relative to control NH_4^+ induced clamp currents was similar, but decreased at pH 6.5 when [NH_3] declined further (Figure 3.5c).

Expression of GmNOD26 in 26972c yeast cultures led to an increase in growth relative to the empty vector controls when grown under limiting nitrogen at low pH (3.5d, see chapter 4). This difference was most pronounced at the lowest pH when NH_4^+ was predominant. To distinguish between NH_3 transport or pH gating in the oocytes, NH_4^+ was replaced by Na^+. The conductance of control oocytes was rather insensitive to pH, decreasing slightly from 19.6 µS at pH 7.5, to 14.3 and 12.9 µS at pH 7.0 and 6.5, respectively (Figure 3.5e). In contrast, the Na^+ conductance of GmNOD26-expressing oocytes was strongly inhibited by low pH, with conductance's of 47.4, 38.2 and 26.2 µS at pH 7.5, 7.0 and 6.5, respectively (Figure 3.5f). This suggests that GmNOD26 cation conductance is gated by pH.

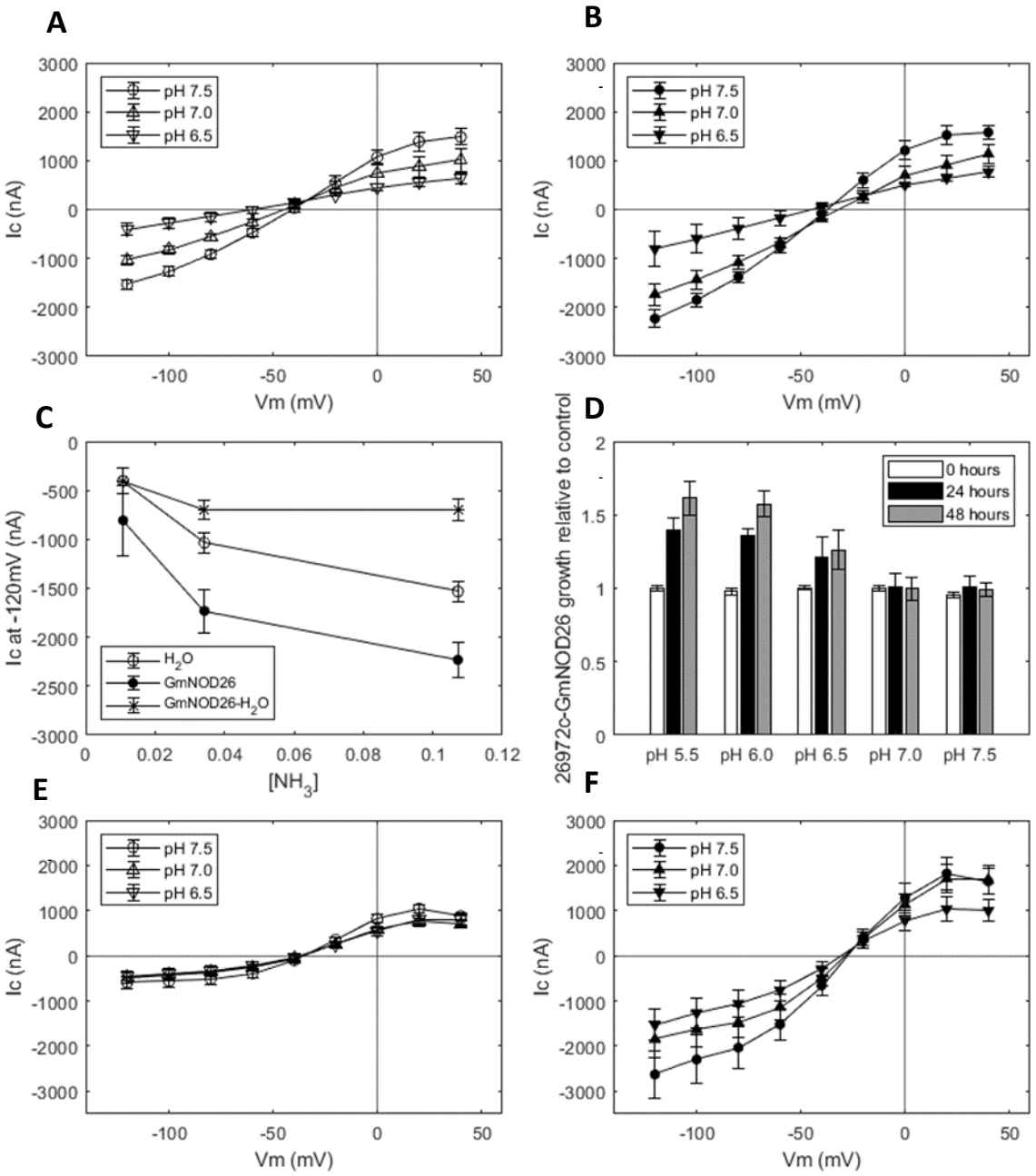

Figure 3.5 External pH gates steady state currents in GmNOD26-expressing *X. laevis* oocytes. (A) Currents in control oocytes. (B) Currents in GmNOD26 expressing oocytes. (C) NH_4^+ induced currents in native and GmNOD26 expressing oocytes clamped at -120 mV plotted as a function of NH_3 calculated from pH. For A-C, the testing solution contained 10 mM NH_4^+ as a chloride salt containing 50 µM Ca^{2+} buffered with HEPES and pH adjusted with TRIS base (pH 6.5 n=8, pH 7.0 n=12, pH 7.5 n=12). (D) Growth of GmNOD26 expressing 26972c yeast on Medium M containing 2% (v/v) galactose and 1 mM NH_4^+ at various pH relative to control (n=4, see chapter 4). (E) Na^+-induced currents in control oocytes. (F) Na^+-induced currents in GmNOD26 expressing oocytes. For E and F, the testing solution contained 50 mM Na^+ as a chloride salt containing 50 µM Ca^{2+} buffered with HEPES and pH adjusted with TRIS base (pH 6.5 n=8, pH 7.0 n=8, pH 7.5 n=12).

3.2.3 Phosphomimetics of S262 alters GmNOD26 cation and water permeability

GmNOD26 is phosphorylated *in vivo* at serine 262 by a calcium-dependent protein kinase (Weaver and Roberts 1992) and this has been shown to enhance water permeability when expressed in *X. laevis* oocytes (Guenther et al. 2003). Expression of a GmNOD26 S262D mutant, which mimics S262 phosphorylation, increased water permeability relative to a phosphor-null S262A mutant expressed in *X. laevis* oocytes (Figure 3.6a). Osmotic water permeabilities were calculated to be 0.0126, 0.0109 and 0.0138 cm/s for Wt, S262D and S262D respectively, while control oocytes exhibit low basal osmotic water permeability, 0.0022 cm/s, several fold lower than the permeability of GmNOD26-expressing oocytes (Figure 3.6b). C-terminal fusion of Wt, S262A and S262D mutants to YFP was used to assess the localisation of the proteins to the oocyte membrane. All constructs localised to the membrane with comparable levels of fluorescence (Figure 3.6c). Control, Wt, S262A and S262D mutants were also probed with the GmNOD26 antibody, a distinct 29 KD protein was successfully identified in Wt and mutant GmNOD26-expressing oocytes (Figure 3.7). This protein was of equal size to that identified in the SM positive control, but this lane also contained a smear of probed protein from 100 to 37 KD. For all homogenised oocyte lysate samples, a cross-reactive band was identified at ~90 KD (Figure 3.7). Although only lysate from a single oocyte was loaded in each gel, variations in the total protein loaded were detected (Appendix 4) and is highlighted by variations in the cross-reactive band (Figure 3.7).

Under voltage clamp conditions, oocytes expressing the phosphor-mimic S262D of GmNOD26 showed smaller sodium-induced inward currents compared to Wt and phosphor-null GmNOD26 proteins (Figure 3.6d; Appendix 5). There was little change in the reversal potential between Wt and mutant proteins expressed in *X. laevis* oocytes, but the phosphor-null mimic shifted to be slightly depolarised: -25.6 mV compared to -27.5 and -27.4 mV in Wt and S262D, respectively. The conductance of the channel was altered: S262A displayed the largest conductivity of 66.9 µS, compared to 47.8 and 52.9 µS for Wt and S262D, respectively. The effect of phosphorylation on the cation permeability of GmNOD26 at more acidic pH was further investigated. Interestingly, the phosphor-null mutant had greater sodium induced inward currents at low pH compared with both the Wt and phosphomimic mutant (Figure 3.6e; Appendix 6).

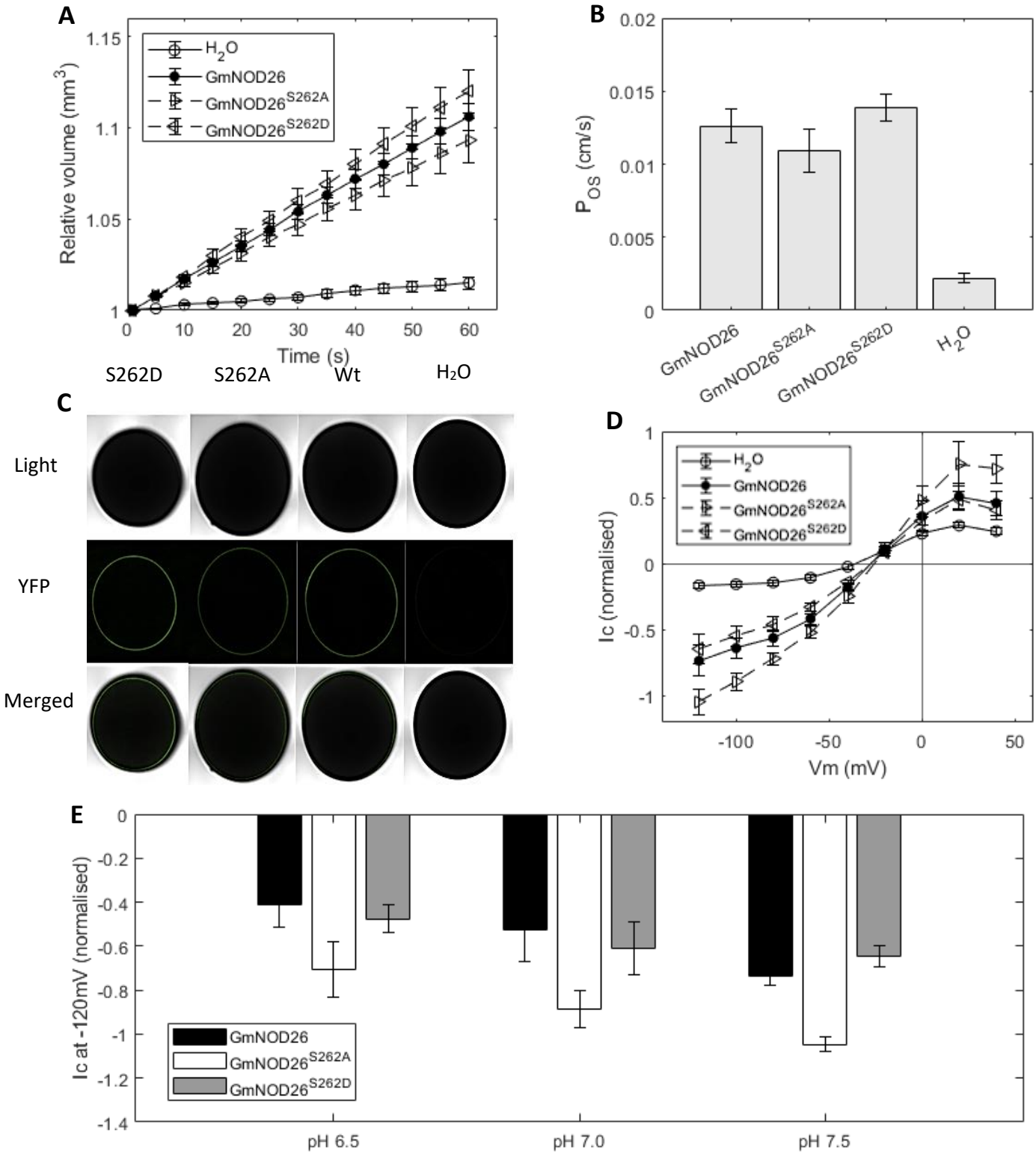

Figure 3.6 Phosphomimetics alter water and cation permeability of GmNOD26. (A) Relative change in volume over 60 seconds in a hypo-osmotic Na^+ testing solution (44 mosmol kg−1). (B) Calculated water permeability. (C) Confocal images of C-terminal YFP fusion to phosphorylation mutant or Wt GmNOD26 expressing oocytes. (D) Relative current-voltage curves in 50 mM NaCl testing solution containing 50 µM Ca^{2+} buffered with HEPES and adjusted to pH 7.5 with TRIS base. (E) Relative Na^+ induced clamp currents at -120 mV in GmNOD26 Wt and phosphorylation mutant expressing oocytes with control oocyte currents subtracted (n = 8).

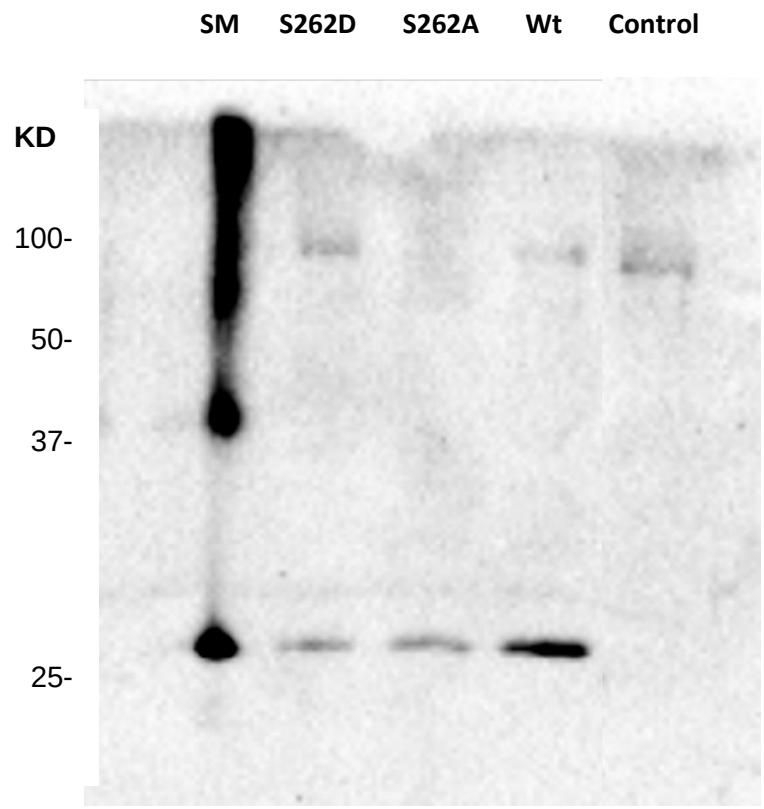

Figure 3.7 GmNOD26 western blot of phosphomimetic-expressing *X. laveis* oocytes. Homogenised oocyte lysate or 10 µg SM was separated on a 12.5% (v/v) SDS PAGE, transferred to nitrocellulose membrane and blotted for the 29 KD GmNOD26 protein and compared against Precision Plus Protein Dual Color Standards (BioRad, USA).

3.2.4 Loop D regulates cation conductance of GmNOD26

Loop D is a highly conserved aquaporin structure which acts as a gating domain regulating water and ion conductivity of aquaporins. Crystal structures of SoPIP2;1 reveal that, depending on the phosphorylation status of the protein, Loop D prevents the central pore from accessing the cytosol (Törnroth-Horsefield et al. 2006). Proline mutagenesis of the Loop D region of HsAQP1 revealed that alterations of three amino acid residues, T157P, D158P and R160P, significantly impaired activation of the channel's cation conductivity, while the alteration G166P increased the conductivity (Yu et al. 2006; Kourghi et al. 2018a). Alignment of the GmNOD26 sequence with other aquaporins reveals that residues corresponding to T176, D177, R179 and G182 are conserved in GmNOD26. Consequently, D177 and R179 were mutated to asparagine (Appendix 7), to remove the charge while retaining polarity.

To determine if Loop D gates ion conductance of GmNOD26, the analogous mutations (Appendix 7) D177N and R179N mutants were expressed in *X. laevis* oocytes. Expression of Wt and mutated forms of GmNOD26 increased the water permeability of oocytes (Figure 3.8a), suggesting that GmNOD26 Loop D mutants were expressed and localised to the oocyte PM; this was confirmed through confocal imaging of YFP-fusion constructs (Figure 3.8c). Interestingly, compared to Wt GmNOD26, water permeation was inhibited by >50% by D177N, but not significantly affected by R179N (Figure 3.7a). This corresponded to water permeabilities of 0.0022, 0.0126, 0.0046 and 0.0093 cm/s for control, Wt, D177N and R179N oocytes, respectively (Figure 3.8b). Site-directed mutagenesis of D192N and R194N in Loop D of GmNOD26 restricted ion conductance when the protein was expressed in oocytes, particularly at more hyperpolarised membrane potentials (Figure 3.8d). The reversal potential shifted from -25 mV in Wt, to -35 mV for mutant GmNOD26, towards the control oocyte reversal potential of -45 mV. A similar shift in conductance was also observed, with oocytes expressing Wt GmNOD26 displaying the largest ion conductance of 47.4 µS, while the conductance of both D177N, 31.0 µS, and R179N, 27.4 µS, shifted towards to control conductance of 20.4 µS (Appendix 5). Western blotting of various GmNOD26 point mutation *X. laveis* oocytes revealed that the Wt, D177N and R179N proteins were expressing well (Figure 3.10). However, there was a low level of V197H; A206C-GmNOD26 protein expressed, emphasised by comparing the cross-reactive band to 29 KD GmNOD26 protein, while there was no expression of the E43N mutant (Figure 3.10). For this reason, the E43N- and V197H; A206C-GmNOD26 mutants were disregarded from electrophysiological reading.

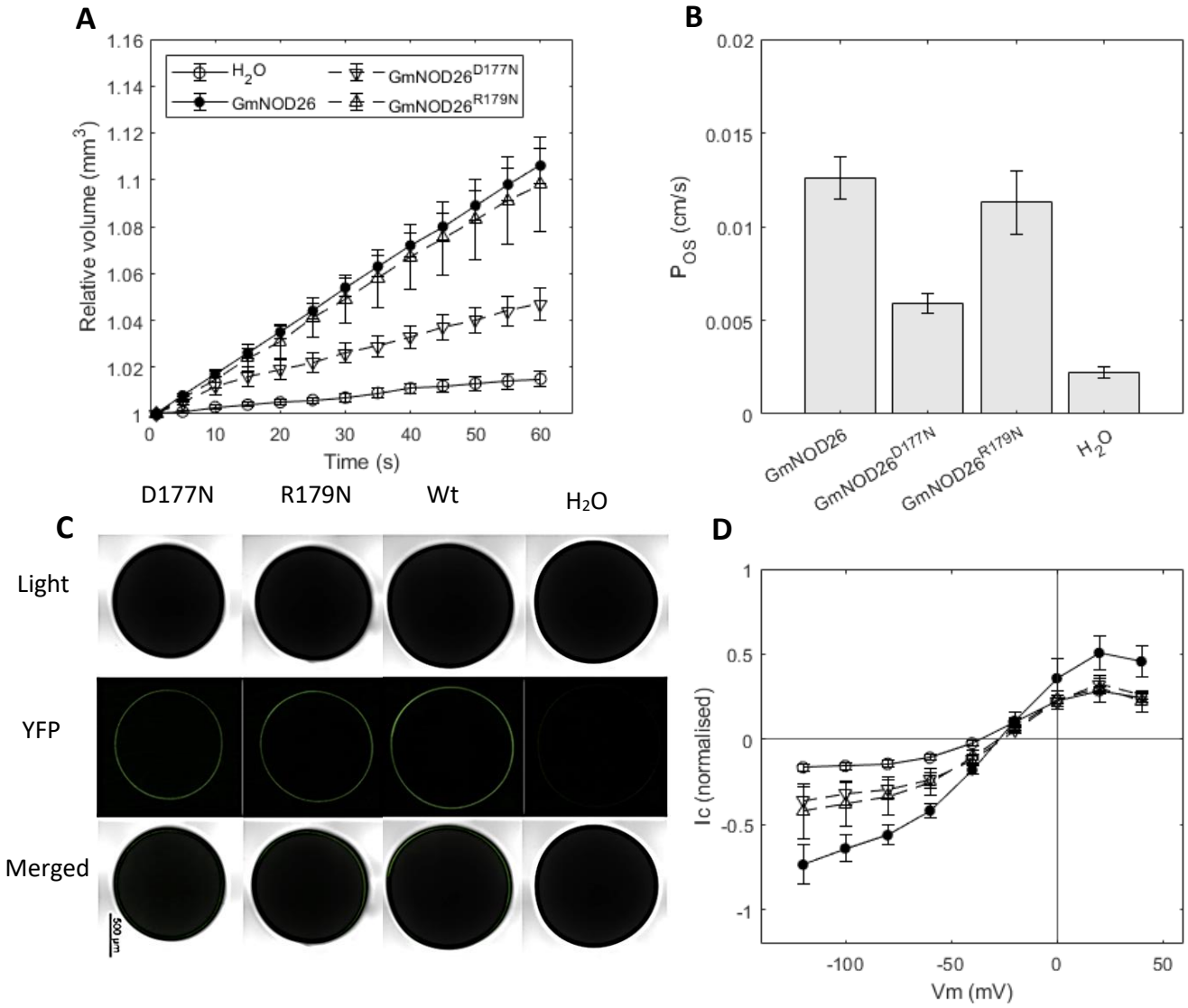

Figure 3.8 Loop D regulates cation conductance of GmNOD26. (A) Relative change in volume over 60 seconds in a hypo-osmotic Na^+ testing solution (44 mosmol kg−1). (B) Calculated water permeability. (C) Confocal images of C-terminal YFP fusion to Loop D mutant or Wt GmNOD26 expressing oocytes. (D) Relative current-voltage curves in 50 mM NaCl testing solution containing 50 µM Ca^{2+} buffered with HEPES and adjusted to pH 7.5 with TRIS base (n = 6).

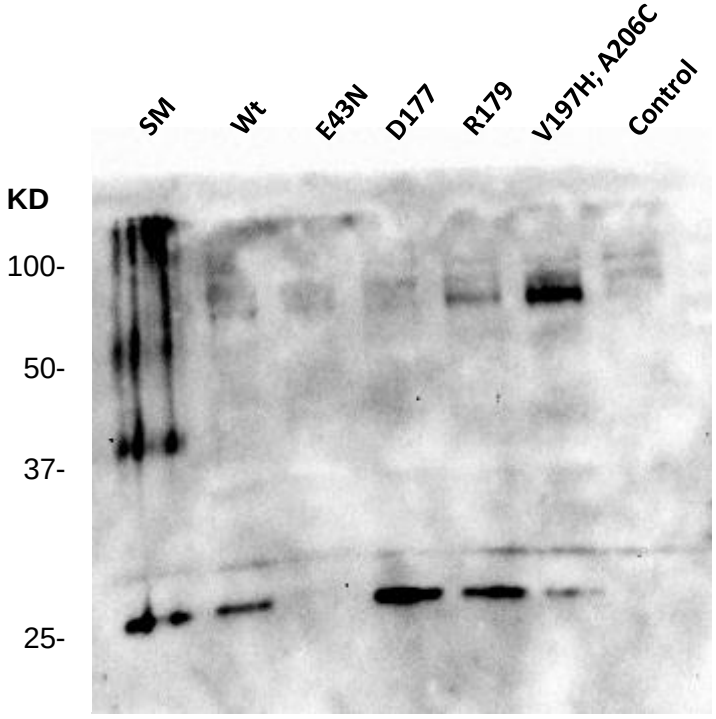

Figure 3.9 Western blot of various GmNOD26 point mutation-expressing *X. laveis* oocytes. Homogenised oocyte lysate or 5 µg SM was separated on a 12.5% (v/v) SDS PAGE, transferred to nitrocellulose membrane and blotted for the 29 KD GmNOD26 protein and compared against Precision Plus Protein Dual Color Standards (BioRad, USA).

3.2.5 Aquaporin inhibitor effect on ion conductance

Various inhibitors of aquaporin cation conductance, and the GmNOD26 antibody, were tested on GmNOD26-expressing *X. laevis* oocytes. When applied to control oocytes there was some variability in the conductance, ranging from 6.6 µS when preincubated with a 1:500 dilution of GmNOD26 antibody, to 18.4 µS when incubated with AqB011 (Figure 3.10). However, these conductance's were less than the ungated sodium induced cation conductance of 31.0 µS observed in GmNOD26-expressing oocytes (Figure 3.10). Neither DMSO nor AqB011 affected the observed monovalent cation conductance of GmNOD26-expressing oocytes (Figure 3.10), and in general the current-voltage curves followed a similar trend. Preincubation with furfural and a 1:500 dilution of GmNOD26 antibody, did decrease the conductivity of the channel, but not to the same extent as application of divalent cations or spermine (Figure 3.10). For furfural, this difference was significantly different to the ungated sodium induced cation conductance, but not for the GmNOD26 antibody, which displayed extremely variable data (Figure 3.10).

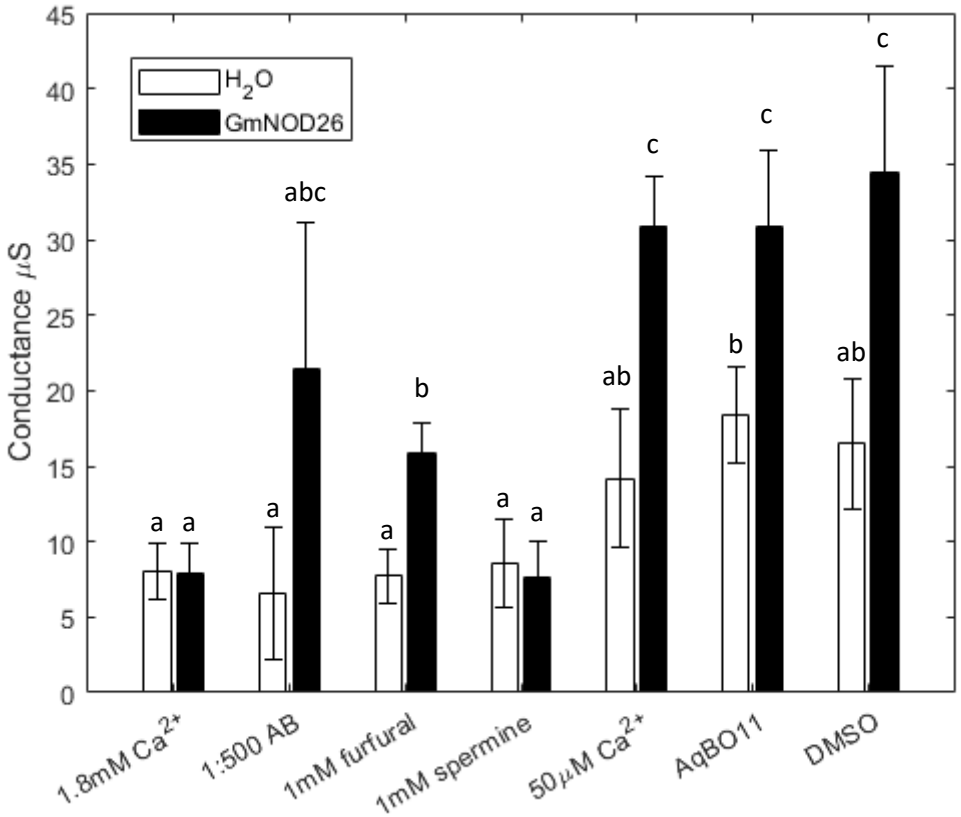

Figure 3.10 Inhibition of monovalent cation induced conductance in GmNOD26. The testing solution consisted of 50 mM Na^+ as a chloride salt containing 50 µM Ca^{2+} buffered with HEPES and pH adjusted with TRIS base in the presence or absence of aquaporin inhibitors. Subscripts represent significance according to Duncan's Post Hoc (n=4).

3.3 Discussion

3.3.1 GmNOD26 resembles the SM-NSCC

A NSCC was previously detected on the soybean SM through patch clamping of isolated symbiosomes (Tyerman et al. 1995; Whitehead et al. 1998; Obermeyer and Tyerman 2005). The channel displayed voltage dependent, SubpicoSeimen conductance and was most permeable to NH_4^+ at physiological concentrations, with time dependent inward currents gated, and rectified, by divalent cations. These properties are distinct from the high affinity ammonium and potassium transport families that are selective for, and function at micromolar concentrations of, specific cations (Schachtman and Schroeder 1994; Howitt and Udvardi 2000). It should also be noted that these channels have not been detected in symbiosome proteomic studies (Saalbach et al. 2002; Wienkoop and Saalbach 2003; Clarke et al. 2015; Luo et al. 2023). I investigated the electrophysiological characteristics of GmNOD26, an aquaporin which constitutes ~10% of the total protein mass (Rivers et al. 1997), by expressing it in *X. laevis* oocytes. GmNOD26 is an excellent candidate for the SM-NSCC due to its high density within the SM, a characteristic shared by the SM-NSCC channel (Tyerman et al. 1995). When expressed in *X. laevis* oocytes, GmNOD26 displays characteristics of an ion channel gated by divalent cations (Figure 3.1), observations similar to those of Tyerman et al. (1995) in symbiosome-attached patches and aligned with the ionic conductance of purified GmNOD26 expressed in lipid bilayers (Weaver et al. 1994). The ionic currents observed in GmNOD26-expressing *X. laevis* oocytes display time and voltage dependency, and are gated by divalent cations in a dose dependent manner (Figure 3.1), characteristics shared by the NSCC characterised in SM patches (Whitehead et al. 1998).

The ion currents in GmNOD26-expressing *X. laevis* oocytes were carried by the monovalent cation, rather than the anion, in solution. When the chloride concentration was maintained at 10 mM and the monovalent cation in solution altered, GmNOD26 displayed a permeability profile of NH_4^+>MeA^+=K^+>Na^+>Choline (Figure 3.2/4). Tyerman et al. (1995) showed that the patch-clamped SM-NSCC was non-selective for cations at high concentrations (150 mM), but selective for NH_4^+ over K^+, at physiological concentrations. A similar permeability profile was established in patches of isolated *L. japonicus* symbiosomes under low divalent cation concentrations, although this channel also appeared to be permeable to calcium (Roberts and Tyerman 2002). Calcium permeability observed in symbiosome patches of *L. japonicus* is unique and not observed in the homologous channel on the soybean SM.

Patches of isolated soybean symbiosomes did not elicit any notable inward currents when the large monovalent cation choline was in solution (Tyerman et al. 1995), similar to my observations with GmNOD26-expressing *X. laevis* oocytes (Figure 3.2-4). This provides further evidence that the ion currents elicited were carried by the monovalent cation and not chloride. Indeed, no monovalent anion induced currents were observed in GmNOD26-expressing *X. laevis* oocytes (Figure 3.2/3). Previously, a correlation between phosphorylation of GmNOD26 and malate uptake by symbiosomes lead to the suggestion that GmNOD26 may be the SM dicarboxylate carrier (Ou Yang et al. 1991). When GmNOD26 was expressed in lipid bilayers, a slight anion:cation preference was observed in the presence of 1.0 M KCl, and there was no significant change in channel activity when KCl was replaced with potassium malate, suggesting that malate and chloride may be transported by the channel (Weaver et al. 1994). However, GmNOD26 expressed in *X. laevis* oocytes has a clear preference for cations over anions, and malate did not stimulate ion currents in these oocytes (Figure 3.2/3). These results, together with other functional characterisation of GmNOD26 have failed to note anion transport (Rivers et al. 1997; Dean et al. 1999; Tyerman and Niemietz 2000; Hwang et al. 2010), providing overwhelming evidence that GmNOD26 does not transport dicarboxylates or other anions.

Polyamines provide a negative feedback loop to regulate nitrogen fixation. In nodules, free polyamine concentrations are comparatively high (Ozawa and Tsuji 1993; Fujihara et al. 1994), likely due to the enhanced production of glutamate during the nitrogen assimilation pathway, which is a precursor for both ureide and polyamine synthesis (Whitehead et al. 2001). In isolated soybean symbiosomes, polyamines stimulate malate uptake in the micromolar range, but inhibit both inward and outward currents observed under patch clamp conditions (Whitehead et al. 2001). This inhibitory effect of spermine on the soybean SM-NSCC was investigated in GmNOD26-expressing *X. laevis* oocytes and similar observations were noted. At concentrations of 1 mM, both inward and outward currents of GmNOD26-expressing oocytes were inhibited to a level similar to high divalent cations, and comparable to control oocytes (Figure 3.8). This inhibition of voltage-dependent cation channels is common among rectifying channels, as the positively charged particles block the ion conducting pore (Armstrong 1969; Nichols and Lopatin 1997).

Whilst controversial, NSCC activity of aquaporins has been reported several times previously, with the human aquaporin 1 (AQP1) found to be a cyclic GMP-gated NSCC permeable to a range of monovalent cations when expressed in *X. laevis* oocytes (Yool et al. 1996; Anthony et al. 2000). Similar observations were made with the *Drosophila* Big Brain aquaporin (Yanochko and Yool 2004), which was also found to be gated by divalent cations, but it was not until more recently that NSCC

activity of plant aquaporins was reported (Byrt et al. 2017). In *Arabidopsis*, AtPIP2;1 is a divalent cation and pH gated NSCC, that when phosphorylated at the C-terminus increases cation conductance and decreases water permeability (Byrt et al. 2017; Qiu et al. 2020). Divalent cation gating of barley PIP2;8 has also been reported, but phosphorylation at the C-terminus increased both cation conductance and water permeability (Tran et al. 2020). Immunogold labelling of PIP1, PIP2 and γ-TIP aquaporin subtypes in soybean nodule sections suggests that these proteins localise to the inner cortical, endodermal and pericycle, but not infected cells (Fleurat-Lessard et al. 2005). This is supported by soybean symbiosome proteomics in which GmNOD26 was the only aquaporin detected in SM fractions (Clarke et al. 2015). Given that no other aquaporins are known to localise to the SM, it is likely that the characterised NSCC activity on the soybean SM is carried by GmNOD26, as shown in this chapter.

3.3.2 GmNOD26 is permeable to NH_4^+ but gated by external pH

The ionic currents elicited in GmNOD26-expressing oocytes appear to decrease with pH (Figure 3.5). Previous characterisation of the SM-NSCC in patch-clamp experiments was performed at pH 7.0 (Tyerman et al. 1995) and the effect of changing pH on the channel was not investigated. This feature makes interpreting NH_3 and NH_4^+ transport in *X. laevis* oocytes difficult, as the NH_4^+ induced currents observed in GmNOD26-expressing oocytes may be the result of an activated endogenous channel following NH_3 transport through GmNOD26. However, given that both Na^+ and NH_4^+ induced currents were reduced by external pH in a similar manner it is likely that the channel itself is gated by protons. When GmNOD26 was expressed in the ammonium transport deficient 26972c strain complementation was observed at low pH (Figure 3.5d, see Chapter 4), suggesting that GmNOD26 can facilitate NH_4^+ transport when required. Gating of other NSCCs by protons (pH) has previously been described (Demidchik et al. 2002; Yu et al. 2001), along with aquaporin transport of water (Tournaire-Roux et al. 2003; Sutka et al. 2005; Verdoucq et al. 2008), glycerol (Mósca et al. 2018) and cation conductivity (Byrt et al. 2017). Proton gating of GmNOD26 is an interesting observation given that the symbiosome space is estimated to be acidic (Udvardi and Day 1989; Pierre et al. 2013). But explains why NH_4^+ induced currents decreased as $[NH_3]$ decreased, as pH was used to manipulate NH_3 concentration. *In planta*, the C-terminal domain of GmNOD26 interacts with cytosolic GS1β and GS1γ, the principal ammonium assimilating enzyme in the nodule infected cell cytosol (Masalkar et al. 2010). GS constitutes ~2% of the nodule cytosolic protein (McParland et al. 1976), and crystal structures reveal an NH_4^+ binding site (Liaw et al. 1995), which when docked to GmNOD26 may alter the enzyme's affinity for NH_4^+.

3.3.3 Ion conductance of GmNOD26 is gated when phosphorylated at serine-262

Mutation of serine 262 to aspartate (S262D), which mimics serine phosphorylation, enhanced water permeability of GmNOD26 when expressed in *X. laevis* oocytes, while mutation of serine 262 to alanine (S262A), which mimics serine in its unphosphorylated state, restricted water permeability (Figure 3.6; (Guenther et al. 2003)). The phosphor-null mutant, S262A, increased the ion conductivity of the channel when expressed in *X. laevis* oocytes compared to Wt and phosphor mutant, S262D (Figure 3.6d). This is in agreement with observations by Lee et al. (1995) who found phosphorylation of S262 resulted in increased voltage-dependent gating and preferential occupancy of lower sub-conductance states of GmNOD26 in planar lipid bilayers. The role of phosphorylation in regulation of cation conductance of aquaporins is still emerging, but tyrosine phosphorylation by protein kinase C has been shown to be essential for the induction of cation currents of HsAQP1 (Zhang et al. 2007). More recently, serine phosphorylation of AtPIP2;1 (Qiu et al. 2020) and HvPIP2;8 (Tran et al. 2020) has been correlated with an increase in ion conductivity. Interestingly, GmNOD26 is the first reported aquaporin where phosphorylation has been shown to lead to a decreased cation conducting state ((Lee et al. 1995); Figure 3.6d). Importantly, these results confirm that the changes in cation conductance upon expression of GmNOD26 in oocytes are caused by the activity of the soybean protein, rather than activation of endogenous channels in the oocytes.

The sodium induced inward currents of Wt GmNOD26 expressed in oocytes switch from behaving in a similar manner to the phosphor-null mutant at pH 7.5, to behaving similarly to the phosphomimic mutant at pH <7.0. This may indicate that Wt GmNOD26 was not phosphorylated when in slightly basic testing solutions but phosphorylated by a native *X. laevis* oocyte protein kinase, eg CK2 (Westmark et al. 2002), when in neutral or acidic testing solutions (Figure 3.6e). This information must be taken into consideration when interpreting the external pH gating data, as the magnitude of the pH dependent gating mechanism may be exaggerated by the super-imposed phosphorylation gating mechanism. *In vivo,* dephosphorylation of GmNOD26 may mitigate the pH gating mechanism observed in the *X. laevis* oocyte system, as greater inward currents are observed in the phosphor-null mutant at low external pH (Figure 3.6e). Phosphorylation of GmNOD26 is regulated developmentally and by osmotic signals, with increasing nodule age and osmotic stress resulting in an increased phosphorylation status (Guenther et al. 2003). Thus, under optimal nitrogen fixing conditions the protein exists in both a unphosphorylated and phosphorylated state, facilitating both ammonium export from, and osmotic adjustment of, the symbiosome. This regulation is largely controlled through the Ca^{2+} dependency of the SM protein kinase, particularly under osmotic stress where rapid Ca^{2+} signalling responses are induced. Ammonium efflux would only be further

enhanced by the cytosolic GS isoforms interacting with the c-terminal of GmNOD26 (Masalkar et al. 2010), which too are post-translationally regulated by phosphorylation (Finnemann and Schjoerring 2000; Lima et al. 2006). In *M. truncatula* root nodules phosphorylation of GS1a reduces the Km for glutamate, which would allow the nitrogen assimilation pathway to continue when substrate concentrations are limiting (Lima et al. 2006).

3.3.4 Loop D is an important regulatory structure of GmNOD26

The complexity of aquaporin transport has been reviewed recently (Tyerman et al. 2021; Henderson et al. 2022). The structural regulation of aquaporins is extensive (Henderson et al. 2022), with gating regions found in M1 (Yanochko and Yool 2004; Yool 2007; Yool and Campbell 2012), Loop B (Yasui et al. 1999) and Loop D (Törnroth-Horsefield et al. 2006; Yu et al. 2006; Kourghi et al. 2018a). The involvement of these regions has largely been determined through resolved crystalline structures of HsAQP1 (Murata et al. 2000; Sui et al. 2001) and SoPIP2;1 (Törnroth-Horsefield et al. 2006), and site-directed mutagenesis. Overwhelming evidence suggest that the monomeric water pore does not permit passage of cations, but rather the central tetrameric pore (Campbell et al. 2012; Kourghi et al. 2018b; Ozu et al. 2018). The crystal structure of SoPIP2;1 suggests that conformational changes to Loop D occlude either the monomeric water pore or central tetrameric pore, altering the transport properties of the channel (Törnroth-Horsefield et al. 2006). It is believed that divalent cation binding or phosphorylation may regulate this conformational change.

Amino acid alignments of GmNOD26 with other studied aquaporins revealed that two of the charged residues in Loop D were conserved, corresponding to D177 and R179 (Appendix 7). In HsAQP1, proline mutagenesis of these residues appears to specifically impair the ion conductance of the channel, with no apparent effect on water transport (Yu et al. 2006; Kourghi et al. 2018a). Similarly, when the equivalent residues were mutated to asparagine to remove the charge while retaining polarity, GmNOD26-expressing oocytes displayed impaired activation of the channel's cation conductivity (Figure 3.7). Interestingly, the D177N mutation also significantly impaired water transport by the channel but did not interfere with its localisation to the oocyte PM (Figure 3.7). These observations provide strong evidence that expression of GmNOD26 in *X. laevis* oocytes was responsible for the observed ion conductance and that Loop D regulates the ion conducting pore.

3.3.5 GmNOD26 is a strong candidate for the SM-NSCC

The importance of NOD26 to symbiotic nitrogen fixation has been emphasised recently by studies with *M. truncatula* knockout mutants, which display symptoms of nitrogen deficiency when grown

under symbiotic conditions (Frare et al. 2022). The results in this chapter, together with preceding studies (Weaver et al. 1994; Rivers et al. 1997; Dean et al. 1999; Tyerman and Niemietz 2000; Hwang et al. 2010) clearly demonstrate that GmNOD26 is a multifunctional plant aquaporin, capable of transporting water, formamide, glycerol, NH_3 and various cations, including NH_4^+. This suggests that the phenotype of the *M. truncatula* nod26 knockout mutants was due to decreased export of ammonium out of the symbiosome and are consistent with GmNOD26 being the major route by which fixed nitrogen is exported to the plant. The capacity for GmNOD26 to transport nitrogenous compounds will further be explored in Chapter 4.

4 Functional characterisation of GmNOD26 in yeast

4.1 Introduction

4.1.1 Transport of ammonia and amino acids from symbiosomes

Although it is believed that NH_4^+ is the primary nitrogen product transported to the cytosol, NH_3 transport can be significant and is largely dependent on the pH of the symbiosome space (Udvardi and Day 1990). Uptake of NH_3 by isolated inside-out symbiosomes is partially inhibited by mercury (Tyerman and Niemietz 2000), a characteristic of ammonia transport shared by GmNOD26 (Hwang et al. 2010). In addition to NH_3 and NH_4^+ transport, labelling experiments have indicated substantial amino acid pools are synthesised under certain microaerobic conditions (Day et al. 2001b). In isolated pea bacteroids, alanine production was largely dependent on bacteroid density, with high bacteroid density activating alanine biosynthesis, attributed to NH_4^+ accumulation (Allaway et al. 2000). Alanine produced by bacteroids is transported to the symbiosome space through general amino acid permeases of the ABC superfamily (Walshaw and Poole 1996; Hosie et al. 2002). The mechanism by which alanine crosses the SM is unknown. Swelling assays of isolated soybean symbiosomes reveals asymmetric alanine transport 100 times greater in the direction out of the symbiosome (Tyerman and Niemietz, unpublished data obtained from Day et al. (2001b)). This transport was strongly inhibited by mercury, and it was suggested that alanine may be transported through GmNOD26 (Day et al. 2001b). Given that water permeability of GmNOD26 is also inhibited by mercury (Rivers et al. 1997; Dean et al. 1999; Hwang et al. 2010), this may have been an artifact induced by the swelling assay and water permeability of the symbiosome is impaired, but warrants investigation of alanine transport by GmNOD26.

Here, ammonia and ammonium transport of GmNOD26 is investigated in the ammonium transport deficient *S. cerevisiae* strains 26972c (*mep1-1*, *mep2-1*, Mep3, ura-) and 31019b (*Mep1-3*Δ, ura-) (Marini et al. 1997). The capacity of GmNOD26 to transport alanine is also explored through heterologous expression in the amino acid transport deficient strain 22Δ10α (MATα gap1-1 put4-1 uga4-1 can1::HisG lyp1- alp1::HisG hip1::HisG dip5::HisG gnp1Δ agp1Δ ura3-118) (Besnard et al. 2016).

4.2 Results

4.2.1 Complementation of ammonium transport deficient *S. cerevisiae*

4.2.1.1 Growth on solid medium

A family of ammonium transporters have been described in *S. cerevisiae*, with two high affinity transporters, Mep1 and Mep2, and a third lower affinity transporter Mep3 (Marini et al. 1994; Marini et al. 1997). In the *S. cerevisiae* strains 26972c (*mep1-1*, *mep2-1*, Mep3, ura-) and 31019b (*Mep1-3*Δ, ura-) ammonium transport is disrupted and growth is not supported on media containing less than 5 mM NH_4^+ (Marini et al. 1997). Here, 26972c and 31019b were transformed with pYES-DEST52 empty and GmNOD26 containing vectors and grown on solid medium M media for 5 days at various NH_4^+ concentrations (Figure 4.1). GmNOD26 rescued growth at lower concentrations of 26972c cells when compared to the empty vector at 1, 2 and 5 mM, but growth decreased with NH_4^+ concentration (Figure 4.1). However, the empty pYES-DEST52 vector 31019b controls displayed growth at all tested ammonium concentrations, emphasised in Appendix 8.

Complementation by GmNOD26 was further investigated through manipulation of the growth medium's pH in the presence of 2 mM NH_3/NH_4^+. At pH 6.0, the ammonia and ammonium availabilities would be 1.4 µM and 1998.6 µM respectively, while at pH 7.0 there would be 14 µM ammonia and 1986 µM ammonium (Boron and De Weer 1976). At higher pH, when the membrane-permeant neutral ammonia species increased, the empty vector 26972c cells were able to grow more readily. At pH 6.0, when NH_4^+ was predominant, GmNOD26 rescued growth of 26972c cells when spotted at a concentration of 10^{-4} (Figure 4.1), while at pH 7.0, when NH_3 concentration increased, rescue occurred at a concentration of 10^{-5}. Bearing in mind the previously demonstrated ammonia permeability of GmNOD26 (Hwang et al. 2010), it is important to demonstrate growth of GmNOD26-expressing 26972c cells at low pH, when little $NH_3$is available, in order to establish cation transport by the channel. In this context, the fact that the relative growth of 26972c GmNOD26-expressing cells did not change significantly over a ~10-fold range of NH_3 availability (Figure 4.1) is consistent with NH_4^+-permeation through the channel. However, it is also possible that the affinity of GmNOD26 for NH_3 is saturated at 1.4 µM. Attempts to manipulate the divalent cation concentration of the growth medium failed as the *S. cerevisiae* cells could not grow in the absence of divalent cations (DNS).

Ammonium was replaced in the media with its toxic analog MeA^+ (Mitsuzawa 2006). *S. cerevisiae* 26972c cells grew readily in the presence of MeA^+ when supplemented with 0.1% (w/v) proline, but when expressing GmNOD26 toxicity was observed (Figure 4.1). In the presence of 100 mM MeA^+,

GmNOD26 clearly enhanced uptake by 26972c cells, with an increase in toxicity observed when spotted at a concentration of 10^{-4} (Figure 4.1). This effect was more pronounced at 200 mM MeA^+ with no apparent toxicity increase relative to pYES-DEST52 containing 26972c cells.

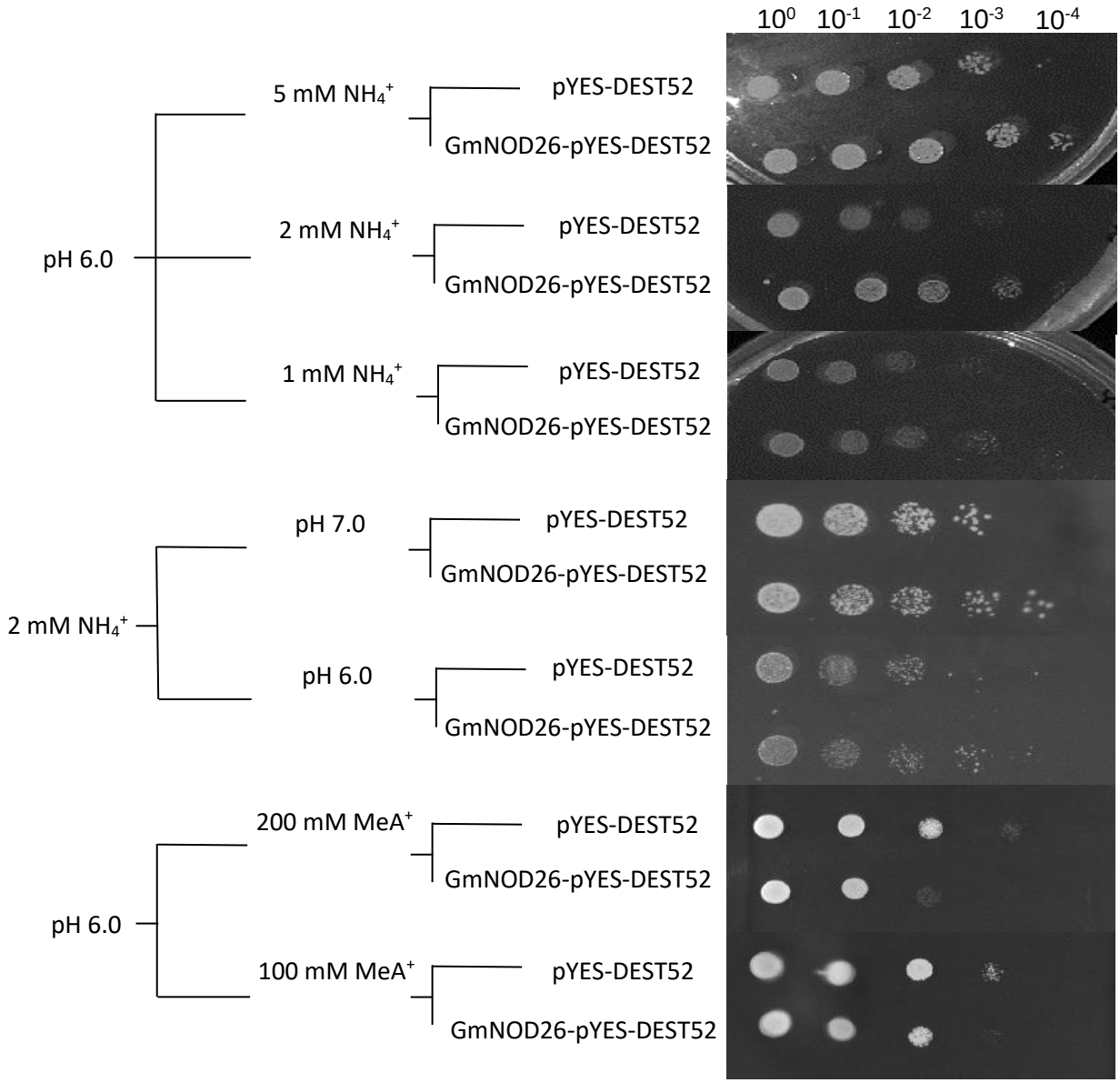

Figure 4.1 Optimising functional complementation of 26972c on Solid medium M. GmNOD26 and empty pYESdest52 vector 26972c transformants were grown in Medium M containing 2% (w/v) glucose and 0.1% (w/v) proline (pH 6.0) overnight, washed twice with sterile water and diluted to an OD600 of 100. Cultures were serially diluted 10-fold and 5 µL spotted onto solid Medium M containing 2% (w/v) galactose and the various treatments.

4.2.1.2 Optimising ammonium concentration in liquid cultures

The ability of GmNOD26 to complement both 26972c and 31019b cells was further investigated in liquid cultures (Figure 4.2, Appendix 8). In both glucose- and galactose-supplemented media, growth of all transformants followed a similar trend (Figure 4.2). In the linear phase of growth, glucose supplemented cells had a typical growth rate of 0.049 to 0.061 OD600/hour, while galactose supplemented cells ranged from 0.049 to 0.057 OD600/hour. At all ammonium concentrations, both empty vector and GmNOD26-expressing 31019b cells grew readily, in agreement with observations on solid media (DNS). It is clear that the 31019b cells made available to me were permeable to ammonium and consequently only 26972c cells, which display characteristics of an ammonium deficient cell line, were used.

The empty pYES-DEST52 vector expressing 26972c cells were unable to grow in liquid media containing 1 mM NH_4^+. When GmNOD26 was expressed under the galactose inducible promoter, growth increased (Figure 4.2c), indicative of NH_4^+ transport through GmNOD26. At 2 mM NH_4^+, growth was slightly increased in the empty vector (0.0942 OD600/hour), but this was far less than that of GmNOD26-expressing cells (0.0300 OD600/hour) (Figure 4.2d). When ammonium concentration was further increased, the empty vector expressing 26972c cells grew readily with growth rates of 0.0315 and 0.104 OD600/hour at 5 and 10 mM NH_4^+ respectively. This was expected as the ammonium transport deficiency of this strain is only observed when the sole nitrogen source is limiting (<2 mM NH_4^+; (Marini et al. 1997)). There was a notable increase in the growth of GmNOD26-expressing cells at 5, but not at 10 mM NH_4^+.

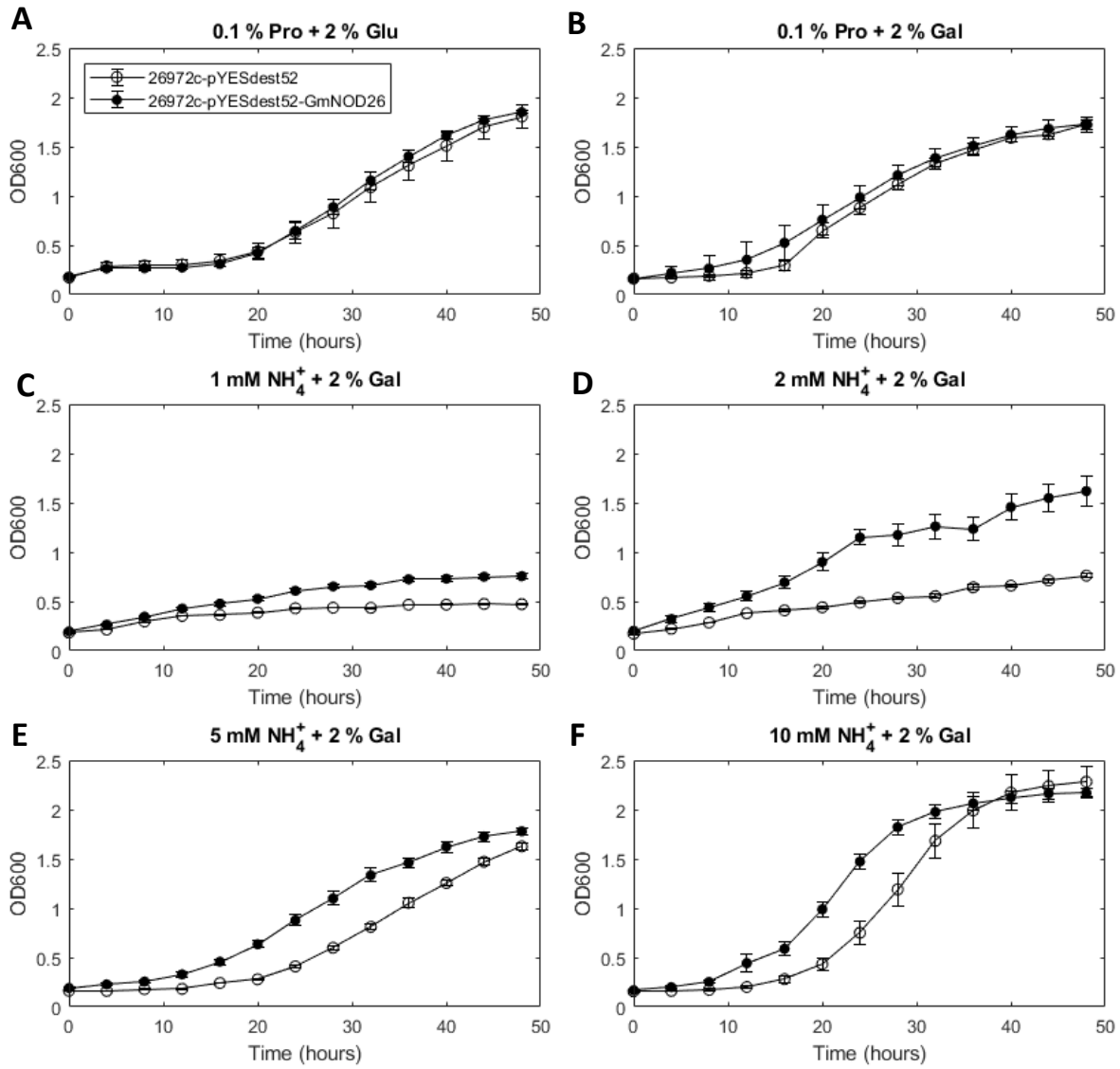

Figure 4.2 Optimising NH_4^+ concentration for GmNOD26 complementation of the ammonium transport deficient yeast strains 26972c. GmNOD26 and empty pYESdest52 vector transformants were grown in 200 µL of Medium M (pH 6.0) containing (A) 2% (w/v) glucose and 0.1% (w/v) proline; or 2% (w/v) galactose and (B) 0.1% (w/v) proline; (C) 1 mM NH_4^+, (D) 2 mM NH_4^+, (E) 5 mM NH_4^+, (F) 10 mM NH_4^+ for 48 hours at 28°C with 200 RPM shaking (n=4).

4.2.1.3 Methylammonium toxicity in liquid cultures

MeA^+ is an analog for ammonium and is toxic to yeast as it can accumulate 1000-fold inside cells and is unable to be metabolised (Marini et al. 1997). Since ammonium transport in the 26972c *S. cerevisiae* strain is disrupted, toxicity to MeA^+ is not observed. When grown in liquid cultures, pYES-DEST52-expressing 26972c cells were able to tolerate MeA^+ concentrations of up to 200 mM, but at 300 mM a moderate toxicity was observed (Figure 4.3). GmNOD26-expressing 26972c grown in media containing both MeA^+ and glucose displayed no detectable toxicity, but when galactose was used as the carbon source, and expression of GmNOD26 was induced, a toxicity phenotype was observed (Figure 4.3). At 100 mM MeA^+, only a slight toxicity was observed, suggesting that the affinity of GmNOD26 for this substrate may be low (Figure 4.3a). When this concentration was increased the effect was more pronounced, and at both 150 and 200 mM there was a clear toxicity of GmNOD26-expressing 26972c cells.

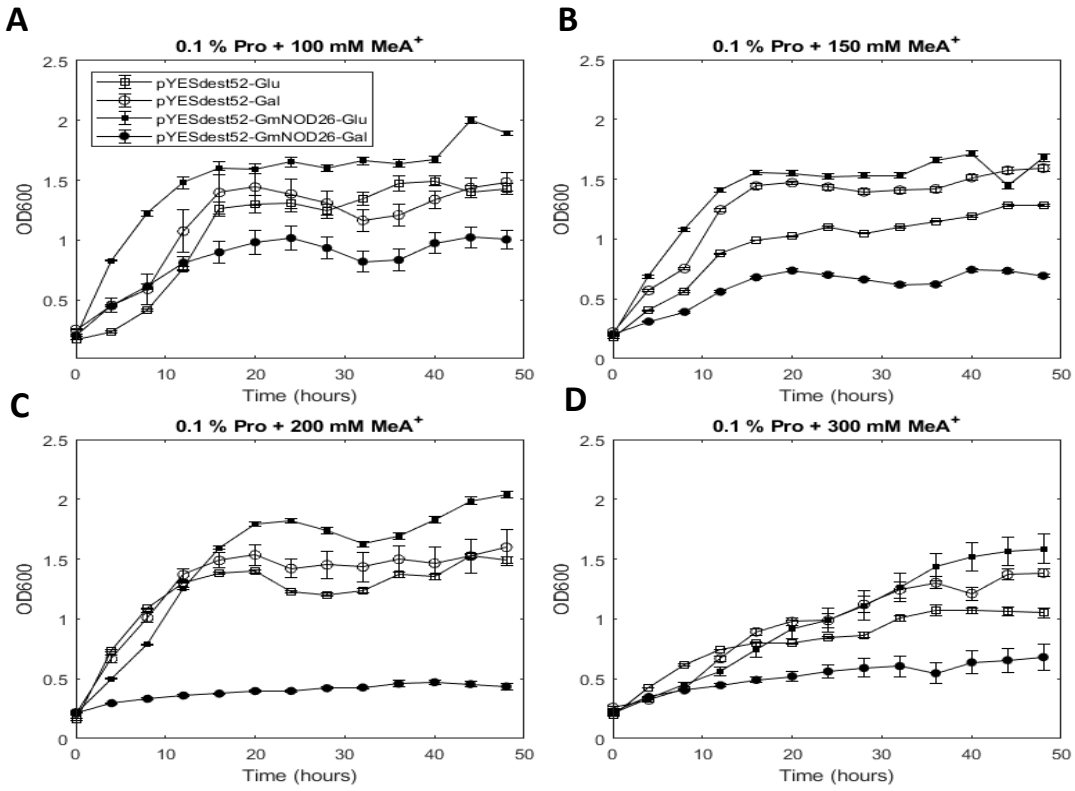

Figure 4.3 Optimising MeA^+ concentration for GmNOD26 complementation of the ammonium transport deficient yeast strain 26972c. GmNOD26 and empty pYESdest52 vector 26972c transformants were grown in 200 µL of Medium M (pH 6.0) containing either 2% (w/v) glucose or galactose and 01.% (w/v) proline with either (A) 100 mM, (B) 150 mM, (C) 200 mM or (D) 300 mM MeA^+ for 48 hours at 28°C with 200 RPM shaking (n=4).

4.2.1.4 The effect of liquid media pH

At acidic pH, when ammonia concentration was low, a clear complementation phenotype was observed in GmNOD26-expressing 26972c cells (Figure 4.4). However, when the pH was increased, growth of the empty vector 26972c cells increased, indicative of ammonia permeating across the yeast PM. During the linear phase of growth, between 20 and 32 hours, a greater growth rate of GmNOD26-expressing 26972c cells is observed when compared with empty-vector-expressing 26972c cells at pH 6.0 (0.0274 OD600/hour). At both pH 5.5 and 6.5 an increase in growth rate was observed, 0.0147 and 0.0061 OD600/hour respectively. But at pH 7.0 and 7.5 there was little change in the growth rate of GmNOD26-expressing 26972c cells compared to the empty vector, with observed changes in growth rate of 0 and 0.0013 OD600/hour respectively. This is shown by the fold changes at 24 and 48 hours (Figure 4.4f), where GmNOD26-expressing 26972c cells grown at pH 5.5 and 6.0 had the greatest change in OD600 compared to the empty vector grown at the specified pH.

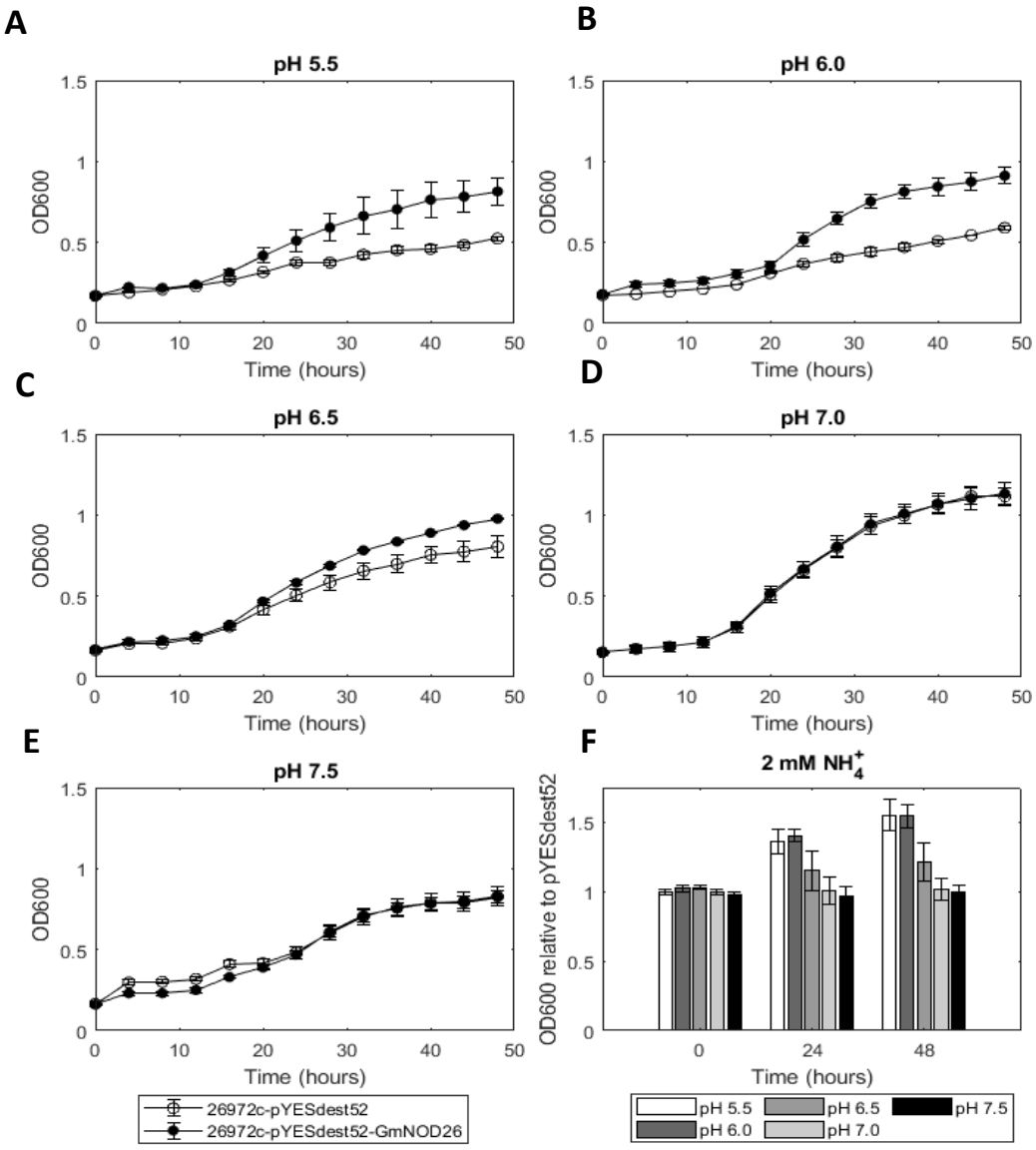

Figure 4.4 The effect of growth medium pH on GmNOD26 complementation of 26972c.

GmNOD26 and empty pYESdest52 vector 26972c transformants were grown in 200 µL of Medium M containing 2% (w/v) galactose and 1 mM NH_4^+ at pH (A) 5.5, (B) 6.0, (C) 6.5, (D) 7.0, or (E) 7.5 for 48 hours at 28°C with 200 RPM shaking (n=4). Growth of GmNOD26 expressing 26972c is shown relative to empty vector expressing 26972c yeast cells (F).

4.2.1.5 Optimised growth condition for GmNOD26-expressing 26972c cells

From the above results, the greatest resolution for GmNOD26 mediated complementation is when 26972c cells are grown at pH 6.0 (Figure 4.4). The optimal concentration to rescue the ammonium deficient growth phenotype was 2 mM NH_4^+, as this concentration was sufficient in supporting growth of GmNOD26-expressing 26972c cells without saturating the strain with free ammonia (Figure 4.2). However, 1 mM NH_4^+ was useful for detecting very small changes in selectivity of GmNOD26-expressing 26972c cells. For cytotoxicity experiments using MeA^+, a concentration of 200 mM was chosen as the complementation is clear and cytotoxicity is not observed in the empty vector cells (Figure 4.3). However, despite optimising the conditions to favour ammonium transport, results need to be interpreted with caution because GmNOD26 can transport ammonia as well (Hwang et al. 2010).

Under the optimised growth conditions, yeast cells expressing GmNOD26 had increased growth on solid medium at limiting NH_4^+ (2 mM). This trend was not observed when proline was provided as the sole nitrogen source, but growth was inhibited in the presence of 200 mM MeA^+ (Figure 4.5a). This difference in growth was more pronounced when cells were grown in liquid cultures where GmNOD26 clearly increased the growth rate (m = 0.0515 OD600/hour) of 26972c cells relative to the empty vector control (m = 0.0356 OD600/hour) under limiting NH_4^+ (Figure 4.5b). This was reversed when NH_4^+ was replaced with its toxic analog MeA^+, where GmNOD26-expressing 26972c cells displayed increased toxicity compared with the empty vector control (Figure 4.5c).

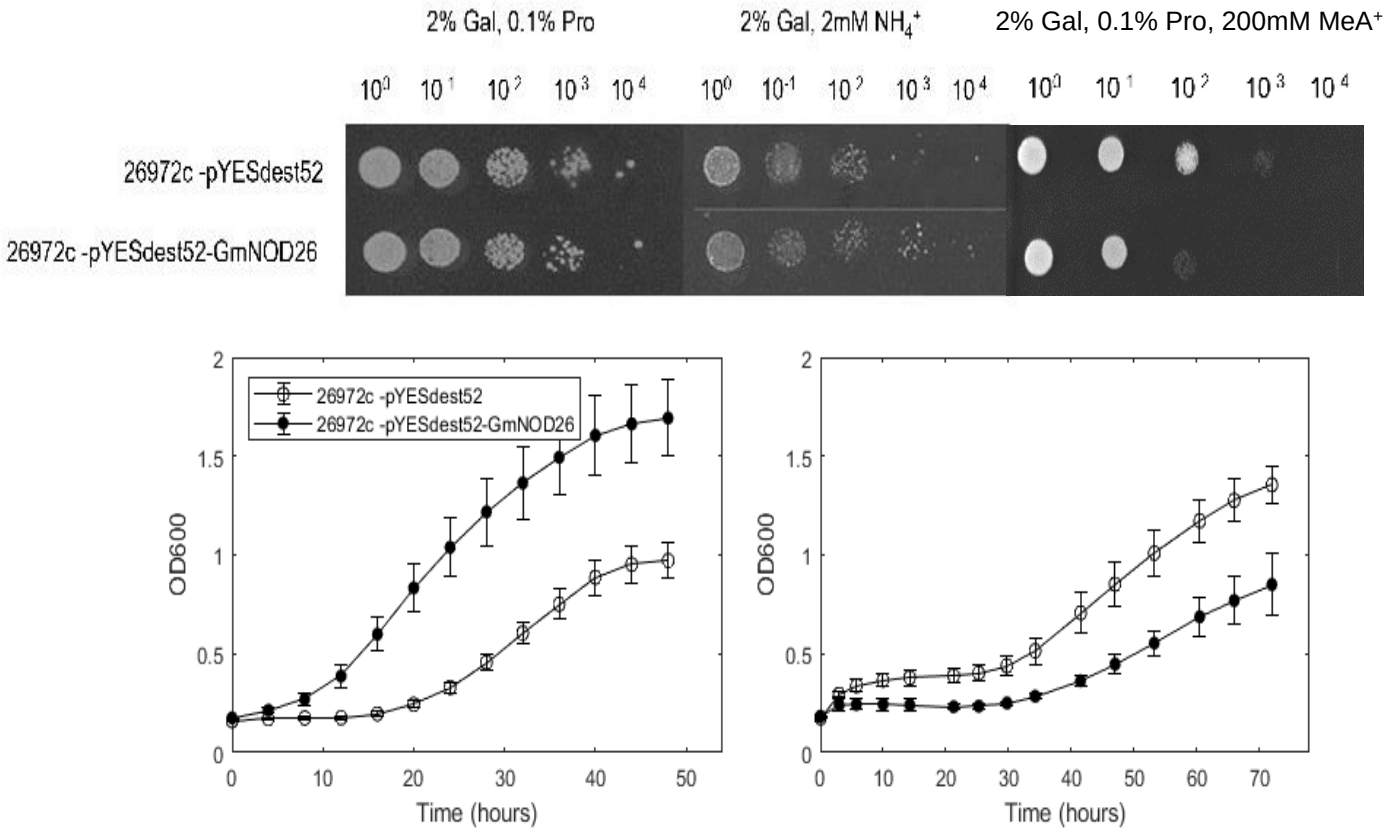

Figure 4.5 Functional complementation of the ammonium transport deficient yeast strain 26972c with GmNOD26. (A) The ammonium transport deficient yeast strain 26972c containing the empty vector and GmNOD26 expressing pYESdest52 vectors were spotted onto Medium M plates containing 2% (w/v) Galactose (Gal) and either 0.1% (w/v) proline (Pro); or 2 mM NH_4^+; or 0.1% (w/v) pro and 200 mM MeA^+ at pH 6.0. Growth curves of GmNOD26 and empty pYESdest52 vector 26972c transformants in Medium M containing 2% (w/v) galactose and either (B) 1 mM NH_4^+, or (C) 0.1% (w/v) proline and 200 mM of cytotoxic MeA_+ at pH 6.0 (n=6).

4.2.1.6 Phosphomemetics of GmNOD26 serine 262 in 26972c cells

The growth of phosphomimic GmNOD26-expressing 26972c cells was similar to the Wt protein (Figure 4.6), but there was a notable change in the OD600 of $GmNOD26^{S262A}$-expressing 26972c cells after 48 hours in limiting NH_4^+ (Figure 4.6c/d). $GmNOD26^{S262A}$ mimics the unphosphorylated serine state and enhanced the rescue phenotype when compared to Wt or phosphorylated $GmNOD26^{S262D}$, this was significant for Wt but not $GmNOD26^{S262D}$. This trend was not observed when grown in the presence of MeA^+ (Figure 4.6), although the cytotoxicity was suboptimum when compared to previous experiments (Figure 4.5). There was no notable change in the growth of any cultures when proline was provided as the nitrogen source (Figure 4.6).

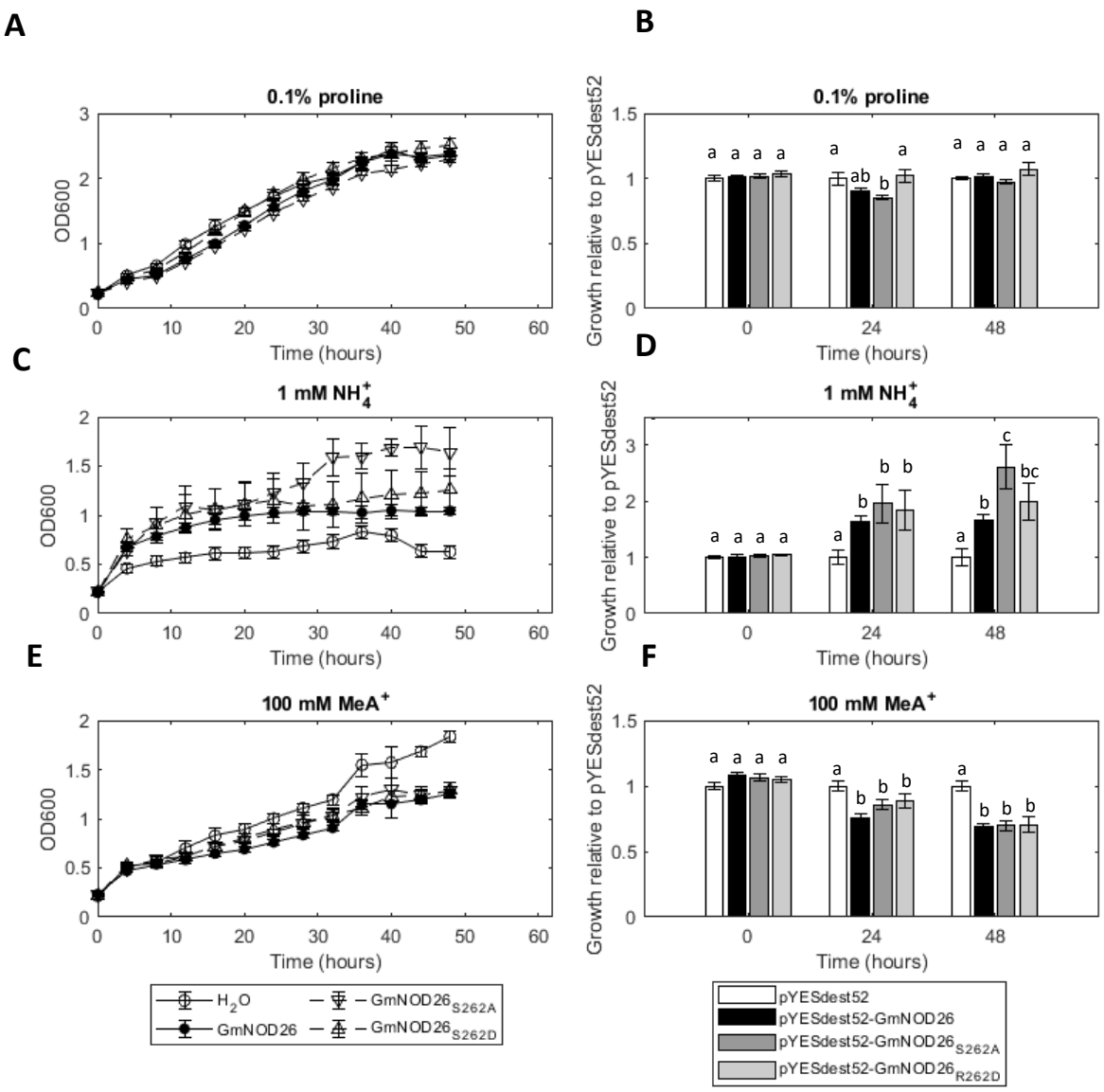

Figure 4.6 Phosphomemtic effect on functional complementation of the ammonium transport deficient yeast strain 26972c with GmNOD26. The ammonium transport deficient yeast strain 26972c containing the empty; GmNOD26; GmNOD26$_{S262A}$; or GmNOD26 $_{S262D}$ expressing pYESdest52 vectors were grown in 200 µL of Medium M (pH 6.0) containing 2% (w/v) galactose with either: 0.1% (w/v) proline (Pro) (A/B); 1 mM NH_4^+ (C/D); or 100 mM MeA^+ (E/F) (n=6). Subscripts depict significance within a timepoint according to Duncan's Post Hoc.

4.2.1.7 Loop D regulates GmNOD26-mediated rescue of 26972c cells on low ammonium

Loop D mutants which alter ion channel activity of GmNOD26 (see 3.2.4) were expressed in 26972c cells and reveal that GmNOD26-mediated ammonium rescue was abolished (Figure 4.7). When empty vector control, Wt, D177N and R179N mutants were grown with proline as the sole nitrogen source, there was little change to the growth rate, but both mutants grew to a greater OD600 (Figure 4.7a/b). When grown under limiting NH_4^+, only Wt GmNOD26-expressing 26972c cells were able to rescue growth (Figure 4.7c/d). Mutation of D177N displayed minimal MeA^+ toxicity at a level that was comparable to that to the empty vector control, but growth of R179N mutant was variable, with growth somewhat comparable to the toxic phenotype observed in Wt GmNOD26 (Figure 4.7e/f).

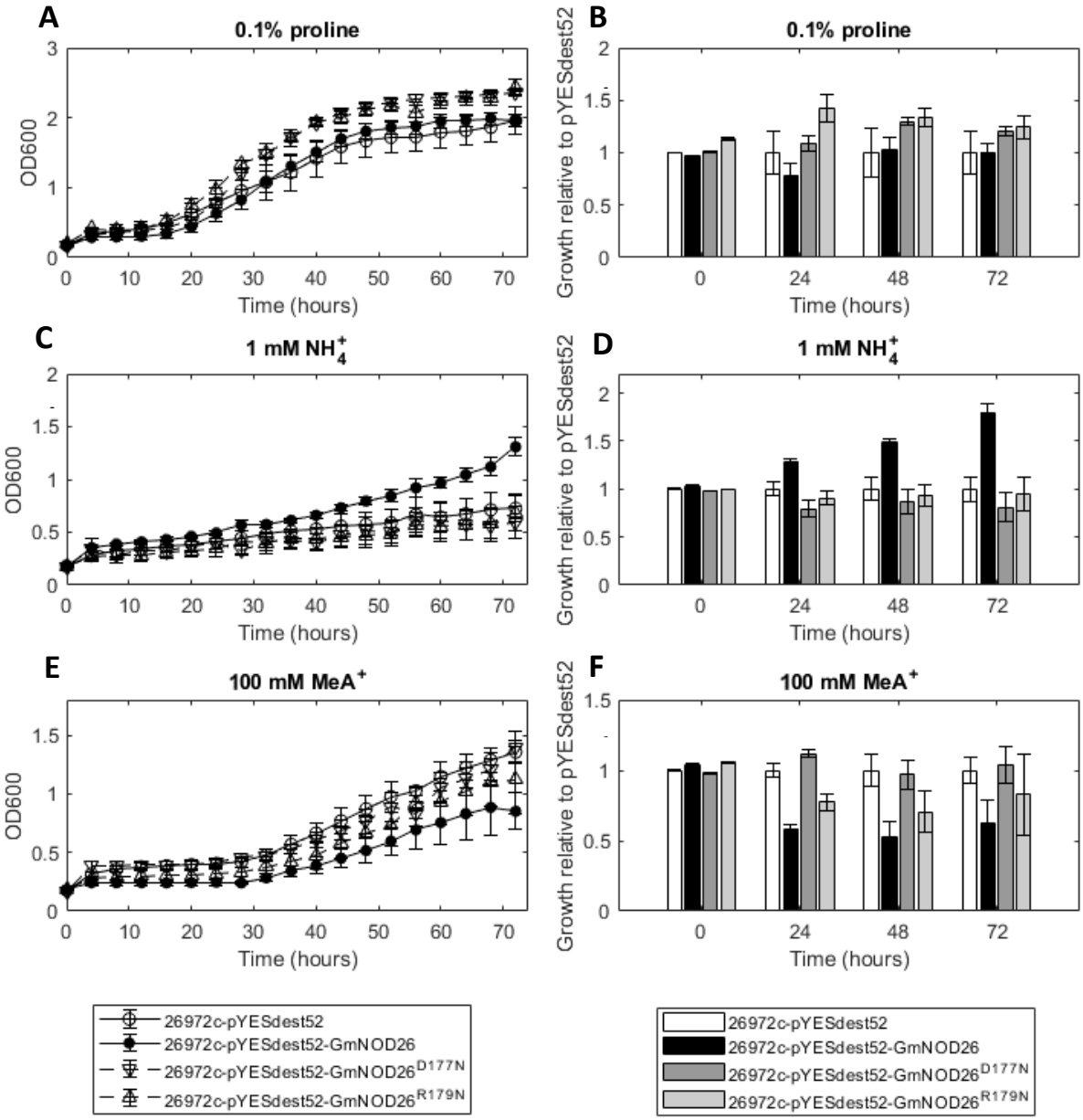

Figure 4.7 Mutations to Loop D reverse complementation of the ammonium transport deficient yeast strain 26972c by GmNOD26. The ammonium transport deficient yeast strain 26972c containing the empty; GmNOD26; $GmNOD26_{D192N}$; or $GmNOD26_{R194N}$ expressing pYESdest52 vectors were grown in 200 µL of Medium M (pH 6.0) containing 2% (w/v) galactose with either: 0.1% (w/v) proline (Pro) (A/B); 1 mM NH_4^+ (C/D); or 100 mM MeA^+ (E/F) (n=6). Subscripts depict significance within a timepoint according to Duncan's Post Hoc.

4.2.1.8 Other mutations also effect GmNOD26-mediated rescue of 26972c cells

HaBIB contains a glutamate in the first transmembrane domain that is conserved across all aquaporins and is important for regulation. When expressed in *X. laevis* oocytes, the mutant HaBIB^{E71N} does not display any typical ion conductivity (Yanochko and Yool 2002; Yanochko and Yool 2004). Interestingly, the analogous mutation in HsAPQ1 had no effect on the ion conductance, but blocked water transport (Yool 2007). The effect of this analogous mutation on ammonium complementation of GmNOD26^{E43N} -expressing 26972c cells was investigated (Figure 4.8). E43N mutation of GmNOD26 reversed complementation, with growth comparable to the empty vector when grown in 1 mM NH_4^+ or 100 mM MeA^+; although there was notable variation in the growth of Wt GmNOD26-expressing cells with proline as the sole nitrogen source after 24 hours (Figure 4.8).

TaTIP2;1 has been shown to facilitate the diffusion of ammonia and is classed as an aqua-ammonia-porins. HsAQP8 shares this feature, but HsAQP1 does not (Jahn et al. 2004). In TaTIP2;1 important regulatory roles have been suggested for I184 and G193 through their mutation to the corresponding amino acids in HsAQP1 (Jahn et al. 2004). In GmNOD26, these residues correspond to V197 and A206 (Appendix 7) and site-directed mutagenesis was performed to mimic the experiments, [V197H, A206C and V197H; A206C (Figure 4.8)]. The growth of cells expressing the V197H single mutation was far greater under control conditions with proline as the sole nitrogen source (Figure 4.8a/b). Under treatment conditions both single mutations, V197H and A206C, did not reverse GmNOD26 complementation of 26972c cells. Growth in 1 mM NH_4^+ was comparable to Wt GmNOD26 but significantly decreased after 48 hours (Figure 4.8c/d). However, the single mutations did abolish GmNOD26 sensitivity to MeA^+ (Figure 4.8e/f). The double mutant V197H; A206C reserved complementation by Wt GmNOD26, with growth significantly similar to the empty pYES-DEST52-expressing cells at all timepoints and sources of nitrogen tested (Figure 4.8).

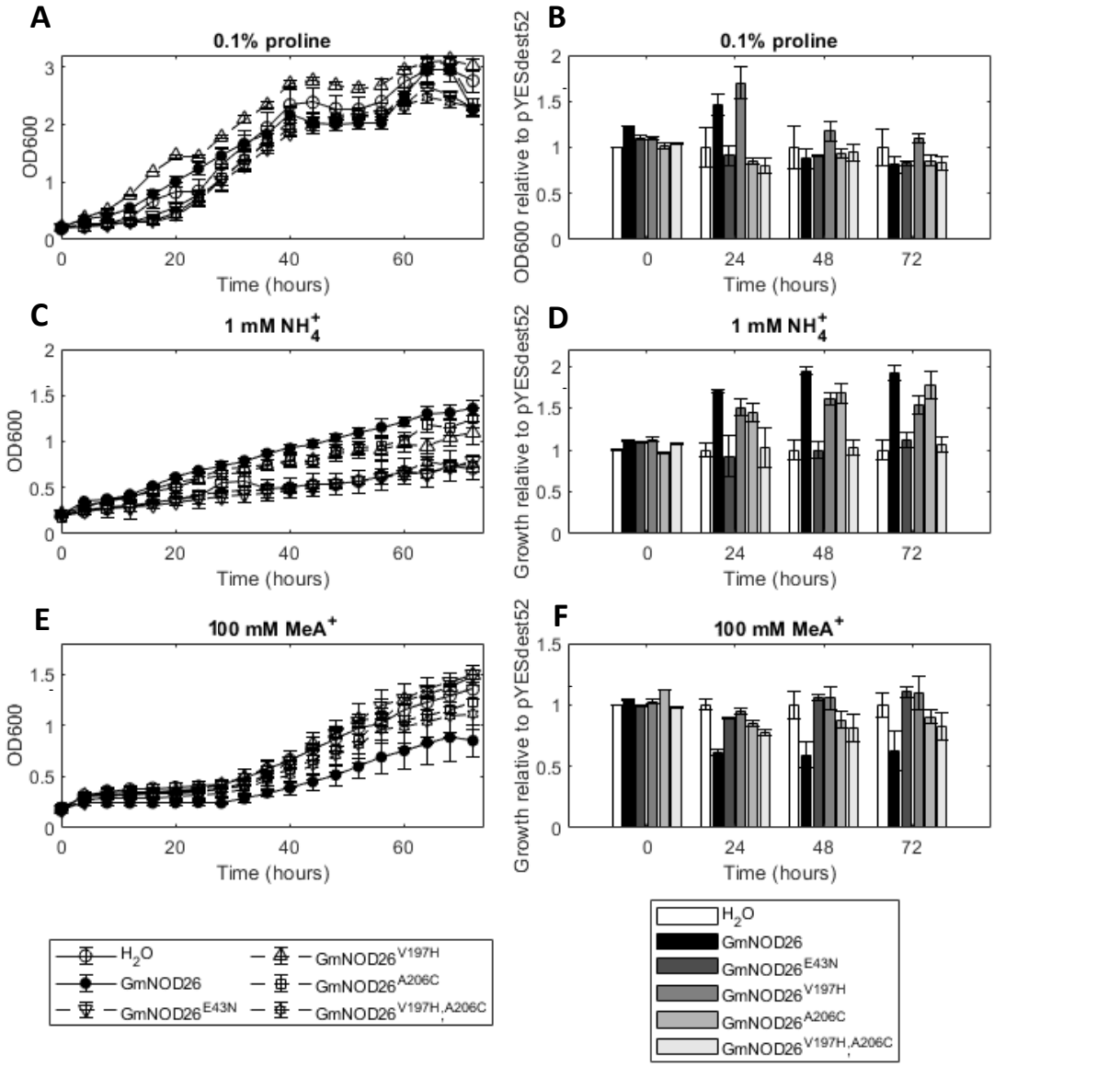

Figure 4.8 Other mutations to GmNOD26 effect complementation of the ammonium transport deficient yeast strain 26972c. The ammonium transport deficient yeast strain 26972c containing the empty; GmNOD26; GmNOD26$_{E43N}$; GmNOD26$_{V197H}$; or GmNOD26$_{A206C}$ expressing pYESdest52 vectors were grown in 200 µL of Medium M (pH 6.0) containing 2% (w/v) galactose with either: 0.1% (w/v) proline (Pro) (A/B); 1 mM NH_4^+ (C/D); or 100 mM MeA^+ (E/F) (n=6). Subscripts depict significance within a timepoint according to Duncan's Post Hoc.

4.2.2 Complementation of amino acid transport deficient *S. cerevisiae* strain

When proteinogenic amino acids or GABA are supplied as the sole nitrogen source, 22Δ10AA (MATα gap1-1 put4-1 uga4-1 can1::HisG lyp1- alp1::HisG hip1::HisG dip5::HisG gnp1Δ agp1Δ ura3-118) is unable to grow except for in the presence of Arg (Besnard et al. 2016). This strain is suitable to assess amino acid transport, in particular alanine, by GmNOD26 and was kindly provided by Guillaume Pilot (Virginia Tech). GmNOD26-expressing 22Δ10AA and parental 23344c cells were serially diluted and spotted onto YNB agar plates containing ammonium, or amino acids as the sole nitrogen source (Figure 4.9). In the presence of 3 mM ammonium, both strains containing the empty or GmNOD26-containing pYESdest52 plasmid grew uniformly on glucose or galactose media. When alanine was supplied as the sole nitrogen source, at 1 or 3 mM, there was minimal growth observed in the empty or GmNOD26-expressing 22Δ10AA cells on galactose media (Figure 4.9). Comparatively the parental strain 23344c grew uniformly as amino acid transport is not disrupted. It was noted that there was increased growth when glucose was the supplied sugar source for 22Δ10AA cells, but this was independent of the presence of GmNOD26 (Figure 4.9). The permeability of GmNOD26 to alanine was also investigated in *X. laevis* oocytes but swelling and content assays identified no significant transport (Appendix 9).

To investigate whether GmNOD26 could transport other amino acids relevant to symbiosis, 22Δ10AA cells were plated on media containing proline, GABA, glutamic acid or aspartic acid as the sole nitrogen source (Figure 4.10). GmNOD26 expression did not enhance growth of 22Δ10AA cells relative to the control, while 23344c cells grew uniformly (Figure 4.10).

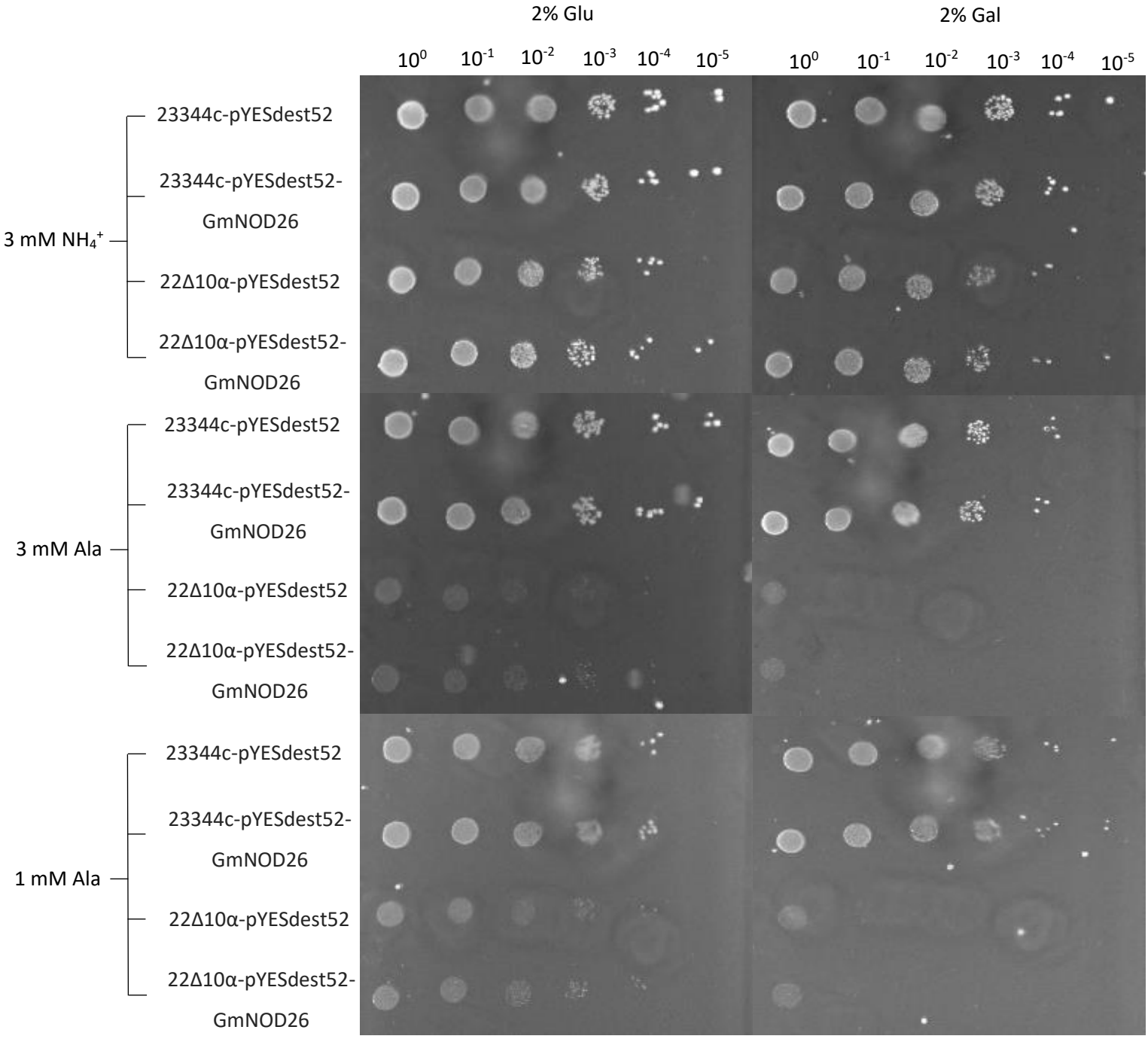

Figure 4.9 GmNOD26 does not complement alanine transport in 22Δ10AA. GmNOD26 and empty pYESdest52 vector 23344c and 22Δ10AA transformants were grown in YNB containing 2% (w/v) glucose and 0.1% (w/v) proline (pH 6.0) overnight, washed twice with sterile water and diluted to an OD600 of 10^0. Cultures were serially diluted 10-fold and 5 µL spotted onto solid YNB containing 2% (w/v) Glucose (Glu) or Galactose (Gal) and either ammonium or alanine as the sole nitrogen source.

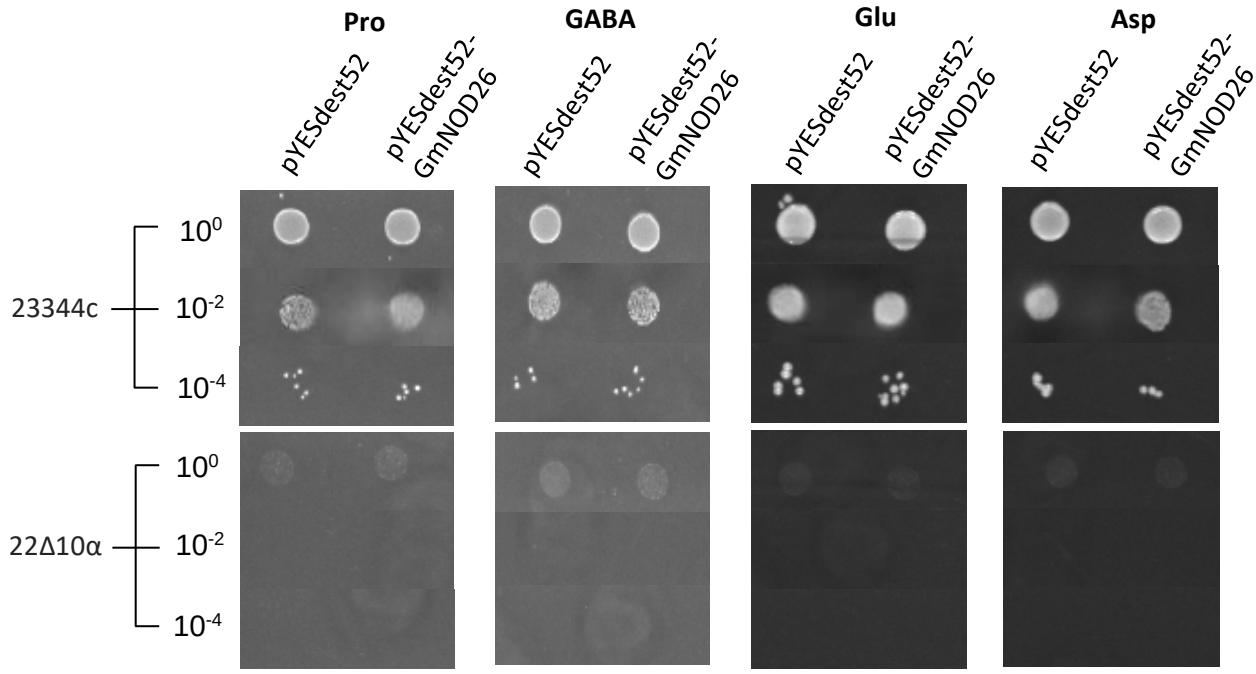

Figure 4.10. GmNOD26 does not transport amino acids. GmNOD26 and empty pYESdest52 vector 23344c and 22Δ10AA transformants were grown in YNB containing 2% (w/v) glucose and 0.1% (w/v) proline (pH 6.0) overnight, washed twice with sterile water and diluted to an OD600 of 10^0. Cultures were serially diluted 10-fold and 5 µL spotted onto solid YNB containing 2% (w/v) galactose with various amino acids as the sole nitrogen source.

4.3 Discussion

4.3.1 GmNOD26 rescues growth of 26972c at low pH

In the *X. laevis* oocyte model, it remains unclear whether ammonia permeable channels are inducing ionic currents through endogenous channel activation due to NH_3 movement, or if NH_4^+ is permeating the channel (Holm et al. 2005; Litman et al. 2009). This confuses the observations of GmNOD26 expressed in *X. laevis* oocytes, which display characteristics of the SM-NSCC channel, but under these conditions appears to be gated by protons. Given that characterisation of the SM-NSCC in patch-clamp experiments was only performed at pH 7.0 (Tyerman et al. 1995), another model must be used. To determine whether GmNOD26 could function at low pH, complementation of the ammonium transport deficient *S. cerevisiae* strains, 26972c and 31019b was performed. It was evident that there was an issue with the 31019b strain, as growth under limiting ammonium was observed (Appendix 8). It is possible that the obtained strain was incorrect or that overtime mutations had accumulated leading to growth on medium containing a low concentration of ammonium. The 26972c strain grew in a manner consistent with disruption in ammonium transport and was complemented by expression of GmNOD26 (Figure 4.5). This is consistent with ammonia/ammonium transport through GmNOD26.

In an attempt to distinguish between ammonia and ammonium transport through GmNOD26, the media pH was varied. Calculations indicate that in liquid media supplemented with 2 mM NH_4Cl at 28°C, there would be 0.445, 1.40, 4.42, 13.9 and 43.4 µM ammonia at pH 5.5, 6.0, 6.5, 7.0 and 7.5, respectively. Complementation was observed at low pH, suggesting that GmNOD26 can facilitate NH_4^+ transport when required (Figure 4.4). A class of so called aquaammoniaporins, which are permeable to both H_2O and NH_3, have been characterised including human AQP3, AQP4, AQP7, AQP8 and HsAQP9, as well as plant aquaporins TaTIP2;1, AtTIP2;1, AtTIP2;3 and GmNOD26 (Jahn et al. 2004; Holm et al. 2005; Dynowski et al. 2008; Hwang et al. 2010; Assentoft et al. 2016). Interestingly RnAQP1 is not permeable to ammonia but point mutations to the aromatic/arginine region can facilitate this movement, suggesting that pore constriction acts as a major selectivity filter (Beitz et al. 2006). Molecular dynamic modelling of AtTIP2;1 suggests that NH_4^+ accumulates at the surface of the protein, but spontaneous permeation events only occur through the monomeric pore as NH_3 (Kirscht et al. 2016). They suggest that NH_4^+ may be deprotonated at the proteins surface to enhance NH_3 transport, this model fits with NH_3-gated NH_4^+ permeation of TaTIP2;1 proposed by Holm et al. (2005) but does not take into consideration the possibility of NH_4^+ permeating the central tetrameric pore, as is shown for other monovalent cations (see chapter 3).

4.3.2 Mutations to GmNOD26 alter 26972c rescue

4.3.2.1 Phosphorylation effect

Previously I (Chapter 3) and other studies (Lee et al. 1995; Guenther et al. 2003) have demonstrated that phosphorylation mimics of S262 alters the transport properties of GmNOD26. This work has been limited to *X. laevis* oocytes and lipid bilayers, for the first time I investigate the effect this has on the replication of *S. cerevisiae* 26972c cells. Growth of the phosphorylation mimics appeared to be similar to the Wt GmNOD26 protein expressed in 26972c, but there was a significant increase in the OD600 of the phosphonull mutant S262A after 48 hours of growth in limiting NH_4^+ (Figure 4.6). This trend was not observed when NH_4^+ was replaced with MeA^+. Although S262 has been shown to be the only targeted phosphorylation site in soybean nodules (Weaver and Roberts 1992), *S. cerevisiae* contain over 110 serine/threonine protein kinases (Brinkworth et al. 2006), and it is highly likely that alternative sites are being phosphorylated *in vivo*. According to NetPhosYeast-1.0 (Ingrell et al. 2007), which predicts the phosphorylation targets of *S. cerevisiae* protein kinases, there are nine serine targets for the GmNOD26 protein sequence. When expressed in *X. laevis* oocytes, $GmNOD26^{S262A}$ displays increased ion conductivity and decreased water permeability ((Lee et al. 1995); Chapter 3), it is unclear what effect these alternative targets may have on the transport properties of GmNOD26, but may confuse the data obtained from specific phosphomimetics.

4.3.2.2 Loop D regulates ammonia/ammonium transport

Mutations to the charged residues of the GmNOD26 Loop D region shifted the reversal potential and reduced the ion conductivity of expressing *X. laevis* oocytes in sodium testing solution (see chapter 3). The important regulatory function of Loop has been demonstrated in both HsAPQ1 and SoPIP2;1, although through differing mechanisms. In SoPIP2;1, calcium binding to the N-terminal region of the protein leads to an interaction with a conserved histidine in the Loop D of PIPs is thought to stabilise the closed monomeric pore of the channel (Törnroth-Horsefield et al. 2006), but this histidine is not present in the Loop D region of GmNOD26. The functional relevance of this mechanism has not been explored in PIPs, although AtPIP2;1 and HvPIP2;8 have been shown to be ion conducting aquaporins gated by divalent cations (Byrt et al. 2017; Tran et al. 2020). As previously discussed, HsAQP1 requires cGMP binding for ion channel activation (Boassa and Yool 2002), through molecular dynamics simulations this binding has been shown to be to the Loop D and facilitate an outward motion of the region, opening the central tetrameric pore (Yu et al. 2006). This was confirmed experimentally through site-directed mutagenesis (Yu et al. 2006) and through inhibition studies with AQB011 (Kourghi et al. 2018a) both of which target the Loop D region of HsAQP1 and result in impaired ion conductance.

To investigate if these mutations effected ammonia/ammonium transport, or reflects a more general gating of ion conductance, GmNOD26 D177N and R179N mutants were expressed in *S. cerevisiae* 26972c cells. Mutations to Loop D were shown to prevent the ability of GmNOD26 to rescue growth of 26972c cells on low ammonium (Figure 4.7), taken together with electrophysiological data provides strong evidence that NH_4^+ may permeable the channel. Surprisingly the D177N mutant did not display symptoms of MeA^+ toxicity differing from the empty vector control, it is unclear why the response to MeA^+ and NH_4^+ would differ. Given that ammonium ions are smaller in nature that methylammonium ions, it would be expected that if NH_4^+ could not permeate then neither should MeA^+. The observed effect may be artefact caused by comparing a low concentration of NH_4^+ to a high concentration of MeA^+, as dissociation of ions may not be equivalent. The data taken together still suggest that mutations to Loop D alter ammonium permeation through GmNOD26. While Loop D mutants successfully localised to the PM of *X. laevis* oocytes (Figure 3.8), caution must be taken when interpretating these mutations in 26972c, as structural changes may influence expression or trafficking of the protein to the PM of *S. cerevisiae.* Similar protein tagging techniques should be employed to confirm successful incorporation to the *S. cerevisiae* PM.

4.3.2.3 4.4.2.3 Other mutations disrupt ammonia/ammonium transport

The MIP family contains a highly conserved glutamate residue in the first transmembrane domain (M1) (Reizer et al. 1993), it is important in maintaining structural integrity of the channel protein though interaction with a histidine residue near M2 (Ren et al. 2001). In HsAQP10 protonation of this histidine residue causes interaction with the conserved glutamate residue and leads to structural rearrangements that widen the monomeric pore to facilitate glycerol permeation (Gotfryd et al. 2018). Mutation of the M1 glutamate to asparagine in the ion-conducting aquaporins HaBIB or HsAQP1 revealed differences in the molecular basis of the ion permeation. $HaBIB^{E71N}$ does not display any typical ion conductivity (Yanochko and Yool 2002; Yanochko and Yool 2004), while the analogous mutation in HsAPQ1 only affected water transport (Yool 2007). The analogous mutant, $GmNOD26^{E43N}$, was expressed in *S. cerevisiae* 26972c cells and behaved in a manner consistent with the empty vector control (Figure 4.8). This suggested that the rescue phenotype was lost, and $GmNOD26^{E43N}$ was unable to facilitate the transport of ammonia/ammonium. In future work, this mutant should be expressed in *X. laevis* oocytes to determine if this mutation is affecting the structure of the monomeric or central tetrameric pore. This would give us a greater understanding of the pathway of ammonia/ammonium transport through GmNOD26.

A subclass of aqua-ammonia-porins, which include soybean GmNOD26, wheat TaTIP2;1 and human HsAQP8, have been described. The important regulatory roles of I184 and G193 have been established through mutation in TaTIP2;1, in which the double mutation which I184H and G193C abolished ammonia transport through the channel (Jahn et al. 2004). Interestingly, when grown on solid medium there was no apparent disruption in the ammonia permeability of TaTIP2;1 by either single mutation. In an attempt to mutate GmNOD26 from an aqua-ammonia-porin into a more traditional water transporting aquaporin such as HsAQP1, V197H, A206C and V197H; A206C mutations were imposed. When grown on medium supplemented with NH_4^+ as the sole nitrogen source, growth was comparable to Wt GmNOD26 but slightly reduced (Figure 4.8). In the double mutant V197H; A206C growth was reduced to a level observed in the empty vector control, indicating that NH_4^+ was no longer transported through GmNOD26. But there was a level of MeA^+ toxicity still present in this mutant. Interestingly MeA^+ toxicity was not observed in either of the single mutants (Figure 4.8), suggesting that the single mutations allowed a reduced passage of NH_4^+, but completely blocked MeA^+. Based on homology modelling and crystalline structures of wheat and *Arabidopsis* TIP2;1 it has been proposed that I184 and G193 allow for a widening on the monomeric water pore that facilitates the movement of ammonia in aqua-ammonia-porins, mutation to the corresponding residues in HsAQP1 restricts this pore resulting in a loss of ammonia transport (Jahn et al. 2004; Kirscht et al. 2016). It is possible that the single mutations in this study, V197H or A206C, may cause a reduction in the monomeric pore diameter that completely blocks the larger MeA^+ cation from being transported but still allows some passage of NH_4^+, as MeA^+ contains a carbon group and two extra hydrogen molecules. Homology modelling should be performed to assess for alterations in the monomeric pore diameter of GmNOD26 mutants.

4.3.3 GmNOD26 facilitates ammonia and ammonium transport but is not permeable to amino acids

The relative contribution of NH_3 or NH_4^+ efflux from symbiosomes remains unclear but is dependent on the pH of the symbiosome space, resting potential of the SM and relative concentration gradient across compartments (Udvardi and Day 1990; Udvardi and Day 1997). Under optimal nitrogen fixing conditions, the symbiosome space would be highly acidic and the SM depolarised, these attributes would favour an efflux of NH_4^+ from the symbiosome space over NH_3. I have shown here that GmNOD26 is the likely pathway for ammonium efflux from symbiosomes, as it displays characteristics of the SM-NSCC (Chapter 3) and can complement ammonium transport deficiency at low pH (Figure 4.4). The docking of GS to GmNOD26 (Masalkar et al. 2010) is logical for NH_4^+ transport through the channel, as it would allow for rapid assimilation to glutamate (Robertson et al. 1975; Liaw et al. 1995) and ensure a favourable concentration gradient of NH_4^+ is maintained.

The observed channel mediated permeability of ammonia across the soybean SM (Niemietz and Tyerman 2000) has been attributed to GmNOD26 (Hwang et al. 2010). The pH of the symbiosome space has been correlated with functional symbiosis is *M. truncatula;* as bacteroids begin to senesce, the pH is rapidly increased (Pierre et al. 2013), likely due to a loss of H^+-ATPase activity which would result in hyperpolarisation of the SM (Udvardi and Day 1989; Rosendahl et al. 1992). Under these conditions the NSCC activity of the membrane would be impaired and NH_3 concentration would increase, favouring NH_3 transport through GmNOD26. The capacity of GmNOD26 to transport both ammonia and ammonium highlights is importance in nitrogen-fixing symbiosis, and this is reenforced through impaired symbiosis in CRISPR/Cas9-mediated NOD26 knockout of *M. truncatula* (Frare et al. 2022).

The relative contribution of amino acids as a fixed nitrogen product remains unclear, but supplying isolated pea and soybean symbiosomes with ^{14}C-malate indicates synthesis and secretion of amino acids across both the bacteroid and symbiosome membranes (Rosendahl et al. 1992). Of these amino acids, alanine production appears to be high (Allaway et al. 2000), excreted from N_2-fixing soybean nodule bacteroids (Waters et al. 1998) and permeable across the SM (Tyerman and Niemietz, unpublished data obtained from (Day et al. 2001b)). However, alanine dehydrogenase mutants in pea bacteroids, unable to synthesis alanine, had no apparent symbiotic phenotype (Allaway et al. 2000). This suggests that symbiosis can function efficiently with NH_3/NH_4^+ as the sole nitrogen source (Day et al. 2001b). Unpublished data by Tyerman and Niemietz reveals asymmetric alanine transport across the SM that is inhibited by mercury, possibly through GmNOD26 (Day et al. 2001b). I expressed GmNOD26 in the amino acid transport deficient *S. cerevisiae* strains 22Δ10AA to screen for amino acid transport via complementation. Expression of GmNOD26 did not enhance growth of 22Δ10AA cells relative to the control when alanine, or any other investigated amino acid was the sole nitrogen source (Figure 4.9/10). In contrast the parental strain, 23344c, which is permeable to amino acids grew uniformly. These data indicate that these amino acids were not transported by GmNOD26 and another protein is responsible for the asymmetric alanine transport reported in isolated soybean symbiosomes. A member of the major facilitator superfamily, GmNPF8.6 has been characterised to transport the tripeptides Ala-Ala-Ala (Mohd Noor 2016). It is not uncommon for members of this family to have a broad spectrum of transport substrates, AtPTR1 is permeable to a range di- and tripeptides, in addition to substrates lacking a peptide bond (Dietrich et al. 2004). There are also numerous members of the ABC superfamily identified through SM proteomic studies (Wienkoop and Saalbach 2003; Clarke et al. 2015; Luo et al. 2023) and are suitable candidates for amino acid export from symbiosomes. These candidates should be investigated in future work.

5 LjALMT1 is a redundant dicarboxylate transporter localised to the root vascular tissue

5.1 Introduction

Carbon uptake by symbiosomes is facilitated by a well characterised but unidentified dicarboxylate carrier. Early work using isolated symbiosomes showed that when malate and succinate were supplied as substrates, uptake rates were sufficient to support estimated nitrogen fixation *in vivo* (Price et al. 1987; Day et al. 1989). Udvardi et al. (1988) further elucidated that the true substrate for the SM-DC is monovalent dicarboxylate anions and calculated the K_m for malate and succinate to be 2 and 15 µM respectively, which would be saturated at physiological concentrations. The carrier has an apparent preference for malate, but also transports a range of other dicarboxylates, as indicated through competitive inhibition of malate uptake into isolated symbiosomes (Ou Yang et al. 1990). Further characterisation reveals that anion uptake by the symbiosome is affected by the rate of bacteroid respiration, energisation across the SM by its ATPase activity and phosphorylation of the carrier, likely by a calcium dependent protein kinase (Ou Yang et al. 1990; Udvardi et al. 1991).

The symbiosome is comparable of the vacuole in normal root cells, making tonoplast dicarboxylate transporters excellent candidates for the SM-DC (Mellor and Werner 1987). Due to the above characterised energetics of the system, the SM-DC essentially acts as an efflux protein, transporting malate out of the plant cytosol and therefore unlikely to complement the growth of dicarboxylate transport deficient *E. coli* strain (CBT315) through cDNA library screening. However as described in Chapter 1.6.1, there are two well characterised tonoplastic dicarboxylate transport families in plants, these are ALMT and tDT, and share many similar characteristics with the described SM-DC. The tonoplast provides extensive candidates for the SM-DC with the ALMT family providing strong candidates, as members of this family of dicarboxylate transporters have been shown to share several functional similarities with the SM-DC, including voltage-dependent gating and regulation by phosphorylation. Although Takanashi et al. (2016) did not identify a symbiosome localised ALMT, the scope of the study may have been insufficient in identifying all ALMT sequences in *L. japonicus* due to the genome coverage at the time. The tDT transport family is a reasonable candidate for the SM-DC due to characterised dicarboxylate transport but the mechanism is distinct, appearing to be antiport - primarily exchanging citrate with malate (Frei et al. 2018).

Proteomic studies on isolated SMs have identified several putative transporters on the SM, but no definitive candidates for the SM-DC (Saalbach et al. 2002; Wienkoop and Saalbach 2003; Clarke et al. 2015; Luo et al. 2023). Far broader transcriptomic data suggests that ALMT transcripts are expressed

in nodule tissues and enhanced in the nitrogen fixing zones (Takanashi et al. 2012; Roux et al. 2014). Here, through homology with the *Arabidopsis* orthologs, the ALMT and tDT gene families have been identified in *L. japonicus* and *M. truncatula*. Publicly available, tissue-specific, transcriptomics data was analysed to provide candidates for the SM-DC based on nodule-enriched expression of ALMT and tDT transcripts that were enhanced in the nitrogen fixing zones. The expression of these candidates in nodules were then confirmed through qRT-PCR prior to in *in vivo* localisation and functional characterisation.

5.2 Results

5.2.1 Identification of ALMT and tDT gene families in model legumes

In 2016, seven *L. japonicus* ALMT proteins were identified using the Kazusa Genome DataBase build 2.5 (Takanashi et al. 2016). The recently updated, high-quality, *L. japonicus* MG20 genome (Li et al. 2020) available through LOTUS BASE was used to identify 13 full-length *L. japonicus* ALMT protein sequences. This was achieved using *Arabidopsis* ALMT protein sequences as BLAST queries and filtering for the presence of Hidden Markov models using HMMER (see 2.10.1). Of the 13 identified *L. japonicus* ALMT protein sequences (Table 5.1), the seven previously characterised transcripts (Lj3g1v0471900.1, Lj1g1v0737300.1, Lj4g1v0452000.1, Lj2g1v0210400.1, Lj4g1v0188700.1, Lj2g1v0415400.1, Lj5g1v0165800.1) were identified along with six putative transcript sequences (Lj3g1v0182300.1, Lj5g1v0341200.1, Lj5g1v0199400.1, Lj5g1v0354000, Lj5g1v0353900, Lj1g1v0728500.1). Nomenclature was assigned through orthology with AtALMTs, with no *L. japonicus* ALMT proteins assigned as ALMT 3, 5, 6, 7, 11 or 14-like (Table 5.1). For most *LjALMT* sequences, the exon number was conserved with its *AtALMT* ortholog, with two exceptions, *LjALMT8* contained one extra, while *LjALMT9.1* contained one less exon. A similar approach was used to identify 16 *M. truncatula* ALMT sequences, but through the NCBI database. Here, no *M. truncatula* ALMT proteins were assigned as *ALMT 1, 3, 5, 6, 11, 13* or *14-like*, and the exon count was mostly conserved with exceptions to the *MtALMT8* subfamily, which contained one extra exon, *MtALMT9.1* with five extra exons and *MtALMT9.1* with one less exon (Table 5.1). These methods were also employed to identify two tDT proteins in both *L. japonicus* and *M. truncatula*, interestingly both model legumes contained twice the exon number of the *Arabidopsis* tDT, but overall protein length was similar to the 540 aa *Arabidopsis* protein (Table 5.2).

5.2.2 Transcriptomic expression of ALMT and tDT gene families in model legumes

To determine the tissue specific expression profile of the identified *ALMT* and *tDT* transcripts in *L. japonicus* and *M. truncatula,* RNA-seq data was analysed in five different tissues (nodule, root, stem, leaf and inflorescence) under symbiotic growth conditions and normalised as specified in 2.10.2. Nine of the 13 identified *LjALMT* and seven of the 16 *MtALMT* transcripts contained publicly available transcriptomics data, which is represented in Figure 5.1.

Of particular interest was nodule-specific expression, due to the possibility of identifying the SM-DC. *LjALMT1* (Lj3g1v0182300) displayed strong nodule-specific expression, along with the *M. truncatula* ortholog *MtALMT8.2* (MTR_2g087285) in this clade. Expression of another *M. truncatula* transcript,

MtALMT9.2 (MTR_6g084680), was enhanced in the nodules, but the *L. japonicus* ortholog *LjALMT9.2* (Lj2g1v0210400) in this clade was expressed across the stem, leaf and inflorescence tissue types (Figure 5.1). Analysis of the *M. truncatula* transcript using Symbimics (Roux et al.) revealed that both *MtALMT8.2* and *MtALMT9.2* contained expression in the nodule tissues, but only *MtALMT8.2* was specific to the nitrogen fixing regions (Appendix 10). The tDT orthologs in *L. japonicus* and *M. truncatula* were not expressed in the nodule tissues and disregarded as candidates for the SM-DC (Figure 5.2).

LjALMT10 (Lj5g1v0199400) was exclusively expressed in the root tissues, but the ortholog *MtALMT10.2* (MTR_1g077670) in this clade displayed a relatively equal distribution of transcript reads that may be enhanced in the nodules, this was not supported by Symbimics data (Appendix 10). Transcript expression of *MtALMT2* (MTR_2g087288) was similar to that of *MtALMT* 10.2, but there was no nodule transcript expression identified in Symbimics (Appendix 10). *LjALMT9.1* (Lj4g1v0452000), *LjALMT12.1* (Lj4g1v0188700) and *LjALMT12.4* (Lj5g1v0353900) transcript expression was predominant in the stem tissue, and this was supported by available transcript expression of *MtALMT12.2* (MTR_5g014310) and *MtALMT9.1* (MTR_8g104110) (Figure 5.1). In *L. japonicus LjALMT12.5* (Lj5g1v0165800) was expressed evenly across both the stem and leaf tissue, while *LjALMT8* (Lj1g1v0737300) expression was found to be predominantly in the inflorescence tissue, but no *M. truncatula* ortholog transcript data was available to support this. Transcript expression of *MtALMT12.4* (MTR_1g115175) displayed a relatively equal distribution of transcript reads with some enhanced in inflorescence expression, but no transcript data was available for the *L. japonicus* ortholog.

Table 5.1 Identification of ALMT proteins in two model legumes. *Arabidopsis* (At) protein sequences were obtained from Dreyer et al. (2012) and used as BLAST queries to identify *M. truncatula* (Mt) proteins using NCBI and *L. japonicus* (Lj) proteins using Lotus Base. The presence of Hidden Markov models (Dreyer et al. 2012) was identified using HMMER. Percentage identity was calculated using ClustalW (Larkin et al. 2007) and compared against the closest *Arabidopsis* ortholog. Novel LjALMT genes have been underlined.

Gene Name	Chromosome	Exon count (At)	Locus tag	Protein accession	Amino acid count	At ortholog (% identity)
LjALMT1	*Chr3*	*6 (6)*	*Lj3g1v0182300*	*Lj3g1v0182300.1*	*426*	*AtALMT1(44)*
LjALMT2	Chr3	6 (6)	Lj3g1v0471900	Lj3g1v0471900.1	473	AtALMT2 (50)
LjALMT4	*Chr5*	*6 (6)*	*Lj5g1v0341200*	*Lj5g1v0341200.1*	*593*	*AtALMT4 (56)*
LjALMT8	Chr1	6 (5)	Lj1g1v0737300	Lj1g1v0737300.1	480	AtALMT8 (52)
LjALMT9.1	Chr4	5 (6)	Lj4g1v0452000	Lj4g1v0452000.1	583	AtALMT9 (59)
LjALMT9.2	Chr2	6 (6)	Lj2g1v0210400	Lj2g1v0210400.1	600	AtALMT9 (57)
LjALMT10	*Chr5*	*6 (6)*	*Lj5g1v0199400*	*Lj5g1v0199400.1*	*484*	*AtALMT10 (46)*
LjALMT12.1	Chr4	6 (6)	Lj4g1v0188700	Lj4g1v0188700.1	537	AtALMT12 (61)
LjALMT12.2	Chr2	6 (6)	Lj2g1v0415400	Lj2g1v0415400.1	544	AtALMT12 (60)
LjALMT12.3	*Chr5*	*6 (6)*	*Lj5g1v0354000*	*Lj5g1v0354000.1*	*514*	*AtALMT12 (56)*
LjALMT12.4	*Chr5*	*6 (6)*	*Lj5g1v0353900*	*Lj5g1v0353900.1*	*494*	*AtALMT12 (55)*
LjALMT12.5	Chr5	6 (6)	Lj5g1v0165800	Lj5g1v0165800.1	465	AtALMT12 (34)
LjALMT13	*Chr1*	*6 (6)*	*Lj1g1v0728500*	*Lj1g1v0728500.1*	*447*	*AtALMT13 (35)*
MtALMT2	Chr2	6 (6)	MTR_2g087288	KEH38993.1	452	AtALMT2 (45)
MtALMT4	Chr1	6 (6)	MTR_1g111250	KEH44248.1	551	AtALMT4 (58)
MtALMT7	Chr4	6 (6)	MTR_4g051575	KEH29773.1	471	AtALMT7 (51)
MtALMT8.1	Chr7	6 (5)	MTR_7g106260	KEH24242.1	479	AtALMT8 (55)
MtALMT8.2	Chr2	6 (5)	MTR_2g087285	KEH38992.1	444	AtALMT8 (46)
MtALMT9.1	Chr8	11 (6)	MTR_8g104110	AET05317.1	578	AtALMT9 (59)
MtALMT9.2	Chr6	6 (6)	MTR_6g084680	KEH27049.1	599	AtALMT3 (56)
MtALMT9.3	Chr8	5 (6)	MTR_8g104130	AET05319.1	568	AtALMT9 (55)
MtALMT10.1	Chr1	6 (6)	MTR_1g077660	KEH42890.1	478	AtALMT10 (48)
MtALMT10.2	Chr1	6 (6)	MTR_1g077670	KEH42891.1	484	AtALMT10 (47)
MtALMT12.1	Chr4	6 (6)	MTR_4g098610	AES90828.1	534	AtALMT12 (61)
MtALMT12.2	Chr5	6 (6)	MTR_5g014310	AES94429.1	549	AtALMT12 (61)
MtALMT12.3	Chr4	6 (6)	MTR_4g098570	AES90824.1	534	AtALMT12 (60)
MtALMT12.4	Chr1	6 (6)	MTR_1g115175	KEH44440.1	532	AtALMT12 (55)
MtALMT12.5	Chr1	6 (6)	MTR_1g115140	KEH44433.1	536	AtALMT12 (53)
MtALMT12.6	Chr7	6 (6)	MTR_7g094770	KEH23744.1	442	AtALMT12 (34)

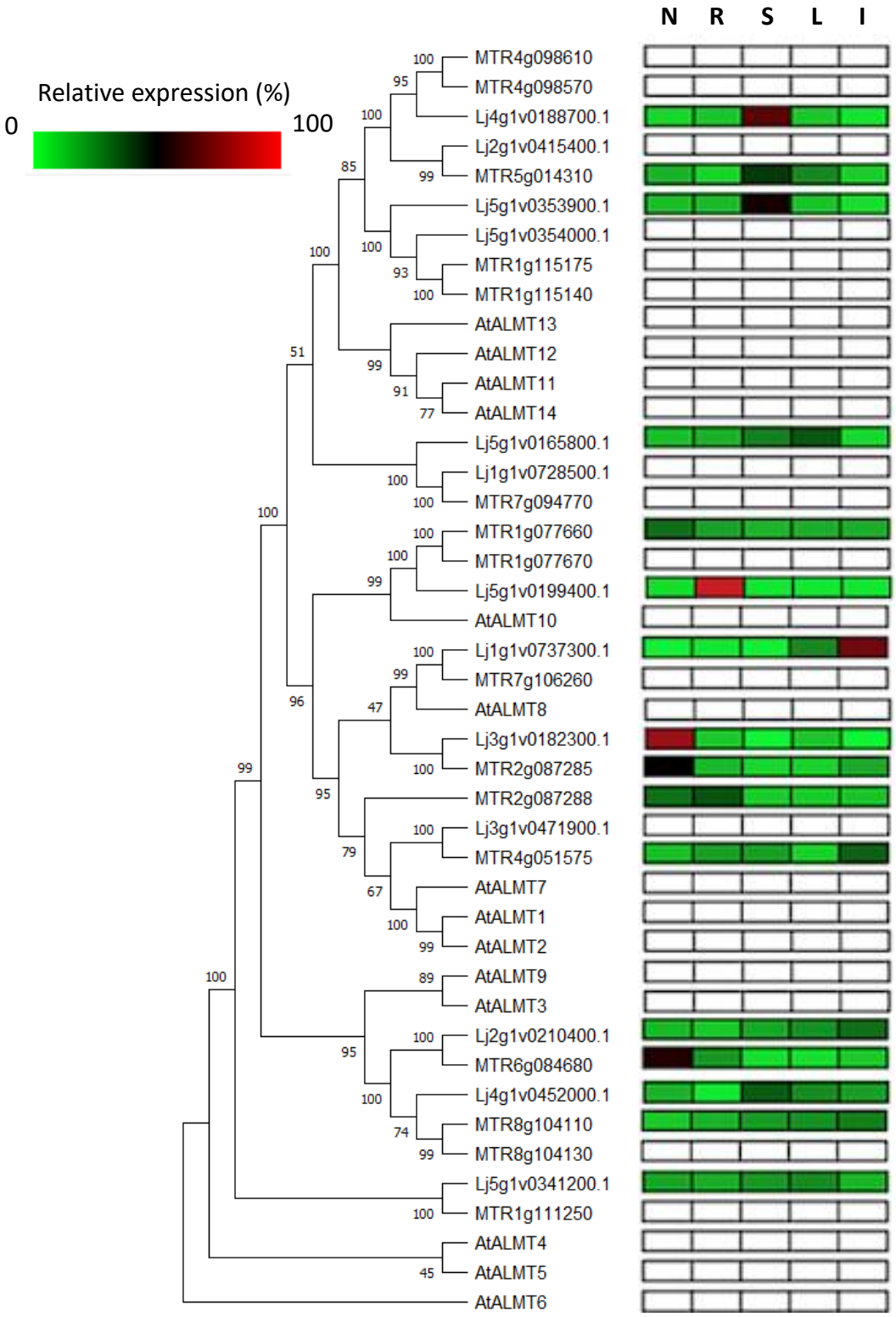

Figure 5.1 Evolution of ALMT family of two model legumes. ALMT amino acid sequences were aligned using Clustal (Larkin et al. 2007) and a maximum likelihood tree with 1000 bootstraps generated using MEGA X (Kumar et al. 2018). Publicly available transcriptomic data was obtained from Genevestigator or Lotus Base and normalised against the maximum expression. This information was used to generate a heatmap and assigned to respective protein, white boxes represent unavailable transcriptomic data. N = nodule, R = root, S = stem, L = leaf, I = inflorescence.

Table 5.2 Identification of tDT proteins in two model legumes. *Arabidopsis* (At) protein sequence was obtained from Emmerlich et al. (2003) and used as BLAST queries to identify *L. japonicus* (Lj) proteins using Lotus Base and *M. truncatula* (Mt) proteins using NCBI. Percentage identity was calculated using ClustalW (Larkin et al. 2007) and compared against the closest *Arabidopsis* ortholog.

Gene Name	Chromosome	Exon count (At)	Locus tag	Protein accession	Amino acid count	At ortholog (% identity)
LjtDT.1	Chr6	6 (3)	Lj6g1v0286400	Lj6g1v0286400.1	534	AttDT (61)
LjtDT.2	Chr4	6 (3)	Lj4g1v0008300	Lj4g1v0008300.1	549	AttDT (62)
MttDT.1	Chr4	6 (3)	MTR_4g133230	AES92729.1	553	AttDT (61)
MttDT.2	Chr2	6 (3)	MTR_2g026030	AES64491.2	528	AttDT (61)

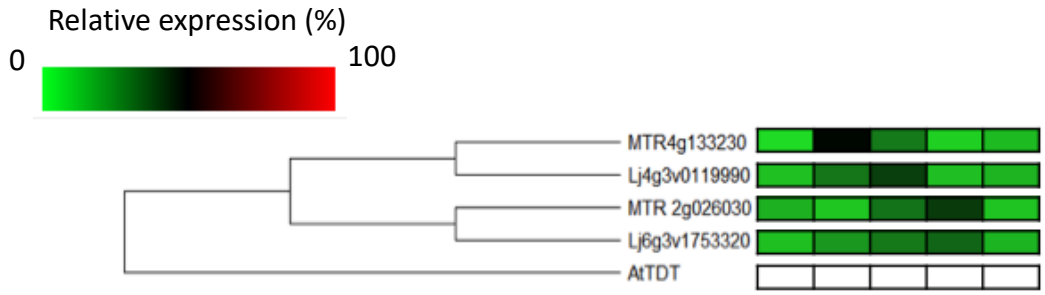

Figure 5.2 Evolution of tDT family of two model legumes. tDT amino acid sequences were aligned using Clustal (Larkin et al. 2007) and a maximum likelihood tree with 1000 bootstraps generated using MEGA X (Kumar et al. 2018). Publicly available transcriptomic data was obtained from Genevestigator or Lotus Base and normalised against the maximum expression. This information was used to generate a heatmap and assigned to respective protein, white boxes represent unavailable transcriptomic data. N = nodule, R = root, S = stem, L = leaf, I = inflorescence.

5.2.3 Growth of Wt *L. japonicus* under symbiotic and non-symbiotic conditions

To gain an understanding of plant development under symbiotic and non-symbiotic conditions, Wt *L. japonicus* were grown under high and low nitrogen conditions in the presence or absence (mock) of *M. loti*. Wt *L. japonicus* were grown for seven days (as specified in 2.3) prior to treatment application. Root and shoot tissues were collected at zero, seven, 14, 21 and 35 days after inoculation (DAI) for biomass quantification. At initial treatment application, zero, or seven DAI, root and shoot biomass was not significant between the four groups (Figure 5.3, Table 5.3/4). For shoot, but not root biomass, the treatment groups were split into 14 DAI, with *M. loti* inoculated plants grown in sufficient nitrogen (2 mM NH_4NO_3) having the greatest shoot biomass (Figure 5.3). This trend continued for the remaining timepoints and was significant for 14, 21 and 35 DAI (Table 5.3). There was similar shoot biomass for *M. loti* inoculated *L. japonicus* plants grown in limiting (10 µM KNO_3) nitrogen and mock treated *L. japonicus* plants containing sufficient (2 mM NH_4NH_3) nitrogen, these measurements were found to be significantly similar 21 and 35 DAI (Figure 5.3, Table 5.3). Mock treated *L. japonicus* plants grown under limiting nitrogen displayed symptoms of stunted growth and did not increase in shoot biomass during the course of the experiment (Figure 5.3).

Changes in root biomass followed a different trend to that of shoot biomass (Figure 5.3). At 21 DAI the mock and *M. loti* treatments split, with significantly more root biomass found in *M. loti* treatments (Figure 5.3, Table 5.4). The *M. loti* inoculated *L. japonicus* plants grown in limiting (10 µM KNO_3) nitrogen developed the greatest root biomass, but this data was variable; at 35 DAI there was a significant split between the limiting and sufficient nitrogen treatments (Figure 5.3, Table 5.4). The root biomass of mock treated *L. japonicus* plants was significantly similar at all timepoints independent of nitrogen application (Figure 5.3, Table 5.4).

Growth studies were repeated under symbiotic (limiting nitrogen and *M. loti* inoculated) or non-symbiotic (sufficient nitrogen with mock inoculation) conditions given that similar increases in biomass were detected under these conditions (Figure 5.4). Samples were collected every week for three weeks with root and shoot tissues used for biomass and qRT-PCR (2.5.2) analysis. Tissue samples from shoot, root and nodule tissues were collected for qRT-PCR 21 DAI under symbiotic conditions. Once again, the changes in root and shoot biomass followed a similar trend, with a significant increase in root biomass detected 21 DAI under symbiotic conditions (Figure 5.5). The typical phenotypic appearance of these plants is visualised in Figure 5.5, with no apparent nutrient limitations to growth, and nodulation only present on inoculated plants from 14 DAI.

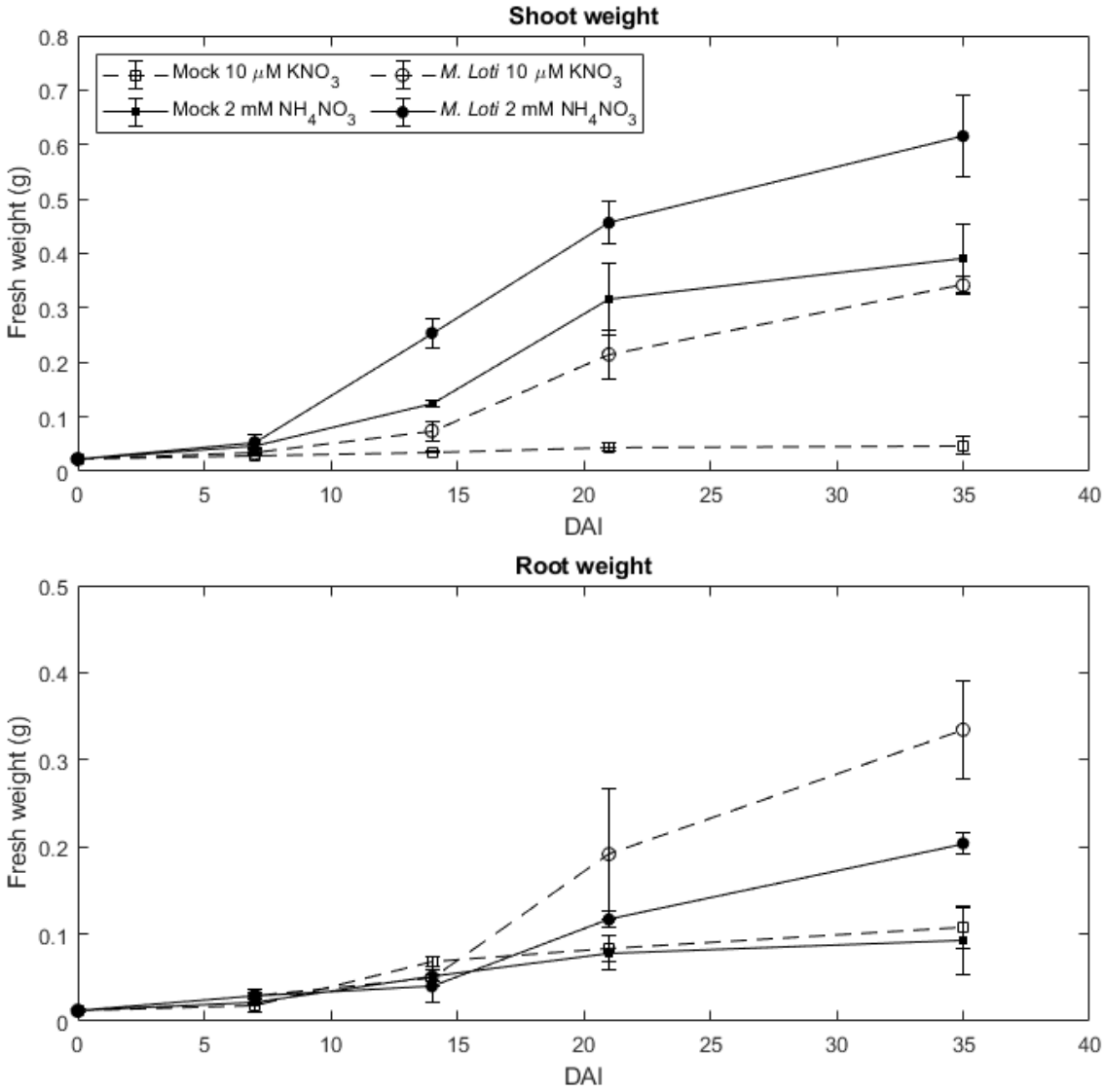

Figure 5.3 The effect of nitrogen application and/or *M. loti* inoculation on Wt *L. japonicus* growth. Seven-day-old *L. japonicus* (MG20) were grown under limiting or optimal nitrogen conditions for 35 days after inoculation (DAI) with *M. loti* or sterile MilliQ water. Root and shoot biomass was harvested at zero, seven, 14, 21 or 35 days after treatment application. For harvests: zero, seven and 14 DAI, six plants were pooled in each replicate; for 21 and 35 DAI two plants were pooled in each replicate (n = 4).

Table 5.3 Significance of nitrogen application and/or *M. loti* inoculation on Wt *L. japonicus* shoot biomass over time according to Duncan's post hoc. Different subscripts indicate a significant difference between groups at a particular timepoint ($\rho < 0.05$) (n = 4).

Nitrogen treatment	Inoculation treatment	Days after inoculation				
		0	**7**	**14**	**21**	**35**
10 µM KNO_3	**Mock**	a	a	a	a	a
	M. loti	a	a	b	b	b
2 mM NH_4NH_3	**Mock**	a	a	c	b	b
	M. loti	a	a	d	c	c

Table 5.4 Significance of nitrogen application and/or *M. loti* inoculation on Wt *L. japonicus* root biomass over time according to Duncan's post hoc. Different subscripts indicate a significant difference between groups at a particular timepoint ($\rho < 0.05$) (n = 4).

Nitrogen treatment	Inoculation treatment	Days after inoculation				
		0	**7**	**14**	**21**	**35**
10 µM KNO_3	**Mock**	a	a	a	a	a
	M. loti	a	a	a	b	c
2 mM NH_4NH_3	**Mock**	a	a	a	a	a
	M. loti	a	a	a	b	b

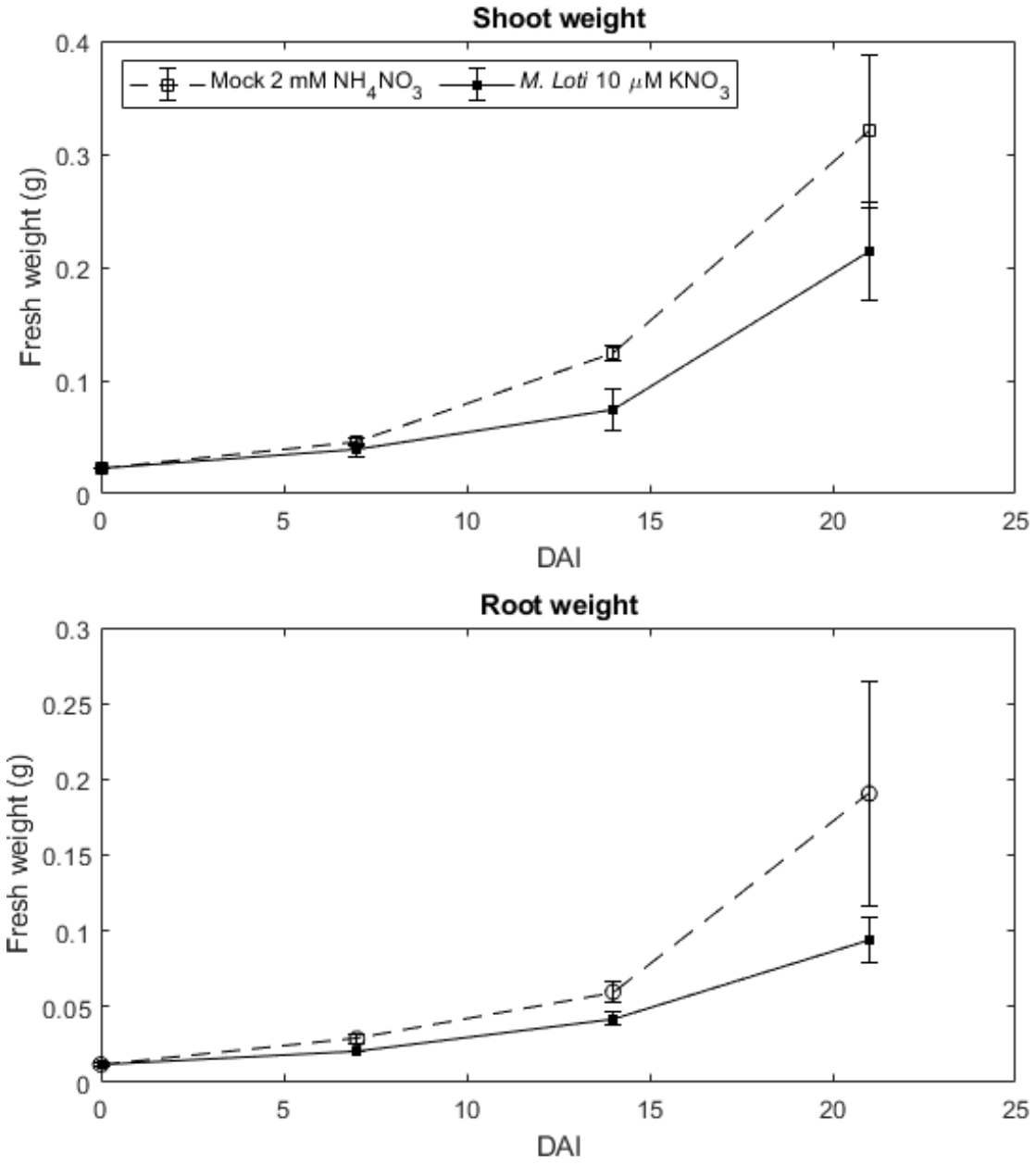

Figure 5.4 Growth of Wt *L. japonicus* plants under symbiotic or nitrogen sufficient conditions. Seven-day-old *L. japonicus* (MG20) were either inoculated with *M. loti* and grown under limiting nitrogen (*M. loti*) or inoculated with sterile MilliQ water and grown under sufficient nitrogen (mock) for 21 days. Root and shoot biomass were harvested at zero, seven, 14 or 21 days after treatment application with tissue snap frozen for RNA extraction. For harvests: zero and seven DAI six plants were pooled in each replicate; for 14 DAI and 21 DAI three plants were pooled in each replicate (n = 4).

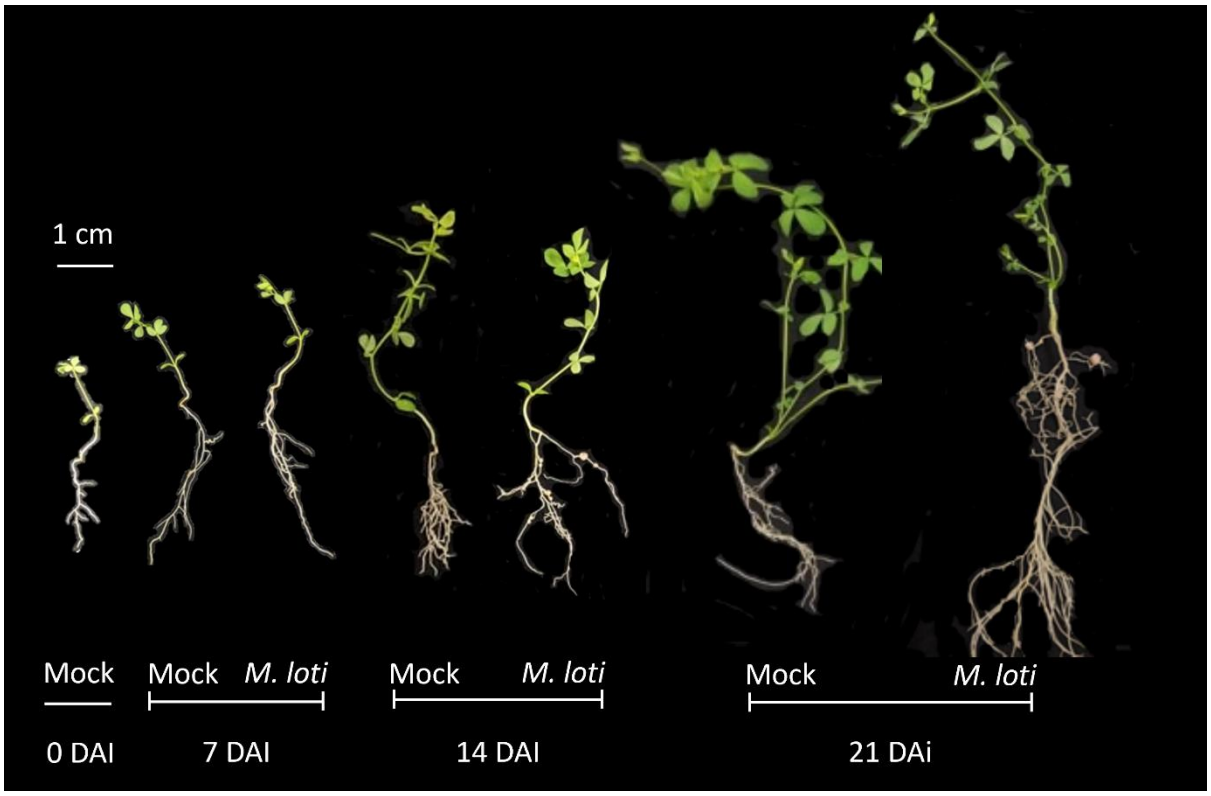

Figure 5.5 Typical phenotypic appearance of Wt *L. japonicus* plants under symbiotic (*M. loti*) or nitrogen sufficient (mock) conditions. Plants were grown as specified in figure 5.4. DAI = days after inoculation.

5.2.4 Gene expression of LjALMT1 under symbiotic and non-symbiotic conditions

5.2.4.1 Transcript expression of LjALMT1 and LjNOD26

Transcript expression of *LjALMT1* and *LjNOD26* was quantified in root and shoot tissues from Wt *L. japonicus* grown under symbiotic or non-symbiotic conditions in the presence of high or low nitrogen. *LjNOD26*, also known as *LIMP2*, is the *L. japonicus* ortholog of *GmNOD26* (Guenther and Roberts 2000), a major component of the SM, and the expression pattern was used as a positive control for symbiotic expression. There was no detectable expression of *LjNOD26* zero DAI in root or shoot tissues (Figure 5.6), furthermore *LjNOD26* expression could not be detected at any timepoint in the shoot tissue of *M. lot*i or mock inoculated Wt *L. japonicus* plants. Expression of *LjNOD26* under symbiotic conditions was first detected seven DAI in root tissues and was approximately half maximal of the level detected 14 and 21 DAI (Figure 5.6). This expression pattern trended with nodule development, phenotypic nodules were not present until 14 DAI (Figure 5.5), but development would precede this. There was a level of *LjNOD26* expression detected in the root tissue of mock treated Wt *L. japonicus* plants, this expression increased with time but was significantly less than in the root tissue of *M. lot*i treated plants (Figure 5.6).

Similar to *LjNOD26*, there was no detectable expression of *LjALMT1* at any timepoint in the shoot tissue of *M. lot*i or mock inoculated Wt *L. japonicus* plants (Figure 5.6). However, expression of *LjALMT1* in the root tissue of Wt *L. japonicus* plants was detected at zero DAI, this level of expression was not significantly different at any timepoint in mock treated plants (Figure 5.6). The expression of *LjALMT1* in the root tissue of *M. lot*i treated plants trended to increase with time, the expression at seven, 14 and 21 DAI was significantly greater than at zero DAI (Figure 5.6). To further investigate the expression profile of *LjALMT1* and *LjNOD26* under symbiotic conditions, the organ specific expression was investigated by excising nodules from root tissue prior to RNA extraction (Figure 5.7). For both *LjALMT1* and *LjNOD26*, expression in the shoot tissue was below the detectable threshold. For *LjNOD26*, expression was predominantly in the nodule tissue, with a normalised expression values of 0.613, significantly greater than the normalised expression of 0.0349 found in the root tissue (Figure 5.7). Expression of *LjALMT1* under symbiotic conditions was similar between the root and nodules, with normalised expression values of 0.281 and 0.253, respectively (Figure 5.7).

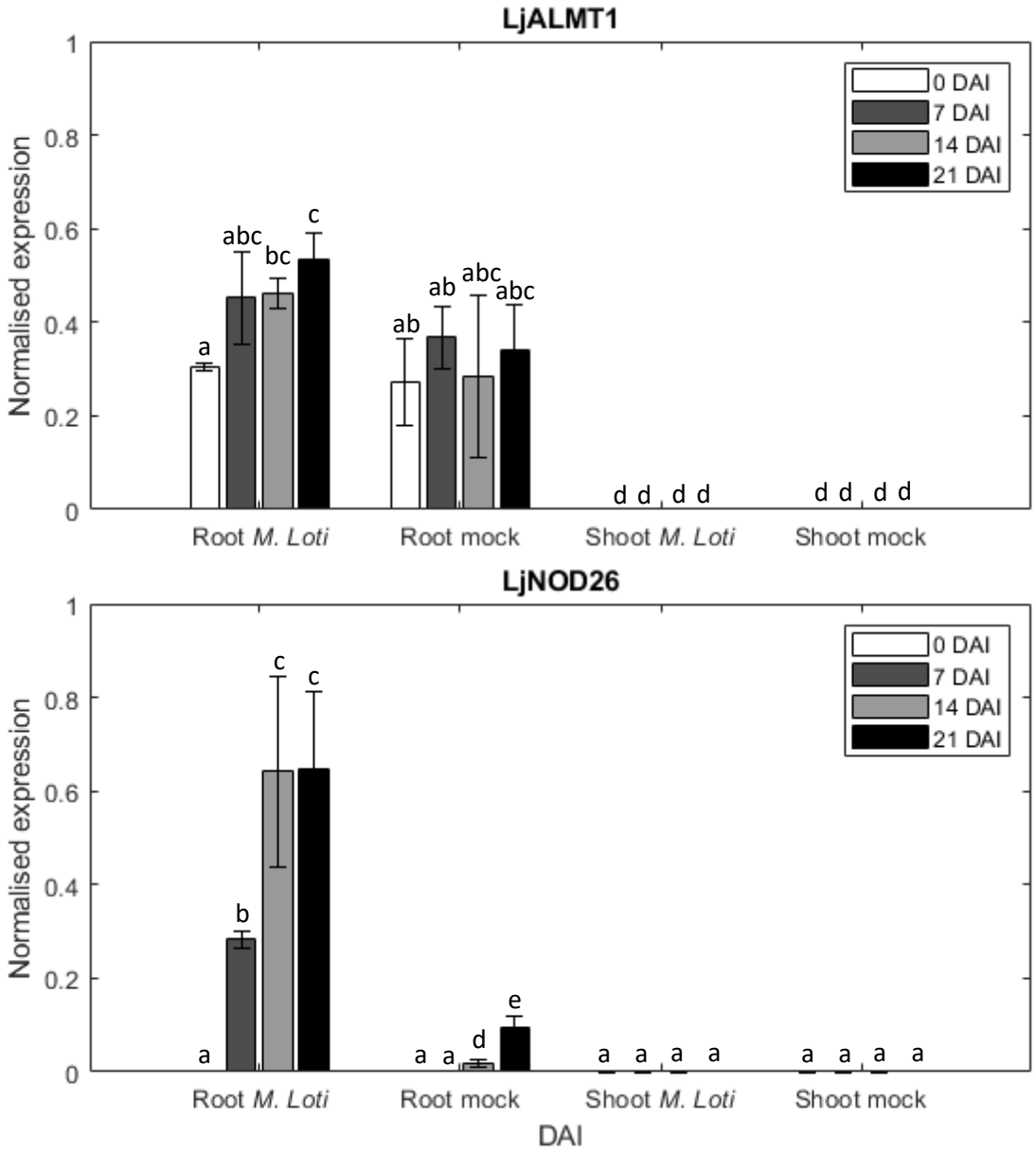

Figure 5.6 Tissue-specific expression of *LjALMT1* and *LjNOD26* under symbiotic or nitrogen sufficient conditions. Seven-day-old L. japonicus (MG20) were either inoculated with *M. loti* and grown under limiting nitrogen (*M. loti*) or inoculated with sterile MilliQ water and grown under sufficient nitrogen (mock) for 21 days. Total RNA was extracted, and cDNA synthesised from root or shoot tissues zero, seven, 14 or 21 days after treatment application prior to qRT-PCR analysis. For harvests: zero and seven DAI six plants were pooled in each replicate; for 14 DAI and 21 DAI three plants were pooled in each replicate (n = 4). Significance across tissue types was determined through Duncan's post hoc (n = 4, subscripts represent post hoc significance).

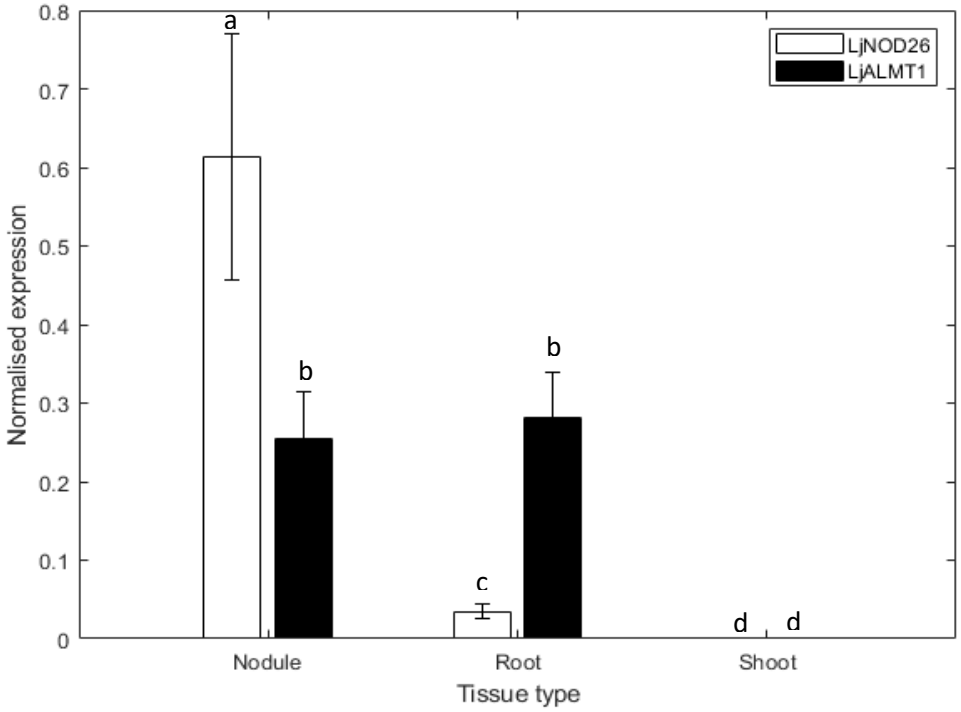

Figure 5.7 Organ-specific expression of *LjALMT1* and *LjNOD26* under symbiotic conditions. Three-weeks after inoculation plant organs were separated for total RNA extraction and cDNA synthesis prior to qRT-PCR analysis. Significance across tissue types was determined through Duncan's post hoc (n = 4, subscripts represent post hoc significance).

5.2.4.2 Spatial activity of the *LjALMT1* and *LjNOD26* regulatory regions

The spatial activity of the *LjALMT1* and *LjNOD26* regulatory regions was investigated through GUS expression (2.6.5, 2.9.3). Following one-hour dark incubation in X-Gluc substrate solution, the empty V48 transformed *L. japonicus* plants displayed no distinct blue staining, indicating that X-Gluc had not been cleaved by GUS and there was no spatial expression of GUS driven by the empty V48 sequence (Figure 5.8). When the root system of *L. japonicus* plants expressing V48 containing the regulatory region of LjNOD26 cloned upstream of GUS were exposed to X-Gluc a distinct blue stain appeared in the nodule tissue (Figure 5.8), suggesting GUS was expressed highly in the nitrogen fixing region of the nodule. GUS expression driven by the *LjNOD26* regulatory element was also present in the root vascular tissue, but this staining was far less distinct than in the nodules (Figure 5.8). The GUS expression driven by the regulatory region of *LjALMT1* displayed a staining pattern distinct from that of *LjNOD26*. The staining was predominantly in the vascular tissue of the *L. japonicus* root system, with this extending around the periphery of the nodule (Figure 5.8). Staining observed in nodule cross sections indicate that this was an extension of the vascular tissue into the

nodule (Figure 5.9) and fit with the transcript expression of *LjALMT1* observed in both the root and nodule (Figure 5.7).

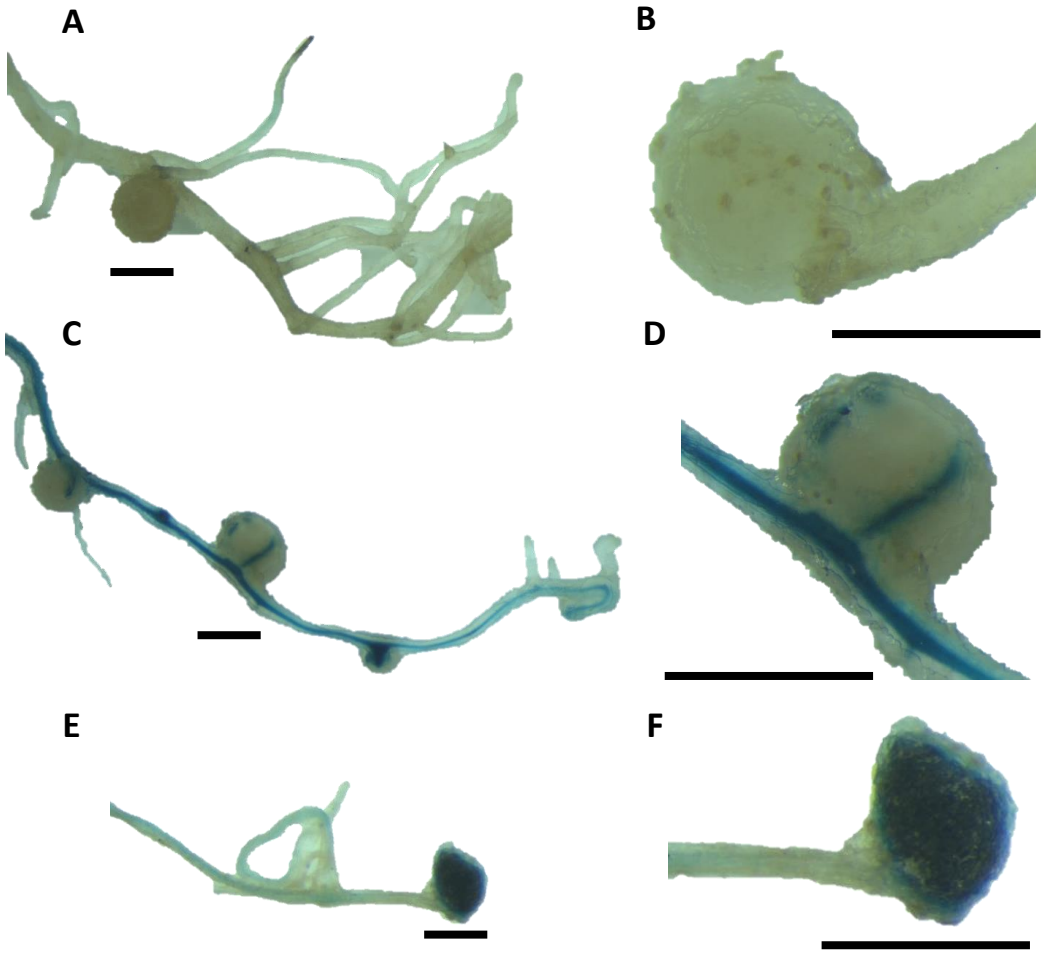

Figure 5.8 GUS expression under the *LjALMT1* and *LjNOD26* promoter. The 2 kb 5' regulatory elements were cloned upstream of the GUS open reading frame in V48 and transformed via hairy root transformation (2.9.2) and infiltrated with X-Gluc (2.9.3) 21 DAI with *M. loti*. A and B empty V48, C and D V48-*LjALMT1*pro, E and F V48-*LjNOD26*pro transformants. Scale = 200 µm.

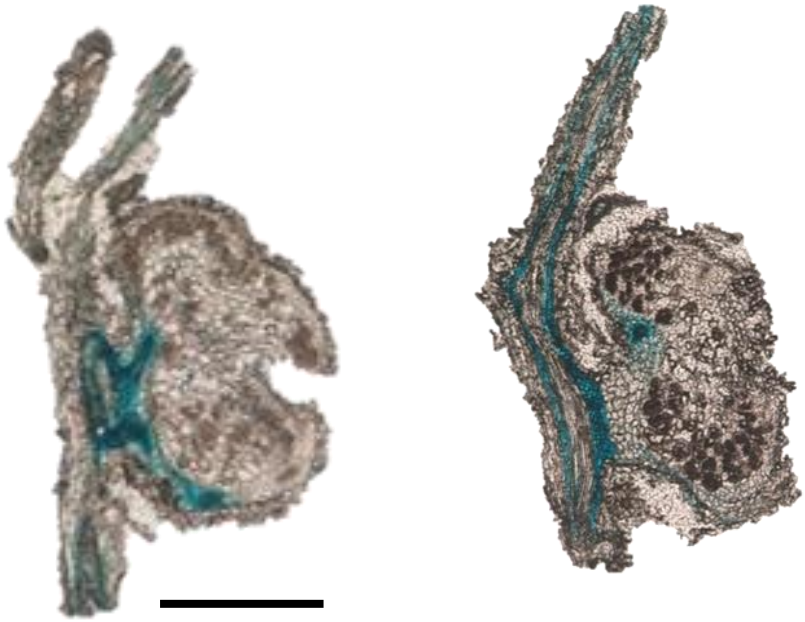

Figure 5.9 Root nodule sections of *LjALMT1* promoter driven GUS expression. X-Gluc infiltrated empty V48-LjALMT1pro transformants were embedded in paraffin, sectioned 10 µm thick and cleared using xylene prior to imaging using an Olympus BX53 upright microscope (Oympus LS, Japan). Scale = 100 µm.

5.2.5 *In vivo* localisation of LjALMT1

The cds of *LjALMT1* or *LjNOD26* were cloned into the N-GFP expression vector, V33, and expressed in *L. japonicus* via hairy root transformation under control of the soybean leghemoglobin promoter. Symbiosomes were counterstained with FM4-64, clearly highlighting the infected cell regions of the 21-day old *L. japonicus* nodule cells, but there was no evidence of GFP signal in empty or LjALMT1 V33 constructs (Figure 5.10). There was substantial GFP signal detected in LjNOD26-V33 expressing *L. japonicus* nodules, although localisation to the SM was unclear (Figure 5.10). The lack of GFP signal in the infected region of LjALMT1-V33-expressing nodules aligns with the GUS staining previously observed (Figure 5.8/9).

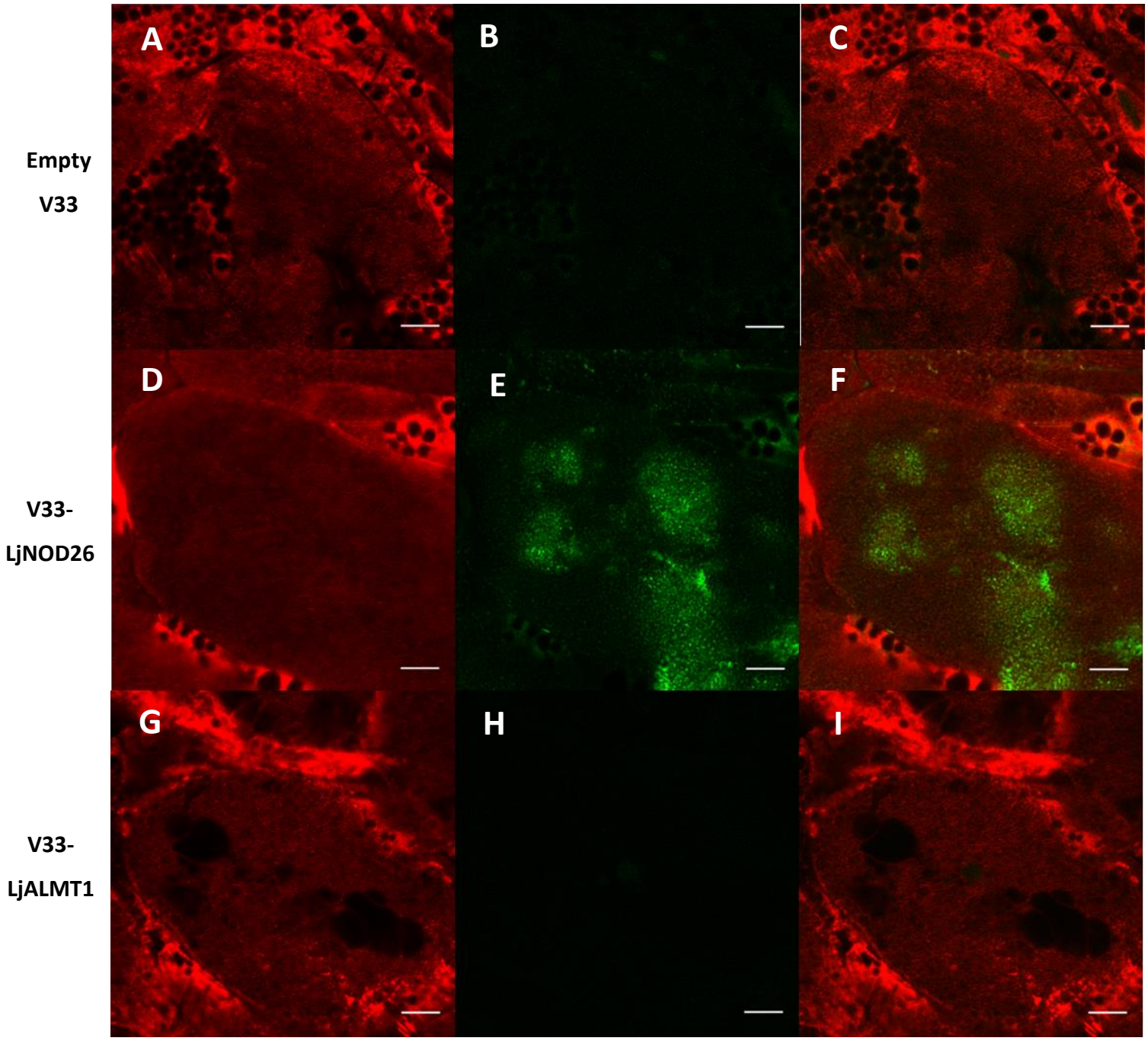

Figure 5.10 Confocal microscopy of *L. japonicus* nodules expressing GFP-fused LjNOD26 and LjALMT1 under the soybean leghaemoglobin promoter. The coding regions of LjNOD26 or LjALMT1 were cloned into V33 and introduced into *L. japonicus* via hairy roots. Confocal images of hand sectioned 21-day old nodules were taken using ZEISS LSM 880 Confocal Laser Scanning Microscope (Carl Zeiss, Germany). (A), (D) and (G), GFP was excited using a 488 nm argon laser and emission recorded 530 nm. B, E and H, the SM was counterstained with FM4–64 and excited using a 510 nm diode pumped solid state laser and emission recorded at 750 nm. (C), (F) and (I), the GFP and FM4-64 images merged. Images were processed using ZEN (black edition) with scale bars representing 10 µm.

The *in vivo* localisation of LjALMT1 was further investigated through fusion of the coding region to the 2 kb 5' regulatory element (2.6.7) and cloning into the gateway enabled C-GFP expression vector, V45. The resulting construct, along with empty and LjNOD26REcds V45 constructs, were expressed in *L. japonicus* via hairy root transformation and grown symbiotically for 21 days. Transgenic nodules expressing the empty V45 did not display any GFP signal in mature *L. japonicus* root nodules (Figure 5.11a-d) but did display GFP signal in the growing root tip (Figure 5.11e/f). Given that Wt *L. japonicus* were not visualised using this technique, it is unclear whether this signal was autofluorescence or leaky GFP expression from V45. Expression of LjNOD26REcds-V45 revealed GFP signal in the nodules, this appeared to be within the large infected cells (Figure 5.12). Confocal microscopy should be employed to confirm this observation. LjALMT1 under its native promoter did not appear to localise within the nodules, with no GFP signal detected in the infected region, but was observed along the root nodule interface (Figure 5.13a/b). Distinct GFP signal was observed along through the vascular tissue of mature *L. japonicus* roots (Figure 5.13c/d). This signal was also observed in the root tip (Figure 5.13e/f) but given that a similar signal was observed in the root tip of empty V45-expressing *L. japonicus* plants (Figure 5.11e/f) it cannot be assumed that this was due to LjALMT1 localisation.

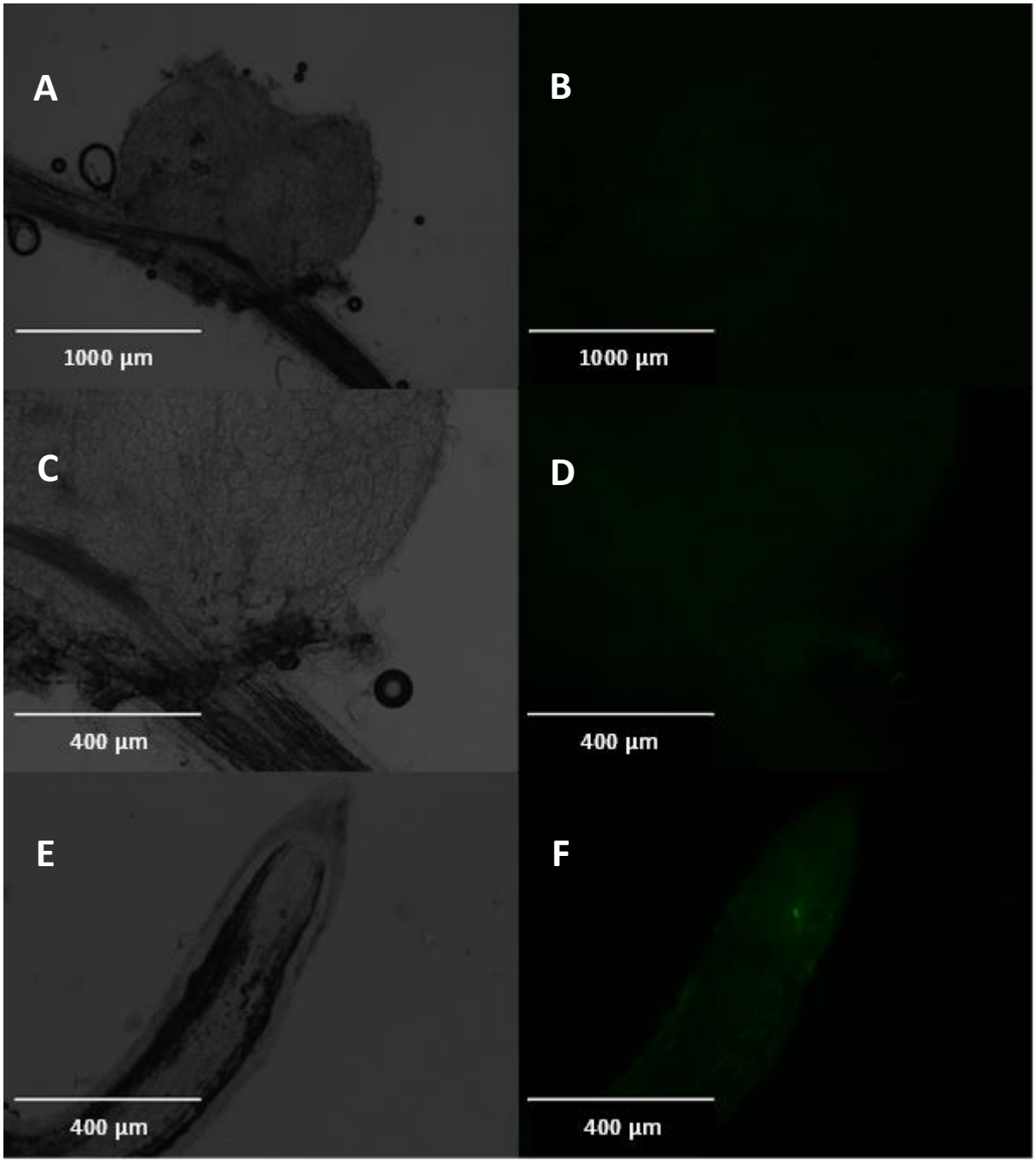

Figure 5.11 Fluorescent microscopy images of root and nodule tissue expressing empty V45. The empty V45 was introduced into *L. japonicus* via hairy roots. Fluorescent microscopy images of 21-day old root nodules were taken using EVOS® FL Auto Imaging System (Thermo Fisher Scientific, USA). (A) white light image of *L. japonicus* root nodule, (B) as (A) but of GFP (482/25 nm Excitation; 524/24 nm Emission). (C) as (A) but under greater magnification, (D) as (C) but of GFP. (E) white light image of *L. japonicus* root tip, (F) as (E) but of GFP highlighting autofluorescence.

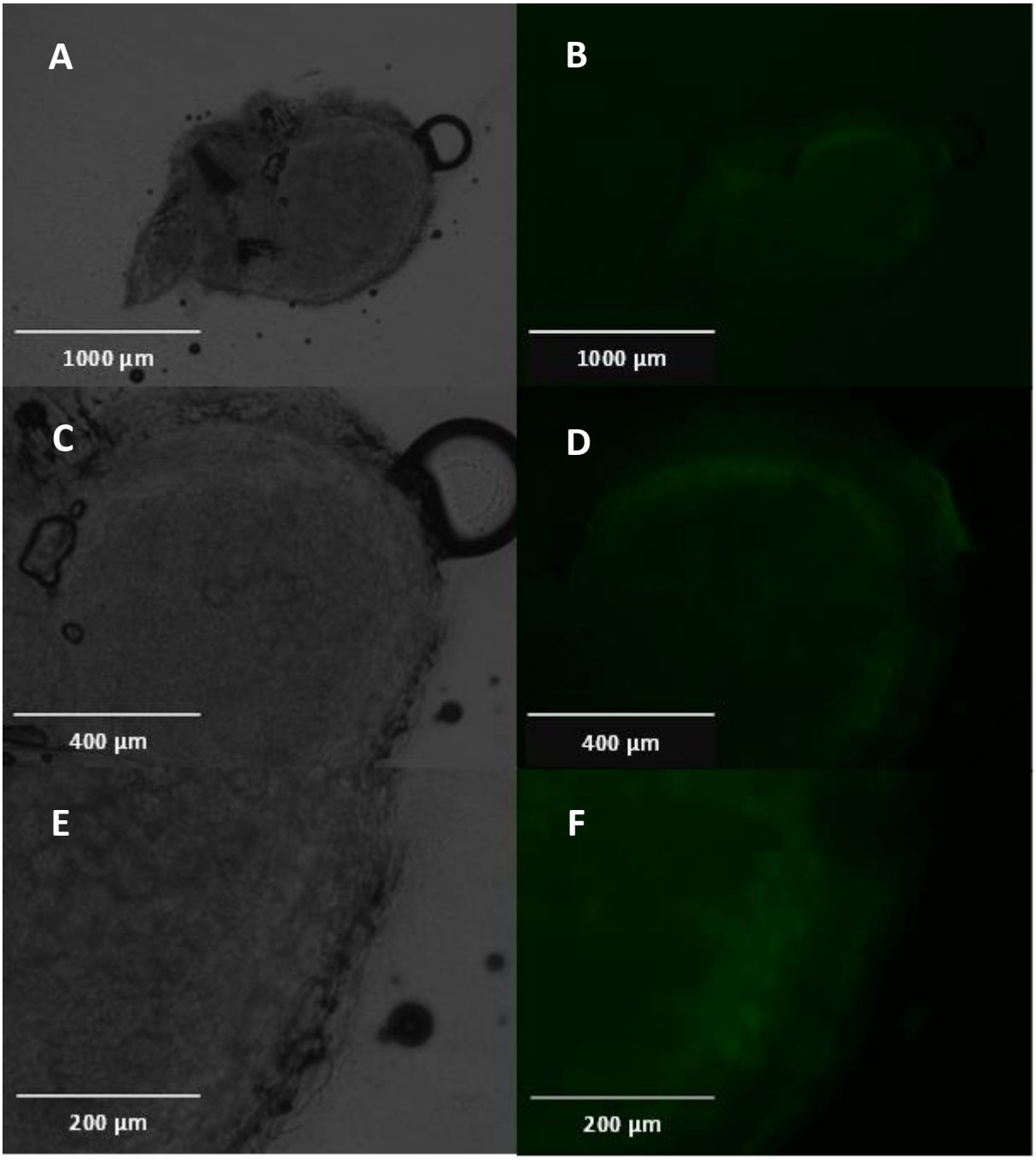

Figure 5.12 GFP localisation LjNOD26 under its native promoter. The fused 2 kb 5' regulatory element and coding regions of LjNOD26 was cloned into V45 and introduced into *L. japonicus* via hairy roots. Fluorescent microscopy images of 21-day old root nodules were taken using EVOS® FL Auto Imaging System (Thermo Fisher Scientific, USA). (A) white light image of *L. japonicus* root nodule, (B) as (A) but of GFP (482/25 nm Excitation; 524/24 nm Emission). (C) and (E), as (A) but under greater magnification. (D) and (F), as (B) but under greater magnification.

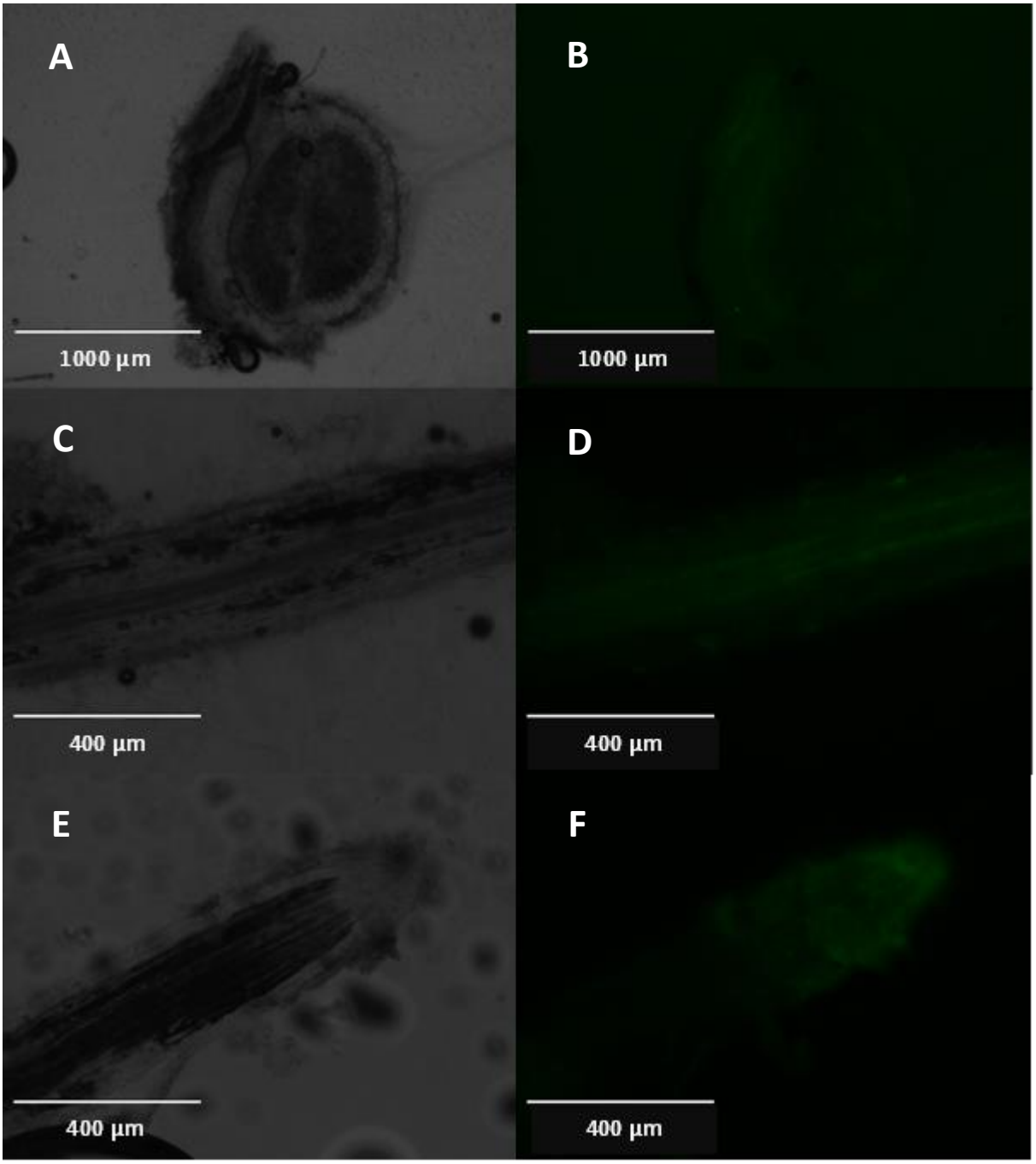

Figure 5.13 GFP localisation LjALMT1 under its native promoter. The fused 2 kb 5' regulatory element and coding regions of LjALMT1 was cloned into V45 and introduced into *L. japonicus* via hairy roots. Fluorescent microscopy images of 21-day old root nodules were taken using EVOS® FL Auto Imaging System (Thermo Fisher Scientific, USA). (A) white light image of *L. japonicus* root nodule, (B) as (A) but of GFP (482/25 nm Excitation; 524/24 nm Emission). (C) white light image of mature *L. japonicus* root, (D) as (C) but of GFP. (E) white light image of *L. japonicus* root tip, (F) as (E) but of GFP.

5.2.6 Growth of LjALMT1 LORE1 mutants

5.2.6.1 Identification of homozygous LjALMT1 LORE1 mutants

L. japonicus mutant population has been established using an endogenous long terminal repeat retrotransposon, Lotus Retrotransposon 1 (LORE1) (Fukai et al. 2010; Fukai et al. 2012; Urbanski et al. 2012). LORE1 is a 5042 bp retrotransposon epigenetically activated during tissue culture resulting in random insertion throughout the genome that can disrupt proper transcription (Madsen et al. 2005; Fukai et al. 2010). In the absence of tissue culture, LORE1 then inactivates and the selfed progeny of the heterozygous M1 population segregate, allowing for detection of homozygous lines in the M2 population (Fukai et al. 2010; Fukai et al. 2012). The M2 ALMT1 LORE1 mutant (30085822) line was obtained from the LORE1 insertion mutant resource (Malolepszy et al. 2016) and contained 5 exonic, 4 intronic, 1 intergenic LORE1 mutations. The M2 progeny were grown under conditions specified in 2.3.1 and gDNA was extracted (2.4.1) for genotyping (2.2.6) of null and mutant segregates. Amplification of the *LjALMT1* 30085822 (882) LORE1 or Wt allele was expected to yield products of 596 or 682 bp respectively (Figure 5.14). Segregation of the 882 LORE1 insertion was expected to be 1:2:1, but the 13 M2 progeny genotyped revealed a segregation of 1.5:1.9:0.6 (Table 5.5). in general, growth of LORE1 mutants was poor in comparison to Wt MG20, of the two homozygous *LjALMT1* LORE1 insertion mutants seed could only be obtained from 882-13. No seed pods successfully developed on the 882-5 line, the filature to seed was also observed in heterozygous and null 882 LORE1 mutants and may be due to another exonic insert in the 822 M2 progeny which has not been characterised in this work.

Table 5.5 Summary of *LjALMT1* (30085822) LORE1 M_2 population segregation. Genotyping of the *LjALMT1* 882 LORE1 M2 population was performed as specified in 2.2.6 and amplified products visualised in Figure 5.14.

	Number of lines	Segregation ratio
Homozygous Wt allele	5	1.5
Heterozygous	6	1.9
Homozygous LORE1 allele	2	0.6

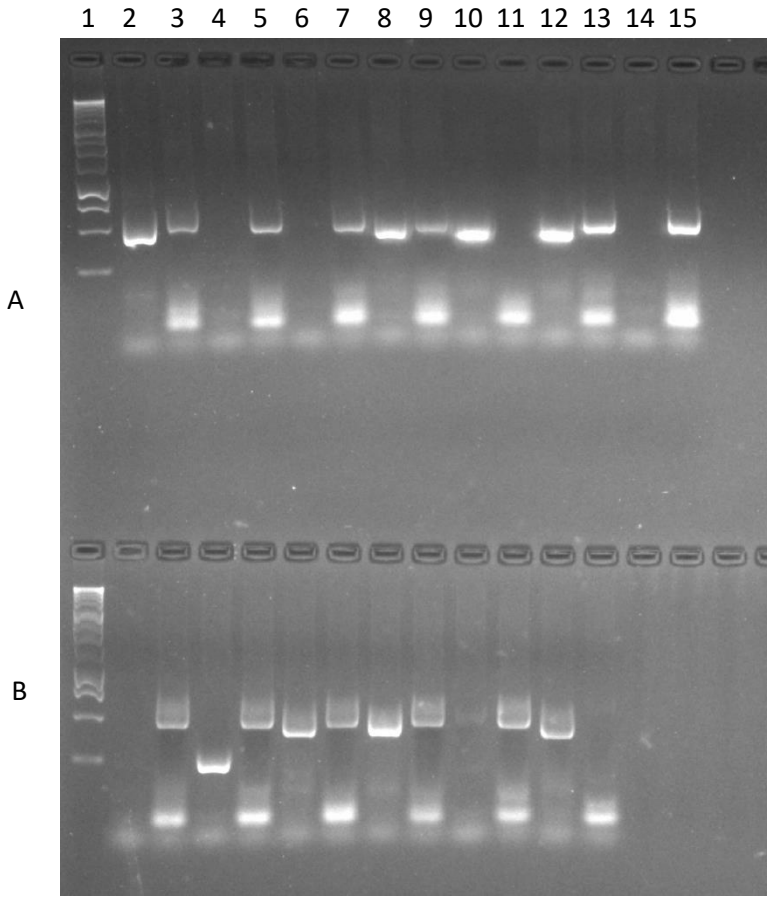

Figure 5.14 Genotyping *LjALMT1* (30085822) LORE1 M_2 population for homozygous LORE1 integration. Genomic DNA was extracted from 21-day old LjALMT1 882 LORE1 M_2 *L. japonicus* plants and used as template for genotyping (2.2.6). PCR products for the Wt and LORE1 alleles were run on a 1.5% (w/v) agarose gel and visualised using GelRed. Lane 1a: Promega (USA) 1kb ladder; Lane 2a: 882-1 LORE1 allele; Lane 3a: 882-1 Wt allele; Lane 4a: 882-2 LORE1 allele; Lane 5a: 882-2 Wt allele; Lane 6a: 882-3 LORE1 allele; Lane 7a: 882-3 Wt allele; Lane 8a: 882-4 LORE1 allele; Lane 9a: 882-4 Wt allele; Lane 10a: 882-5 LORE1 allele; Lane 11a: 882-5 Wt allele; Lane 12a: 882-6 LORE1 allele; Lane 13a: 882-6 Wt allele; Lane 14a: 882-7 LORE1 allele; Lane 15a: 882-7 Wt allele; Lane 1b: Promega (USA) 1kb ladder; Lane 2b: 882-8 LORE1 allele; Lane 3b: 882-8 Wt allele; Lane 4b: 882-9 LORE1 allele; Lane 5b: 882-9 Wt allele; Lane 6b: 882-10 LORE1 allele; Lane 7b: 882-10 Wt allele; Lane 8b: 882-11 LORE1 allele; Lane 9b: 882-11 Wt allele; Lane 10b: 882-12 LORE1 allele; Lane 11b: 882-12 Wt allele; Lane 12b: 882-13 LORE1 allele; Lane 13b: 882-13 Wt allele.

5.2.6.2 LjALMT1 LORE1 mutant phenotype

The phenotypic effect of the LjALMT1 exonic insertion was compared in homozygous *LjALMT1*-LORE1 (882-13) or *LjALMT1*-null (882-3) M3 progeny. *L. japonicus* plants were grown under symbiotic conditions (as specified in 2.3) with biomass and nodule number recorded 21 and 60 DAI. In general, the phenotypic appearance of both null and LORE1 insertional mutants was poor, with the stem predominantly maroon with an exception in the rapidly growing portions (Figure 5.15). This was not observed in Wt MG20 *L. japonicus* plants (Figure 5.5). The shoot biomass 21 DAI was not significant between the three lines, but 60 DAI the *LjALMT1*-null line has a significant decrease compared to the *LjALMT1*-LORE1 and Wt MG20 lines (Figure 5.15). Root biomass between the three lines was similar 21 DAI but was significantly greater in the Wt MG20 compared the *LjALMT1*-null line. The root weight in the *LjALMT1*-LORE1 line was significantly greater than the *LjALMT1*-null line 60 DAI, but not significant from the Wt MG20 line (Figure 5.15). Nodule number followed a similar trend to root biomass, 21 DAI there was significantly less nodules on the *LjALMT1*-null lines compared to both the Wt MG20 and *LjALMT1*-LORE1 lines. The nodule number of the *LjALMT1*-LORE1 line was significantly greater than both the *LjALMT1*-null and Wt MG20 lines 60 DAI (Figure 5.15).

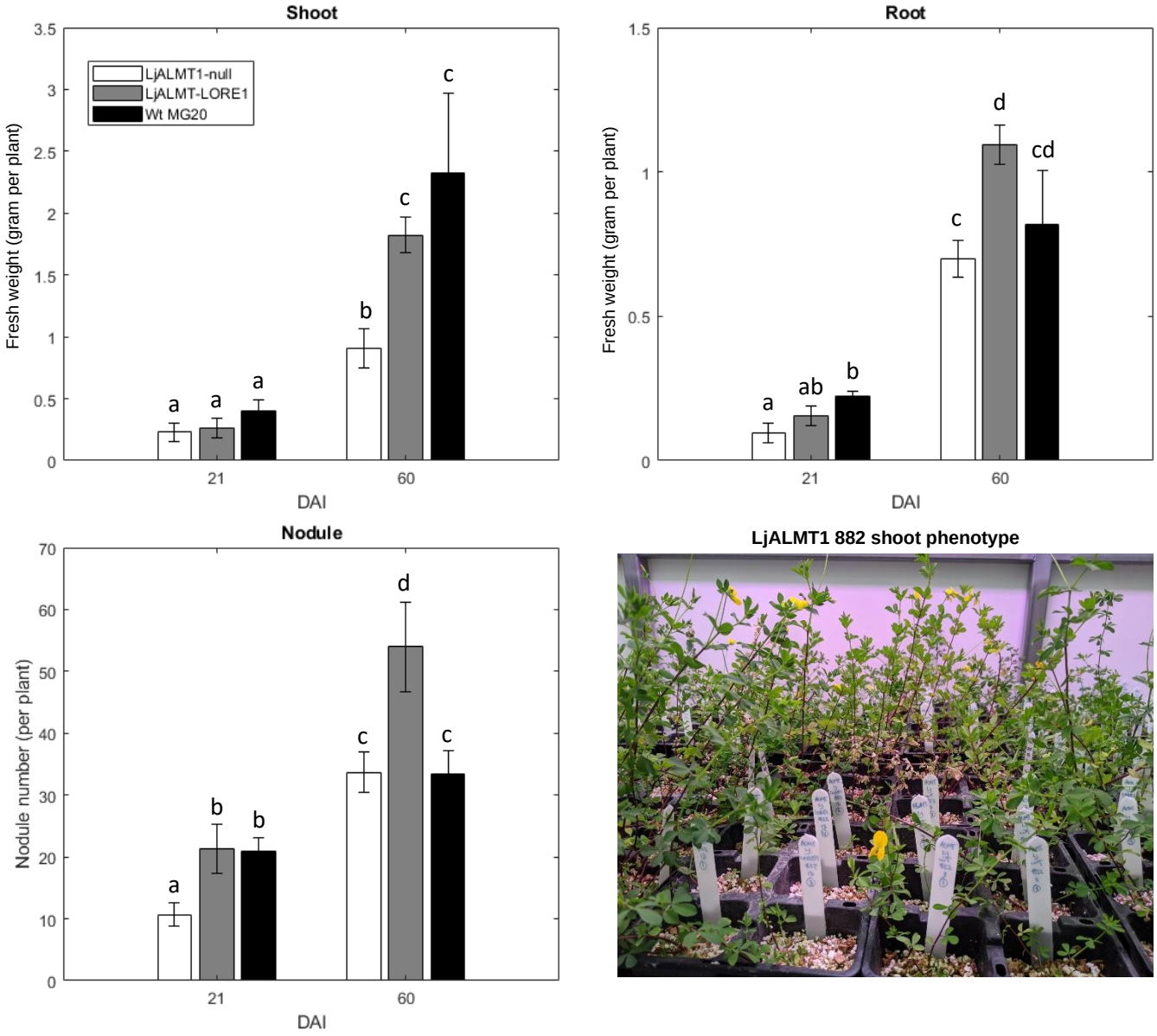

Figure 5.15 Growth LjALMT1 (30085822) LORE1 mutants under symbiotic conditions. Seven-day-old *L. japonicus* homozygous M3 LORE1 insertional, null or Wt MG20 plants were inoculated with *M. loti* and grown under limiting nitrogen for 60 days. Biomass and nodule number was recorded 21 and 60 DAI (n = 8, subscripts represent post hoc significance). Shoot phenotype was recorded 45 DAI.

5.2.7 Functional characterisation of LjALMT1 in *X. laevis* oocytes

LjALMT1 was expressed in *X. laevis* oocytes to determine if the channel was active and stimulated by malate. Initial clamping of oocytes 48 hours post injection with 32 ng cRNA displayed poor membrane integrity and unstable currents in excess of 10 µA (DNS). To reveal the transport properties of LjALMT1 in *X. laevis* oocytes, further optimisation of the cRNA injection was required.

5.2.7.1 Optimising cRNA injections

To optimise the quantity of cRNA injected for appropriate expression of LjALMT1 oocytes were injected with 8, 16 or 32 ng of cRNA for 24 hours. Oocytes injected for this shorter period displayed improved membrane integrity and stable currents (Figure 5.16). Control oocytes were not stimulated by basal or malate testing solutions with conductance's of 2.7 and 4.0 µS, respectively. For all investigated LjALMT1 cRNA concentrations, oocytes displayed enhanced ionic currents in both basal and malate testing solutions. In general, the magnitude of the current increased with cRNA concentration, but was similar between 16 and 32 ng of cRNA (Figure 5.16). When injected with 32 ng of cRNA the conductivity of the channel in basal and malate testing solution was similar, 16.3 and 15.0 µS, respectively. At 16 ng of cRNA the malate stimulation was more pronounced, with conductivities of 9.5 and 17.7 µS, respectively.

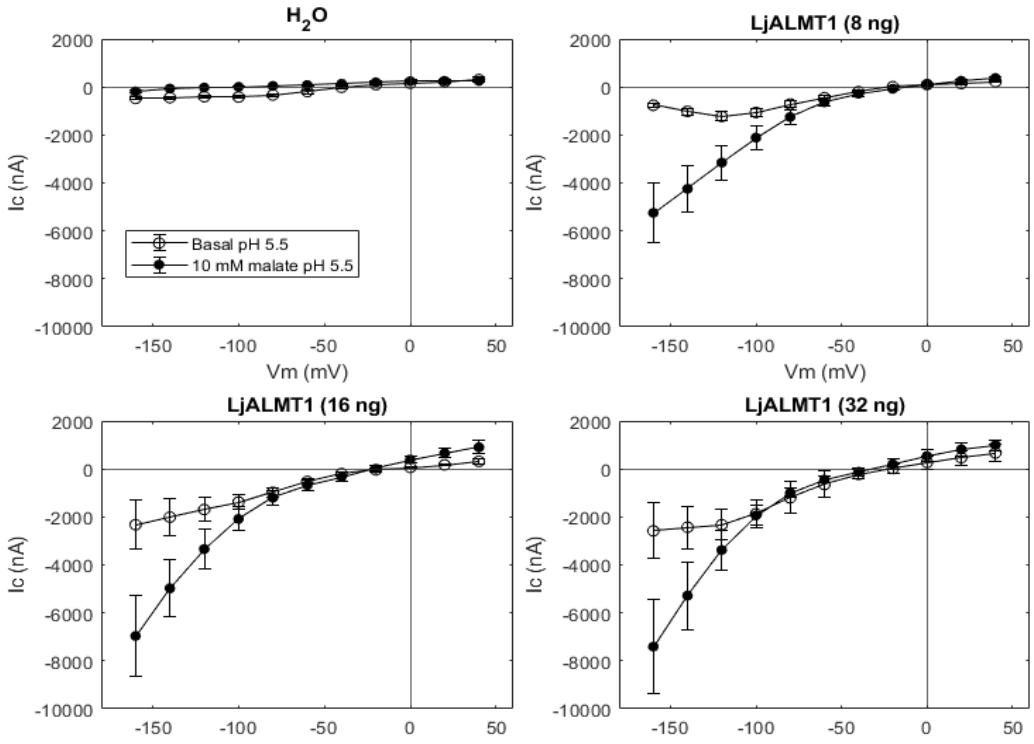

Figure 5.16 Effect of cRNA concentration on malate induced currents in LjALMT1-expressing *X. laevis* oocytes. Testing solutions contained either 0 mM (basal) or 10 mM malic acid (malate) with 0.5 mM $CaCl_2$, buffered to pH 5.5 with BTP and osmolality was adjusted to 220 mosmol kg^{-1} with D-mannitol (n = 8 from two oocyte harvests).

5.2.7.2 Aluminium activation and GABA inhibition of malate-induced ionic currents

To investigate previously characterised properties of ALMT proteins, I expressed LjALMT1 in *X. laevis* oocytes and used two-electrode voltage clamp to determine if it was activated by aluminium and if GABA had any effect on the transport in ND88 testing solution. Ionic currents in control oocytes were not stimulated by perfusion with ND88 solution, nor were they activated by $AlCl_3$ or inhibited by GABA, with conductivities between 2.0 and 2.6 µS observed. LjALMT1-expressing oocytes displayed strong ionic current activation, with conductivity of 40.7 µS in ND88 testing solution and displayed a bell-shaped current-voltage curve, closing the channel at more negative membrane potentials (Figure 5.17). When $AlCl_3$ was added to the ND88 testing solution, LjALMT1-expressing oocytes displayed enhanced ionic conductance, 43.7 µS, and the capacity to remain open at more negative membrane potentials (Figure 5.17). GABA application was opposing to $AlCl_3$, with an observed decrease in channel conductivity, 34.5 µS, and a more pronounced bell-shaped current-voltage curve (Figure 5.17).

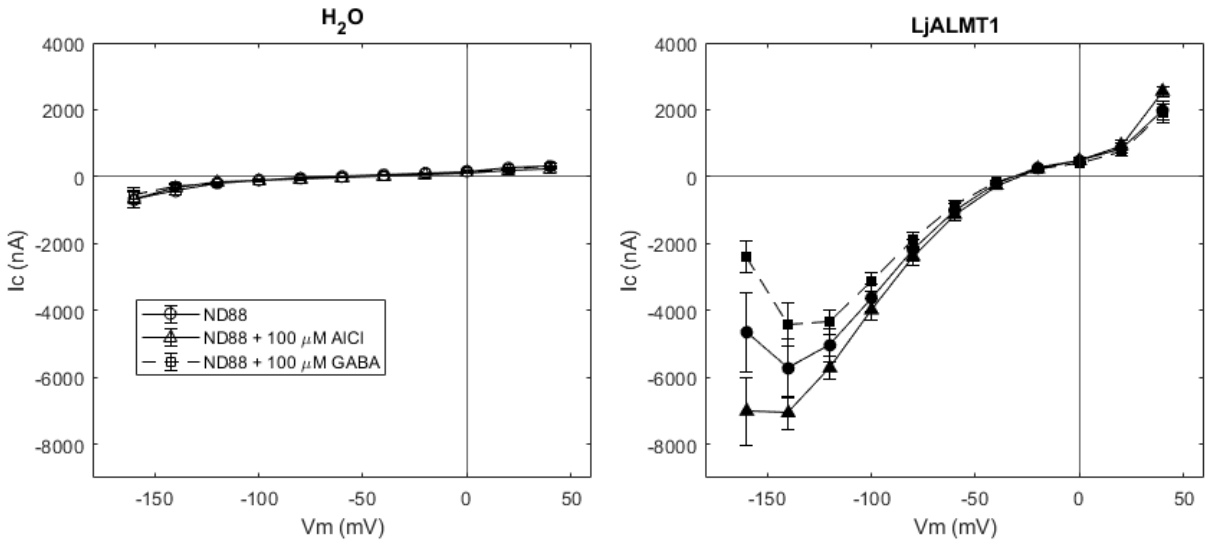

Figure 5.17 TEVC of LjALMT1-expressing *X. laevis* oocytes in ND88. Testing solutions contained 88 mM NaCl, 1 mM KCl, 2.4 mM $NaHCO_3$, 6.2 mM $Ca(NO_3)_2$, 8.5 mM $CaCl_2$, 0.82 mM $MgCl_2$ and buffered to pH 4.5 with HCl ± 100 µM $AlCl_3$ or ± 100 µM GABA. For all solutions osmolality was adjusted to 220 mosmol kg−1 with D-mannitol (n = 6 from two oocyte harvests).

5.2.7.3 Malate preloading enhances ionic currents

To determine if the ionic currents observed in LjALMT1-expressing oocytes were carried by anions, in particular malate, oocytes were preloaded with 46 nL of 100 mM malic acid pH 7.5. Loading with malate depolarised both control and LjALMT1-expressing oocytes, but this depolarisation was much more substantial in LjALMT1-expressing oocytes. This is reflected in the reversal potentials with

control oocytes reversing between -72.3 and -47.7 mV, while in LjALMT1-expressing oocytes this was far more depolarised, at pH 5.5 this was between -30.7 and -32.9 mV, but trended somewhat more hyperpolarised at pH 7.5, reversing between -36.5 and -37.1 mV (Figure 5.18).

As previously described, the ion conductance of control and LjALMT1-expressing oocytes was calculated using the slope of the linear portion of the current-voltage curve across the reversal potential (Figure 5.18). In control oocytes preloaded with malate the conductance was low in all testing solutions, ranging between 2.71 and 8.34 µS. However, the conductance of malate preloaded LjALMT1-expressing oocytes was far greater, this was most pronounced in at pH 5.5 with external application of malate, with a channel conductivity of 93.0 µS (Figure 5.18). In the absence of external malate, the channel remained active with a conductance of 62.8 µS. Interestingly at pH 5.5, the external malate application enhanced the ionic conductance to a level that reversed the bell-shaped current-voltage curve allowing linear channel conductance at more negative membrane potentials (Figure 5.18). The conductivity of LjALMT1-expressing oocytes preloaded with malate appeared to lose most of its external malate stimulation at pH 7.5, with conductivities of 62.8 and 67.6 µS for basal and malate testing solutions, respectively (Figure 5.18). It is also noted that the external malate stimulation at pH 7.5 is insufficient to rectify the bell-shaped current-voltage curve (Figure 5.18).

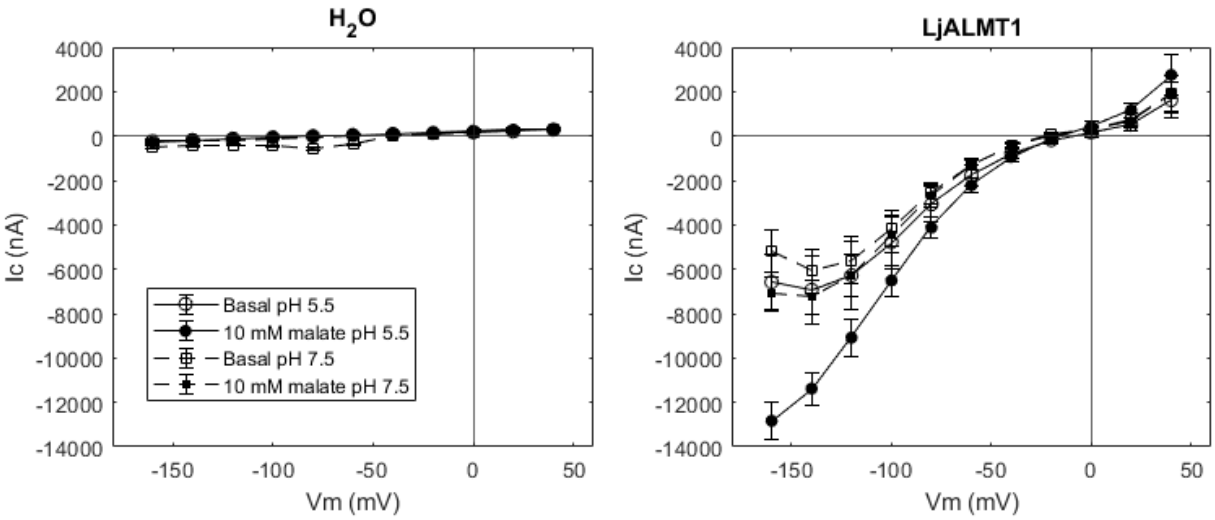

Figure 5.18 TEVC of LjALMT1-expressing *X. laevis* oocytes preloaded with malate in malate and basal testing solution. Testing solutions contained either 0 mM (basal) or 10 mM malic acid (malate) with 0.5 mM $CaCl_2$, buffered to pH 5.5 or 7.5 with BTP and osmolality was adjusted to 220 mosmol kg^{-1} with D-mannitol (n = 12 from three oocyte harvests).

5.2.7.4 [^{14}C] malate transport by LjALMT1-expressing oocytes

The cytosol of *X. laevis* oocytes can contain a high concentration of chloride and given the strong ionic current activation of LjALMT1-expressing oocytes in ND88 solution, [^{14}C] malate studies were employed to confirm direct transport of malate by LjALMT1. Control oocytes incubated in [^{14}C] malate at pH 5.5 for 15 minutes had a [^{14}C] malate flux of 662 pmol/oocyte/minute, this was significantly lower than the 2420 pmol/oocyte/minute flux observed in LjALMT1-expressing oocytes (Figure 5.19). The [^{14}C] malate flux of control and LjALMT1-expressing oocytes was insensitive to the SM-DC inhibitor, phthalonic acid (Figure 5.19).

Taken together with electrophysiological recordings these data strongly suggest direct transport of malate by LjALMT1.

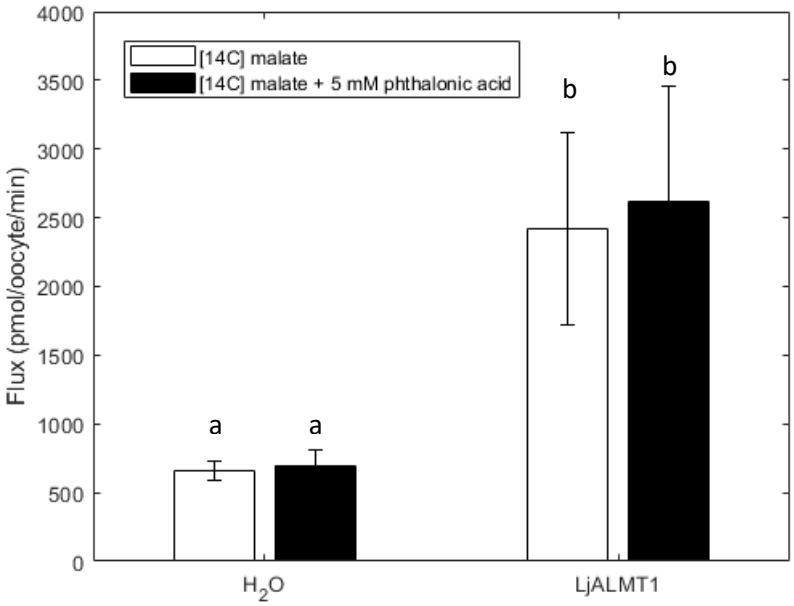

Figure 5.19 Radiolabeled malate uptake by LjALMT1 expressing oocytes. Oocytes injected with dH_2O or 16 ng LjALMT1 cRNA were incubated in [^{14}C] malate at pH 5.5 for 15 minutes and digested in nitric acid for determination of malate uptake. Uptake solution contained a total of 2 mM malic acid (malate) ± 5 mM phthalonic acid with 0.5 mM $CaCl_2$, buffered to pH 5.5 with BTP and osmolality adjusted to 220 mosmol kg^{-1} with D-mannitol (n = 16 from two oocyte harvests).

5.3 Discussion

5.3.1 Expression pattern of LjALMTs

The ALMT family were initially characterised due to their role in aluminium tolerance with the root tip expressed TaALMT1 shown to export organic acids into the soil and cause aluminium to chelate into non-toxic complexes (Sasaki et al. 2004). Since then, functional roles in stomatal movement, inflorescence, organic acid accumulation in fruit, signalling and soil interactions have been proposed and not all ALMTs have been observed to have a role in aluminium tolerance (Barbier-Brygoo et al. 2011; Ryan et al. 2011; Chen et al. 2013; Takanashi et al. 2016; Gutermuth et al. 2018; Pantoja 2021). In this chapter I successfully identified novel *ALMT* transcripts in the *L. japonicus* genome and proposed candidates for the SM-DC. Previously, (Takanashi et al. 2016) identified seven *L. japonicus ALMT* genes in the Kazusa genome database (ver. 2.5), using the MG20 genome (Li et al. 2020) available through LOTUS BASE, I identified a further six putative *L. japonicus ALMT* gene sequences (Table 5.1). Two tDT transporters in *L. japonicus* were also identified but did not appear to be expressed in the nodule tissues and have not been investigated in this study (Table 5.2, Figure 5.2).

Similar expression patterns were observed between Takanashi et al. (2016) and the publicly available transcriptomics analysed here. Nomenclature by Takanashi et al. (2016) are denoted by $_{Tak}$. *LjALMT9.1* and *LjALMT12.1* here, corresponding to *LjALMT5* $_{Tak}$ and *LjALMT6* $_{Tak}$, respectively, were all shown to be expressed through the stem and leaf tissues. *LjALMT12.5* also followed this expression pattern but Takanashi et al. (2016) failed to identify expression of the corresponding *LjALMT7*$_{Tak}$. The publicly available transcriptomic data of *LjALMT8* could explain why Takanashi et al. (2016) did not detect any expression in the corresponding *LjALMT1*$_{Tak}$, as it is mainly expressed in the inflorescence tissue, which was not investigated by this group. There was no transcriptomic expression *LjALMT2, LjALMT4 LjALMT12.2* and *LjALMT12.3*, interestingly two of those genes were previously investigated (Takanashi et al. 2016). *LjALMT2*$_{Tak}$, corresponding to *LjALMT12.2* was expressed in the leaf and stem tissues, while *LjALMT4*$_{Tak}$, corresponding to *LjALMT2*, was expressed specifically in the nodules (Takanashi et al. 2016). It is unclear why these transcripts were not detected in publicly available transcriptomics data.

The expression pattern of the 13 *L. japonicus ALMT* transcripts along with their *M. truncatula* orthologs identified two possible candidates for the SM-DC, *LjALMT1* and *LjALMT9.2*. The nodule localised *LjALMT4*$_{Tak}$ is not considered a candidate for the SM-DC as it has been shown to localised to the nodule vascular bundles rather than the infected region (Takanashi et al. 2016). *LjALMT9.2* was initially considered a candidate due to nodule-specific expression of the orthologous *MtALMT9.2*

(Figure 5.1, Appendix 10). However, *LjALMT9.2* in this study corresponds to *LjALMT3*$_{Tak}$ in the Kazusa genome database, detailed qRT-PCR by Takanashi et al. (2016) has shown that this transcript is expressed mostly in the leaf tissue. Of the putative transporters identified in this study, only *LjALMT1* appeared to be expressed in the nodule and remains unstudied.

5.3.2 LjALMT1 is expressed through the root vascular tissue

The transcriptomic expression profile of *LjALMT1* was validated through tissue specific qRT-PCR. Transcript expression of *LjALMT1* does not appear to be specific to the nodule tissues, but rather expressed throughout the root nodule system (Figure 5.7). Many SM localised proteins display a nodule specific expression pattern, as observed in *LjNOD26* (Figure 5.7); for *LjALMT1* to be involved in dicarboxylate transport across the SM, it must be expressed in the infected region of the nodule. I used *LjNOD26 (LIMP2)* as a positive control for symbiosome specific expression, although localisation has not been confirmed, Guenther and Roberts (2000) have shown nodule specific expression through Northern blot analysis. Further evidence that LjNOD26 is the symbiosome localised GmNOD26 ortholog is provided by Takanashi et al. (2012), with tissue-specific transcriptomics of *L. japonicus* nodules identifying four aquaporins, but only *LjNOD26* was expressed in the infected region. The functional role of LjALMT1 is unlikely to be essential for symbiosis as expression occurs independent of *M. loti* inoculation (Figure 5.6). By contrast, *LjNOD26* is only expressed under symbiotic conditions, and peaks around nodule maturity. In this work, it was occasionally observed that mock treated Wt *L. japonicus* plants developed nodules, this could be due to contamination by a wild rhizobial strains or *M. loti*. This level of nodulation was never to the extent of *M. loti* inoculated plants but may explain why *LjNOD26* expression was detected in the root tissue of mock treated plants 21 DAI.

The spatial activity of the *LjALMT1* regulatory region was investigated through GUS expression. *LjALMT1* appeared to be expressed throughout the vascular tissue of the root and extending around the periphery of the nodule through the vascular bundles (Figure 5.8). The spatial expression pattern of *LjALMT1* is reminiscent of the *ALMT1* genes from *Arabidopsis* and white lupin (Kobayashi et al. 2007; Zhou et al. 2020). In both these plants the *ALMT1* regulatory elements drive GUS expression in the vascular tissue and root tip, but the effect symbiosis and nodule development had on this expression in white lupin was not investigated. Given that the spatial activity of the *LjALMT1* promoter is not observed in the infected region of the nodule, it is unlikely that that LjALMT1 would localise to the SM. Fitting with the anticipated nodule specific expression of *LjNOD26* (Guenther and Roberts 2000), the regulatory region driving GUS expression was specific to the nodules and observed throughout the infected region (Figure 5.8). Due to the limitations of transient hairy root

transformation, the *LjALMT1* and *LjNOD26* regulatory regions could only be investigated in the root system of transgenic *L. japonicus.* It was not possible to assess these regulatory regions in the shoot tissues, although transcript data would not suggest expression here. It is also noted that the inflorescent or pod tissues were not investigated.

5.3.3 Localisation of LjALMT1 in *L. japonicus*

Initially, I expressed LjALMT1 or LjNOD26 tagged to GFP under control of the soybean leghemoglobin promoter. This regulatory region is specific to nodule cells and has been previously used to demonstrate SM localisation (Clarke et al. 2015), particularly when expression by the native regulatory region does not generate sufficient GFP signal. There was no GFP signal detected in empty vector or LjALMT1 expressing *L. japonicus* nodules, but notable GFP signal detected in the infected cells expressing LjNOD26 (Figure 5.9). The SM was counterstained with FM4-64, but the GFP signal from LjNOD26 under the soybean leghemoglobin promoter did not clearly localise to this membrane. It is possible that the expression of LjNOD26 under the soybean leghemoglobin promoter was too high for appropriate localisation, to my knowledge this regulatory element has not been used in *L. japonicus* previously. Optimisation of the technique is required, but in the scope of this study appropriate localisation of LjNOD26 to the SM is not required.

Given that *LjALMT1* expression is observed in the root and nodule vascular tissues, rather than throughout the nodule infected region as is observed for leghemoglobin, it was more appropriate to assess localisation under the native regulatory region. For this I fused the regulatory and coding regions of LjALMT1 or LjNOD26, and subsequently fused GFP to the c-terminal through introduction into V45. Under its native promoter, LjALMT1 appeared to be localised to the PM of the cells lining the vascular tissue throughout the root system (Figure 5.13). Localisation of ALMT genes is largely performed in model cells to confirm localisation to the PM or tonoplast (Yamaguchi et al. 2005; Kovermann et al. 2007; Pineros et al. 2008; Ligaba et al. 2012; Liang et al. 2013). For this reason, it is difficult to compare the localisation of LjALMT1 with that of other organisms, but it is likely LjALMT1 does localise to the PM, as is observed in root expressed ALMT1s from other plant species (Yamaguchi et al. 2005; Kobayashi et al. 2007; Pineros et al. 2008; Liang et al. 2013; Zhou et al. 2020) GFP signal was also observed in the root tip when expressing GFP tagged LjALMT1 (Figure 5.13), this would be expected based on the previously observed GUS histochemical staining (Figure 5.8). However, it is unclear whether this signal was truly related to the localisation of LjALMT1, as a similar, but weaker GFP signal was observed in empty V45 transformants (Figure 5.11), likely caused by autofluorescence or leaky GFP expression. The localisation of LjALMT1 under its native regulatory confirmed that this protein was not localised in the symbiotic regions of the nodule. However,

LjNOD26 under its native promoter appeared to localise within the large infected cells (Figure 5.12), whether this was to the SM still remains to be confirmed through confocal microscopy.

5.3.4 LjALMT1 is a functional dicarboxylate carrier

Initially, oocytes injected with LjALMT1 cRNA for 48-hours displayed poor membrane integrity, when attempting to clamp these oocytes the resting membrane potential was often positive. The typical resting membrane potential of healthy control oocytes is usually between -60 and -80 mV. This indicated that LjALMT1 was being expressed at a level toxic to the oocyte; after optimising the concentration and timing of cRNA injections all subsequent experiments were performed 24-hours post injection with 16 ng LjALMT1 cRNA. This aligns with what is found in the literature, with 16 to 46 ng of ALMT cRNA typically injected into *X. laevis* oocytes (Sasaki et al. 2004; Gruber et al. 2010; Ramesh et al. 2015). When bathed in ND88 testing solution at pH 4.5 LjALMT1 displayed a bell-shaped current-voltage curve, typical of the ALMT12 subfamily localised in guard cells (Meyer et al. 2010). The conductivity of the channel was somewhat enhanced by extracellular aluminium application, but not essential for activation (Figure 5.17). Variability in aluminium activation of ALMT channels is typical; activation of TaALMT1 and AtALMT1 is greatly enhanced by extracellular aluminium (Sasaki et al. 2004; Kovermann et al. 2007) whereas AtALMT12 and ZmALMT1 are relatively insensitive to its application (Pineros et al. 2008; Meyer et al. 2010). Of particular interest is the capacity for LjALMT1 to remain open at more negative membrane potentials in the presence of aluminium (Figure 5.17). The C-terminus of ALMTs has been associated with voltage dependent gating at negative membrane potentials (Mumm et al. 2013; Qin et al. 2022) and aluminium activation (Ligaba et al. 2013), although the occurrence of both has not been previously reported in a single ALMT until now. The ionic currents stimulated by LjALMT1-expressing *X. laevis* oocytes were also negatively regulated by GABA (Figure 5.17). TaALMT1 is thought to transport both malate and GABA, with external GABA application displaying inhibitory effects on the malate-induced currents of TaALMT1-expressing *X. laevis* oocytes (Ramesh et al. 2015; Long et al. 2020). Given that a similar response is observed here, it is likely that LjALMT1 may also transport GABA.

Although it is primarily believed that ALMTs are selective to dicarboxylates, they are somewhat permeable to other physiologically relevant anions (Pineros et al. 2008). Initial malate permeability of TaALMT1 was inferred as aluminium enhanced inward currents were only observed when preloaded with malate, it was assumed the endogenous malate concentration was insufficient in generating detectable currents (Sasaki et al. 2004; Pineros et al. 2008). Since these initial observations, numerous ALMTs have been characterised without the need for malate preloading, including here in LjALMT1. To determine if an increase in intracellular malate increased the LjALMT1-

mediated conductivity, I preloaded oocytes with 46 nL of 100 mM malic acid pH 7.5. Indeed, the magnitude of the current at more negative membrane potentials was increased (Figure 5.16, 5.18). External malate enhanced this in a typical ALMT manner, but interestingly decreased the voltage dependent gating observed in ND88 solution (Figure 5.17). To further confirm that malate was directly transported through LjALMT1, [^{14}C] malate was used as a radiotracer. These experiments confirmed that the observed malate-induced currents in LjALMT1-expressing oocytes were carried by malate. Uptake of [^{14}C] malate was not inhibited by phthalonate in control or LjALMT1-expressing oocytes, further biochemical confirmation that LjALMT1 is not the SM-DC. Future work should investigate the permeability of physiologically relevant anions such as Cl^-, NO_3^-, and SO_4^{2-}, given that LjALMT1 is expressed in the root vascular tissue, they may play important roles in signal perception and transduction.

5.3.5 Transport by LjALMT1 may be redundant

Functional characterisation of LjALMT1 was further investigated through use of the LORE1 mutant population (Fukai et al. 2010; Fukai et al. 2012; Urbanski et al. 2012; Malolepszy et al. 2016). I successfully identified homozygous null and LORE1 lines for the LjALMT1 allele. Unfortunately, growth of null and LORE1 LjALMT1 allelic mutants was poor in comparison to Wt MG20 *L. japonicus,* and other exonic LORE1 mutations in the 30085822 M2 progeny may be present, making interpretation of results not definitive. The exonic LORE1 mutation in the LjALMT1 gene did not decrease shoot or root biomass, nor nodule number when compared to the null or Wt MG20 lines after 21 days of symbiotic growth (Figure 5.15). Interestingly the nodule number after 60 days of symbiotic growth was significantly higher in the LjALMT1-LORE1 mutant than in the null or Wt MG20 lines. This could suggest that LjALMT1 transport may be important in regulating nodule number, perhaps through dicarboxylate signalling or as a mechanism to recapture dicarboxylates metabolised in the nodules. However, growth studies should be repeated before any conclusions are drawn, and root architecture should be investigated under aluminium stress. It is possible that transport by LjALMT1 is redundant; *LjALMT2* is expressed in the nodule vascular tissue (Takanashi et al. 2016) and transcriptomics suggests that *LjALMT10* is expressed throughout the root tissues. The similar expression pattern observed in these transporters, along with the remaining uncharacterised *L. japonicus* ALMT proteins may explain why no deleterious phenotype has been detected. It is likely that both LjALMT1 and LjALMT2 would provide an apoplastic route for malate movement within the nodule, and that LjALMT1 may be more generally involved in dicarboxylate, or GABA, movement through the root vasculature.

6 GmNPF1.2 is a dicarboxylate transporter on the SM

6.1 Introduction

6.1.1 Dicarboxylate transport across the soybean SM

As previously described in 1.7.1, carbon uptake by symbiosomes is facilitated by a well characterised but unidentified dicarboxylate carrier (see chapter 1 and 5 for summary). Early work using isolated symbiosomes showed that when malate and succinate were supplied as substrates, uptake rates were sufficient to support estimated nitrogen fixation *in vivo* (Price et al. 1987; Day et al. 1989). The carrier has an apparent preference for malate, but also transports a range of other dicarboxylates (Ou Yang et al. 1990). Udvardi et al. (1988) further elucidated that the true substrate for the SM-DC is monovalent dicarboxylate anions and calculated the K_m for malate and succinate to be 2 and 15 µM respectively. It has been suggested that dicarboxylate uptake by the symbiosome is uniport, driven by the energisation of the SM and stimulated by phosphorylation (Ou Yang et al. 1990; Udvardi et al. 1991). The SM-DC is thought to act as an efflux protein, transporting one monovalent malate anion out of the plant's cytosol for each proton pumped across the SM by its H^+-ATPase activity.

6.1.2 Dicarboxylate transport in non-legume symbioses

The non-legume *A. glutinosa* forms an actinorhizal symbiosis with the filamentous soil bacterium *Frankia*, whereby the symbiotic interface is invaginated and the PM of the infected cell is not completely enclosed (Mylona et al. 1995). There has been little biochemical characterisation of this symbiosis due to the difficulty to study and its agricultural relevance. A nodule specific member of the NPF family, AgDCAT1, was localised to the symbiotic interface and shown to transport dicarboxylates when expressed in the dicarboxylate transport deficient *E. coli* strain CBT315 and in *X. laevis* oocytes (Jeong et al. 2004). Substrate specificity was investigated through [^{14}C] malate uptake and showed that both succinate and fumarate were competitive for the transporter. These data are reminiscent of the dicarboxylate carrier characterised on the soybean SM. However, given that NPFs are generally regarded as proton symporters (Corratgé-Faillie and Lacombe 2017), and the symbiosome has an acid interior (Bhandari and Nicholas 1985; Blumwald et al. 1985; Udvardi and Day 1989), seemingly the energetics are not aligned. Indeed, a proton-symporter would likely transport its substrate out of the symbiosome. However, not all NPFs act as symporters *per se*.

6.1.3 NPF transporters

NPFs belong to the major facilitator superfamily, and most of the characterisation of this superfamily has been performed in *Arabidopsis*, where 53 members are found (Léran et al. 2014). The substrate preferences of NPFs are extremely broad, with anion, peptide, amino acid, plant hormone and glucosinolate transport characterised in various *Arabidopsis* family members (Corratgé-Faillie and Lacombe 2017). The crystal structure of AtNPF6.3 has been resolved, suggesting a symport mechanism of transport (Parker and Newstead 2014). A proton binding motif named ExxER/K on transmembrane helix 1 (TMH1), as well as two salt bridges that form between residues on TMH1 and TMH7 or TMH4 and TMH10, have been suggested to facilitate the conformational change required for proton symport (Longo et al. 2018). Interestingly, these structural features are not strictly conserved across plant genomes, suggesting that some NPFs have evolved uniport or antiport mechanisms (Longo et al. 2018). A subfamily of NPFs, the so-called NAXT proteins, are thought to facilitate the uniport of nitrate out of the plant cell's cytosol, coupled to proton-pumping by the PM H^+-ATPase and driven by the electrochemical gradient across the PM (Segonzac et al. 2007). Biochemically, this is essentially the transport mechanism described for isolated soybean symbiosomes, making the NPF family excellent candidates for the SM-DC (Booth et al. 2021).

6.1.4 NPF transporters expressed exclusively in soybean nodules

Eight members of the NPF family have been found to be exclusively expressed in soybean nodules ((Severin et al. 2010), Table 6.1). These include *GmNPF1.2* (Glyma.08G037200), *GmNPF5.2* (Glyma.06G145200), *GmNPF5.3* (Glyma.04G220700), *GmNPF2.24* (Glyma.11G224400), *GmNPF5.25* (Glyma.11G224200), *GmNPF5.29* (Glyma.18G033900), *GmNPF5.30* (Glyma.11G223900) and *GmNPF8.6* (Glyma.02G224600). Five of these were identified also in proteomic studies of the soybean SM ((Clarke et al. 2015), Table 6.1), and NPFs have been detected also in the SM proteome of *L. japonicus* (Wienkoop and Saalbach 2003). Localisation of the 2kb 5' regulatory sequence of *GmNPF5.24* and *GmNPF5.25* was investigated through fusion to the GUS reporter gene, with histological straining showing that expression of these proteins was specific to the nodule (Clarke et al. 2015). *GmNPF5.25* was expressed in both the infected and uninfected cells, while *GmNPF5.24* was specific to the infected cells (Clarke et al. 2015). GUS staining driven by the 2kb 5' regulatory sequence of *GmNPF1.2* has also been investigated, with staining comparable to GmNPF5.24 (Penelope Smith, Appendix 12). Localisation of GmNPF1.2, GmNPF5.24 and GmNPF5.29 to the SM was confirmed through C-terminal fusion to GFP ((Clarke et al. 2015); Penelope Smith, Appendix 13).

Table 6.1 Tissue-specific expression of NPF family members in soybean nodules. Normalised transcript reads extracted from SoyBase based on transcriptomics data collected from (Severin et al. 2010). Reads were normalised (reads/kilobase/million) for leaf (L), flower (F), pod (P), seed (Se), root (R) and nodule (N) tissues. Proteins identified in the soybean SM proteome Clarke et al. (2015) are indicated by ✓.

Name	Accession no.	L	F	P	Se	R	N	SM
GmNPF1.2	Glyma.08G037200	0	0	0	0	0	155	✓
GmNPF5.2	Glyma.06G145200	0	0	0	0	0	74	
GmNPF5.3	Glyma.04G220700	0	0	0	0	0	139	
GmNPF2.24	Glyma.11G224400	-	-	-	-	-	-	✓
GmNPF5.25	Glyma.11G224200	0	0	0	0	0	61	✓
GmNPF5.29	Glyma.18G033900	-	-	-	-	-	-	✓
GmNPF5.30	Glyma.11G223900	0	0	0	0	0	96	
GmNPF8.6	Glyma.02G224600	0	0	0	0	0	31	✓

6.1.5 Functions of nodule enhanced NPFs

Data on the potential substrates for the nodule enhanced NPFs is limited. Di- and tripeptide transport by these proteins was investigated in *the S. cerevisiae* mutant ptr2 (LR2 strain), which is unable to grow on media containing small peptides as the sole nitrogen source (Tanaka and Fink 1985; Rentsch et al. 1995). Mohd Noor (2016) found that only GmNPF8.6 was able to transport di- and tripeptides, where a growth complementation phenotype was observed for the peptides Ala-Ala-Aa, Gly-Pro and Val-Leu. *The L. japonicus* ortholog of this transporter, LjNPF8.6, has been reported to transport nitrate when expressed in *X. laevis* oocytes (Valkov et al. 2017). The capacity of LjNPF8.6 to transport dicarboxylates was also investigated in the *E. coli* dicarboxylate transport mutant CBT315 strain, but no complementation was observed when malate was provided as the carbon source. Other than these reports, the substrate specificity of these proteins remains largely unstudied, with no anion, amino acid, plant hormone or glucosinolate transport investigated. Here, I focus on the anion permeability of the nodule enhanced soybean NPF subfamily, with a key focus on dicarboxylates.

6.2 Results

6.2.1 NPF-induced anion currents in *X. laevis* oocytes

The NPF proteins upregulated in nodules were expressed in *X. laevis* oocytes to determine if any anion stimulated currents could be induced. Anions were externally applied to the *X. laevis* oocytes 48 hours post injection with 46 ng of GmNPF1.2; GmNPF5.2; GmNPF5.3; GmNPF5.24; GmNPF5.25; GmNPF5.29; GmNPF5.30; GmNPF8.6 cRNA, or an equivalent volume of nuclease free water. Externally applied anions are capable of transactivating proteins expressed on the *X. laevis* oocyte PM, as demonstrated for the nitrate-inducible nitrate transporter from *Arabidopsis* (Tsay et al. 1993).

The resting membrane potential of *X. laevis* oocytes shifted to a more depolarised state when expressing members of the soybean NPF family and bathed in basal testing solution, indicating successful incorporation of the transporters into the oocyte PM, and altered transport properties (Table 6.2). This shift was from -74 ± 7.6 mV in water injected control oocytes to: -43 ± 3.0 mV in GmNPF1.2; -44 ± 10.9 mV in GmNPF5.2; -46 ± 1.8 mV in GmNPF5.3; -46 ± 7.2 mV in GmNPF5.24; -36 ± 4.7 mV in GmNPF5.25; -22 ± 5.1 mV in GmNPF5.29; -41 ± 2.8 mV in GmNPF5.30; and -38 ± 2.0 mV in GmNPF8.6 expressing oocytes (n = 3 ± SE; Table 6.2). The basal solution contains a low concentration of buffered ions (0.5 mM $CaCl_2$), suggesting that the increase in inward current is likely carried by anions moving out of the NPF-expressing *X. laevis* oocytes rather than due to an influx of cations. The selectivity of the expressed channels was investigated under voltage clamp conditions when the *X. laevis* oocytes were perfused with a solution containing 10 mM of the various anions. While no significant shifts in the reversal potential was observed for any of the externally applied anions, at more negative membrane potentials under voltage-clamp conditions activity with some of the anions was observed (See Figure 6.1).

Table 6.2 Membrane potential of control and NPF-expressing oocytes 48 hours post injection. Vm was measured in basal testing solution (n = 3).

	Vm (mV)	SE
H_2O	-74	7.6
GmNPF1.2	-43	3.0
GmNPF5.2	-44	10.9
GmNPF5.3	-46	1.8
GmNPF5.24	-46	7.3
GmNPF5.25	-36	4.7
GmNPF5.29	-22	5.1
GmNPF5.30	-41	2.8
GmNPF8.6	-38	2.0

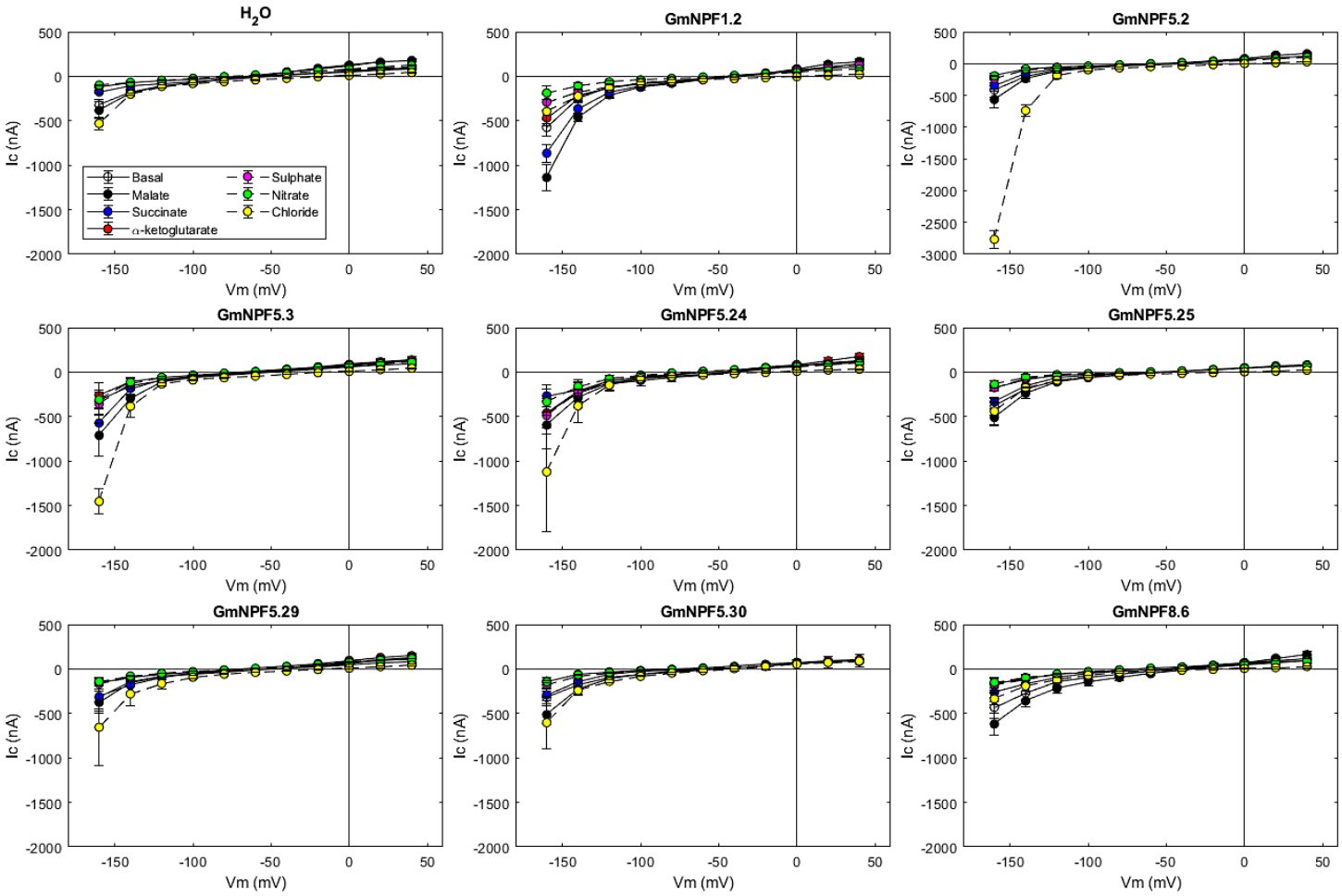

Figure 6.1 Oocytes expressing GmNPF1.2 display malate and succinate stimulated currents. Testing solutions contained a basal solution of 0.5 mM $CaCl_2$, buffered to pH 5.5 with BTP, osmolality adjusted to 220 mosmol kg^{-1} with D-mannitol and containing 10 mM of either malate; succinate; α-ketoglutarate; sulphate; nitrate; or chloride (for H_2O and NPF1.2 expressing oocytes: n = 12 from three oocyte harvests for basal and plus dicarboxylic acids, n = 6 from two oocyte harvests for remaining solutions; for NPF5.2, 5.3, 5.24, 5.25, 5.29, 5.30 and 8.6 expressing oocytes: n = 6 from two oocyte harvests for basal and dicarboxylic acids, n = 3 from a single oocyte harvest for remaining solutions).

For water injected control oocytes the I_c at -160 mV of the tested anions ranged from -324 ± 61.9 nA in basal solution to -530 ± 70.1 nA with externally applied chloride (Figure 6.1). This established a baseline conductivity for endogenous channel activity on the *X. laevis* oocyte membrane. The I_c at -160 mV of GmNPF1.2 expressing oocytes was significantly greater in basal (-575 ± 70.1 nA, p = 0.046), malate (-1137 ± 148.2 nA, $p = 1 \times 10^{-4}$) and succinate (-865 ± 97.4 nA, $p = 2 \times 10^{-4}$) testing solutions; but not significant when α-ketoglutarate (-468 ± 82.6 nA, p = 0.174), sulphate (-290 ± 92.7 nA, p = 0.774), nitrate (-187 ± 74.9 nA, p = 0.237) or chloride (-394 ± 136.6 nA, p = 0.595) were applied (compared to the basal testing solution of water injected control oocytes; significance

calculated through Students t-test (Figure 6.1). Of the expressed GmNPF5 proteins, only GmNPF5.2, GmNPF5.3 and GmNPF5.24 showed any anion stimulated currents, all for chloride with I_c at -160 mV of -2765 ± 136.1 nA ($p = 1 \times 10^{-8}$), -1454 ± 143.4 nA ($p = 2 \times 10^{-4}$) and -1121 ± 671.9 nA (p = 0.0155) respectively (Figure 6.1). While GmNPF5.3 did show minor malate-stimulated currents (I_c of -710 ± 235.3 nA at -160 mV) but this was not statistically significant (p = 0.0545) (Figure 6.2). Malate-induced currents were observed in GmNPF8.6 expressing oocytes (I_c of -618 ± 127.0 nA at -160 mV, p = 0.0337), but other anions, including succinate, had negligible effect (Figure 6.1).

The malate-stimulated currents observed in oocytes expressing GmNPF1.2, GmNPF5.3 and GmNPF8.6 are of particular interest in the context of the dicarboxylate transporter previously observed on the SM (Udvardi et al. 1988). Both GmNPF1.2 and GmNPF8.6 depolarised the reversal potential when malate was externally applied, but this shift was less pronounced with the other soybean NPFs (Figure 6.2).

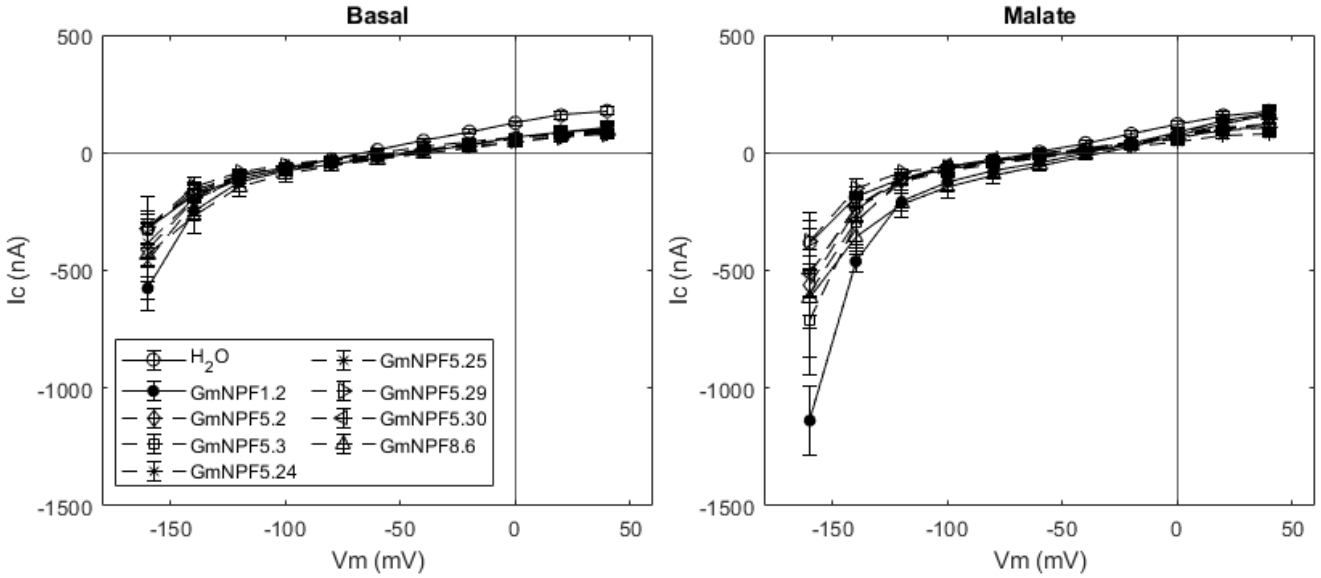

Figure 6.2 Malate-stimulated ion currents in NPF expressing oocytes. Testing solutions contained either 0 mM (basal) or 10 mM malic acid (malate) with 0.5 mM $CaCl_2$, buffered to pH 5.5 with BTP and osmolality adjusted to 220 mosmol kg^{-1} with D-mannitol (for H_2O and NPF1.2 expressing oocytes: n = 12 from three oocyte harvests; for NPF5.2, 5.3, 5.24, 5.25, 5.29, 5.30 and 8.6 expressing oocytes: n = 6 from two oocyte harvests).

6.2.2 Large ionic currents are observed in GmNPF1.2 expressing oocytes preloaded with malate

To further investigate the malate stimulated currents observed with GmNPF1.2, GmNPF5.3 and GmNPF8.6, oocytes were preloaded with 46 nL of 100 mM malic acid pH 7.5, as previously described for TaALMT1 (Sasaki et al. 2004). Loading with malate depolarised both water injected control and NPF-expressing oocytes, but the NPFs tended to be more depolarised than the control. This is reflected in the current-time traces, where larger inward and outward currents were observed in all malate-injected oocytes relative to the uninjected controls (Figure 6.3). The magnitude of the current in GmNPF1.2-expressing oocytes was far greater than that of control, GmNPF5.3 or GmNPF8.6 expressing oocytes, in both basal (Figure 6.3) and malate testing solutions, as reflected in the current-voltage curves (Figure 6.4).

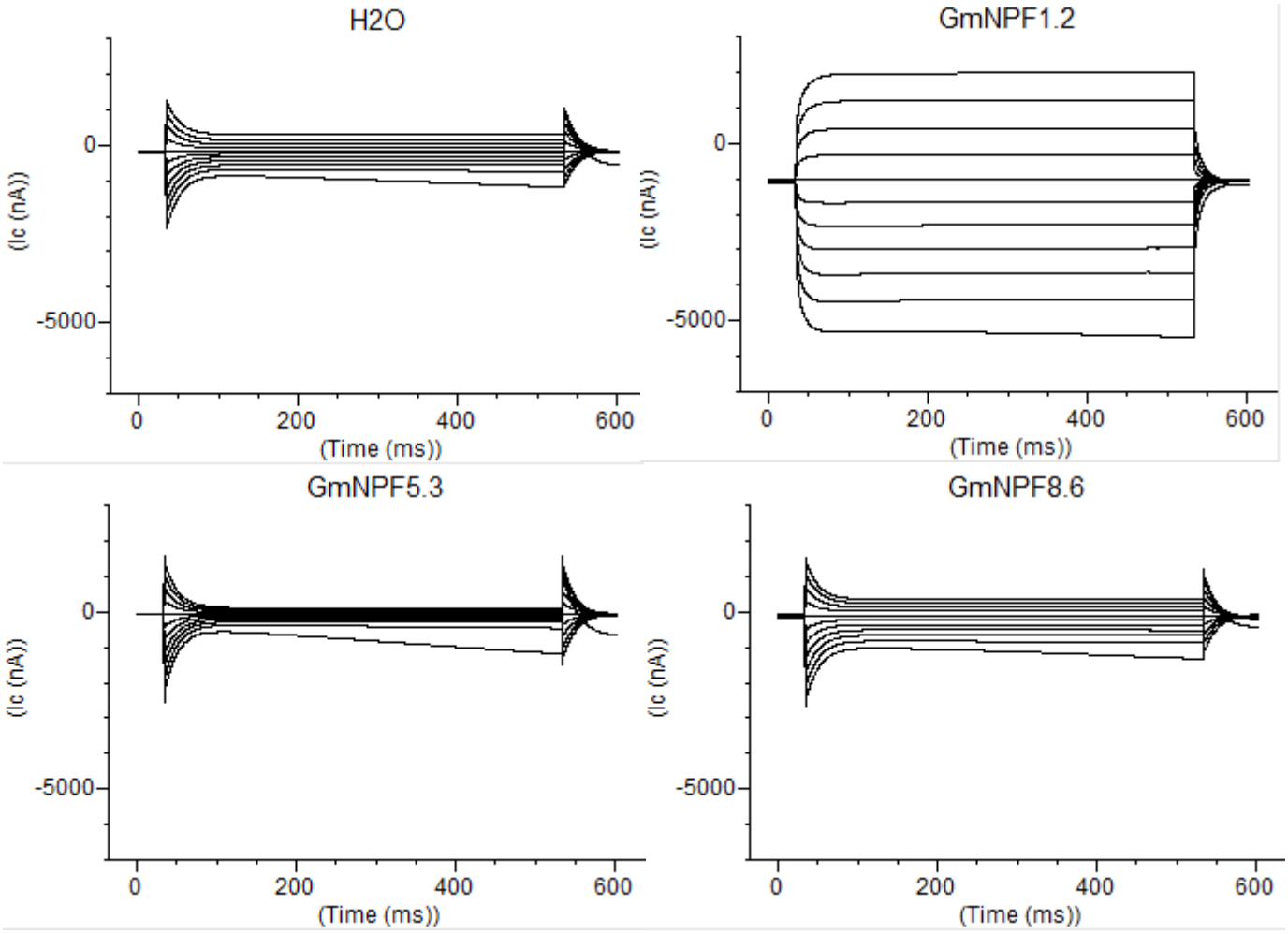

Figure 6.3 Current-time traces of control and NPF-expressing oocytes ± malate injection. Representative traces of control or NPF-expressing oocytes clamped at -40 mV with the membrane potential decreased from 40 to -160 mV in increments of 20 mV for 0.5 s, followed by -40 mV for 0.5 s. Testing solution contained 0.5 mM $CaCl_2$, buffered to pH 5.5 with BTP and osmolality adjusted to 220 mosmol kg^{-1} with D-mannitol.

The reversal potential of GmNPF1.2-expressing oocytes was similar in both basal and malate testing solutions at pH 5.5 (-16.4 and -17.8 mV, respectively). In contrast, the reversal potential of control oocytes was more hyperpolarised and displayed a slight shift from -29.2 mV in basal to -24.1 mV in malate testing solution (Figure 6.4). The reversal potential in GmNPF5.3 and GmNPF8.6 expressing oocytes was more depolarised than the controls, -20.9 mV and -25.6 mV, respectively, but not to the same extent as GmNPF1.2 (Figure 6.4). The ion conductance of control and NPF-expressing oocytes was calculated using the slope of the linear portion of the current-voltage curve across the reversal potential (Figure 6.4). In basal testing solution the conductance of control, GmNPF5.3 and GmNPF8.6-expressing oocytes was low, 4.77, 4.45 and 2.94 µS respectively, but was much greater in GmNPF1.2-expressing oocytes (16.1 µS. For GmNPF1.2). This conductivity increased to 25.5 µS with external application of malate. While conductance also increased in control, GmNPF5.3 and GmNPF8.6-expressing oocytes, the magnitude was much less, 6.28, 5.91 and 4.22 µS respectively.

From these results, I conclude that GmNPF1.2 but not GmNPF5.3 or GmNPF8.6, facilitates bidirectional transport of malate and that the transporter is transactivated by external malate.

Similar results were found at pH 7.5, but the reversal potential of GmNPF1.2-expressing oocytes was more hyperpolarised than at pH 5.5 (-27.4 mV in basal solution, shifting more depolarised by external application of malate -22.2 mV; Figure 6.4b). In contrast there was no substantial shift in the reversal potential of control oocytes at pH 7.5 when bathed in basal or malate testing solutions (Figure 6.4a). In malate-testing solution at pH 7.5, the reversal potential of GmNPF5.3 and GmNPF8.6-expressing oocytes was similar to control oocytes (Figure 6.4c-d). Interestingly, in basal solution at pH 7.5, the reversal potentials of GmNPF5.3 and GmNPF8.6-expressing oocytes were similar to those for GmNPF1.2. Taken together, these results suggest that there was no transactivation of GmNPF5.3 and GmNPF8.6 by malate and that the previously observed ion currents when not preloaded with malate (Figure 6.1) may be carried by another anion. GmNPF5.3 displays large ionic currents when bathed in external chloride testing solution (Figure 6.1), and movement of this anion out of the oocyte may be responsible for the slight stimulation by malate. The conductance of control and GmNPF-expressing oocytes at pH 7.5 was similar to those observed at pH 5.5, although it was slightly reduced for GmNPF1.2 (-25.5 µS at pH 5.5 and -22.5 µS) at pH 7.5 in malate testing solution. This suggests that GmNPF1.2 is a malate carrier relatively insensitive to pH.

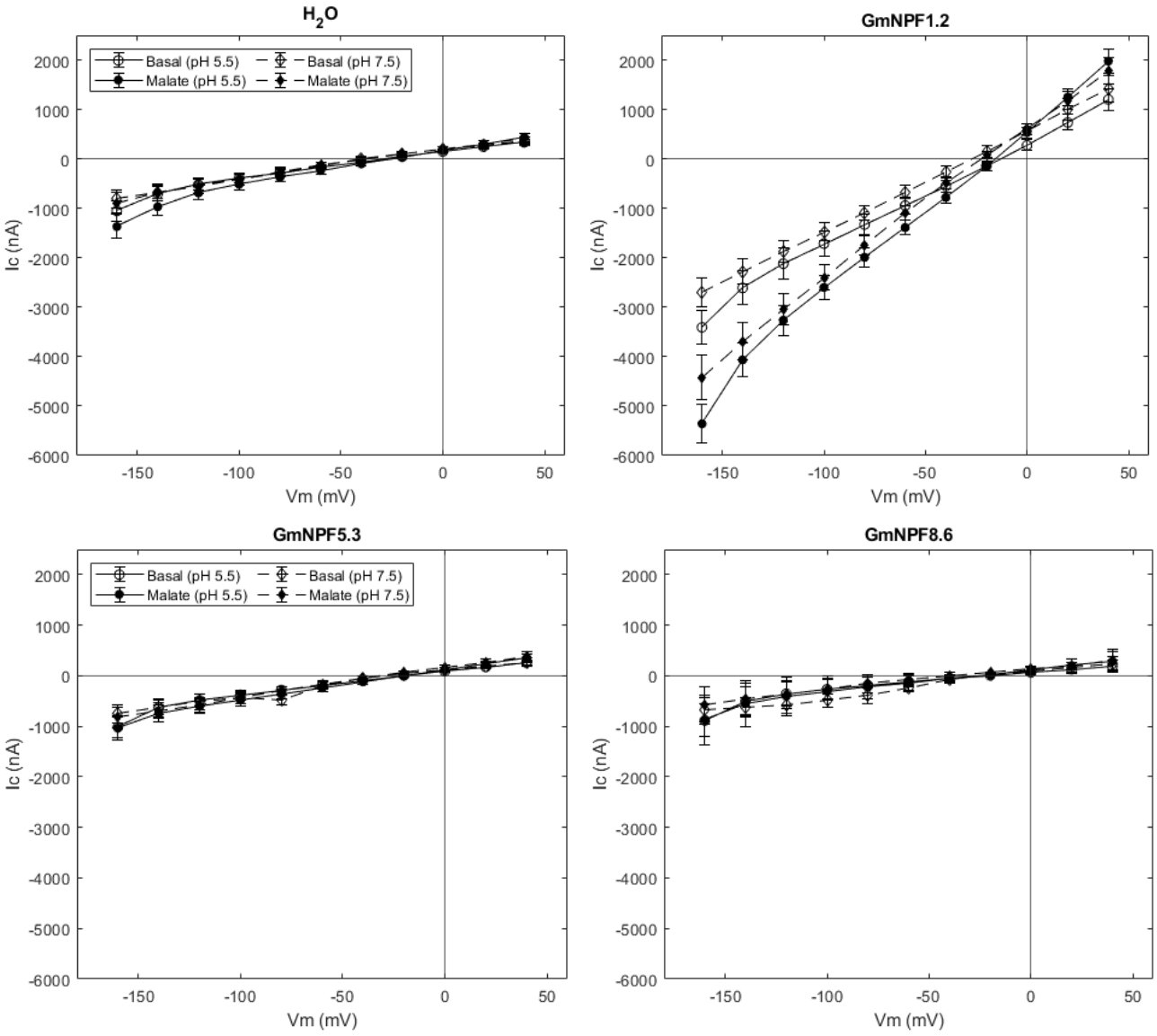

Figure 6.4 GmNPF1.2-expressing oocytes display large ionic currents when preloaded with malate. Oocytes were injected with 46 nL 100 mM malic acid pH 7.5 one hour prior to electrophysiological recordings. Testing solutions contained either 0 mM (basal) or 10 mM malic acid (malate) with 0.5 mM $CaCl_2$, buffered to pH 5.5 or 7.5 with BTP and osmolality adjusted to 220 mosmol kg^{-1} with D-mannitol (for: water injected and GmNPF1.2, n = 12 from three oocyte harvests; GmNPF5.3, n = 3 from a single oocyte harvest; GmNPF8.6, n = 8 from two oocyte harvests).

6.2.3 GmNPF1.2 also transports succinate

Radio tracer studies with isolated symbiosomes (Udvardi et al. 1988) showed that the SM dicarboxylate carrier also catalyses uptake of succinate but not α-ketoglutarate. Likewise, GmNPF1.2 expressed in *X. laevis* oocytes displays succinate-stimulated currents, but α-ketoglutarate had little effect (Figure 6.1). Transactivation of GmNPF1.2 was further investigated in malate-injected oocytes. Externally applied malate generated the largest transactivation of malate efflux from GmNPF1.2-expressing oocytes, but succinate also showed some transactivation, while α-ketoglutarate followed the same trend as the basal solution (Figure 6.5). While the reversal potential in basal, malate, succinate and α-ketoglutarate solutions remained relatively constant (-18.8 mV, -22.3 mV, -19.6 mV and 20.9 mV respectively), the conductivity varied. For GmNPF1.2 expressing oocytes the conductance of the solutions was 8.44 µS, 12.76 µS, 9.92 µS and 8.77 µS respectively. This conductivity was greater than for control oocytes; 4.04 µS, 5.81 µS, 7.45 µS, 6.69 µS respectively (Figure 6.5), suggesting that GmNPF1.2 malate stimulated currents can be transactivated by both malate and succinate but not α-ketoglutarate.

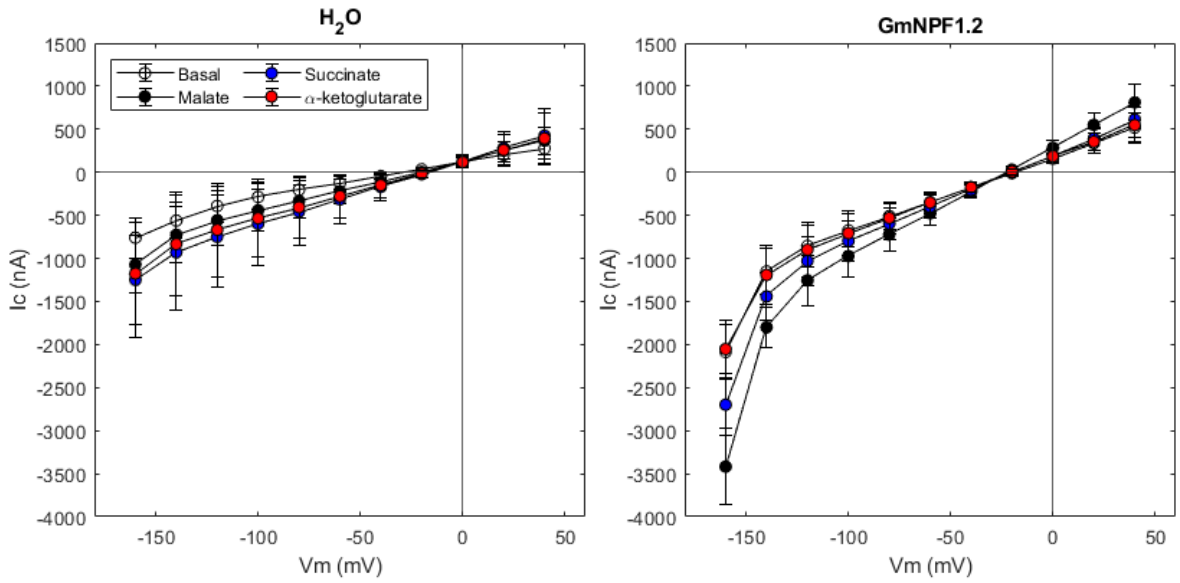

Figure 6.5 Ionic currents in GmNPF1.2-expressing oocytes are transactivated by malate and succinate. Oocytes were injected with 46 nL 100 mM malic acid pH 7.5 one hour prior to electrophysiological recordings. Testing solutions contained a basal solution of 0.5 mM $CaCl_2$, buffered to pH 5.5 with BTP, osmolality adjusted to 220 mosmol kg^{-1} with D-mannitol and containing 10 mM of either: malic; succinic; or α-ketoglutaric acid (n = 6 from two oocyte harvests).

Further evidence that GmNPF1.2 can facilitate transport of succinate comes from experiments with succinate injected oocytes (Figure 6.6). Oocytes from a single harvest were preloaded with either 100 mM malate (pH 7.5) or succinate (pH 7.5) one hour prior to electrophysiological recordings. Control oocytes were slightly more depolarised when preloaded with malate than succinate (reversal potentials in basal testing solution of -36.2 mV and -40.5 mV, respectively; Figure 6.6), but preloading either malate or succinate into NPF1.2-expressing oocytes further depolarised the reversal potentials to -19.1 and 15.9 mV respectively (Figure 6.6). In general, control oocytes had less endogenous activation by succinate preloading compared to malate, with a conductance of 2.42 µS for succinate and 5.45 µS for malate preloaded oocytes when bathed in basal testing solution (Figure 6.6). Malate preloaded GmNPF1.2-expressing oocytes had the greatest conductance in both basal, 17.5 µS, and malate, 28.5 µS, testing solutions, but significant conductance was also observed in succinate preloaded oocytes. For succinate preloaded GmNPF1.2-expressing oocytes this conductance was 11.19 µS in basal and 17.5 µS in malate testing solutions, far greater than the 2.42 and 2.58 µS conductance of control oocytes preloaded with succinate and bathed in these solutions (Figure 6.6).

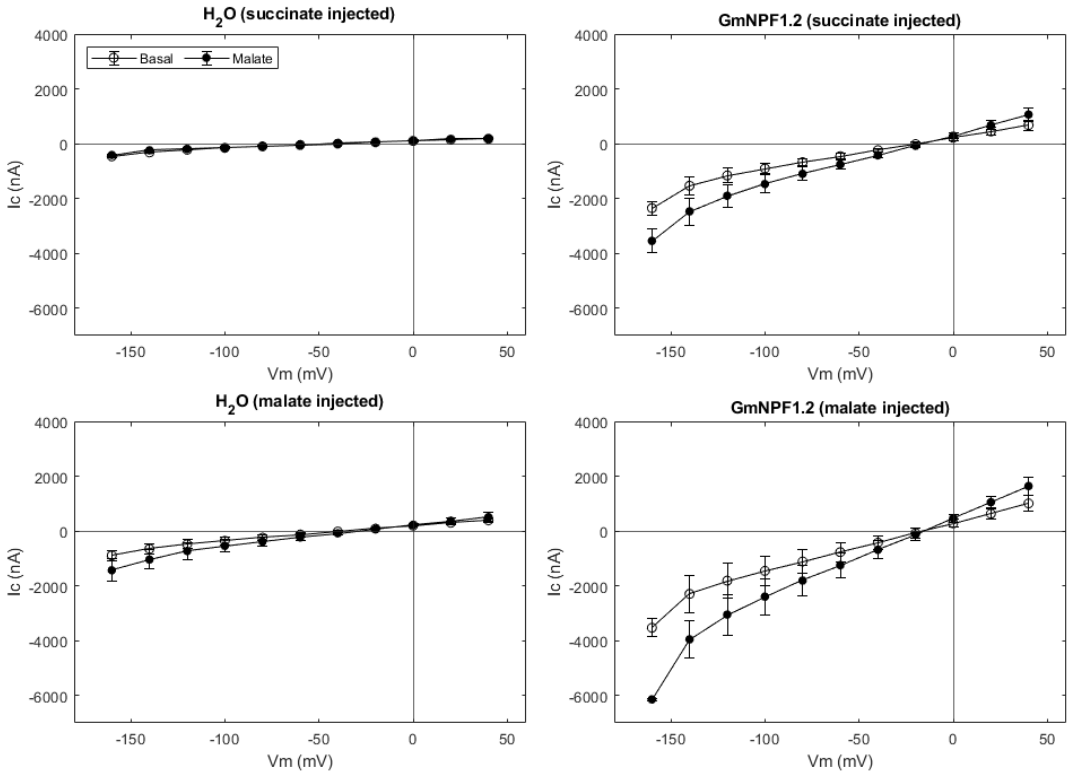

Figure 6.6 Both malate and succinate induce large ionic currents in GmNPF1.2 expressing oocytes. Oocytes were injected with 46 nL 100 mM malate or succinate at pH 7.5 one hour prior to electrophysiological recordings. Testing solutions contained either 0 mM (basal) or 10 mM malate with 0.5 mM $CaCl_2$, buffered to pH 5.5 with BTP and osmolality adjusted to 220 mosmol kg^{-1} with D-mannitol (n = 3 oocytes from a single oocyte harvest).

6.2.4 Phthalonic acid inhibits malate transactivation of GmNPF1.2

Malate uptake into isolated symbiosomes is partially inhibited by phthalonic acid (Udvardi et al. 1988), an inhibitor of mitochondrial citrate and oxoglutarate transporters (Day and Wiskich 1981). The effect of this compound on GmNPF1.2 was investigated in *X. laevis* oocytes under electrophysiological conditions (Figure 6.7). For both control and GmNPF1.2-expressing oocytes, addition of 5 mM phthalonic acid had little effect on the reversal potential when bathed in basal or malate testing solutions, ranging from -24.2 to -20.1 mV in control, and -15.3 to -17.8 mV in GmNPF1.2 expressing oocytes. Phthalonate did, however, inhibit the conductance of GmNPF1.2 expressing oocytes in malate testing solution, from 25.5 to 19.0 µS (Figure 6.7). Negligible effect was observed on control oocytes (Figure 6.7). Since phthalonate shifted the conductance of the malate testing solution towards that of the basal solution, it appears that it inhibits malate transactivation of the channel.

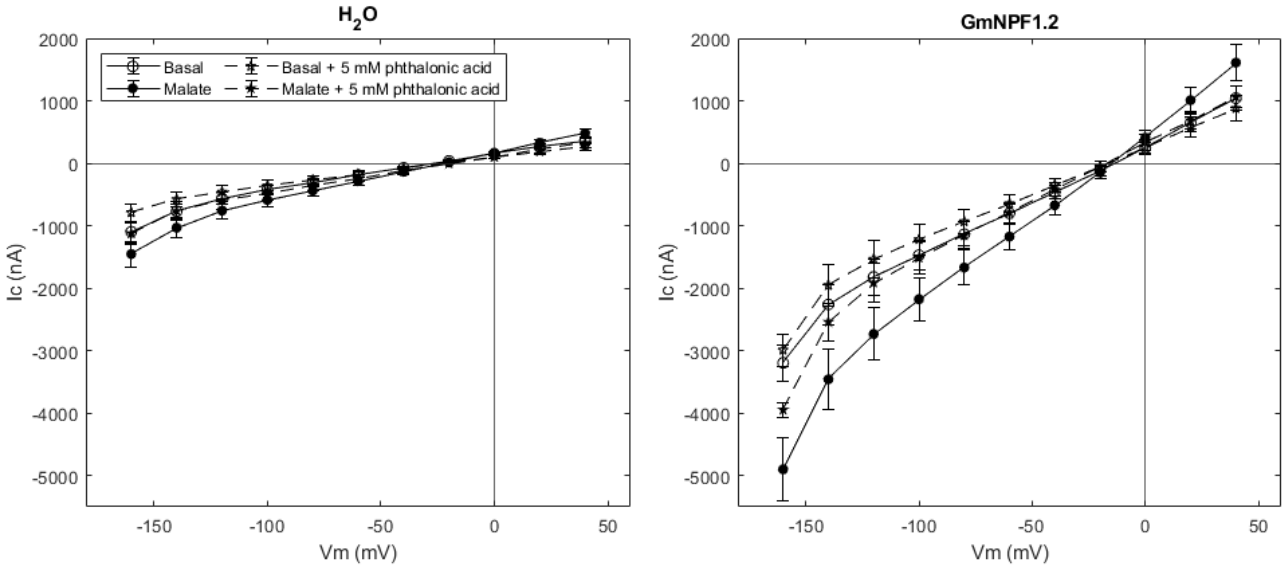

Figure 6.7 GmNPF1.2 malate induced currents are inhibited by phthalonic acid. Testing solutions contained either 0 mM (basal) or 10 mM malate ± 5 mM phthalonic acid with 0.5 mM $CaCl_2$, buffered to pH 5.5 with BTP and osmolality adjusted to 220 mosmol kg^{-1} with D-mannitol (n = 16 from four oocyte harvests).

6.2.5 [^{14}C] malate transport by GmNPF1.2-expressing oocytes

To determine if the observed anion stimulated currents in GmNPF1.2-expressing oocytes were truly carried by movement of malate through the channel and not stimulated by another anion moving out of the oocyte, [^{14}C] malate transport was investigated. Oocytes were incubated in 2 mM malate containing the [^{14}C] radiotracer and sampled over 60 minutes (Figure 6.8). GmNPF1.2-expressing oocytes took up more [^{14}C] malate compared to the control oocytes over a 15-minute time course [42 nmol/oocyte vs 24 nmol/oocyte ($p = 0.046$)]. There was no significant difference in the uptake of [^{14}C] malate at longer time points, but the overall trend of [^{14}C] malate uptake by control oocytes appeared to be linear while in GmNPF1.2-expressing oocytes it trended logarithmic. The [^{14}C] malate uptake time course of control and GmNPF1.2-expressing oocytes was used to establish the linear phase of malate uptake. After five and 15 minutes of incubation with [^{14}C] malate the flux of GmNPF1.2-expressing oocytes was greater than control oocytes, but after 30 minutes the rates equilibrated. Hence further experiments were performed with 15 minutes of [^{14}C] malate incubation as this appeared to be in the linear phase of uptake (Figure 6.8).

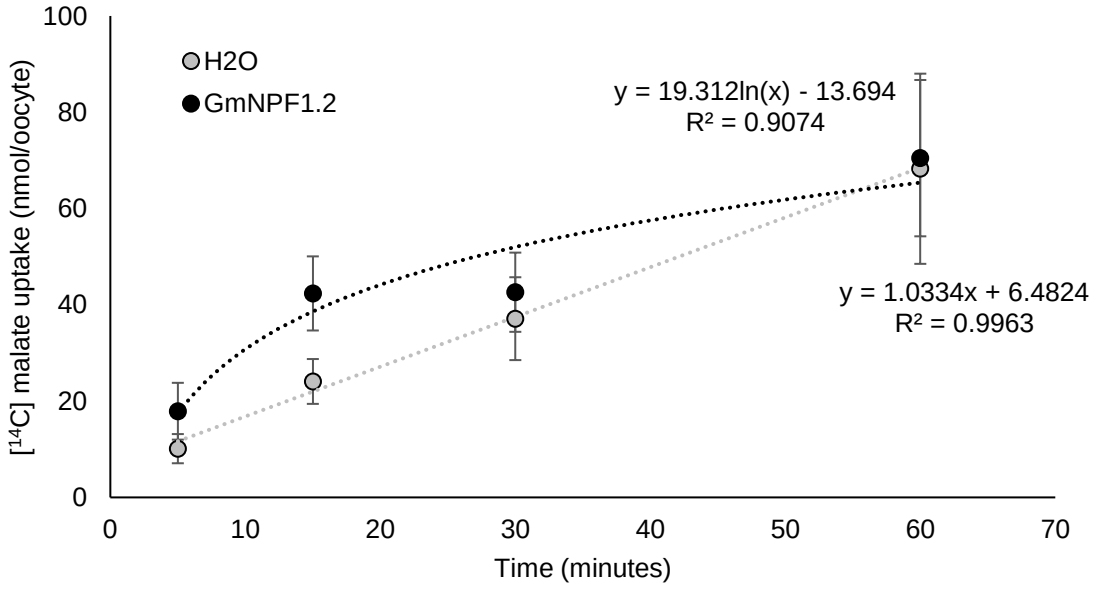

Figure 6.8 Radiolabeled malate uptake by GmNPF1.2 expressing oocytes over 60 minutes. Oocytes injected with dH2O or 46 ng GmNPF1.2 cRNA were incubated in [^{14}C] malate at pH 5.5 over time and digested in nitric acid for determination of malate uptake. The uptake solution contained a total of 2 mM malic acid (malate) with 0.5 mM $CaCl_2$, buffered to pH 5.5 with BTP and osmolality adjusted to 220 mosmol kg^{-1} with D-mannitol (n = 5 from a single oocyte harvest; T-test indicates significance only at 15 minutes).

To confirm that malate was taken up by GmNPF1.2, [^{14}C] malate uptake studies were repeated with a 15-minute incubation. [^{14}C] malate flux by control oocytes was 662 pmol/oocyte/minute was comparable to the flux of control oocytes in previous studies (Gruber et al. 2010) and not significantly affected by addition of 5 mM phthalonic acid to the uptake buffer (Figure 6.9). A flux of 1294 pmol/oocyte/minute was observed in GmNPF1.2-expressing oocytes, significantly greater than in control oocytes, and incubation with phthalonic acid reduced the uptake to a level comparable to the control (Figure 6.9). Using LjALMT1 (see chapter 5) as a positive control, a rate of 2420 pmol/oocyte/minute was recorded, which was insensitive to phthalonic acid (Figure 6.9).

Taken together, these data suggest that GmNPF1.2 is capable of transporting malate and that the channel is inhibited by phthalonic acid.

A [^{14}C] malate efflux experiment was setup to determine if GmNPF1.2 transported malate bidirectionally dependent on the concentration of malate (Appendix 11). GmNPF1.2-expressing oocytes had an accelerated rate of [^{14}C] malate efflux over 15 minutes and sampling of the oocytes post efflux revealed a greater concentration of [^{14}C] malate remained in the control oocytes (Appendix 11). Taking into account the total concentration of malate, control oocytes took up ~45% less [^{14}C] malate in the initial uptake buffer (Appendix 11), although this is not reflected by the initial uptake time course (Figure 6.8). Efflux experiments were repeated by preloading oocytes with 46 nL [^{14}C] malate and sampling the buffer as described in methods 2.7.5. [^{14}C] malate flux over two minutes was greater in GmNPF1.2-expressing oocytes both 24 and 48 hours post cRNA injection. This flux was greater in LjALMT1- expressing oocytes but was not significantly inhibited by phthalonate (Figure 6.10). After 5 minutes incubation in efflux buffer all oocytes were comparable and the flux rate had significantly decreased (Figure 6.10).

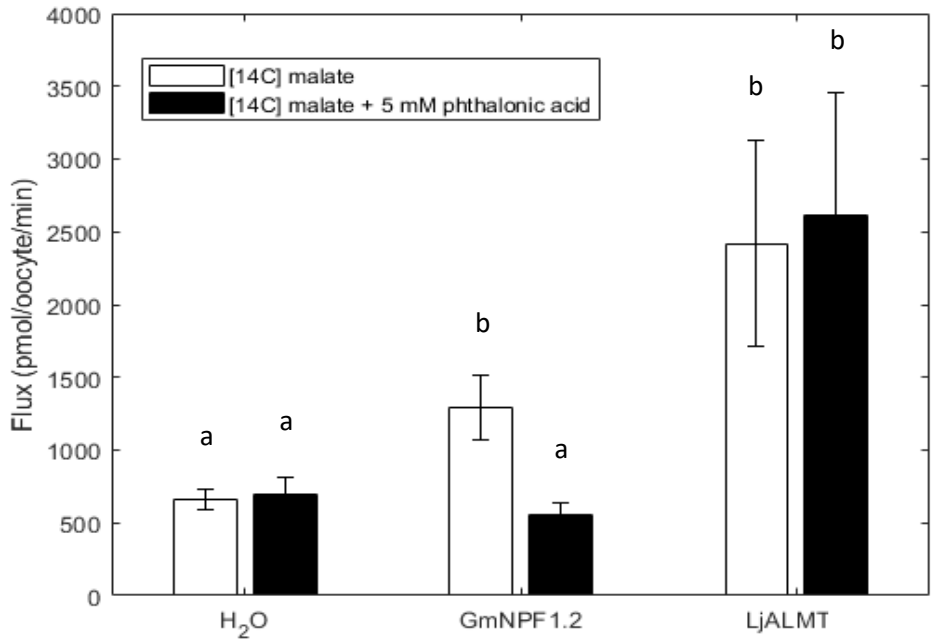

Figure 6.9 Radiolabeled malate uptake by GmNPF1.2 expressing oocytes. Oocytes injected with dH_2O, 46 ng GmNPF1.2 cRNA, or 16 ng LjALMT1 cRNA were incubated in [^{14}C] malate at pH 5.5 for 15 minutes and digested in nitric acid for determination of malate uptake. Uptake solution contained a total of 2 mM malic acid (malate) ± 5 mM phthalonic acid with 0.5 mM $CaCl_2$, buffered to pH 5.5 with BTP and osmolality adjusted to 220 mosmol kg^{-1} with D-mannitol (n = 16 from two oocyte harvests).

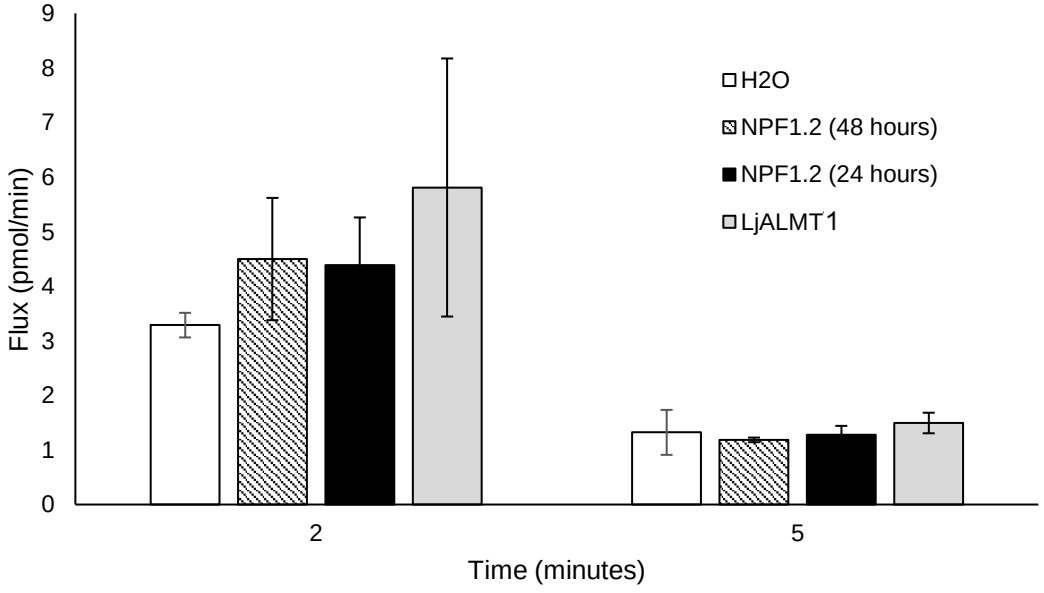

Figure 6.10 Radiolabeled malate efflux by GmNPF1.2 expressing oocytes. Oocytes injected with dH_2O or 46 ng GmNPF1.2, or LjALMT1 cRNA 24 or 48 hours prior to injection with 46 nL [^{14}C] malate and radioactivity of the bathing solution recorded. Bathing solution contained 0.5 mM $CaCl_2$, buffered to pH 5.5 with BTP and osmolality adjusted to 220 mosmol kg^{-1} with D-mannitol (n = 8 from a single oocyte harvest; One-Way ANOVA indicates data is ns for each timepoint).

6.3 Discussion

6.3.1 GmNPF1.2 is a dicarboxylate carrier on the SM

Eight NPF proteins show enhanced expression in nodules compared to other tissues (Table 6.1), but their transport specificity remains largely unstudied. The localisation of GmNPF1.2, GmNPF5.24 and GmNPF5.25 to the infected region of soybean nodules was shown by promoter-GUS fusion experiments ((Clarke et al. 2015); PMC, Appendix 13), suggests a role in symbiotic nitrogen fixation. Of the eight NPFs screened through two-electrode voltage clamping of *X. laevis* oocytes, five putative anion channels - GmNPF1.2; GmNPF5.2; GmNPF5.3; GmNPF5.24; and GmNPF8.6 - elicited detectable whole cell currents when exposed to external anions (Figure 6.1). Transactivation of GmNPF1.2-expressing oocytes by dicarboxylates is of particular interest given the importance of their uptake by symbiosomes to support nitrogen fixation. Isolated symbiosomes are permeable to malate and succinate but poorly permeable to α-ketoglutarate, glutamate, and pyruvate (Price et al. 1987). Results with GmNPF1.2-expressing oocytes were remarkably similar, showing transactivation by malate and succinate, but not α-ketoglutarate (Figure 6.1). Oocytes expressing GmNPF1.2 were not transactivated by any of the other tested anions (nitrate, sulphate, or chloride), indicating a level of specificity for dicarboxylates.

Transactivation of a channel heterologously expressed in the *X. laevis* oocyte expression system must be interpreted with caution. With respect to anion induced transactivation at positive membrane potentials, the increase in positive current may be carried by either the externally applied anion entering through the heterologously expressed channel, or movement of another ion in/out of the *X. laevis* oocyte through an endogenous transport system. At negative membrane potentials, the increase in negative current is likely carried by the movement of cations out of the *X. laevis* oocytes through endogenous transporters, this may be a response to externally applied anions entering the oocyte through the heterologous channel. This mechanism is inherently bias when artificially manipulating the membrane potential, and biochemical changes must be considered for all voltage steps in the clamping protocol. The biological relevance of transactivation is unknown outside of this heterologous expression system. Given that the SM-DC is driven largely by a concentration gradient maintained by bacteroid respiration, it is unclear why malate inside the symbiosome space would stimulate malate uptake or whether this observation is an artifact induced through the heterologous expression system. However, malate and succinate preloading experiments confirmed that when the concentration gradient was favourable, malate could be transported through GmNPF1.2 (Figure 6.4), as shown previously in *X. laevis* oocytes expressing the wheat (*Triticum aestivum*) or barley (*Hordeum vulgare*) ALMT1 (Sasaki et al. 2004; Gruber et al.

2010). GmNPF5.3- or GmNPF8.6-expressing oocytes, on the other hand, showed no such increase in conductance when preloaded with malate (Figure 6.4).

The magnitude of outward currents elicited in HvALMT1 was dependent on the external anion in solution, with externally applied malate, fumarate and citrate transactivating the channel. Likewise, patch clamping of tobacco (*Nicotiana benthamiana*) vacuoles heterologously expressing AtALMT9 displayed selectivity for malate and fumarate over chloride (Kovermann et al. 2007) and later work revealed that the probability of the channel being open was increased by cytosolic malate or fumarate (De Angeli et al. 2013b). These studies provide a precedent that transactivation by externally applied anion is indicative of the transport properties of the channel. Transactivation of GmNPF1.2-expressing oocytes was observed when preloaded with malate and succinate, but not α-ketoglutarate (Figure 6.5), which is consistent with the transport properties of the SM dicarboxylate carrier. The magnitude of transactivation (malate>succinate> α-ketoglutarate) is also similar to the apparent K_m for these substrates in isolated symbiosomes (Udvardi et al. 1988; Ou Yang et al. 1990).

GmNPF1.2-expressing oocytes appear permeable to both malate and succinate, as preloading with either of them led to increased conductivity (Figure 6.6). In contrast, preloading of TaALMT1 with citrate did not generate the same increase in inward current as malate, suggesting that this channel is permeable to malate but not citrate (Sasaki et al. 2004). Preloading of GmNPF1.2-expressing oocytes with citrate or α-ketoglutarate was not attempted in this study but warrants further investigation. Phthalonate, an inhibitor of the SM-DC (Udvardi et al. 1988), inhibited transactivation of NPF1.2 expressing oocytes. This inhibition was not absolute, but nor was it in isolated symbiosomes (Udvardi et al. 1988).

Radiotracer experiments confirmed that the observed malate-induced currents in GmNPF1.2-expressing oocytes were carried by malate. Uptake of [^{14}C] malate by GmNPF1.2-expressing oocytes was significantly greater than in control oocytes and was inhibited by phthalonate (Figure 6.9), consistent with the characteristics of the SM dicarboxylate carrier (Udvardi et al. 1988).

Taken together with the spatial expression (Appendix 12) and localisation data (Appendix 13) of GmNPF1.2 in soybean, showing expression in the infected regions of the nodule and localisation the SM, the results described here strongly suggest that GmNPF1.2 is a SM localised dicarboxylate transporter. Support for a critical role of GmNPF1.2 in nitrogen fixation is also supported by preliminary RNAi experiments (Appendix 14), where a reduction of nitrogen fixation rates is observed. These experiments need to be repeated so that the level of RNAi knockdown can be established.

6.3.2 Transport properties of the other SM NPF proteins

6.3.2.1 Transport of inorganic anions by NPFs

Nitrate plays a significant role in regulating nitrogen fixing symbioses, with suppression of nodulation and inhibition of nitrogen fixation in mature nodules occurring under high soil nitrate availability (Streeter and Wong 1988). Permeability of isolated symbiosomes to nitrate is high and at 10 mM is capable of completely dissipating the membrane potential, essentially switching off the carbon and nitrogen exchange (Udvardi and Day 1989). An inorganic anion transporter which falls into the major facilitator superfamily, NOD70, has already been characterised on the SM of both soybean and *L. japonicus* (Vincill et al. 2005). It was suggested that NOD70, which displays a permeability profile similar to that observed for anions in isolated symbiosomes (nitrate > nitrite > chloride > acetate = dicarboxylates), may be at least partially responsible for the inhibition of nitrogen fixation by uncoupling the H^+-ATPase activity across the SM in response to elevated cytosolic nitrate (Vincill et al. 2005). However, since GmNOD70 appears to have low affinity (1-3 mM) for nitrate, it is possible that other transporters contribute to the observed dissipation of the electrochemical potential across the SM by added nitrate.

Three of the eight NPFs screened in this study displayed significant transactivation by external chloride, but not other anions (Figure 6.1); these all belong to subfamily five (GmNPF5.2, GmNPF5.3 and GmNPF5.24). As previously mentioned, isolated symbiosomes are permeable to chloride, but the physiological relevance of this is poorly established; roles in bacteroid metabolism, maintenance of the electrochemical gradient, or in osmotic adjustment have been suggested (Udvardi and Day 1989; Vincill et al. 2005). In the published literature, the substrate specificity of NPF subfamily five is diverse, with the first characterised member, AtNPF5.2 transporting di- and tri- peptides (Karim et al. 2007). A number of nitrate permeable channels in this subfamily have also been identified, largely through [^{15}N] nitrate accumulation in NPF-expressing oocytes, as demonstrated with AtNPF5.5 (Chiba et al. 2015). More recently, redundancy in the *Arabidopsis* vacuolar efflux system has been established, with five low affinity nitrate permeable NPFs of subfamily five characterised (He et al. 2017; Lu et al. 2022b). None of the soybean enhanced NPFs in this study displayed any transactivation by nitrate; but it is difficult to characterise low affinity nitrate transport under electrophysiological conditions in *X. laevis* oocytes, as whole cell currents are often small, with an I_c at -60 mV of -50 to -100 nA typical (Lu et al. 2022b). A more in-depth analysis of soybean nodule-enhanced NPFs using [^{15}N] nitrate is warranted.

6.3.2.2 Transport of other compounds by NPFs

Electrophysiology is limited by its ability to screen only charged molecules and for this reason the transport of anions has been investigated here. However, due to the diverse substrate specificity of NPFs in other species, it is possible that the nodule-enhanced NPFs may transport compounds other than anions. Previous work has demonstrated di and tri-peptide transport by GmNPF8.6 when expressed in the *S. cerevisiae ptr2* mutant (Mohd Noor 2016), but not by the seven other nodule-enhanced NPFs in soybean. In this study, GmNPF8.6-expressing oocytes appeared to be transactivated by malate, but much less than GmNPF1.2-expressing oocytes (Figure 6.1). However, after preloading GmNPF8.6-expressig oocytes with malate, it was clear that it is not permeable to dicarboxylates (Figure 6.3). Interestingly, the *L. japonicus* ortholog of this gene is reported to facilitate nitrate (but not malate) transport, although di- and tri-peptide transport was not investigated (Valkov et al. 2017). In *Arabidopsis,* AtNRT1.2 has been shown to transport auxin (Kanno et al. 2012), and given the permeability of the SM to auxin, it may be possible that one of the nodule enhanced NPFs facilitates this uptake. Although AtNPF1.2 is classified in the NPF1 subfamily, it displays only a 25% similarity in amino acid sequence to GmNPF1.2, the dicarboxylate carrier characterised in this study.

7 General discussion

7.1 Aims

The capacity for legumes to harness gaseous nitrogen through symbiotic nitrogen fixation is of great agricultural importance. For thousands of years legumes have been grown in crop rotations to improve soil nitrogen availability and yield of subsequent crops (White 1970). These practices are still of economic and environmental significance today, reducing the commercial reliance on synthetic nitrogen fertilisers. Understanding the genetic and molecular basis of symbiotic nitrogen fixation is fundamental in improving its efficiency, or perhaps incorporating the symbiosis into cereal crops (Udvardi and Poole 2013). The legume-rhizobia symbiosis is initiated through NOD factor recognition that triggers signalling pathways, ultimately leading to the development of the infection thread and nodule organogenesis. Within the nodule, differentiated bacteroids are symbiotic auxotrophs excluded from the plant cytosol by the SM. This membrane directly controls metabolite transport between the symbionts, and understanding its transport processes is crucial in improving BNF. Many transport processes of the SM have been biochemically characterised, but the molecular identity of these transporters remains unidentified (see chapter 1). In this project, I have focused on the primary nutrient exchange across the SM, identifying the transport proteins responsible for the provision of reduced carbon from the plant to the bacteroid and efflux of fixed nitrogen from the bacteroid to the plant.

7.2 Transport of fixed nitrogen

A number of previous studies have shown that nitrogen fixed in the bacteroid may exist as NH_3, NH_4^+ or amino acids within the symbiosome space, but it is likely that of these NH_4^+ is a major form and needs to be transported across the SM. Transport of NH_4^+ in patch-clamped SM was shown to occur through a voltage dependent NSCC of SubpicoSeimen conductance present at high density in the SM patches and rectified by divalent cations (Tyerman et al. 1995; Whitehead et al. 1998; Obermeyer and Tyerman 2005). Those characteristics of the SM-NSCC are reminiscent of recently described aquaporin-mediated ion transport in various membrane systems (Weaver et al. 1994; Yool et al. 1996; Yu et al. 2006; Byrt et al. 2017). GmNOD26 is an aquaporin known to localise to the SM (Rivers et al. 1997; Fleurat-Lessard et al. 2005; Clarke et al. 2015) and constitutes ~10% of the SM total protein mass (Rivers et al. 1997). Other studies showed that GmNOD26 is also a diffusive pathway for NH_3 efflux from symbiosomes (Hwang et al. 2010), and behaves as an ion channel when expressed in lipid bilayers, albeit with an anion:cation preference (Weaver et al. 1994). Taking these earlier studies as a cue, I have further characterised the transport properties of GmNOD26 in *X. laevis* oocytes and yeast, showing that it transports monovalent cations and is the likely pathway for NH_4^+ efflux from symbiosomes.

7.2.1 Distinguishing exogenously expressed GmNOD26 activity from endogenous *X. laevis* channels.

Typically, when investigating the monovalent cation conductivity of a foreign protein expressed in *X. laevis* oocytes, the testing solution will also contain divalent cations, usually 1 mM Mg^{2+} and 1.8 mM Ca^{2+}. This is largely to modulate the activity of endogenous voltage-gated channels, with endogenous activity of oocyte NSCCs being particularly problematic (Terhag et al. 2010). These channels are permeable to a range of monovalent cations, including NH_4^+, and are rectified by divalent cations (Burckhardt and Frömter 1992; Burckhardt and Burckhardt 1997; Arellano et al. 1995). It is possible that previous characterisation of GmNOD26 in *X. laevis* oocytes used a high concentration of divalent cations, and the channel's cation conductivity was masked. However, given that the pharmacological signatures of the endogenous *X. laevis* NSCC and GmNOD26 are so similar, it poses the question, is the NSCC activity of GmNOD26-expressing *X. laevis* oocytes an artifact? The experiments described in this thesis indicate that this is not the case.

1. The time dependent ionic currents observed in GmNOD26-expressing *X. laevis* oocytes were not evident in control oocytes but do resemble the SM-NSCC traces seen in symbiosome patches by Tyerman et al. (1995).
2. Aquaporins typically display low open ion channel probabilities, making characterisation in heterologous systems difficult - as noted with HsAQP1 (Yu et al. 2006). However, a number of groups have identified specific regions of aquaporins that when mutated alter their ion channel activity without affecting water permeability (Boassa and Yool 2002; Yu et al. 2006; Kourghi et al. 2018a). Site-directed mutagenesis of the Loop D regulatory region of GmNOD26, based on the HsAQP1 structural mutants, particularly the R194N mutation, restricted ion conductance without an apparent effect on the water permeability of GmNOD26.
3. Phosphomimetics of S262 in GmNOD26 provide further structural evidence that the ionic currents were carried by the heterologously expressed channel, rather than the endogenous NSCC. In line with previous observations, phosphorylation of GmNOD26 enhanced its water permeability (Guenther et al. 2003) but reduced the ionic conductivity (Lee et al. 1995). This is the first time that the 'switch' between ion and water conducting states of GmNOD26 has been demonstrated in *a X. laevis* oocytes, confirming that this ion conductance is carried by cations rather than anions. Through maintaining chloride concentrations, I was able to establish a permeability profile of NH_4^+>MeA^+=K^+>Na^+>Choline, which is reminiscent of the SM-NSCC (Tyerman et al. 1995).

It is apparent that GmNOD26 is a multifunctional aquaporin, permeable to water, formamide, glycerol, NH_3 (Rivers et al. 1997; Wallace et al. 2002; Hwang et al. 2010) and now also cations (this thesis). Taken together, these studies show that GmNOD26 is capable of handling two of the three possible nitrogen sources produced by bacteroids, NH_3 and NH_4^+. However, my experiments with *S. cerevisiae* mutants suggest strongly that GmNOD26 is not involved in amino acid transport.

7.2.2 Regulation of GmNOD26 activity

Given that the symbiosome space is acidic, it is surprising that GmNOD26 is be gated by protons. Unfortunately, initial characterisation of the SM-NSCC in patches was only performed at pH 7.0 (Tyerman et al. 1995), and the effect of pH on the channel *in planta* is unknown. Future work should investigate the conductivity of the SM-NSCC at varying pH using patch clamping of isolated symbiosomes and manipulating the pH of the pipette solution. It should also be borne in mind that proton gating of GmNOD26 in *X. laevis* oocytes may be different *in planta*. I observed greater sodium induced inward currents in the phosphonull mutant at low pH compared to both the Wt and phosphomimic mutant. The sodium induced inward currents of Wt GmNOD26-expressing *X. laevis* oocytes switch from behaving in a similar manner to the phosphonull mutant at pH 7.5, to behaving similarly to the phosphomimic mutant at pH <7.0. This may indicate that the Wt GmNOD26 protein is not phosphorylated when in slightly basic testing solutions but becomes phosphorylated by a native *X. laevis* oocyte protein kinase, such as CK2 (Westmark et al. 2002), when in neutral or acidic testing solutions. That is, the magnitude of the pH dependent gating mechanism may be exaggerated by the additional phosphorylation gating mechanism. Though the phosphomimetics provides some evidence for this, it would be useful to employ a phosphor-specific antibody for GmNOD26 (anti-GC12P) to confirm these observations (see (Guenther et al. 2003)). However, even those experiments could be complicated by other phosphorylation targets of *X. laevis* oocyte protein kinases.

In addition to the above, the NSCC activity of GmNOD26 on the SM *in planta* may be altered due to its binding of GS. It has been established that the C-terminal domain of GmNOD26 interacts with cytosolic glutamine synthetase GS1β and GS1γ (Masalkar et al. 2010), and that the true substrate of GS is NH_4^+ (Liaw et al. 1995). Given that GS contains a high affinity NH_4^+ site, docking to GmNOD26 could enhance the sink strength for NH_4^+ through the central pore formed by the GmNOD26 tetramer. Additionally, conformational changes to the protein structure may directly alter its transport status. In HsAQP1, the C-terminal domain is an important regulatory region for ion channel activation (Boassa and Yool 2002), and the phosphorylation site of GmNOD26 at S262 is located on the C-terminus of the protein.

7.2.3 Further studies with GmNOD26

Although this thesis provides strong evidence that GmNOD26 acts as a NSCC and transports ammonium in heterologous systems, further characterisation of GmNOD26 *in planta* is required, for example using transgenics to alter its expression. The use of RNAi or CRISPR technologies would allow for the symbiotic phenotype of GmNOD26 to be characterised. Unfortunately, such experiments were outside the scope of this thesis due to time constraints, but I am currently preparing an RNAi construct for future knock-down of GmNOD26 in the nodules on hairy roots of *G. max*. If my interpretation of the results presented here are correct, then knocking down the expression of the SM-NSCC should significantly impact the plant's capacity to fix biological nitrogen (bearing in mind that some fixed nitrogen may still exit the symbiosome as amino

acids). A reduction in symbiotic phenotype has already been shown in CRISPR/Cas9-mediated knockout of MtNOD26 (Frare et al. 2022). In addition to measuring nitrogen fixation rates and plant growth characteristics, it would be useful to perform patch-clamp experiments with the transgenic symbiosomes to directly observe changes to the activity of the SM-NSCC.

7.3 Transport of reduced carbon

The demand for fixed carbon in nodules is very large compared to the rest of the plant, consuming up to 25% of total photosynthate Schubert (1981); (Vance 2008). This carbon is largely supplied to nodules as sucrose before it is metabolised to dicarboxylates that must permeate the symbiosome to support a functioning symbiosis (Gordon et al. 1985; Udvardi and Day 1997; Booth et al. 2021). The transport properties of the ALMT family closely resemble that of the SM-DC, but these proteins have not been identified in SM proteomics (Wienkoop and Saalbach 2003; Saalbach et al. 2002; Clarke et al. 2015; Luo et al. 2023). Using the updated MG20 genome of the model legume *L. japonicus* I identified 13 full-length ALMT transcripts, with six of these being putative ALMT sequences. Of the six uncharacterised transcripts, *LjALMT1* appeared to be expressed in the nodules, but in a detailed analysis I was able to show that it was mainly expressed through the vascular tissue of the root and nodule rather than in the infected region. This analysis builds on the work by Takanashi et al. (2016), suggesting that an ALMT protein is not responsible for dicarboxylate transport across the SM.

During *Frankia* symbiosis in the non-legume *A. glutinosa*, an NPF protein is responsible for dicarboxylate transport across the symbiotic interface of infected nodule cells (Jeong et al. 2004). In soybean, eight NPF transcripts are expressed exclusively in the nodules (Severin et al. 2010), and five of these have been identified in SM proteomics (Clarke et al. 2015). I have investigated the capacity for these proteins to transport dicarboxylates through expression in *X. laevis* oocyte. For all eight soybean NPFs, the resting membrane potential of *X. laevis* oocytes shifted to a more depolarised state suggesting an altered biochemical status. Three of the NPFs, GmNPF1.2, GmNPF5.3 and GmNPF8.6, displayed malate-stimulated currents, but through malate preloading I was able to demonstrate that only GmNPF1.2 carried large ionic currents. This technique is common practice when characterising malate export through channels expressed in *X. laevis* oocytes and has been used extensively for the ALMT family (Sasaki et al. 2004; Pineros et al. 2008).

Radiotracer experiments confirmed that the observed malate-induced currents in GmNPF1.2-expressing oocytes were carried by malate. Uptake of [^{14}C] malate by GmNPF1.2-expressing *X. laevis* oocytes was significantly greater than in control oocytes and this uptake was inhibited by phthalonic acid a known inhibitor of the SM dicarboxylate carrier (Udvardi et al. 1988). Ou Yang et al. (1990) further investigated the substrate specificity of the SM dicarboxylate carrier through competitive inhibition of [^{14}C] malate uptake, and respiration of substrates in isolated symbiosomes. They found that succinate, fumarate, oxaloacetate,

α-Ketoglutarate, malonate and phthalonate all reduced malate uptake, but only succinate, oxaloacetate and fumarate were able to stimulate endogenous O_2 uptake, suggesting that only succinate, fumarate and oxaloacetate were transported across the SM at sufficient rates to stimulate bacteroid respiration. Since some organic acids appear to inhibit malate uptake by the SM dicarboxylate carrier without directly being transported through it, these experiments were not repeated in GmNPF1.2-expressing oocytes.

The transport activity of GmNPF1.2 displayed a preference for malate over succinate but no other organic acids, which closely resembles the preferences of the SM-DC characterised in isolated symbiosomes (Udvardi et al. 1988; Ou Yang et al. 1990). Taken together with the inhibition by phthalonic acid, the spatial expression (Appendix 12) and localisation data (Appendix 13) of GmNPF1.2 in soybean indicating expression in the infected regions of the nodule and localisation to the SM, it appears that GmNPF1.2 is in fact the symbiosome dicarboxylate carrier. The critical role of GmNPF1.2 in nitrogen fixation has been further supported by preliminary RNAi experiments (Appendix 14), where a reduction of nitrogen fixation rates is observed. These experiments need to be repeated, so that the level of RNAi knockdown can be established, and further replicates generated. Mutant populations of *M. truncatula* and *L. japonicus* exist, an investigation into the phenotype of the NPF1.2 orthologs in these species is warranted. Given that soybean and *L. japonicus* both form determinate type nodules, it would be expected that the function of this protein would be homologous. There are six NPFs expressed in the indeterminate nodules of *M. truncatula,* it is likely that one of these proteins would function as a dicarboxylate carrier, but this remains to be determined.

7.4 Conclusions and Further Experiments

The data presented here suggest that the principal exchange of fixed carbon (organic acids) for fixed nitrogen (ammonia and ammonium) across the soybean SM is catalysed by GmNPF1.2, the SM dicarboxylate carrier, and GmNOD26, the SM non-selective monovalent cation channel. These findings are fundamental for our understanding of the legume-rhizobia symbiosis and are essential for transferring the symbiotic relationship to other crop species.

However, further experimentation is required to confirm the importance of the two transport systems *in planta.* Transgenic transformation techniques must be employed to confirm the symbiotic phenotypes using knock-down via RNAi of the proteins initially to confirm their functions. In addition to phenotypic measurements (plant growth, N-fixation rates, nodule development), transport activity of isolated symbiosomes could be performed, assuming that nodule development is not too severely compromised. Once their functional roles are confirmed, overexpression of these proteins, individually and together could be employed to determine if we can enhance nitrogen fixation in soybean. Evidence for this is found within the literature, in soybean, fixed nitrogen is transport to the xylem mainly as ureides through ureide permeases localised to the nodule inner cortex and vascular bundle. Overexpression of ureide permease 1

results in enhanced BNF, and ultimately whole plant carbon and nitrogen gains (Carter and Tegeder 2016; Lu et al. 2022a). This process increases the overall sink strength for fixed nitrogen, but it is unknown at what point the SM transporters themselves may become saturated with their substrates. Overexpression of GmNPF1.2 and/or GmNOD26 may further enhance the sink strength for BNF through similar but distinct mechanisms and could be employed in unison with the overexpression of ureide permeases. It is unclear whether simple overexpression of GmNOD26 would enhance BNF, given that this protein is already so highly expressed on the SM. More directional approaches may be required, such as the use of CRISPR technologies to specifically mutate S262 into its ion conducting, unphosphorylated state.

Reference list

Agre P (2004) Aquaporin water channels (Nobel Lecture). Angew Chem Int Ed Engl 43 (33):4278-4290. doi:10.1002/anie.200460804

Ahmad P (2015) Legumes under Environmental Stress: Yield, Improvement and Adaptations. John Wiley & Sons Inc, Chichester, UK. doi:10.1002/9781118917091

Allaway D, Lodwig EM, Crompton LA, Wood M, Parsons R, Wheeler TR, Poole PS (2000) Identification of alanine dehydrogenase and its role in mixed secretion of ammonium and alanine by pea bacteroids. Mol Microbiol 36 (2):508-515. doi:10.1046/j.1365-2958.2000.01884.x

Andreev IM, Dubrovo PN, Krylova VV, Izmailov SF (1999) Functional identification of ATP-driven Ca^{2+} pump in the peribacteroid membrane of broad bean root nodules. FEBS Lett 447 (1):49-52. doi:10.1016/S0014-5793(99)00262-8

Andreev IM, Krylova VV, Zartdinova RF, Izmailov SF (2019) Ca^{2+}-ATPase of the Symbiosome Membrane from Broad Bean Root Nodules: Novel Results Supporting the Mechanism of Transmembrane Translocation of Ca^{2+}. Russ J Plant Physiol 66 (2):345-349. doi:10.1134/S1021443719020043

Anthony TL, Brooks HL, Boassa D, Leonov S, Yanochko GM, Regan JW, Yool AJ (2000) Cloned human aquaporin-1 is a cyclic GMP-gated ion channel. Mol Pharmacol 57 (3):576-588. doi:10.1124/mol.57.3.576

Appleby CA (1984) Leghemoglobin and Rhizobium Respiration. Annu Rev Plant Physiol 35 (1):443-478. doi:10.1146/annurev.pp.35.060184.002303

Arellano RO, Woodward RM, Miledi R (1995) A monovalent cationic conductance that is blocked by extracellular divalent cations in *Xenopus* oocytes. J Physiol 484 (Pt 3) (Pt 3):593-604. doi:10.1113/jphysiol.1995.sp020689

Armstrong CM (1969) Inactivation of the potassium conductance and related phenomena caused by quaternary ammonium ion injection in squid axons. J Gen Physiol 54 (5):553-575. doi:10.1085/jgp.54.5.553

Armstrong EL, Heenan DP, Pate JS, Unkovich MJ (1996) Nitrogen benefits of lupins, field pea, and chickpea to wheat production in south-eastern Australia. Aust J Agric Res 48 (1):39-48. doi:https://doi.org/10.1071/A96054

Assentoft M, Kaptan S, Schneider HP, Deitmer JW, de Groot BL, MacAulay N (2016) Aquaporin 4 as a NH_3 Channel. J Biol Chem 291 (36):19184-19195. doi:10.1074/jbc.M116.740217

Barbier-Brygoo H, De Angeli A, Filleur S, Frachisse JM, Gambale F, Thomine S, Wege S (2011) Anion channels/transporters in plants: from molecular bases to regulatory networks. Annu Rev Plant Biol 62:25-51. doi:10.1146/annurev-arplant-042110-103741

Bauer W (1981) Infection of legumes by rhizobia. Annu Rev Plant Physiol 32 (1):407-449

Beeler T, Bruce K, Dunn T (1997) Regulation of cellular Mg^{2+} by *Saccharomyces cerevisiae*. Biochim Biophys Acta 1323 (2):310-318. doi:10.1016/s0005-2736(96)00199-x

Beitz E, Wu B, Holm LM, Schultz JE, Zeuthen T (2006) Point mutations in the aromatic/arginine region in aquaporin 1 allow passage of urea, glycerol, ammonia, and protons. Proc Natl Acad Sci USA 103 (2):269-274. doi:10.1073/pnas.0507225103

Bergersen FJ (1980) Methods for evaluating biological nitrogen fixation. J. Wiley,

Bergersen FJ, Brockwell J, Gault RR, Lj M, Peoples M, Turner GL (1989) Effects of available soil nitrogen and rates of inoculation on nitrogen fixation by irrigated soybeans and evaluation of δ15N methods for measurement. Aust J Agric Res 40 (4):763-780. doi:https://doi.org/10.1071/AR9890763

Bergersen FJ, Goodchild DJ (1973) Cellular Location and Concentration of Leghaemoglobin in Soybean Root Nodules. Aust J Biol Sci 26 (4):741-756

Besnard J, Pratelli R, Zhao C, Sonawala U, Collakova E, Pilot G, Okumoto S (2016) UMAMIT14 is an amino acid exporter involved in phloem unloading in *Arabidopsis* roots. J Exp Bot 67 (22):6385-6397. doi:10.1093/jxb/erw412

Bhandari B, Nicholas DJ (1985) Proton motive force in washed cells of *Rhizobium japonicum* and bacteroids from *Glycine max*. J Bacteriol 164 (3):1383-1385. doi:10.1128/jb.164.3.1383-1385.1985

Blesh J, Drinkwater LE (2013) The impact of nitrogen source and crop rotation on nitrogen mass balances in the Mississippi River Basin. Ecol Appl 23 (5):1017-1035. doi: https://doi.org/10.1890/12-0132.1

Blumwald E, Fortin MG, Rea PA, Verma DP, Poole RJ (1985) Presence of Host-Plasma Membrane Type H-ATPase in the Membrane Envelope Enclosing the Bacteroids in Soybean Root Nodules. Plant Physiol 78 (4):665-672. doi:10.1104/pp.78.4.665

Boassa D, Yool AJ (2002) A fascinating tail: cGMP activation of aquaporin-1 ion channels. Trends Pharmacol Sci 23 (12):558-562. doi:10.1016/s0165-6147(02)02112-0

Boldt M, Burckhardt G, Burckhardt BC (2003) NH_4^+ conductance in *Xenopus laevis* oocytes. III. Effect of NH_3. Pflugers Arch 446 (6):652-657. doi:10.1007/s00424-003-1122-z

Booth NJ, Smith PMC, Ramesh SA, Day DA (2021) Malate Transport and Metabolism in Nitrogen-Fixing Legume Nodules. Molecules 26 (22). doi:10.3390/molecules26226876

Boron WF, De Weer P (1976) Intracellular pH transients in squid giant axons caused by CO_2, NH_3, and metabolic inhibitors. J Gen Physiol 67 (1):91-112. doi:10.1085/jgp.67.1.91

Brear E, Day D, Smith P (2013) Iron: an essential micronutrient for the legume-rhizobium symbiosis. Front Plant Sci 4 (359). doi:10.3389/fpls.2013.00359

Brear EM, Bedon F, Gavrin A, Kryvoruchko IS, Torres-Jerez I, Udvardi MK, Day DA, Smith PMC (2020) GmVTL1a is an iron transporter on the symbiosome membrane of soybean with an important role in nitrogen fixation. New Phytol 228 (2):667-681. doi:10.1111/nph.16734

Brewin NJ (1991) Development of the legume root nodule. Annu Rev Cell Biol 7:191-226. doi:10.1146/annurev.cb.07.110191.001203

Brinkworth RI, Munn AL, Kobe B (2006) Protein kinases associated with the yeast phosphoproteome. BMC Bioinform 7:47. doi:10.1186/1471-2105-7-47

Broughton WJ, Dilworth MJ (1971) Control of leghaemoglobin synthesis in snake beans. Biochem J 125 (4):1075-1080. doi:10.1042/bj1251075

Bruning B, Rozema J (2013) Symbiotic nitrogen fixation in legumes: Perspectives for saline agriculture. Environ Exp Bot 92:134-143. doi:https://doi.org/10.1016/j.envexpbot.2012.09.001

Burckhardt BC, Burckhardt G (1997) NH_4^+ conductance in *Xenopus laevis* oocytes. I. Basic observations. Pflugers Arch 434 (3):306-312. doi:10.1007/s004240050401

Burckhardt BC, Frömter E (1992) Pathways of NH_3/NH_4^+ permeation across *Xenopus laevis* oocyte cell membrane. Pflugers Arch 420 (1):83-86. doi:10.1007/bf00378645

Byrt CS, Zhao M, Kourghi M, Bose J, Henderson SW, Qiu J, Gilliham M, Schultz C, Schwarz M, Ramesh SA, Yool A, Tyerman S (2017) Non-selective cation channel activity of aquaporin AtPIP2;1 regulated by Ca^{2+} and pH. Plant Cell Environ 40 (6):802-815. doi:10.1111/pce.12832

Cakmak I (2000) Possible roles of zinc in protecting plant cells from damage by reactive oxygen species. New Phytol 146 (2):185-205. doi:10.1046/j.1469-8137.2000.00630.x

Campbell EM, Birdsell DN, Yool AJ (2012) The activity of human aquaporin 1 as a cGMP-gated cation channel is regulated by tyrosine phosphorylation in the carboxyl-terminal domain. Mol Pharmacol 81 (1):97-105. doi:10.1124/mol.111.073692

Carter AM, Tegeder M (2016) Increasing nitrogen fixation and seed development in soybean requires complex adjustments of nodule nitrogen metabolism and partitioning processes. Curr Biol 26 (15):2044-2051

Catalano CM, Lane WS, Sherrier DJ (2004) Biochemical characterization of symbiosome membrane proteins from *Medicago truncatula* root nodules. Electrophoresis 25 (3):519-531. doi:10.1002/elps.200305711

Chalk PM (1997) Dynamics of biologically fixed N in legume-cereal rotations: a review. Aust J Agric Res 49 (3):303-316. doi:https://doi.org/10.1071/A97013

Chen G, Wang L, Chen Q, Qi K, Yin H, Cao P, Tang C, Wu X, Zhang S, Wang P, Wu J (2019) PbrSLAH3 is a nitrate-selective anion channel which is modulated by calcium-dependent protein kinase 32 in pear. BMC Plant Biol 19 (1):190. doi:10.1186/s12870-019-1813-z

Chen ZC, Yokosho K, Kashino M, Zhao FJ, Yamaji N, Ma JF (2013) Adaptation to acidic soil is achieved by increased numbers of cis-acting elements regulating ALMT1 expression in *Holcus lanatus*. Plant J 76 (1):10-23. doi:10.1111/tpj.12266

Chiasson DM, Loughlin PC, Mazurkiewicz D, Mohammadidehcheshmeh M, Fedorova EE, Okamoto M, McLean E, Glass ADM, Smith SE, Bisseling T, Tyerman SD, Day DA, Kaiser BN (2014) Soybean SAT1 (Symbiotic Ammonium Transporter 1) encodes a bHLH transcription factor involved in nodule growth and NH_4^+ transport. Proc Natl Acad Sci USA 111 (13):4814-4819. doi:10.1073/pnas.1312801111

Chiba Y, Shimizu T, Miyakawa S, Kanno Y, Koshiba T, Kamiya Y, Seo M (2015) Identification of Arabidopsis thaliana NRT1/PTR FAMILY (NPF) proteins capable of transporting plant hormones. J Plant Res 128 (4):679-686. doi:10.1007/s10265-015-0710-2

Christenhusz M, Byng J (2016) The number of known plant species in the world and its annual increase, vol 261. doi:10.11646/phytotaxa.261.3.1

Christopher SF, Lal R (2007) Nitrogen Management Affects Carbon Sequestration in North American Cropland Soils. Crit Rev Plant Sci 26 (1):45-64. doi:10.1080/07352680601174830

Clarke VC, Loughlin PC, Day DA, Smith PMC (2014) Transport processes of the legume symbiosome membrane. Front Plant Sci 5:699-699. doi:10.3389/fpls.2014.00699

Clarke VC, Loughlin PC, Gavrin A, Chen C, Brear EM, Day DA, Smith PM (2015) Proteomic analysis of the soybean symbiosome identifies new symbiotic proteins. Mol Cell Proteomics 14 (5):1301-1322. doi:10.1074/mcp.M114.043166

Cooper JE (2004) Multiple Responses of Rhizobia to Flavonoids During Legume Root Infection. In: Advances in Botanical Research, vol 41. Academic Press, pp 1-62. doi:https://doi.org/10.1016/S0065-2296(04)41001-5

Corratgé-Faillie C, Lacombe B (2017) Substrate (un)specificity of Arabidopsis NRT1/PTR FAMILY (NPF) proteins. J Exp Bot 68 (12):3107-3113. doi:10.1093/jxb/erw499

Davidson AL, Dassa E, Orelle C, Chen J (2008) Structure, function, and evolution of bacterial ATP-binding cassette systems. Microbiol Mol Biol Rev 72 (2):317-364. doi:10.1128/MMBR.00031-07

Day DA, Kaiser BN, Thomson R, Udvardi MK, Moreau S, Puppo A (2001a) Nutrient transport across symbiotic membranes from legume nodules. Funct Plant Biol 28 (7):669-676

Day DA, Poole PS, Tyerman SD, Rosendahl L (2001b) Ammonia and amino acid transport across symbiotic membranes in nitrogen-fixing legume nodules. Cell Mol Life Sci 58 (1):61-71. doi:10.1007/PL00000778

Day DA, Price GD, Udvardi MK (1989) Membrane Interface of the *Bradyrhizobium japonicum-Glycine max* Symbiosis: Peribacteroid Units From Soyabean Nodules. Funct Plant Biol 16 (1):69-84

Day DA, Wiskich JT (1981) Effect of phthalonic acid on respiration and metabolite transport in higher plant mitochondria. Arch Biochem Biophys 211 (1):100-107. doi:https://doi.org/10.1016/0003-9861(81)90434-3

De Angeli A, Baetz U, Francisco R, Zhang J, Chaves MM, Regalado A (2013a) The vacuolar channel VvALMT9 mediates malate and tartrate accumulation in berries of *Vitis vinifera*. Planta 238 (2):283-291. doi:10.1007/s00425-013-1888-y

De Angeli A, Zhang J, Meyer S, Martinoia E (2013b) AtALMT9 is a malate-activated vacuolar chloride channel required for stomatal opening in *Arabidopsis*. Nat Commun 4:1804. doi:10.1038/ncomms2815

Dean RM, Rivers RL, Zeidel ML, Roberts DM (1999) Purification and functional reconstitution of soybean nodulin 26. An aquaporin with water and glycerol transport properties. Biochem 38 (1):347-353. doi:10.1021/bi982110c

Delgado MJ, Tresierra-Ayala A, Talbi C, Bedmar EJ (2006) Functional characterization of the Bradyrhizobium japonicum modA and modB genes involved in molybdenum transport. Microbiology 152 (1):199-207. doi:https://doi.org/10.1099/mic.0.28347-0

Demidchik V, Davenport RJ, Tester M (2002) Nonselective cation channels in plants. Annu Rev Plant Biol 53:67–107. doi:https://doi.org/10.1146/annurev.arplant.53.091901.161540

Díaz CL, Grønlund M, Schlaman HRM, Spaink HP (2005) Induction of hairy roots for symbiotic gene expression studies. In: Márquez AJ (ed) Lotus japonicus Handbook. Springer Netherlands, Dordrecht, pp 261-277. doi:10.1007/1-4020-3735-X_26

Dietrich D, Hammes U, Thor K, Suter-Grotemeyer M, Flückiger R, Slusarenko AJ, Ward JM, Rentsch D (2004) AtPTR1, a plasma membrane peptide transporter expressed during seed germination and in vascular tissue of *Arabidopsis*. Plant J 40 (4):488-499. doi:10.1111/j.1365-313X.2004.02224.x

Dilworth M, Glenn A (1982) Movements of ammonia in *Rhizobium leguminosarum*. J Gen Microbiol 128:29-37.

Dilworth M, Glenn A (1984) How does a legume nodule work? Trends Biochem Sci 9 (12):519-523. doi:https://doi.org/10.1016/0968-0004(84)90280-9

Djordjevic MA, Redmond JW, Batley M, Rolfe BG (1987) Clovers secrete specific phenolic compounds which either stimulate or repress nod gene expression in *Rhizobium trifolii*. EMBO J 6 (5):1173-1179

Do THT, Martinoia E, Lee Y (2018) Functions of ABC transporters in plant growth and development. Curr Opin Plant Biol 41:32-38. doi:https://doi.org/10.1016/j.pbi.2017.08.003

Downie JA (2010) The roles of extracellular proteins, polysaccharides and signals in the interactions of rhizobia with legume roots. FEMS Microbiol Rev 34 (2):150-170. doi:10.1111/j.1574-6976.2009.00205.x

Downie JA (2014) Legume nodulation. Curr Biol 24 (5):184-190. doi:https://doi.org/10.1016/j.cub.2014.01.028

Dreyer I, Gomez-Porras J, Riaño-Pachón DM, Hedrich R, Geiger D (2012) Molecular evolution of slow and quick anion channels (SLACs and QUACs/ALMTs). Frontiers in plant science 3:263. doi:10.3389/fpls.2012.00263

Durmort C, Brown JS (2015) Chapter 10 - Streptococcus pneumoniae Lipoproteins and ABC Transporters. In: Brown J, Hammerschmidt S, Orihuela C (eds) Streptococcus Pneumoniae. Academic Press, Amsterdam, pp 181-206. doi:https://doi.org/10.1016/B978-0-12-410530-0.00010-7

Dynowski M, Mayer M, Moran O, Ludewig U (2008) Molecular determinants of ammonia and urea conductance in plant aquaporin homologs. FEBS Lett 582 (16):2458-2462. doi:10.1016/j.febslet.2008.06.012

Emmerlich V, Linka N, Reinhold T, Hurth MA, Traub M, Martinoia E, Neuhaus HE (2003) The plant homolog to the human sodium/dicarboxylic cotransporter is the vacuolar malate carrier. Proc Natl Acad Sci USA 100 (19):11122-11126. doi:10.1073/pnas.1832002100

Evans J, O'Connor G, Turner G, Coventry D, Fettell N, Mahoney J, Armstrong E, Walsgott D (1989) N_2 fixation and its value to soil N increase in lupin, field pea and other legumes in south-eastern Australia. Aust J Agric Res 40 (4):791-805. doi:https://doi.org/10.1071/AR9890791

Fedorova E, Thomson R, Whitehead LF, Maudoux O, Udvardi MK, Day DA (1999) Localization of H^+ATPases in soybean root nodules. Planta 209 (1):25-32

Ferguson BJ, Indrasumunar A, Hayashi S, Lin MH, Lin YH, Reid DE, Gresshoff PM (2010) Molecular analysis of legume nodule development and autoregulation. J Integr Plant Biol 52 (1):61-76. doi:10.1111/j.1744-7909.2010.00899.x

Finnemann J, Schjoerring JK (2000) Post-translational regulation of cytosolic glutamine synthetase by reversible phosphorylation and 14-3-3 protein interaction. Plant J 24 (2):171-181. doi:https://doi.org/10.1046/j.1365-313x.2000.00863.x

Fischer HM (1994) Genetic regulation of nitrogen fixation in rhizobia. Microbiol Rev 58 (3):352-386

Fleurat-Lessard P, Michonneau P, Maeshima M, Drevon JJ, Serraj R (2005) The distribution of aquaporin subtypes (PIP1, PIP2 and gamma-TIP) is tissue dependent in soybean (*Glycine max*) root nodules. Ann Bot 96 (3):457-460. doi:10.1093/aob/mci195

Fortin MG, Morrison NA, Verma DP (1987) Nodulin-26, a peribacteroid membrane nodulin is expressed independently of the development of the peribacteroid compartment. Nucleic Acids Res 15 (2):813-824. doi:10.1093/nar/15.2.813

Frare R, Stritzler M, Gómez C, Tajima H, Pascuan C, López-Fernández M, Bottero E, Nikel PI, Alleva K, Ayub N, Blumwald E, Soto G (2022) Retrotransposon and CRISPR/Cas9-mediated knockout of NOD26 impairs the legume-rhizobia symbiosis. Plant Cell Tissue Organ Cult 151:1-13. doi:10.1007/s11240-022-02357-7

Frei B, Eisenach C, Martinoia E, Hussein S, Chen XZ, Arrivault S, Neuhaus HE (2018) Purification and functional characterization of the vacuolar malate transporter tDT from *Arabidopsis*. J Biol Chem 293 (11):4180-4190. doi:10.1074/jbc.RA117.000851

Fujihara S, Abe H, Minakawa Y, Akao S, Yoneyama T (1994) Polyamines in nodules from various plant-microbe symbiotic associations. Plant Cell Physiol 35 (8):1127-1134

Fukai E, Soyano T, Umehara Y, Nakayama S, Hirakawa H, Tabata S, Sato S, Hayashi M (2012) Establishment of a *Lotus japonicus* gene tagging population using the exon-targeting endogenous retrotransposon LORE1. Plant J 69 (4):720-730. doi:10.1111/j.1365-313X.2011.04826.x

Fukai E, Umehara Y, Sato S, Endo M, Kouchi H, Hayashi M, Stougaard J, Hirochika H (2010) Derepression of the plant Chromovirus LORE1 induces germline transposition in regenerated plants. PLoS Genet 6 (3):e1000868. doi:10.1371/journal.pgen.1000868

Garg N, Geetanjali (2009) Symbiotic Nitrogen Fixation in Legume Nodules: Process and Signaling: A Review. In: Lichtfouse E, Navarrete M, Debaeke P, Véronique S, Alberola C (eds) Sustainable Agriculture. Springer Netherlands, Dordrecht, pp 519-531. doi:10.1007/978-90-481-2666-8_32

Geiger D, Scherzer S, Mumm P, Stange A, Marten I, Bauer H, Ache P, Matschi S, Liese A, Al-Rasheid KAS, Romeis T, Hedrich R (2009) Activity of guard cell anion channel SLAC1 is controlled by drought-stress signaling kinase-phosphatase pair. Proc Natl Acad Sci USA 106 (50):21425-21430. doi:10.1073/pnas.0912021106

Gietz RD, Woods RA (2002) Transformation of yeast by lithium acetate/single-stranded carrier DNA/polyethylene glycol method. Meth Enzymol 350:87-96. doi:10.1016/s0076-6879(02)50957-5

González-Andrés F, James E (2016) Biological Nitrogen Fixation and Beneficial Plant-Microbe Interactions. Cham: Springer. doi:10.1007/978-3-319-32528-6

González-Guerrero M, Escudero V, Saéz Á, Tejada-Jiménez M (2016) Transition metal transport in plants and associated endosymbionts: arbuscular mycorrhizal fungi and rhizobia. Front Plant Sci 7:1088

González-Guerrero M, Matthiadis A, Sáez Á, ngela, Long TA (2014) Fixating on metals: new insights into the role of metals in nodulation and symbiotic nitrogen fixation. Front Plant Sci 5:45

Gordon A, Ryle G, Mitchell D, Powell DC (1985) The flux of 14C-labelled photosynthate through soyabean root nodules during N2 fixation. J Exp Bot 36 (5):756-769

Gordon AJ, Lea PJ, Rosenberg C, Trinchant J-C (2001) Nodule formation and function. In: Plant nitrogen. Springer, pp 101-146

Gotfryd K, Mósca AF, Missel JW, Truelsen SF, Wang K, Spulber M, Krabbe S, Hélix-Nielsen C, Laforenza U, Soveral G, Pedersen PA, Gourdon P (2018) Human adipose glycerol flux is regulated by a pH gate in AQP10. Nat Commun 9 (1):4749. doi:10.1038/s41467-018-07176-z

Gottesman MM, Ambudkar SV (2001) Overview: ABC transporters and human disease. J Bioenerg Biomembr 33 (6):453-458. doi:10.1023/a:1012866803188

Gregorich E, Drury C, Baldock J (2001) Changes in Soil Carbon Under Long-Term Maize in Monoculture and Legume-Based Rotation, vol 81. doi:10.4141/S00-041

Gruber B, Ryan P, Richardson A, Tyerman S, Ramesh S, Hebb D, Howitt S, Delhaize E (2010) HvALMT1 from barley is involved in the transport of organic anions. J Exp Bot 61:1455-1467. doi:10.1093/jxb/erq023

Guasch LM, de Felipe MR, Fernández-Pascual M (2001) Effects of different O_2 concentrations on nitrogenase activity, respiration, and O_2 diffusion resistance in *Lupinus albus* cv. Multolupa nodules. J Plant Physiol 158 (11):1395-1402. doi:https://doi.org/10.1078/0176-1617-00577

Guenther JF, Nouth C, Galetovic MP, Wallace IS, et al. (2003) Phosphorylation of soybean nodulin 26 on serine 262 enhances water permeability and is regulated developmentally and by osmotic signals. Plant Cell 15 (4):981-991

Guenther JF, Roberts DM (2000) Water-selective and multifunctional aquaporins from *Lotus japonicus* nodules. Planta 210 (5):741-748. doi:10.1007/s004250050675

Guether M, Balestrini R, Hannah M, He J, Udvardi MK, Bonfante P (2009) Genome-wide reprogramming of regulatory networks, transport, cell wall and membrane biogenesis during *arbuscular mycorrhizal* symbiosis in *Lotus japonicus*. New Phytol 182 (1):200-212. doi:10.1111/j.1469-8137.2008.02725.x

Gutermuth T, Herbell S, Lassig R, Brosché M, Romeis T, Feijó JA, Hedrich R, Konrad KR (2018) Tip-localized Ca^{2+} -permeable channels control pollen tube growth via kinase-dependent R- and S-type anion channel regulation. New Phytol 218 (3):1089-1105. doi:10.1111/nph.15067

Hageman RV, Burris RH (1978) Nitrogenase and nitrogenase reductase associate and dissociate with each catalytic cycle. Proc Natl Acad Sci USA 75 (6):2699-2702. doi:10.1073/pnas.75.6.2699

Hakoyama T, Niimi K, Watanabe H, Tabata R, Matsubara J, Sato S, Nakamura Y, Tabata S, Jichun L, Matsumoto T, Tatsumi K, Nomura M, Tajima S, Ishizaka M, Yano K, Imaizumi-Anraku H, Kawaguchi M, Kouchi H, Suganuma N (2009) Host plant genome overcomes the lack of a bacterial gene for symbiotic nitrogen fixation. Nature 462 (7272):514-517. doi:10.1038/nature08594

Hakoyama T, Niimi K, Yamamoto T, Isobe S, Sato S, Nakamura Y, Tabata S, Kumagai H, Umehara Y, Brossuleit K, Petersen TR, Sandal N, Stougaard J, Udvardi MK, Tamaoki M, Kawaguchi M, Kouchi H, Suganuma N (2012) The integral membrane protein SEN1 is required for symbiotic nitrogen fixation in *Lotus japonicus* nodules. Plant Cell Physiol 53 (1):225-236. doi:10.1093/pcp/pcr167

He Y-N, Peng J-S, Cai Y, Liu D-F, Guan Y, Yi H-Y, Gong J-M (2017) Tonoplast-localized nitrate uptake transporters involved in vacuolar nitrate efflux and reallocation in *Arabidopsis*. Sci Rep 7 (1):1-9

Henderson SW, Nourmohammadi S, Ramesh SA, Yool AJ (2022) Aquaporin ion conductance properties defined by membrane environment, protein structure, and cell physiology. Biophys Rev 14 (1):181-198. doi:10.1007/s12551-021-00925-3

Hirsch A (1992) Developmental biology of legume nodulation. New Phytol 122:211-237

Hodge T, Colombini M (1997) Regulation of metabolite flux through voltage-gating of VDAC channels. J Membr Biol 157 (3):271-279. doi:10.1007/s002329900235

Holm LM, Jahn TP, Møller ALB, Schjoerring JK, Ferri D, Klaerke DA, Zeuthen T (2005) NH_3 and NH_4^+permeability in aquaporin-expressing *Xenopus* oocytes. Pflügers Archiv 450 (6):415-428. doi:10.1007/s00424-005-1399-1

Hoover TR, Imperial J, Ludden PW, Shah VK (1989) Homocitrate is a component of the iron-molybdenum cofactor of nitrogenase. Biochemistry 28 (7):2768-2771. doi:10.1021/bi00433a004

Hosie AH, Allaway D, Poole PS (2002) A monocarboxylate permease of *Rhizobium leguminosarum* is the first member of a new subfamily of transporters. J Bacteriol 184 (19):5436-5448. doi:10.1128/jb.184.19.5436-5448.2002

Howitt SM, Udvardi MK (2000) Structure, function and regulation of ammonium transporters in plants. Biochimica et biophysica acta 1465 (1-2):152-170. doi:10.1016/s0005-2736(00)00136-x

Howitt SM, Udvardi MK, Day DA, Gresshoff PM (1986) Ammonia Transport in Free-living and Symbiotic Rhizobium sp. ANU289. Microbiol 132 (2):257-261. doi:https://doi.org/10.1099/00221287-132-2-257

Hruz T, Laule O, Szabo G, Wessendorp F, Bleuler S, Oertle L, Widmayer P, Gruissem W, Zimmermann P (2008) Genevestigator V3: A Reference Expression Database for the Meta-Analysis of Transcriptomes. Adv Bioinform 2008:1-5. doi:10.1155/2008/420747

Hughes R, Herridge D (1989) Effect of tillage on yield, nodulation and nitrogen fixation of soybean in far north-coastal New South Wales. Aust J Exp Agric 29 (5):671-677. doi:https://doi.org/10.1071/EA9890671

Hurth MA, Suh SJ, Kretzschmar T, Geis T, Bregante M, Gambale F, Martinoia E, Neuhaus HE (2005) Impaired pH Homeostasis in *Arabidopsis* Lacking the Vacuolar Dicarboxylate Transporter and Analysis of Carboxylic Acid Transport across the Tonoplast. Plant Physiol 137 (3):901. doi:10.1104/pp.104.058453

Hwang JH, Ellingson SR, Roberts DM (2010) Ammonia permeability of the soybean nodulin 26 channel. FEBS Lett 584 (20):4339-4343. doi:https://doi.org/10.1016/j.febslet.2010.09.033

Imaizumi-Anraku H, Kawaguchi M, Koiwa H, Akao S, Syōno K (1997) Two Ineffective-Nodulating Mutants of *Lotus japonicus*—Different Phenotypes Caused by the Blockage of Endocytotic Bacterial Release and Nodule Maturation. Plant Cell Physiol 38 (7):871-881. doi:10.1093/oxfordjournals.pcp.a029246

Imes D, Mumm P, Bohm J, Al-Rasheid KA, Marten I, Geiger D, Hedrich R (2013) Open stomata 1 (OST1) kinase controls R-type anion channel QUAC1 in *Arabidopsis* guard cells. Plant J 74 (3):372-382. doi:10.1111/tpj.12133

Ingestad T, Lund A (1979) Nitrogen Stress in Birch Seedlings. Physiol Plant 45 (1):137-148. doi:10.1111/j.1399-3054.1979.tb01678.x

Ingrell CR, Miller ML, Jensen ON, Blom N (2007) NetPhosYeast: prediction of protein phosphorylation sites in yeast. Bioinformatics 23 (7):895-897. doi:10.1093/bioinformatics/btm020

Jahn TP, Møller ALB, Zeuthen T, Holm LM, Klærke DA, Mohsin B, Kühlbrandt W, Schjoerring JK (2004) Aquaporin homologues in plants and mammals transport ammonia. FEBS Lett 574 (1-3):31-36. doi:10.1016/j.febslet.2004.08.004

Jeong J, Suh S, Guan C, Tsay YF, Moran N, Oh CJ, An CS, Demchenko KN, Pawlowski K, Lee Y (2004) A nodule-specific dicarboxylate transporter from alder is a member of the peptide transporter family. Plant Physiol 134 (3):969-978. doi:10.1104/pp.103.032102

Kaiser BN, Finnegan PM, Tyerman SD, Whitehead LF, Bergersen FJ, Day DA, Udvardi MK (1998) Characterization of an ammonium transport protein from the peribacteroid membrane of soybean nodules. Science 281 (5380):1202-1206. doi:10.1126/science.281.5380.1202

Kaiser BN, Moreau S, Castelli J, Thomson R, Lambert A, Bogliolo S, Puppo A, Day DA (2003) The soybean NRAMP homologue, GmDMT1, is a symbiotic divalent metal transporter capable of ferrous iron transport. Plant J 35 (3):295-304. doi:10.1046/j.1365-313X.2003.01802.x

Kaldenhoff R, Fischer M (2006) Functional aquaporin diversity in plants. Biochim Biophys Acta Biomembr 1758 (8):1134-1141. doi:https://doi.org/10.1016/j.bbamem.2006.03.012

Kanno Y, Hanada A, Chiba Y, Ichikawa T, Nakazawa M, Matsui M, Koshiba T, Kamiya Y, Seo M (2012) Identification of an abscisic acid transporter by functional screening using the receptor complex as a sensor. Proc Natl Acad Sci USA 109 (24):9653-9658. doi:10.1073/pnas.1203567109

Karim S, Holmström KO, Mandal A, Dahl P, Hohmann S, Brader G, Palva ET, Pirhonen M (2007) AtPTR3, a wound-induced peptide transporter needed for defence against virulent bacterial pathogens in *Arabidopsis*. Planta 225 (6):1431-1445. doi:10.1007/s00425-006-0451-5

Keeney DR (1982) Nitrogen Management for Maximum Efficiency and Minimum Pollution1. In: Stevenson FJ (ed) Nitrogen in Agricultural Soils. Agronomy Monograph, vol 22. American Society of Agronomy, Crop Science Society of America, Soil Science Society of America, Madison, WI, pp 605-649. doi:10.2134/agronmonogr22.c16

Kennedy IR, Rigaud J, Trinchant JC (1975) Nitrate reductase from bacteroides of *Rhizobium japonicum*: enzyme characteristics and possible interaction with nitrogen fixation. Biochim Biophys Acta 397 (1):24-35

Kereszt A, Mergaert P, Kondorosi E (2011) Bacteroid development in legume nodules: evolution of mutual benefit or of sacrificial victims? Mol Plant Microbe Interact 24 (11):1300-1309. doi:10.1094/mpmi-06-11-0152

Kerner J, Lee K, Tandler B, Hoppel CL (2012) VDAC proteomics: Post-translation modifications. Biochim Biophys Acta Biomembr 1818 (6):1520-1525. doi:https://doi.org/10.1016/j.bbamem.2011.11.013

Kirscht A, Kaptan SS, Bienert GP, Chaumont F, Nissen P, de Groot BL, Kjellbom P, Gourdon P, Johanson U (2016) Crystal Structure of an Ammonia-Permeable Aquaporin. PLoS Biol 14 (3):e1002411. doi:10.1371/journal.pbio.1002411

Kobayashi Y, Hoekenga OA, Itoh H, Nakashima M, Saito S, Shaff JE, Maron LG, Piñeros MA, Kochian LV, Koyama H (2007) Characterization of AtALMT1 expression in aluminum-inducible malate release and its role for rhizotoxic stress tolerance in *Arabidopsis*. Plant Physiol 145 (3):843-852. doi:10.1104/pp.107.102335

Kourghi M, De Ieso M, Nourmohammadi S, Pei J, Yool A (2018a) Identification of Loop D Domain Amino Acids in the Human Aquaporin-1 Channel Involved in Activation of the Ionic Conductance and Inhibition by AqB011. Front Chem 6. doi:10.3389/fchem.2018.00142

Kourghi M, Nourmohammadi S, Pei JV, Qiu J, McGaughey S, Tyerman SD, Byrt CS, Yool AJ (2017) Divalent Cations Regulate the Ion Conductance Properties of Diverse Classes of Aquaporins. Int J Mol Sci 18 (11). doi:10.3390/ijms18112323

Kourghi M, Pei JV, De Ieso ML, Nourmohammadi S, Chow PH, Yool AJ (2018b) Fundamental structural and functional properties of Aquaporin ion channels found across the kingdoms of life. Clin Exp Pharmacol 45 (4):401-409. doi:https://doi.org/10.1111/1440-1681.12900

Kovermann P, Meyer S, Hörtensteiner S, Picco C, Scholz-Starke J, Ravera S, Lee Y, Martinoia E (2007) The *Arabidopsis* vacuolar malate channel is a member of the ALMT family. Plant J 52 (6):1169-1180. doi:10.1111/j.1365-313X.2007.03367.x

Krusell L, Krause K, Ott T, Desbrosses G, Krämer U, Sato S, Nakamura Y, Tabata S, James EK, Sandal N, Stougaard J, Kawaguchi M, Miyamoto A, Suganuma N, Udvardi MK (2005) The sulfate transporter SST1 is crucial for symbiotic nitrogen fixation in Lotus japonicus root nodules. The Plant cell 17 (5):1625-1636. doi:10.1105/tpc.104.030106

Krylova V, Andreev IM, Zartdinova R, Izmailov SF (2013) Biochemical characteristics of the Ca^{2+} pumping ATPase in the peribacteroid membrane from broad bean root nodules. Protoplasma 250 (2):531-538. doi:10.1007/s00709-012-0436-0

Kumar S, Stecher G, Li M, Knyaz C, Tamura K (2018) MEGA X: Molecular Evolutionary Genetics Analysis across Computing Platforms. Mol Biol Evol 35 (6):1547-1549. doi:10.1093/molbev/msy096

Kuzma MM, Hunt S, Layzell DB (1993) Role of Oxygen in the Limitation and Inhibition of Nitrogenase Activity and Respiration Rate in Individual Soybean Nodules. Plant Physiol 101 (1):161-169. doi:10.1104/pp.101.1.161

Larkin MA, Blackshields G, Brown NP, Chenna R, McGettigan PA, McWilliam H, Valentin F, Wallace IM, Wilm A, Lopez R, Thompson JD, Gibson TJ, Higgins DG (2007) Clustal W and Clustal X version 2.0. Bioinformatics 23 (21):2947-2948. doi:10.1093/bioinformatics/btm404

Latham MC (1997) Human nutrition in the developing world / Michael C. Latham. FAO food and nutrition series, 1014-3181 ; no. 29., vol Accessed from https://nla.gov.au/nla.cat-vn4247929. Food and Agriculture Organization of the United Nations, Rome

Lea PJ, Morot-Gaudry J-F (2000) Plant Nitrogen. Berlin/Heidelberg: Springer Berlin Heidelberg, Berlin/Heidelberg. doi:10.1007/978-3-662-04064-5

Lee JW, Zhang Y, Weaver CD, Shomer NH, Louis CF, Roberts DM (1995) Phosphorylation of nodulin 26 on serine 262 affects its voltage-sensitive channel activity in planar lipid bilayers. J Biol Chem 270 (45):27051-27057. doi:10.1074/jbc.270.45.27051

Lee M, Choi Y, Burla B, Kim YY, Jeon B, Maeshima M, Yoo JY, Martinoia E, Lee Y (2008) The ABC transporter AtABCB14 is a malate importer and modulates stomatal response to CO_2. Nat Cell Biol 10 (10):1217-1223. doi:10.1038/ncb1782

Léran S, Varala K, Boyer JC, Chiurazzi M, Crawford N, Daniel-Vedele F, David L, Dickstein R, Fernandez E, Forde B, Gassmann W, Geiger D, Gojon A, Gong JM, Halkier BA, Harris JM, Hedrich R, Limami AM, Rentsch D, Seo M, Tsay YF, Zhang M, Coruzzi G, Lacombe B (2014) A unified nomenclature of NITRATE TRANSPORTER 1/PEPTIDE TRANSPORTER family members in plants. Trends Plant Sci 19 (1):5-9. doi:10.1016/j.tplants.2013.08.008

LeVier K, Day DA, Guerinot ML (1996) Iron Uptake by Symbiosomes from Soybean Root Nodules. Plant Physiol 111 (3):893-900. doi:10.1104/pp.111.3.893

Li H, Jiang F, Wu P, Wang K, Cao Y (2020) A High-Quality Genome Sequence of Model Legume *Lotus japonicus* (MG-20) Provides Insights into the Evolution of Root Nodule Symbiosis. Genes 11 (5). doi:10.3390/genes11050483

Liang C, Piñeros MA, Tian J, Yao Z, Sun L, Liu J, Shaff J, Coluccio A, Kochian LV, Liao H (2013) Low pH, aluminum, and phosphorus coordinately regulate malate exudation through GmALMT1 to improve soybean adaptation to acid soils. Plant Physiol 161 (3):1347-1361. doi:10.1104/pp.112.208934

Liaw SH, Kuo I, Eisenberg D (1995) Discovery of the ammonium substrate site on glutamine synthetase, a third cation binding site. Protein Sci 4 (11):2358-2365. doi:10.1002/pro.5560041114

Ligaba A, Dreyer I, Margaryan A, Schneider DJ, Kochian L, Piñeros M (2013) Functional, structural and phylogenetic analysis of domains underlying the Al sensitivity of the aluminum-activated malate/anion transporter, TaALMT1. Plant J 76 (5):766-780. doi:https://doi.org/10.1111/tpj.12332

Ligaba A, Kochian L, Pineros M (2009) Phosphorylation at S384 regulates the activity of the TaALMT1 malate transporter that underlies aluminum resistance in wheat. Plant J 60 (3):411-423. doi:10.1111/j.1365-313X.2009.03964.x

Ligaba A, Maron L, Shaff JON, Kochian L, PiÑEros M (2012) Maize ZmALMT2 is a root anion transporter that mediates constitutive root malate efflux. Plant Cell Environ 35 (7):1185-1200. doi:https://doi.org/10.1111/j.1365-3040.2011.02479.x

Lima L, Seabra A, Melo P, Cullimore J, Carvalho H (2006) Post-translational regulation of cytosolic glutamine synthetase of *Medicago truncatula*. J Exp Bot 57 (11):2751-2761. doi:10.1093/jxb/erl036

Lin CW, Chang HB, Huang HJ (2005) Zinc induces mitogen-activated protein kinase activation mediated by reactive oxygen species in rice roots. Plant Physiol Biochem 43 (10-11):963-968. doi:10.1016/j.plaphy.2005.10.001

Litman T, Søgaard R, Zeuthen T (2009) Ammonia and Urea Permeability of Mammalian Aquaporins. Handb Exp Pharmacol 190:327-358. doi:10.1007/978-3-540-79885-9_17

Liu S, Liao LL, Nie MM, Peng WT, Zhang MS, Lei JN, Zhong YJ, Liao H, Chen ZC (2020) A VIT-like transporter facilitates iron transport into nodule symbiosomes for nitrogen fixation in soybean. New Phytol 226 (5):1413-1428. doi:https://doi.org/10.1111/nph.16506

Liu Z, Kong X, Long Y, Liu S, Zhang H, Jia J, Cui W, Zhang Z, Song X, Qiu L, Zhai J, Yan Z (2023) Integrated single-nucleus and spatial transcriptomics captures transitional states in soybean nodule maturation. Nat Plants 9 (4):515-524. doi:10.1038/s41477-023-01387-z

Lodwig E, Poole P (2003) Metabolism of Rhizobium Bacteroids. Crit Rev Plant Sci 22 (1):37-78. doi:10.1080/713610850

Lodwig EM, Hosie AHF, Bourdes A, Findlay K, Allaway D, Karunakaran R, Downie JA, Poole PS (2003) Amino-acid cycling drives nitrogen fixation in the legume-Rhizobium symbiosis. Nature 422 (6933):722. doi:10.1038/nature01527

Long Y, Tyerman SD, Gilliham M (2020) Cytosolic GABA inhibits anion transport by wheat ALMT1. New Phytol 225 (2):671-678. doi:https://doi.org/10.1111/nph.16238

Longo A, Miles NW, Dickstein R (2018) Genome Mining of Plant NPFs Reveals Varying Conservation of Signature Motifs Associated With the Mechanism of Transport. Front Plant Sci 9:1668. doi:10.3389/fpls.2018.01668

Lu MZ, Carter AM, Tegeder M (2022a) Altering ureide transport in nodulated soybean results in whole-plant adjustments of metabolism, assimilate partitioning, and sink strength. J Plant Physiol 269:153613. doi:10.1016/j.jplph.2021.153613

Lu YT, Liu DF, Wen TT, Fang ZJ, Chen SY, Li H, Gong JM (2022b) Vacuolar nitrate efflux requires multiple functional redundant nitrate transporter in *Arabidopsis thaliana*. Front Plant Sci 13:926809. doi:10.3389/fpls.2022.926809

Luo Y, Liu W, Sun J, Zhang Z-R, Yang W-C (2023) Quantitative proteomics reveals key pathways in the symbiotic interface and the likely extracellular property of soybean symbiosome. J Genet Genomics 50 (1):7-19. doi:https://doi.org/10.1016/j.jgg.2022.04.004

Madsen LH, Fukai E, Radutoiu S, Yost CK, Sandal N, Schauser L, Stougaard J (2005) LORE1, an active low-copy-number TY3-gypsy retrotransposon family in the model legume *Lotus japonicus*. Plant J 44 (3):372-381

Maierhofer T, Diekmann M, Offenborn JN, Lind C, Bauer H, Hashimoto K, KA SA-R, Luan S, Kudla J, Geiger D, Hedrich R (2014) Site- and kinase-specific phosphorylation-mediated activation of SLAC1, a guard cell anion channel stimulated by abscisic acid. Sci Signal 7 (342):ra86. doi:10.1126/scisignal.2005703

Malolepszy A, Mun T, Sandal N, Gupta V, Dubin M, Urbanski D, Shah N, Bachmann A, Fukai E, Hirakawa H, Tabata S, Nadzieja M, Markmann K, Su J, Umehara Y, Soyano T, Miyahara A, Sato S, Hayashi M, Stougaard J, Andersen SU (2016) The LORE1 insertion mutant resource. Plant J 88 (2):306-317. doi:10.1111/tpj.13243

Marini AM, Soussi-Boudekou S, Vissers S, Andre B (1997) A family of ammonium transporters in *Saccharomyces cerevisiae*. Mol Cell Biol 17 (8):4282-4293. doi:10.1128/mcb.17.8.4282

Marini AM, Springael JY, Frommer WB, André B (2000) Cross-talk between ammonium transporters in yeast and interference by the soybean SAT1 protein. Mol Microbiol 35 (2):378-385. doi:10.1046/j.1365-2958.2000.01704.x

Marini AM, Vissers S, Urrestarazu A, André B (1994) Cloning and expression of the MEP1 gene encoding an ammonium transporter in *Saccharomyces cerevisiae*. EMBO J 13 (15):3456-3463. doi:10.1002/j.1460-2075.1994.tb06651.x

Márquez AJ, Stougaard J, Udvardi M, Parniske M, Spaink H, Saalbach G, Webb J, Chiurazzi M (2005) *Lotus japonicus* handbook. Dordrecht: Springer Netherlands, Dordrecht. doi:10.1007/1-4020-3735-X

Masalkar P, Wallace IS, Hwang JH, Roberts DM (2010) Interaction of Cytosolic Glutamine Synthetase of Soybean Root Nodules with the C-terminal Domain of the Symbiosome Membrane Nodulin 26 Aquaglyceroporin. J Biol Chem 285 (31):23880-23888

Mathews A, Carroll BJ, Gresshoff PM (1989) Development of *Bradyrhizobium* infections in supernodulating and non-nodulating mutants of soybean (*Glycine max* [L.] Merrill). Protoplasma 150 (1):40-47. doi:10.1007/BF01352919

Mellor RB, Werner D (1987) Peribacteroid membrane biogenesis in mature legume root nodules. Symbiosis 3(1):75-100

Meyer S, Mumm P, Imes D, Endler A, Weder B, Al-Rasheid KAS, Geiger D, Marten I, Martinoia E, Hedrich R (2010) AtALMT12 represents an R-type anion channel required for stomatal movement in *Arabidopsis* guard cells. Plant J 63 (6):1054-1062. doi:10.1111/j.1365-313X.2010.04302.x

Meyer S, Scholz-Starke J, De Angeli A, Kovermann P, Burla B, Gambale F, Martinoia E (2011) Malate transport by the vacuolar AtALMT6 channel in guard cells is subject to multiple regulation. Plant J 67 (2):247-257. doi:10.1111/j.1365-313X.2011.04587.x

Miller PR, McConkey BG, Clayton GW, Brandt SA, Staricka JA, Johnston AM, Lafond GP, Schatz BG, Baltensperger DD, Neill KE (2002) Pulse Crop Adaptation in the Northern Great Plains. J Agron 94:261-272. doi:10.2134/agronj2002.2610

Mitsuzawa H (2006) Ammonium transporter genes in the fission yeast *Schizosaccharomyces pombe*: role in ammonium uptake and a morphological transition. Genes Cells 11 (10):1183-1195. doi:https://doi.org/10.1111/j.1365-2443.2006.01014.x

Mohd Noor S, Day D, Smith P (2015) The Symbiosome Membrane. In: Biological Nitrogen Fixation. pp 683-694. doi:10.1002/9781119053095.ch68

Mohd Noor SN (2016) Characterization of transport proteins on the symbiosome membrane of Glycine max. The University of Sydney, Sydney

Moling S, Bisseling T (2015) Evolution of Rhizobium Nodulation: From Nodule-Specific Genes (Nodulins) to Recruitment of Common Processes. In: Bruijn FJd (ed) Biological Nitrogen Fixation, vol 1. John Wiley & Sons, Inc., In Biological Nitrogen Fixation, F. J. de Bruijn (Ed.). . doi:doi:10.1002/9781119053095.ch4

Moreau S, Thomson RM, Kaiser BN, Trevaskis B, Guerinot ML, Udvardi MK, Puppo A, Day DA (2002) GmZIP1 Encodes a Symbiosis-specific Zinc Transporter in Soybean. J Biol Chem 277 (7):4738-4746

Mósca AF, de Almeida A, Wragg D, Martins AP, Sabir F, Leoni S, Moura TF, Prista C, Casini A, Soveral G (2018) Molecular Basis of Aquaporin-7 Permeability Regulation by pH. Cells 7 (11). doi:10.3390/cells7110207

Mumm P, Imes D, Martinoia E, Al-Rasheid KAS, Geiger D, Marten I, Hedrich R (2013) C-Terminus-Mediated Voltage Gating of *Arabidopsis* Guard Cell Anion Channel QUAC1. Molecular plant 6 (5):1550-1563. doi:https://doi.org/10.1093/mp/sst008

Mun T, Bachmann A, Gupta V, Stougaard J, Andersen SU (2016) Lotus Base: An integrated information portal for the model legume *Lotus japonicus*. Sci Rep 6 (1):39447. doi:10.1038/srep39447

Murata K, Mitsuoka K, Hirai T, Walz T, Agre P, Heymann JB, Engel A, Fujiyoshi Y (2000) Structural determinants of water permeation through aquaporin-1. Nature 407 (6804):599-605. doi:10.1038/35036519

Myers R (1988) Nitrogen management of upland crops: from cereals to food legumes to sugar cane. In: Advances in Nitrogen Cycling in Agricultural Ecosystems. CAB International, Oxford, UK, pp 257–273

Mylona P, Pawlowski K, Bisseling T (1995) Symbiotic Nitrogen Fixation. Plant Cell 7 (7):869-885. doi:10.1105/tpc.7.7.869

Nagel R, Elliott A, Masel A, Birch RG, Manners JM (1990) Electroporation of binary Ti plasmid vector into *Agrobacterium tumefaciens* and *Agrobacterium rhizogenes*. FEMS Microbiol Lett 67 (3):325-328. doi:10.1111/j.1574-6968.1990.tb04041.x

Nedumaran S, Abinaya P, Jyosthnaa P, Shraavya B, Rao P, Bantilan C (2015) Grain Legumes Production, Consumption and Trade Trends in Developing Countries. Working Paper Series No. 60.

Negi J, Matsuda O, Nagasawa T, Oba Y, Takahashi H, Kawai-Yamada M, Uchimiya H, Hashimoto M, Iba K (2008) CO2 regulator SLAC1 and its homologues are essential for anion homeostasis in plant cells. Nature 452 (7186):483-486. doi:10.1038/nature06720

Nichols CG, Lopatin AN (1997) Inward rectifier potassium channels. Annu Rev Physiol 59:171-191. doi:10.1146/annurev.physiol.59.1.171

Niemietz CM, Tyerman SD (2000) Channel-mediated permeation of ammonia gas through the peribacteroid membrane of soybean nodules. FEBS Lett 465 (2-3):110-114. doi:10.1016/S0014-5793(99)01729-9

Norden A, Perry V, Martin F, NeSmith J (1977) Effect of Age of Bahiagrass Sod on Succeeding Peanut Crops. Peanut Sci 4 (2):71-74. doi:10.3146/i0095-3679-4-2-7

Nunes MR, van Es HM, Schindelbeck R, Ristow AJ, Ryan M (2018) No-till and cropping system diversification improve soil health and crop yield. Geoderma 328:30-43. doi:https://doi.org/10.1016/j.geoderma.2018.04.031

O'Hara GW, Dilworth MJ, Boonkerd N, Parkpian P (1988) Iron-deficiency specifically limits nodule development in peanut inoculated with *Bradyrhizobium* sp. New Phytol 108 (1):51-57. doi:10.1111/j.1469-8137.1988.tb00203.x

Obermeyer G, Tyerman SD (2005) NH_4^+ currents across the peribacteroid membrane of soybean. Macroscopic and microscopic properties, inhibition by Mg^{2+}, and temperature dependence indicate a SubpicoSiemens channel finely regulated by divalent cations. Plant Physiol 139 (2):1015-1029. doi:10.1104/pp.105.066670

Okamoto S, Yoro E, Suzaki T, Kawaguchi M (2013) Hairy Root Transformation in *Lotus japonicus*. Bio-protocol 3 (12):e795. doi:10.21769/BioProtoc.795

Oldroyd GED, Downie JA (2004) Calcium, kinases and nodulation signalling in legumes. Nat Rev Mol Cell Biol 5 (7):566-576. doi:10.1038/nrm1424

Oldroyd GED, Downie JA (2008) Coordinating Nodule Morphogenesis with Rhizobial Infection in Legumes. Annu Rev Plant Biol 59 (1):519-546. doi:10.1146/annurev.arplant.59.032607.092839

Olness A (2005) Effect of organic carbon on available water in soil. Soil Sci v. 170 (no. 2):pp. 90-101-2005 v.2170 no.2002. doi:10.1097/00010694-200502000-00002

Ott T, van Dongen JT, Gunther C, Krusell L, Desbrosses G, Vigeolas H, Bock V, Czechowski T, Geigenberger P, Udvardi MK (2005) Symbiotic leghemoglobins are crucial for nitrogen fixation in legume root nodules but not for general plant growth and development. Curr Biol 15 (6):531-535. doi:10.1016/j.cub.2005.01.042

Ou Yang L-J, Udvardi MK, Day DA (1990) Specificity and regulation of the dicarboxylate carrier on the peribacteroid membrane of soybean nodules. Planta 182 (3):437. doi:10.1007/BF02411397

Ou Yang L-J, Whelan J, Weaver CD, Roberts DM, Day DA (1991) Protein phosphorylation stimulates the rate of malate uptake across the peribacteroid membrane of soybean nodules. FEBS Lett 293 (1):188-190. doi:https://doi.org/10.1016/0014-5793(91)81183-9

Ozawa T, Tsuji T (1993) A possible role for polyamines in the repression of growth of *Bradyrhizobium japonicum* bacteroids in soybean nodules. Plant Cell Physiol 34 (6):899-904

Ozu M, Galizia L, Acuña C, Amodeo G (2018) Aquaporins: More Than Functional Monomers in a Tetrameric Arrangement. Cells 7 (11). doi:10.3390/cells7110209

Palmer CM, Guerinot ML (2009) Facing the challenges of Cu, Fe and Zn homeostasis in plants. Nat Chem Biol 5 (5):333-340. doi:10.1038/nchembio.166

Pantoja O (2021) Recent advances in the physiology of ion channels in plants. Annu Rev Plant Biol 72:463-495

Parker JL, Newstead S (2014) Molecular basis of nitrate uptake by the plant nitrate transporter NRT1.1. Nature 507 (7490):68-72. doi:10.1038/nature13116

Pau RN, Lawson DM (2002) Transport, homeostasis, regulation, and binding of molybdate and Tungstate to proteins. Met Ions Biol Syst 39:31-74

Peoples M, Herridge, DF., Ladha, JK. (1995) Biological nitrogen fixation: An efficient source of nitrogen for s nable agricultural production? Plant Soil 174:3-28

Peters N, Verma D (1990) Phenolic compounds as regulators of gene expression in plant-microbe interactions. Mol Plant Microbe Interact 3 (1):4-8

Phillips DA (1992) Flavonoids: Plant Signals to Soil Microbes. In: Stafford HA, Ibrahim RK (eds) Phenolic Metabolism in Plants. Springer US, Boston, MA, pp 201-231. doi:10.1007/978-1-4615-3430-3_7

Pierre O, Engler G, Hopkins J, Brau F, Boncompagni E, HÉRouart D (2013) Peribacteroid space acidification: a marker of mature bacteroid functioning in *Medicago truncatula* nodules. Plant Cell Environ 36 (11):2059-2070. doi:https://doi.org/10.1111/pce.12116

Pineros MA, Cancado GM, Maron LG, Lyi SM, Menossi M, Kochian LV (2008) Not all ALMT1-type transporters mediate aluminum-activated organic acid responses: the case of ZmALMT1 - an anion-selective transporter. Plant J 53 (2):352-367. doi:10.1111/j.1365-313X.2007.03344.x

Postgate J (1998) Nitrogen Fixation, 3rd ed. Cambridge University Press,

Prell J, White JP, Bourdes A, Bunnewell S, Bongaerts RJ, Poole PS (2009) Legumes regulate Rhizobium bacteroid development and persistence by the supply of branched-chain amino acids. Proc Natl Acad Sci USA 106 (30):12477-12482. doi:10.1073/pnas.0903653106

Price GD, Day DA, Gresshoff PM (1987) Rapid Isolation of Intact Peribacteroid Envelopes from Soybean Nodules and Demonstration of Selective Permeability to Metabolites. J Plant Physiol 130 (2):157-164. doi:https://doi.org/10.1016/S0176-1617(87)80219-5

Qin L, Tang LH, Xu JS, Zhang XH, Zhu Y, Zhang CR, Wang MH, Liu XL, Li F, Sun F, Su M, Zhai Y, Chen YH (2022) Cryo-EM structure and electrophysiological characterization of ALMT from *Glycine max* reveal a previously uncharacterized class of anion channels. Sci Adv 8 (9):eabm3238. doi:10.1126/sciadv.abm3238

Qiu J, McGaughey SA, Groszmann M, Tyerman SD, Byrt CS (2020) Phosphorylation influences water and ion channel function of AtPIP2;1. Plant Cell Environ 43 (10):2428-2442. doi:https://doi.org/10.1111/pce.13851

Ramesh SA, Tyerman SD, Xu B, Bose J, Kaur S, Conn V, Domingos P, Ullah S, Wege S, Shabala S, Feijó JA, Ryan PR, Gilliham M (2015) GABA signalling modulates plant growth by directly regulating the activity of plant-specific anion transporters. Nat Commun 6:7879. doi:10.1038/ncomms8879

Ramos F, Wiame JM (1979) Synthesis and activation of asparagine in asparagine auxotrophs of *Saccharomyces cerevisiae*. Eur J Biochem 94 (2):409-417. doi:10.1111/j.1432-1033.1979.tb12908.x

Reckling M, Bergkvist G, Watson CA, Stoddard FL, Zander PM, Walker RL, Pristeri A, Toncea I, Bachinger J (2016) Trade-Offs between Economic and Environmental Impacts of Introducing Legumes into Cropping Systems. Front Plant Sci 7 (669). doi:10.3389/fpls.2016.00669

Reizer J, Reizer A, Saier MH, Jr. (1993) The MIP family of integral membrane channel proteins: sequence comparisons, evolutionary relationships, reconstructed pathway of evolution, and proposed functional differentiation of the two repeated halves of the proteins. Crit Rev Biochem Mol Biol 28 (3):235-257. doi:10.3109/10409239309086796

Ren G, Reddy VS, Cheng A, Melnyk P, Mitra AK (2001) Visualization of a water-selective pore by electron crystallography in vitreous ice. Proc Natl Acad Sci USA 98 (4):1398-1403. doi:10.1073/pnas.98.4.1398

Rentsch D, Laloi M, Rouhara I, Schmelzer E, Delrot S, Frommer WB (1995) NTR1 encodes a high affinity oligopeptide transporter in *Arabidopsis*. FEBS Lett 370 (3):264-268. doi:10.1016/0014-5793(95)00853-2

Reumann S, Maier E, Heldt HW, Benz R (1998) Permeability properties of the porin of spinach leaf peroxisomes. Eur J Biochem 251 (1-2):359-366. doi:10.1046/j.1432-1327.1998.2510359.x

Rivers RL, Dean RM, Chandy G, Hall JE, Roberts DM, Zeidel ML (1997) Functional analysis of nodulin 26, an aquaporin in soybean root nodule symbiosomes. J Biol Chem 272 (26):16256-16261. doi:10.1074/jbc.272.26.16256

Roberts DM, Tyerman SD (2002) Voltage-dependent cation channels permeable to NH_4^+, K^+, and Ca^{2+} in the symbiosome membrane of the model legume *Lotus japonicus*. Plant Physiol 128 (2):370-378

Robertson J, Lyttleton P (1984) Division of peribacteroid membranes in root nodules of white clover. J Cell Sci 69 (1):147-157

Robertson JG, Farnden KJF, Warburton MP, Banks JAM (1975) Induction of Glutamine Synthetase During Nodule Development in Lupin. Funct Plant Biol 2 (3):265-272

Robertson JG, Warburton MP, Lyttleton P, Fordyce AM, Bullivant S (1978) Membranes in lupin root nodules. II. Preparation and properties of peribacteroid membranes and bacteroid envelope inner membranes from developing lupin nodules. J Cell Sci 30 (1):151

Rolfe BG, Gresshoff PM (1988) Genetic Analysis of Legume Nodule Initiation. Annu Rev Plant Physiol 39 (1):297-319. doi:10.1146/annurev.pp.39.060188.001501

Rosendahl L, Dilworth MJ, Glenn AR (1992) Exchange of Metabolites Across the Peribacteroid Membrane in Pea Root Nodules. J Plant Physiol 139 (5):635-638. doi:https://doi.org/10.1016/S0176-1617(11)80385-8

Rosendahl L, Jochimsen B (1995) In vitro indole-3-acetic acid uptake in symbiosomes from soybean (*Glycine max L.*) root nodules. Symbiosis 19:99-110. doi:http://hdl.handle.net/10222/77445

Roth LE, Stacey G (1989) Cytoplasmic membrane systems involved in bacterium release into soybean nodule cells as studied with two *Bradyrhizobium japonicum* mutant strains. Eur J Cell Biol 49 (1):24-32

Roux B, Rodde N, Jardinaud M-F, Timmers T, Sauviac L, Cottret L, Carrère S, Sallet E, Courcelle E, Moreau S, Debellé F, Capela D, de Carvalho-Niebel F, Gouzy J, Bruand C, Gamas P (2014) An integrated analysis of plant and bacterial gene expression in symbiotic root nodules using laser-capture microdissection coupled to RNA sequencing. Plant J 77 (6):817-837. doi:10.1111/tpj.12442

Rubio LM, Ludden PW (2005) Maturation of Nitrogenase: a Biochemical Puzzle. J Bacteriol 187 (2):405-414. doi:10.1128/jb.187.2.405-414.2005

Ruttan VW, Conway G (1998) The Doubly Green Revolution: Food for All in the Twenty-First Century. Popul Dev Rev 24 (2):394. doi:10.2307/2807982

Ryan J, Masri S, Pala M, Singh M (2009) Nutrient Dynamics in a Long-Term Cereal-Based Rotation Trial in a Mediterranean Environment: Nitrogen Forms, vol 40. doi:10.1080/00103620802695149

Ryan PR, Tyerman SD, Sasaki T, Furuichi T, Yamamoto Y, Zhang WH, Delhaize E (2011) The identification of aluminium-resistance genes provides opportunities for enhancing crop production on acid soils. J Exp Bot 62 (1):9-20. doi:10.1093/jxb/erq272

Saalbach G, Erik P, Wienkoop S (2002) Characterisation by proteomics of peribacteroid space and peribacteroid membrane preparations from pea (*Pisum sativum*) symbiosomes. Proteomics 2 (3):325-337. doi:10.1002/1615-9861(200203)2:3<325::AID-PROT325>3.0.CO;2-W

Sainz M, Calvo-Begueria L, Pérez-Rontomé C, Wienkoop S, Abián J, Staudinger C, Bartesaghi S, Radi R, Becana M (2015) Leghemoglobin is nitrated in functional legume nodules in a tyrosine residue within the heme cavity by a nitrite/peroxide-dependent mechanism. Plant J 81 (5):723-735. doi:10.1111/tpj.12762

Sambrook J, Russell D (2001) Molecular Cloning: A Laboratory Manual. Cold Spring Harbor Lab Press, NY

Sasaki T, Yamamoto Y, Ezaki B, Katsuhara M, Ahn SJ, Ryan PR, Delhaize E, Matsumoto H (2004) A wheat gene encoding an aluminum-activated malate transporter. Plant J 37 (5):645-653. doi:10.1111/j.1365-313X.2003.01991.x

Schachtman DP, Schroeder JI (1994) Structure and transport mechanism of a high-affinity potassium uptake transporter from higher plants. Nature 370 (6491):655-658. doi:10.1038/370655a0

Scherzer S, Maierhofer T, Al-Rasheid KA, Geiger D, Hedrich R (2012) Multiple calcium-dependent kinases modulate ABA-activated guard cell anion channels. Mol Plant 5 (6):1409-1412. doi:10.1093/mp/sss084

Schneider S, Schintlmeister A, Becana M, Wagner M, Woebken D, Wienkoop S (2019) Sulfate is transported at significant rates through the symbiosome membrane and is crucial for nitrogenase biosynthesis. Plant Cell Environ 42 (4):1180-1189. doi:10.1111/pce.13481

Schubert KR (1981) Enzymes of Purine Biosynthesis and Catabolism in Glycine max: I. comparison of activities with N_2 fixation and composition of xylem exudate during nodule development. Plant Physiol 68 (5):1115-1122. doi:10.1104/pp.68.5.1115

Seefeldt LC, Hoffman BM, Dean DR (2009) Mechanism of Mo-dependent nitrogenase. Annu Rev Biochem 78:701-722. doi:10.1146/annurev.biochem.78.070907.103812

Segonzac C, Boyer JC, Ipotesi E, Szponarski W, Tillard P, Touraine B, Sommerer N, Rossignol M, Gibrat R (2007) Nitrate efflux at the root plasma membrane: identification of an *Arabidopsis* excretion transporter. Plant Cell 19 (11):3760-3777. doi:10.1105/tpc.106.048173

Severin AJ, Woody JL, Bolon Y-T, Joseph B, Diers BW, Farmer AD, Muehlbauer GJ, Nelson RT, Grant D, Specht JE, Graham MA, Cannon SB, May GD, Vance CP, Shoemaker RC (2010) RNA-Seq Atlas of *Glycine max*: A guide to the soybean transcriptome. BMC Plant Biol 10 (1):160. doi:10.1186/1471-2229-10-160

Shah VK, Brill WJ (1973) Nitrogenase. IV. Simple method of purification to homogeneity of nitrogenase components from *Azotobacter vinelandii*. Biochim Biophys Acta 305 (2):445-454. doi:10.1016/0005-2728(73)90190-4

Sharma T, Dreyer I, Kochian L, Piñeros MA (2016) The ALMT Family of Organic Acid Transporters in Plants and Their Involvement in Detoxification and Nutrient Security. Front Plant Sci 7:1488-1488. doi:10.3389/fpls.2016.01488

Shavrukov Y, Bovill J, Afzal I, Hayes JE, Roy SJ, Tester M, Collins NC (2013) HVP10 encoding V-PPase is a prime candidate for the barley HvNax3 sodium exclusion gene: evidence from fine mapping and expression analysis. Planta 237 (4):1111-1122. doi:10.1007/s00425-012-1827-3

Shaw BD (1983) Non-coordinate Regulation of Rhizobium Nitrogenase Synthesis by Oxygen: Studies with Bacteroids from Nodulated *Lupinus angustifolius*. Microbiology 129 (3):849-857. doi:https://doi.org/10.1099/00221287-129-3-849

Shelden MC, Howitt SM, Kaiser BN, Tyerman SD (2009) Identification and functional characterisation of aquaporins in the grapevine, *Vitis vinifera*. Funct Plant Biol 36 (12):1065-1078

Soltis DE, Soltis PS, Morgan DR, Swensen SM, Mullin BC, Dowd JM, Martin PG (1995) Chloroplast gene sequence data suggest a single origin of the predisposition for symbiotic nitrogen fixation in angiosperms. Proc Natl Acad Sci USA 92 (7):2647-2651

Sprent JI, Ardley J, James EK (2017) Biogeography of nodulated legumes and their nitrogen-fixing symbionts. New Phytol 215 (1):40-56. doi:10.1111/nph.14474

Stein LY, Klotz MG (2016) The nitrogen cycle. Curr Biol 26 (3):R94-98. doi:10.1016/j.cub.2015.12.021

Streeter J, Wong PP (1988) Inhibition of legume nodule formation and N_2 fixation by nitrate. Crit Rev Plant Sci 7 (1):1-23. doi:10.1080/07352688809382257

Streeter JG (1981) Seasonal Distribution of Carbohydrates in Nodules and Stem Exudate from Field-grown Soya Bean Plants*. Annals of Botany 48 (4):441-450. doi:10.1093/oxfordjournals.aob.a086148

Streeter JG (1985) Nitrate inhibition of legume nodule growth and activity : I. Long term studies with a continuous supply of nitrate. Plant Physiol 77 (2):321-324

Streeter JG (1989) Estimation of Ammonium Concentration in the Cytosol of Soybean Nodules. Plant Physiol 90 (3):779-782. doi:10.1104/pp.90.3.779

Streeter JG (1995) Integration of Plant and Bacterial Metabolism in Nitrogen Fixing Systems. In: Tikhonovich IA, Provorov NA, Romanov VI, Newton WE (eds) Nitrogen Fixation: Fundamentals and Applications: Proceedings of the 10th International Congress on Nitrogen Fixation, St. Petersburg, Russia, May 28–June 3, 1995. Springer Netherlands, Dordrecht, pp 67-76. doi:10.1007/978-94-011-0379-4_9

Stumpf DK, Burris RH (1979) A micromethod for the purification and quantification of organic acids of the tricarboxylic acid cycle in plant tissues. Anal Biochem 95 (1):311-315. doi:https://doi.org/10.1016/0003-2697(79)90221-5

Suganuma N, Nakamura Y, Yamamoto M, Ohta T, Koiwa H, Akao S, Kawaguchi M (2003) The *Lotus japonicus* Sen1 gene controls rhizobial differentiation into nitrogen-fixing bacteroids in nodules. Mol Genet Genomics 269 (3):312-320. doi:10.1007/s00438-003-0840-4

Sui H, Han BG, Lee JK, Walian P, Jap BK (2001) Structural basis of water-specific transport through the AQP1 water channel. Nature 414 (6866):872-878. doi:10.1038/414872a

Sullivan P (2003) Overview of Cover Crops and Green Manures. Sustain Agric:1-11

Sun S-J, Qi G-N, Gao Q-F, Wang H-Q, Yao F-Y, Hussain J, Wang Y-F (2016) Protein kinase OsSAPK8 functions as an essential activator of S-type anion channel OsSLAC1, which is nitrate-selective in rice. Planta 243 (2):489-500. doi:10.1007/s00425-015-2418-x

Sutka M, Alleva K, Parisi M, Amodeo G (2005) Tonoplast vesicles of *Beta vulgaris* storage root show funtional aquaporins regulated by protons. Biol Cell 97 (11):837-846. doi:10.1042/BC20040121

Szalay A (1964) Cation exchange properties of humic acids and their importance in the geochemical enrichment of UO2++ and other cations. Geochim Cosmochim Acta 28 (10):1605-1614. doi:https://doi.org/10.1016/0016-7037(64)90009-2

Szczyglowski K, Kapranov P, Hamburger D, de Bruijn FJ (1998) The *Lotus japonicus* LjNOD70 nodulin gene encodes a protein with similarities to transporters. Plant Mol Biol 37 (4):651-661. doi:10.1023/a:1006043428636

Tadege M, Wen J, He J, Tu H, Kwak Y, Eschstruth A, Cayrel A, Endre G, Zhao PX, Chabaud M, Ratet P, Mysore KS (2008) Large-scale insertional mutagenesis using the Tnt1 retrotransposon in the model legume *Medicago truncatula*. Plant J 54 (2):335-347. doi:10.1111/j.1365-313X.2008.03418.x

Takanashi K, Sasaki T, Kan T, Saida Y, Sugiyama A, Yamamoto Y, Yazaki K (2016) A Dicarboxylate Transporter, LjALMT4, Mainly Expressed in Nodules of *Lotus japonicus*. Mol Plant Microbe Interact 29 (7):584-592. doi:10.1094/mpmi-04-16-0071-r

Takanashi K, Takahashi H, Sakurai N, Sugiyama A, Suzuki H, Shibata D, Nakazono M, Yazaki K (2012) Tissue-Specific Transcriptome Analysis in Nodules of *Lotus japonicus*. Mol Plant Microbe Interact 25 (7):869-876. doi:10.1094/MPMI-01-12-0011-R

Takanashi K, Yazaki K (2014) ABC Proteins and Other Transporters in *Lotus japonicus* and *Glycine max*, vol 22. In: Geisler M. (eds) Plant ABC Transporters. Signaling and Communication in Plants. Springer, Cham,

Takano J, Wada M, Ludewig U, Schaaf G, von Wirén N, Fujiwara T (2006) The *Arabidopsis* major intrinsic protein NIP5;1 is essential for efficient boron uptake and plant development under boron limitation. Plant Cell 18 (6):1498-1509. doi:10.1105/tpc.106.041640

Tanaka J, Fink GR (1985) The histidine permease gene (HIP1) of *Saccharomyces cerevisiae*. Gene 38 (1-3):205-214. doi:10.1016/0378-1119(85)90219-7

Tate R, Riccio A, Merrick M, Patriarca EJ (1998) The Rhizobium etli amtB gene coding for an NH_4^+ transporter is down-regulated early during bacteroid differentiation. Mol Plant Microbe Interact 11 (3):188-198. doi:10.1094/mpmi.1998.11.3.188

Taylor PM, Kaur S, Mackenzie B, Peter GJ (1996) Amino-acid-dependent modulation of amino acid transport in *Xenopus laevis* oocytes. J Exp Biol 199 (Pt 4):923-931. doi:10.1242/jeb.199.4.923

Tegeder M (2012) Transporters for amino acids in plant cells: some functions and many unknowns. Curr Opin Plant Biol 15 (3):315-321. doi:https://doi.org/10.1016/j.pbi.2012.02.001

Terhag J, Cavara NA, Hollmann M (2010) Cave Canalem: how endogenous ion channels may interfere with heterologous expression in *Xenopus* oocytes. Methods 51 (1):66-74. doi:10.1016/j.ymeth.2010.01.034

Thimann KV (1936) On the Physiology of the Formation of Nodules on Legume Roots. Proceedings of the National Academy of Sciences of the United States of America 22 (8):511-514. doi:10.1073/pnas.22.8.511

Thöny-Meyer L, Künzler P (1996) The *Bradyrhizobium japonicum* aconitase gene (acnA) is important for free-living growth but not for an effective root nodule symbiosis. J Bacteriol 178 (21):6166-6172. doi:10.1128/jb.178.21.6166-6172.1996

Tomatsu H, Takano J, Takahashi H, Watanabe-Takahashi A, Shibagaki N, Fujiwara T (2007) An *Arabidopsis thaliana* high-affinity molybdate transporter required for efficient uptake of molybdate from soil. Proc Natl Acad Sci USA 104 (47):18807-18812. doi:10.1073/pnas.0706373104

Törnroth-Horsefield S, Wang Y, Hedfalk K, Johanson U, Karlsson M, Tajkhorshid E, Neutze R, Kjellbom P (2006) Structural mechanism of plant aquaporin gating. Nature 439 (7077):688-694. doi:10.1038/nature04316

Tournaire-Roux C, Sutka M, Javot H, Gout E, Gerbeau P, Luu DT, Bligny R, Maurel C (2003) Cytosolic pH regulates root water transport during anoxic stress through gating of aquaporins. Nature 425 (6956):393-397. doi:10.1038/nature01853

Tran ST, Horie T, Imran S, Qiu J, McGaughey S, Byrt CS, Tyerman SD, Katsuhara M (2020) A Survey of Barley PIP Aquaporin Ionic Conductance Reveals Ca^{2+}-Sensitive HvPIP2;8 Na^+ and K^+ Conductance. Int J Mol Sci 21 (19). doi:10.3390/ijms21197135

Tsay YF, Schroeder JI, Feldmann KA, Crawford NM (1993) The herbicide sensitivity gene CHL1 of *Arabidopsis* encodes a nitrate-inducible nitrate transporter. Cell 72 (5):705-713. doi:10.1016/0092-8674(93)90399-b

Tyerman SD (2002) Nonselective Cation Channels. Multiple Functions and Commonalities. Plant Physiol 128 (2):327-328. doi:10.1104/pp.900021

Tyerman SD, McGaughey SA, Qiu J, Yool AJ, Byrt CS (2021) Adaptable and Multifunctional Ion-Conducting Aquaporins. Annu Rev Plant Biol 72 (1):703-736. doi:10.1146/annurev-arplant-081720-013608

Tyerman SD, Niemietz CM (2000) Solute and Water Permeation Across the Symbiosome Membrane of Legumes. In: Hohmann S, Nielsen S (eds) Molecular Biology and Physiology of Water and Solute Transport. Springer US, Boston, MA, pp 319-329. doi:10.1007/978-1-4615-1203-5_44

Tyerman SD, Whitehead LF, Day DA (1995) A channel-like transporter for NH_4^+ on the symbiotic interface of N_2-fixing plants. Nature 378 (6557):629

Udvardi M, Poole PS (2013) Transport and Metabolism in Legume-Rhizobia Symbioses. Annu Rev Plant Biol 64 (1):781-805. doi:10.1146/annurev-arplant-050312-120235

Udvardi MK, Day DA (1989) Electrogenic ATPase Activity on the Peribacteroid Membrane of Soybean (*Glycine max L.*) Root Nodules. Plant Physiol 90 (3):982. doi:10.1104/pp.90.3.982

Udvardi MK, Day DA (1990) Ammonia (C-Methylamine) Transport across the Bacteroid and Peribacteroid Membranes of Soybean Root Nodules. Plant Physiol 94 (1):71-76. doi:10.1104/pp.94.1.71

Udvardi MK, Day DA (1997) Metabolite transport across symbiotic membranes of legume nodules. Annu Rev Plant Biol 48 (1):493-523. doi:10.1146/annurev.arplant.48.1.493

Udvardi MK, Lister DL, Day DA (1991) ATPase activity and anion transport across the peribacteroid membrane of isolated soybean symbiosomes. Arch Microbiol 156 (5):362-366. doi:10.1007/BF00248711

Udvardi MK, Price GD, Gresshoff PM, Day DA (1988) A dicarboxylate transporter on the peribacteroid membrane of soybean nodules. FEBS Lett 231 (1):36-40. doi:https://doi.org/10.1016/0014-5793(88)80697-5

Underwood W, Somerville SC (2017) Phosphorylation is required for the pathogen defense function of the *Arabidopsis* PEN3 ABC transporter. Plant Signal Behav 12 (10):e1379644. doi:10.1080/15592324.2017.1379644

Urbanski DF, Malolepszy A, Stougaard J, Andersen SU (2012) Genome-wide LORE1 retrotransposon mutagenesis and high-throughput insertion detection in *Lotus japonicus*. Plant J 69 (4):731-741. doi:10.1111/j.1365-313X.2011.04827.x

Vahisalu T, Kollist H, Wang Y-F, Nishimura N, Chan W-Y, Valerio G, Lamminmäki A, Brosché M, Moldau H, Desikan R, Schroeder JI, Kangasjärvi J (2008) SLAC1 is required for plant guard cell S-type anion channel function in stomatal signalling. Nature 452 (7186):487-491. doi:10.1038/nature06608

Valkov VT, Rogato A, Alves LM, Sol S, Noguero M, Léran S, Lacombe B, Chiurazzi M (2017) The Nitrate Transporter Family Protein LjNPF8.6 Controls the N-Fixing Nodule Activity. Plant Physiol 175 (3):1269-1282. doi:10.1104/pp.17.01187

Van Eunen K, Bouwman J, Daran-Lapujade P, Postmus J, Canelas AB, Mensonides FI, Orij R, Tuzun I, Van den Brink J, Smits GJ, Van Gulik WM, Brul S, Heijnen JJ, De Winde JH, De Mattos MJ, Kettner C, Nielsen J, Westerhoff HV, Bakker BM (2010) Measuring enzyme activities under standardized in vivo-like conditions for systems biology. FEBS J 277 (3):749-760. doi:10.1111/j.1742-4658.2009.07524.x

Vance CP (2008) Carbon and Nitrogen Metabolism in Legume Nodules. In: Dilworth MJ, James EK, Sprent JI, Newton WE (eds) Nitrogen-fixing Leguminous Symbioses. Springer Netherlands, Dordrecht, pp 293-320. doi:10.1007/978-1-4020-3548-7_10

Varinderpal S, Bijay S, Yadvinder S, Thind HS, Gobinder S, Satwinderjit K, Kumar A, Vashistha M (2012) Establishment of threshold leaf colour greenness for need-based fertilizer nitrogen management in irrigated wheat (*Triticum aestivum L.*) using leaf colour chart. Field Crops Res 130:109-119. doi:https://doi.org/10.1016/j.fcr.2012.02.005

Verdoucq L, Grondin A, Maurel C (2008) Structure-function analysis of plant aquaporin AtPIP2;1 gating by divalent cations and protons. Biochem J 415 (3):409-416. doi:10.1042/bj20080275

Verma DP, Kazazian V, Zogbi V, Bal AK (1978) Isolation and characterization of the membrane envelope enclosing the bacteroids in soybean root nodules. J Cell Biol 78 (3):919-936. doi:10.1083/jcb.78.3.919

Vessey JK (2003) Plant growth promoting rhizobacteria as biofertilizers. Plant Soil 255 (2):571-586. doi:10.1023/A:1026037216893

Vessey JK, Pawlowski K, Bergman B (2005) Root-based N_2-fixing symbioses: Legumes, actinorhizal plants, *Parasponia sp.* and cycads. Plant Soil 266 (1):205-230. doi:10.1007/s11104-005-0871-1

Vincent J, Humphrey BA (1963) Partition of divalent cations between bacterial wall and cell contents. Nature 199 (4889):149-151

Vincill ED, Szczyglowski K, Roberts DM (2005) GmN70 and LjN70. Anion Transporters of the Symbiosome Membrane of Nodules with a Transport Preference for Nitrate. Plant Physiol 137 (4):1435-1444

Vitha S (2007) Histochemical localization of β-glucuronidase (GUS) reporter activity in plant tissues. Microscopy and Imaging Center

Walker RL, Burns IG, Moorby J (2001) Responses of plant growth rate to nitrogen supply: a comparison of relative addition and N interruption treatments. J Exp Bot 52 (355):309-317. doi:10.1093/jexbot/52.355.309

Wallace IS, Wills DM, Guenther JF, Roberts DM (2002) Functional selectivity for glycerol of the nodulin 26 subfamily of plant membrane intrinsic proteins. FEBS Lett 523 (1-3):109-112. doi:10.1016/s0014-5793(02)02955-1

Walshaw DL, Poole PS (1996) The general L-amino acid permease of *Rhizobium leguminosarum* is an ABC uptake system that also influences efflux of solutes. Mol Microbiol 21 (6):1239-1252. doi:10.1046/j.1365-2958.1996.00078.x

Wandrey M, Trevaskis B, Brewin N, Udvardi MK (2004) Molecular and Cell Biology of a Family of Voltage-Dependent Anion Channel Porins in *Lotus japonicus*. Plant Physiol 134 (1):182. doi:10.1104/pp.103.031484

Waters JK, Hughes BL, 2nd, Purcell LC, Gerhardt KO, Mawhinney TP, Emerich DW (1998) Alanine, not ammonia, is excreted from N_2-fixing soybean nodule bacteroids. Proc Natl Acad Sci USA 95 (20):12038-12042. doi:10.1073/pnas.95.20.12038

Weaver CD, Roberts DM (1992) Determination of the site of phosphorylation of nodulin 26 by the calcium-dependent protein kinase from soybean nodules. Biochemistry 31 (37):8954-8959. doi:10.1021/bi00152a035

Weaver CD, Shomer NH, Louis CF, Roberts DM (1994) Nodulin 26, a nodule-specific symbiosome membrane protein from soybean, is an ion channel. J Biol Chem 269 (27):17858-17862

Weil R, A. Weismiller R, S. Turner R (1990) Nitrate Contamination of Groundwater under Irrigated Coastal Plain Soils. J Environ Qual 19:441-448. doi:10.2134/jeq1990.00472425001900030015x

Westmark CJ, Ghose R, Huber PW (2002) Phosphorylation of *Xenopus* transcription factor IIIA by an oocyte protein kinase CK2. Biochem J 362 (Pt 2):375-382. doi:10.1042/0264-6021:3620375

White KD (1970) Fallowing, Crop Rotation, and Crop Yields in Roman Times. Agricultural History 44 (3):281-290

Whitehead L, Tyerman S, Day D (2001) Polyamines as potential regulators of nutrient exchange across the peribacteroid membrane in soybean root nodules. Funct Plant Biol 28:677-683. doi:10.1071/PP01025

Whitehead LF, Day DA (1997) The peribacteroid membrane. Physiol Plant 100 (1):30-44. doi:10.1111/j.1399-3054.1997.tb03452.x

Whitehead LF, Day DA, Tyerman SD (1998) Divalent cation gating of an ammonium permeable channel in the symbiotic membrane from soybean nodules. Plant J 16 (3):313-324. doi:10.1046/j.1365-313x.1998.00298.x

Wienkoop S, Saalbach G (2003) Proteome analysis. Novel proteins identified at the peribacteroid membrane from *Lotus japonicus* root nodules. Plant Physiol 131 (3):1080-1090. doi:10.1104/pp.102.015362

Wittenberg JB, Wittenberg BA, Day DA, Udvardi MK, Appleby CA (1996) Siderophore-bound iron in the peribacteriod space of soybean root nodules. Plant Soil 178 (2):161-169. doi:10.1007/BF00011579

Yamaguchi M, Sasaki T, Sivaguru M, Yamamoto Y, Osawa H, Ahn SJ, Matsumoto H (2005) Evidence for the Plasma Membrane Localization of Al-activated Malate Transporter (ALMT1). Plant Cell Physiol 46 (5):812-816. doi:10.1093/pcp/pci083

Yanochko GM, Yool AJ (2002) Regulated cationic channel function in *Xenopus* oocytes expressing Drosophila big brain. J Neurosci 22 (7):2530-2540. doi:10.1523/JNEUROSCI.22-07-02530.2002

Yanochko GM, Yool AJ (2004) Block by extracellular divalent cations of Drosophila big brain channels expressed in *Xenopus* oocytes. Biophys J 86 (3):1470-1478. doi:10.1016/s0006-3495(04)74215-0

Yao P, Vincent JM (1969) Host Specificity In The Root Hair "Curling Factor" of Rhizobium Spp. Aust J Biol Sci 22 (2):413-424

Yasui M, Hazama A, Kwon T-H, Nielsen S, Guggino WB, Agre P (1999) Rapid gating and anion permeability of an intracellular aquaporin. Nature 402 (6758):184-187

Ye J, Coulouris G, Zaretskaya I, Cutcutache I, Rozen S, Madden TL (2012) Primer-BLAST: a tool to design target-specific primers for polymerase chain reaction. BMC Bioinform 13:134. doi:10.1186/1471-2105-13-134

Yool AJ (2007) Functional domains of aquaporin-1: keys to physiology, and targets for drug discovery. Curr Pharm Des 13 (31):3212-3221. doi:10.2174/138161207782341349

Yool AJ, Campbell EM (2012) Structure, function and translational relevance of aquaporin dual water and ion channels. Mol Aspects Med 33 (5-6):553-561. doi:10.1016/j.mam.2012.02.001

Yool AJ, Stamer WD, Regan JW (1996) Forskolin stimulation of water and cation permeability in aquaporin1 water channels. Science 273 (5279):1216-1218

Yu J, Yool AJ, Schulten K, Tajkhorshid E (2006) Mechanism of Gating and Ion Conductivity of a Possible Tetrameric Pore in Aquaporin-1. Structure 14 (9):1411-1423. doi:https://doi.org/10.1016/j.str.2006.07.006

Yu L, Moshelion M, Moran N (2001) Extracellular protons inhibit the activity of inward-rectifying potassium channels in the motor cells of *Samanea saman* pulvini. Plant Physiol 127 (3):1310-1322

Zhang W, Zitron E, Hoömme M, Kihm L, Morath C, Scherer D, Hegge S, Thomas D, Schmitt CP, Zeier M (2007) Aquaporin-1 channel function is positively regulated by protein kinase C. The Journal of biological chemistry 282 (29):20933-20940

Zheng L, White RH, Dean DR (1997) Purification of the *Azotobacter vinelandii* nifV-encoded homocitrate synthase. J Bacteriol 179 (18):5963-5966. doi:10.1128/jb.179.18.5963-5966.1997

Zhou Y, Neuhäuser B, Neumann G, Ludewig U (2020) LaALMT1 mediates malate release from phosphorus-deficient white lupin root tips and metal root to shoot translocation. Plant Cell Environ 43 (7):1691-1706. doi:https://doi.org/10.1111/pce.13762

Zizi M, Byrd C, Boxus R, Colombini M (1998) The Voltage-Gating Process of the Voltage-Dependent Anion Channel Is Sensitive to Ion Flow. Biophys J 75 (2):704-713. doi:https://doi.org/10.1016/S0006-3495(98)77560-5

Appendices

A1. Gateway vector maps used in this thesis

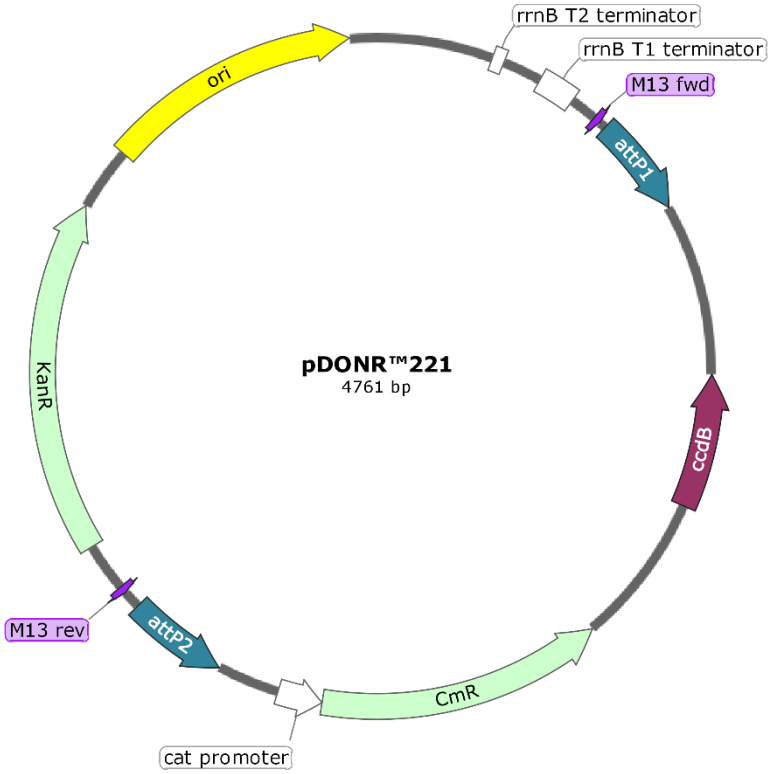

Figure A1 1. pDONR™221 plasmid obtained from Invitrogen (USA). AttB containing PCR products were recombined with pDONR™221 using Gateway™ BP Clonase™ and selected on LB agar containing 50 µg/mL Kanamycin. The generated entry vector contained the sequence of interest flanked by AttL sites and was maintained in DH5α due to the removal of the toxic ccdB gene. Map was generated and annotated using SnapGene.

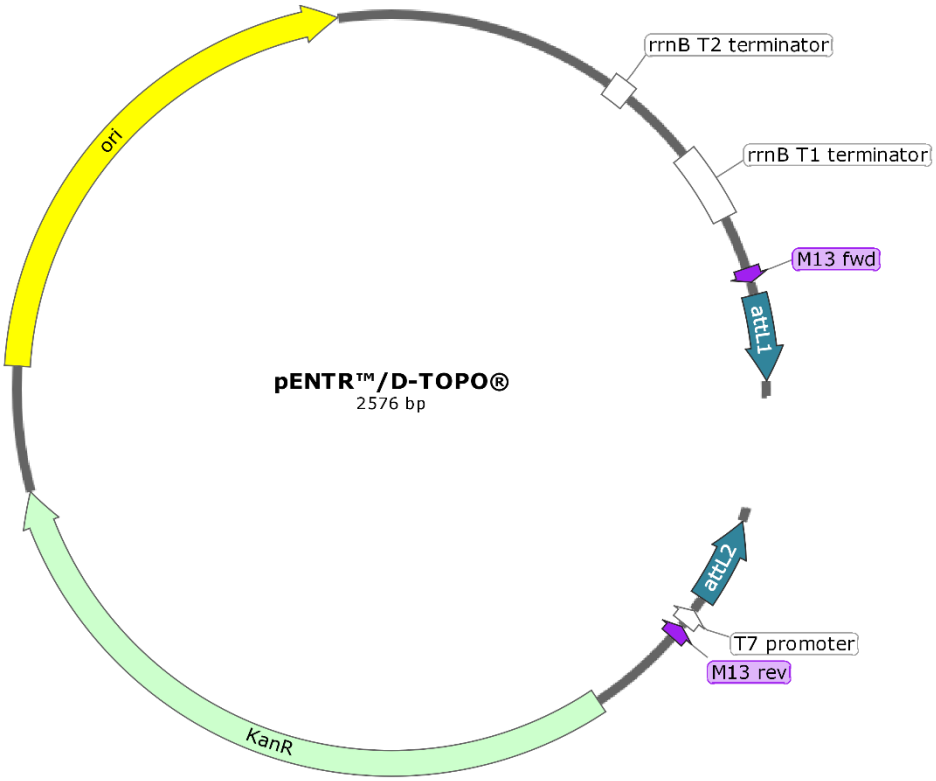

Figure A1 2 pENTR™/D-TOPO™ plasmid obtained from Invitrogen (USA). PCR products containing a 5' CACC overhang were recombined with pENTR™/D-TOPO™ which has been linearised through activity of Topoisomerase I and selected on LB agar containing 50 µg/mL Kanamycin. The generated entry vector contained the sequence of interest flanked by AttL sites and was maintained in DH5α. Map was generated and annotated using SnapGene.

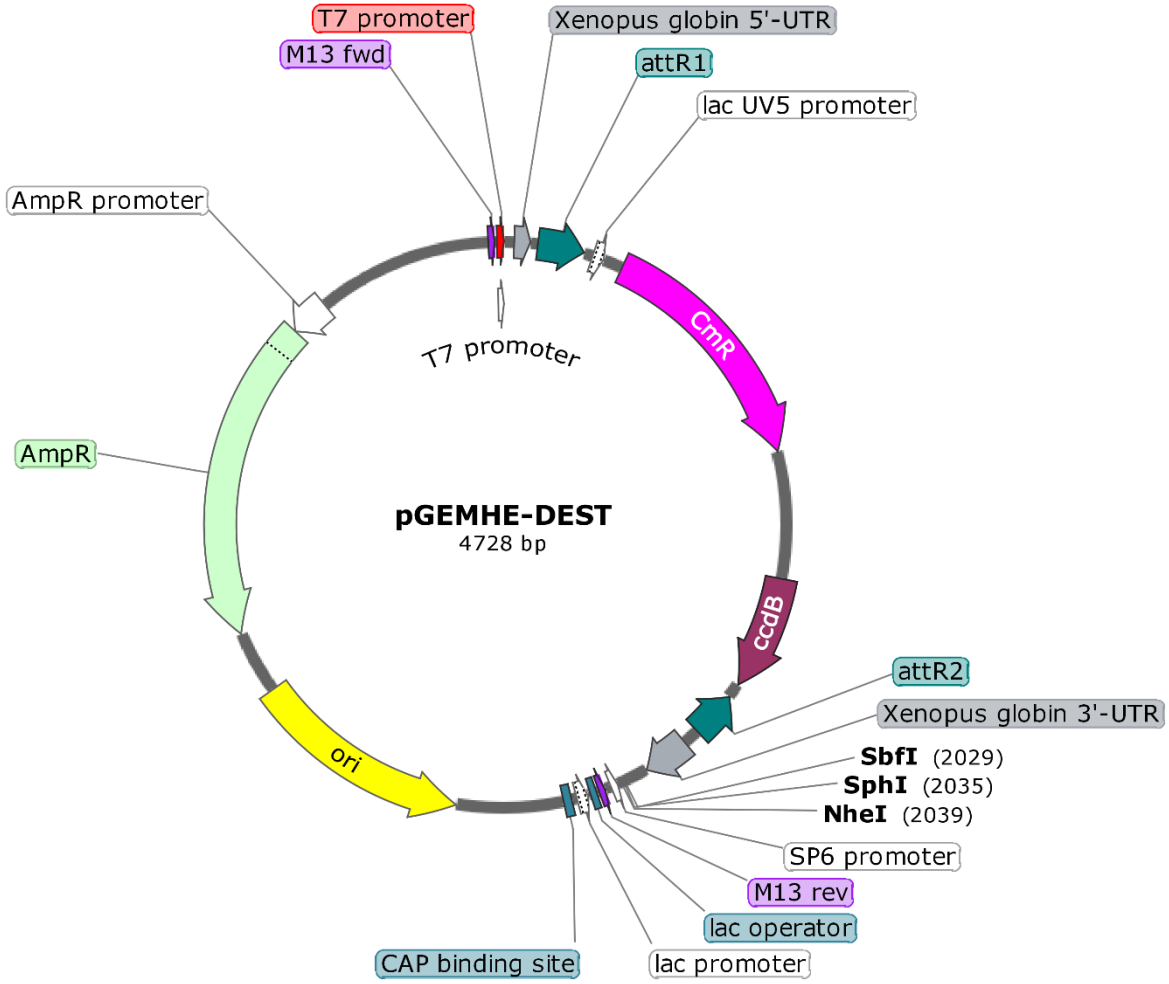

Figure A1 3. pGEMHE-DEST plasmid obtained from Sunita Ramesh (Adelaide University, Australia). Entry vectors containing gene coding sequence of interest flanked by AttL sites was recombined with pGEMHE-DEST using Gateway™ LR Clonase™ II and selected on LB agar containing 100 µg/mL Ampicillin. The generated expression clone was maintained in DH5α due to the removal of the toxic ccdB gene. For expression in *X. laevis* oocytes the generated expression clone was linearised using: SbfI; or SphI; or NheI, prior to cRNA synthesis using the mMESSAGE mMACHINE® T7 Transcription kit (Thermo Fisher Scientific, Australia). Map was generated and annotated using SnapGene.

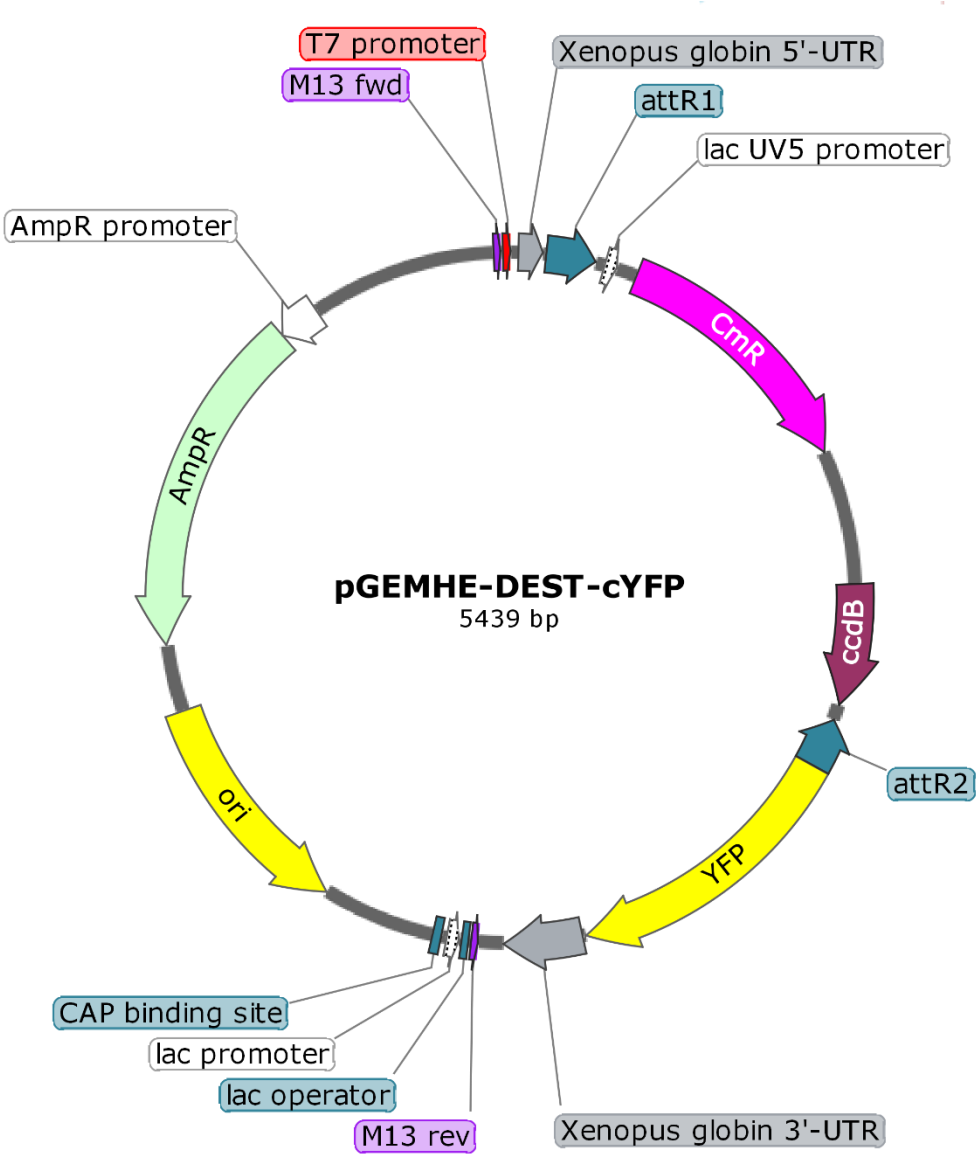

Figure A1 4. pGEMHE-DEST-cYFP plasmid obtained from Sunita Ramesh (Adelaide University, Australia). Entry vectors containing gene coding sequence of interest without the stop codon and flanked by AttL sites was recombined with pGEMHE-DEST-cYFP using Gateway™ LR Clonase™ II and selected on LB agar containing 100 µg/mL Ampicillin. The generated expression clone was maintained in DH5α due to the removal of the toxic ccdB gene. For expression in X. laevis oocytes the generated expression clone was linearised using: SbfI; or SphI; or NheI, prior to cRNA synthesis using the mMESSAGE mMACHINE® T7 Transcription kit (Thermo Fisher Scientific, Australia). Map was generated and annotated using SnapGene.

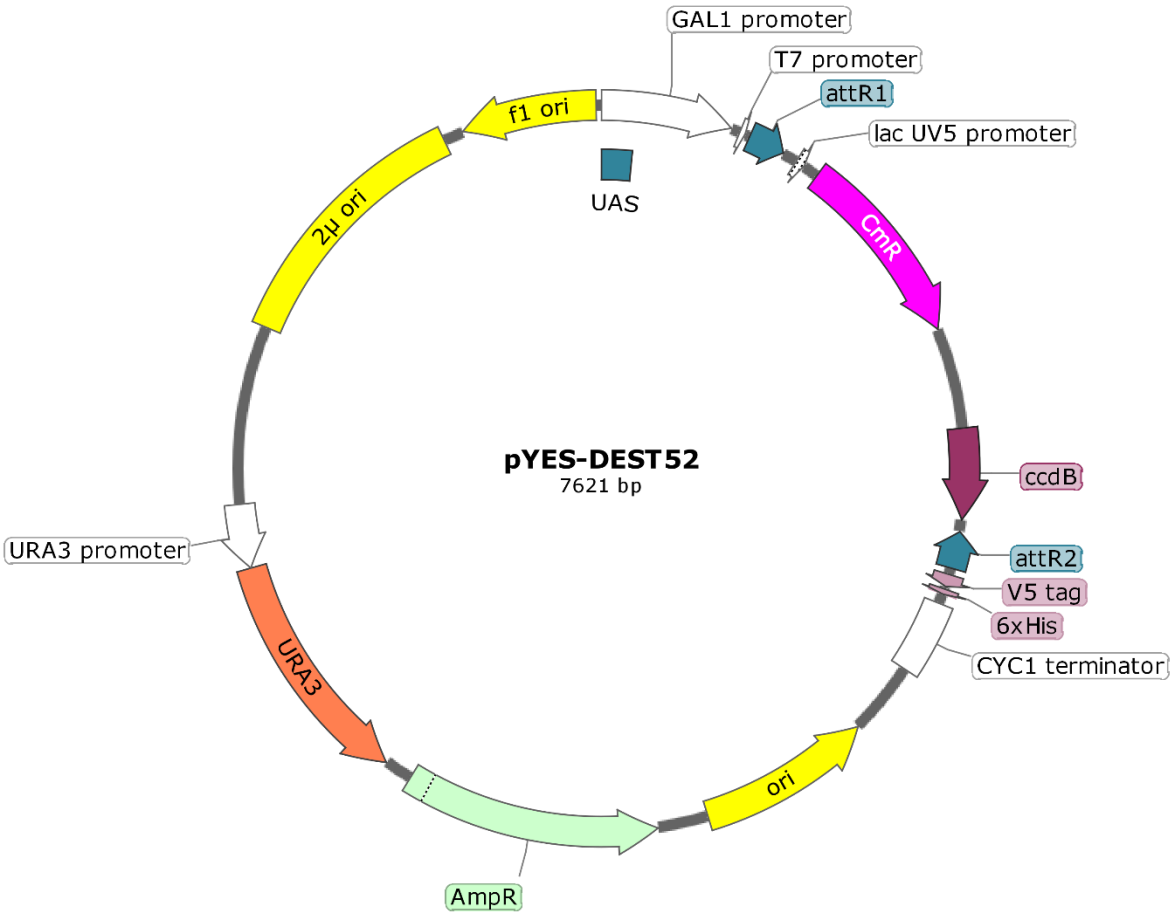

Figure A1 5. pYES-DEST52 plasmid obtained from Sunita Ramesh (Adelaide University, Australia). Entry vectors containing gene coding sequence of interest flanked by AttL sites was recombined with pYES-DEST52 using Gateway™ LR Clonase™ II and selected on LB agar containing 100 µg/mL Ampicillin. The generated expression clone was maintained in DH5α due to the removal of the toxic ccdB gene. pYES-DEST52 expression clones were transformed into the *S. cerevisiae* strains 26972c, 22Δ10AA or 23344c and grown in the absence of uracil for selection (URA3). Gene expression was under the control of the galactose inducible (GAL1) promoter. Map was generated and annotated using SnapGene.

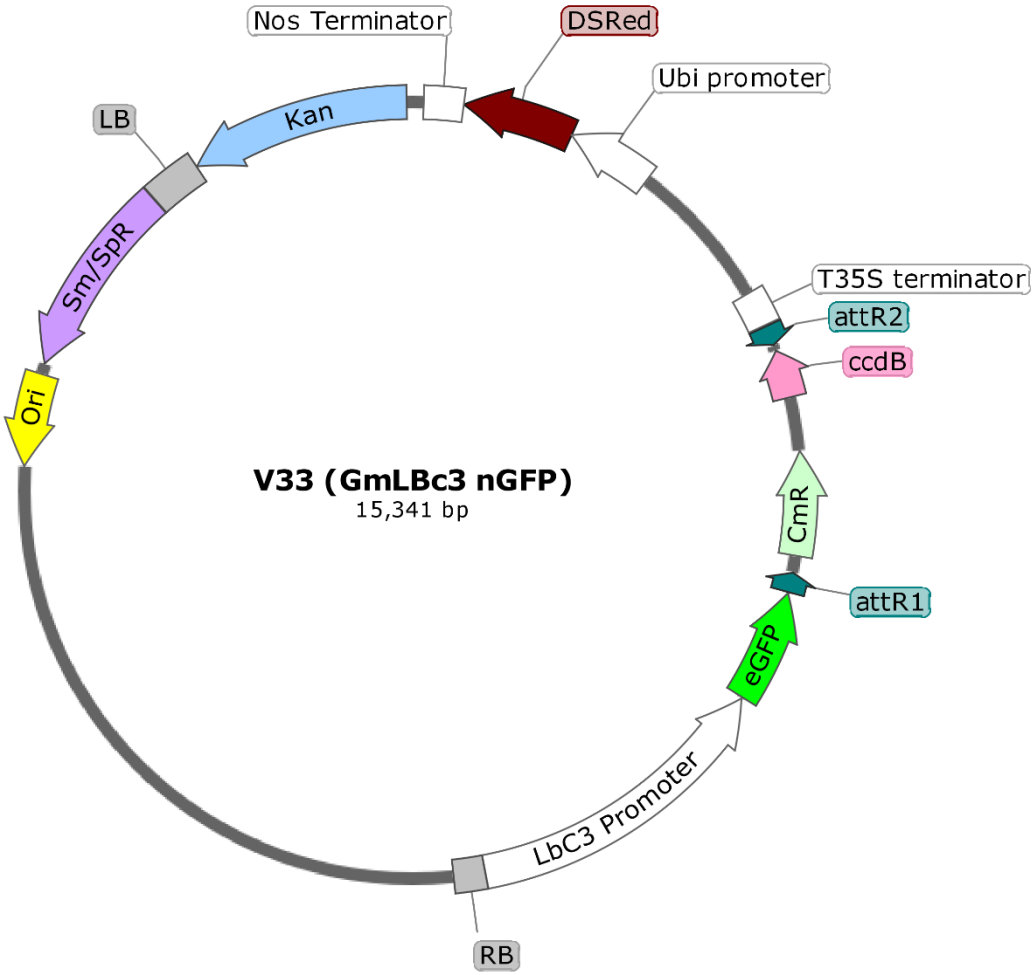

Figure A1 6. V33 plasmid obtained from Penelope Smith (La Trobe University, Australia). Entry vectors containing coding region of interest flanked by AttL sites was recombined with V33 using Gateway™ LR Clonase™ II and selected on LB agar containing 100 µg/mL Spectinomycin. The generated expression clone was maintained in DH5α due to the removal of the toxic ccdB gene. V33 expression clones were transformed into *L. japonicus* through hairy root transformation and selected for expression of DSRed. Successful transformants were analysed through confocal microscopy. Expression of the GFP-protein of interest was driven by the nodule specific GmLbC3 5' regulatory element to determine where the protein of interest was localised within *L. japonicus* nodules. Map was generated and annotated using SnapGene.

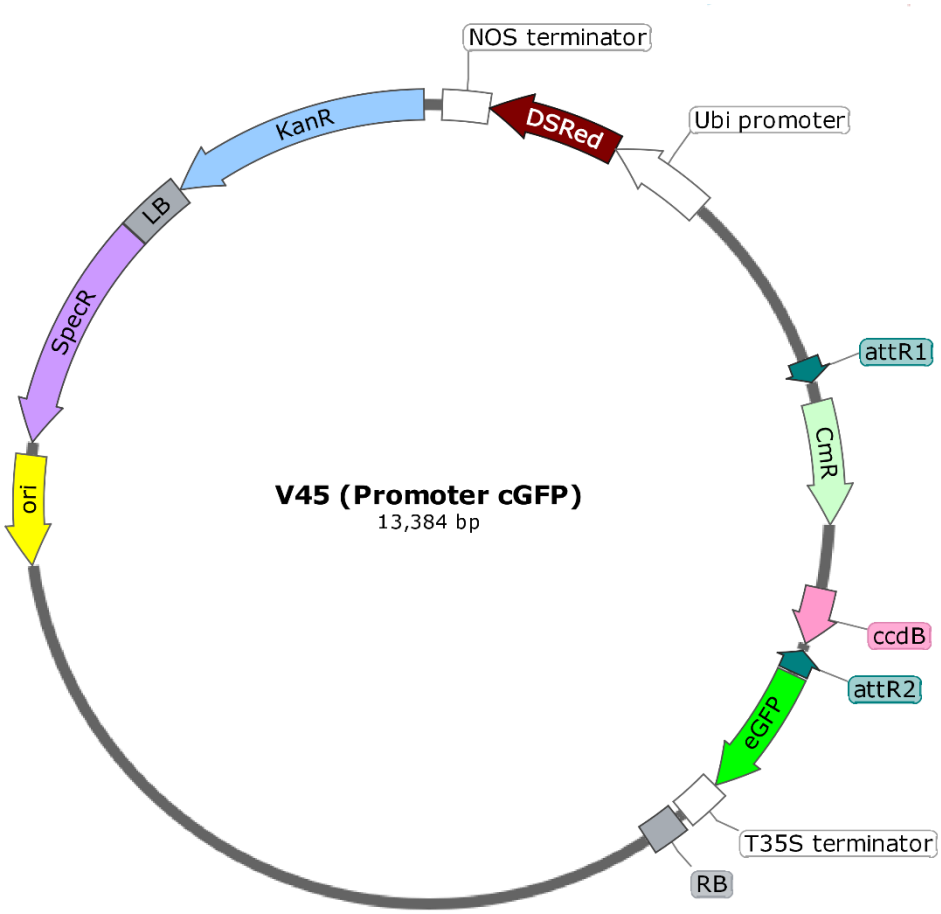

Figure A1 7. V45 plasmid obtained from Penelope Smith (La Trobe University, Australia). Entry vectors containing a 5' regulatory element and coding region of interest fusion flanked by AttL sites was recombined with V45 using Gateway™ LR Clonase™ II and selected on LB agar containing 100 µg/mL Spectinomycin. The generated expression clone was maintained in DH5α due to the removal of the toxic ccdB gene. V45 expression clones were transformed into *L. japonicus* through hairy root transformation and selected for expression of DSRed. Successful transformants were analysed through confocal microscopy. Expression of the GFP-protein of interest was driven by the native 5' regulatory element to determine where the protein of interest was localised within *L. japonicus*. Map was generated and annotated using SnapGene.

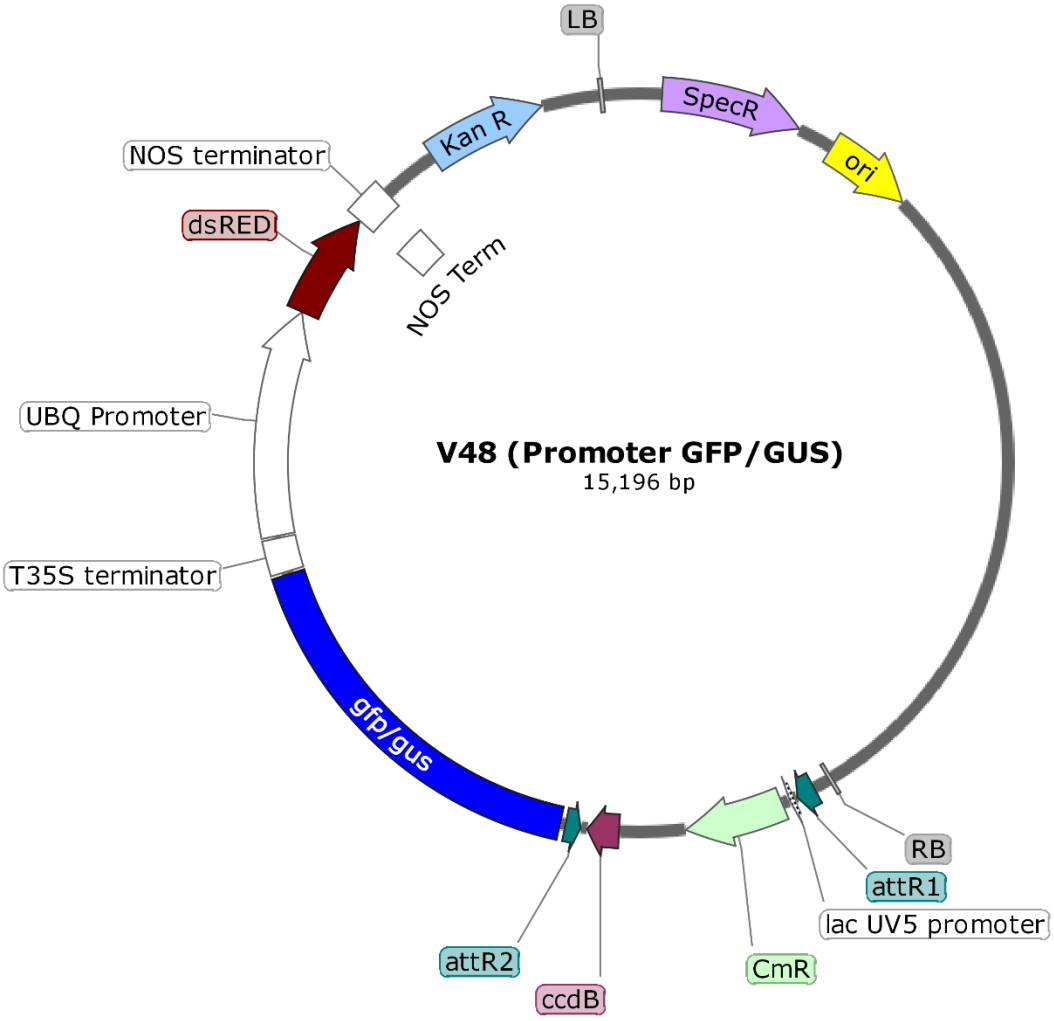

Figure A1 8. V48 plasmid obtained from Penelope Smith (La Trobe University, Australia). Entry vectors containing 5' regulatory element of interest flanked by AttL sites was recombined with V48 using Gateway™ LR Clonase™ II and selected on LB agar containing 100 µg/mL Spectinomycin. The generated expression clone was maintained in DH5α due to the removal of the toxic ccdB gene. V48 expression clones were transformed into *L. japonicus* through hairy root transformation and selected for expression of DSRed. Successful transformants were analysed using the GUS reporter gene driven by the 5' regulatory element of interest. Map was generated and annotated using SnapGene.

A2. Cloned PCR products were sequenced by AGRF and aligned with the LotusBase sequences

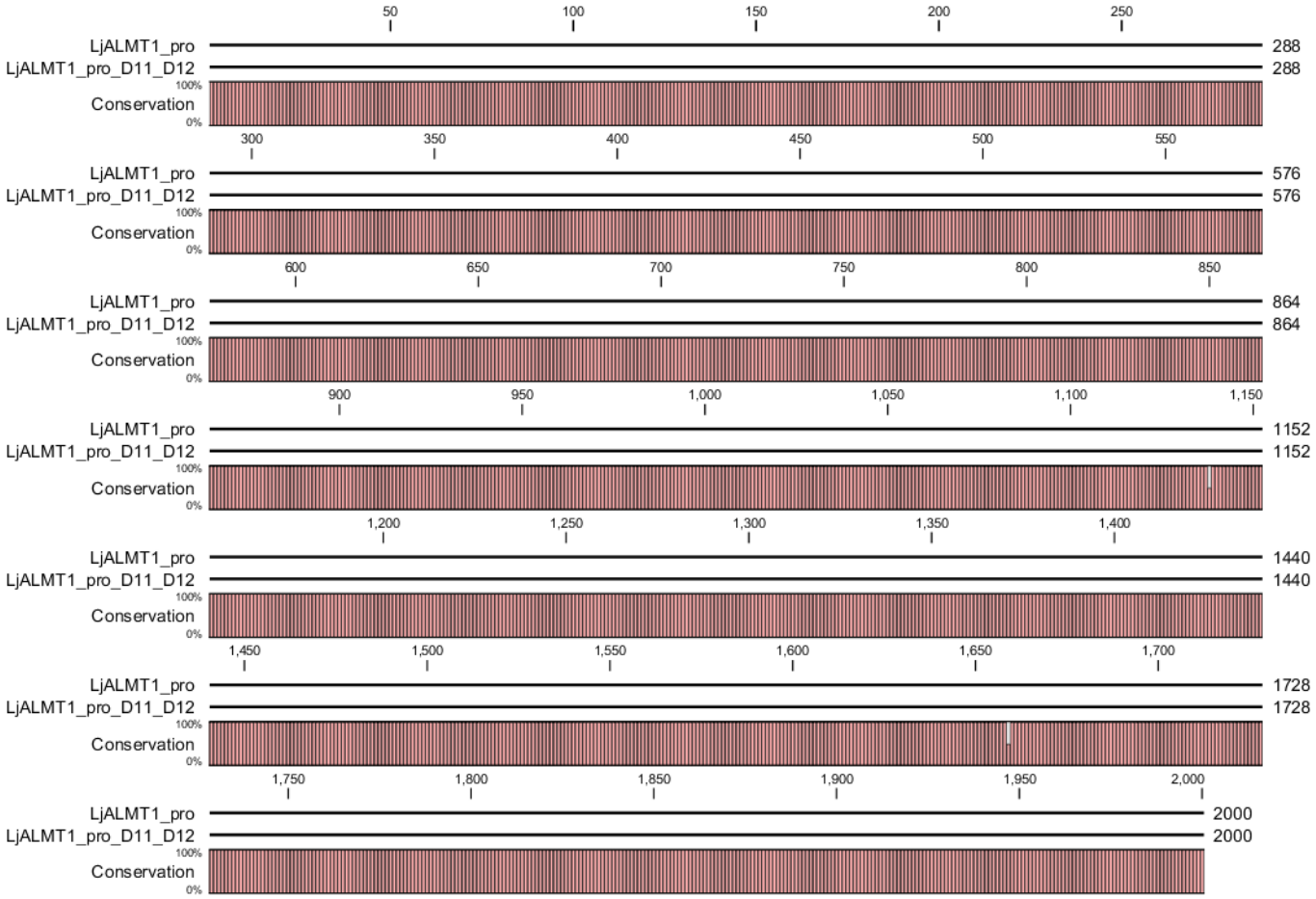

Figure A2 1. Alignment of cloned and publicly available 5' LjALMT1 regulatory element. Cloned sequence was sanger sequenced at AGRF while the publicly available sequence was obtained from LotusBase. Alignment was completed using CLC sequence viewer. Two SNPs detected at A1138G and A1659C.

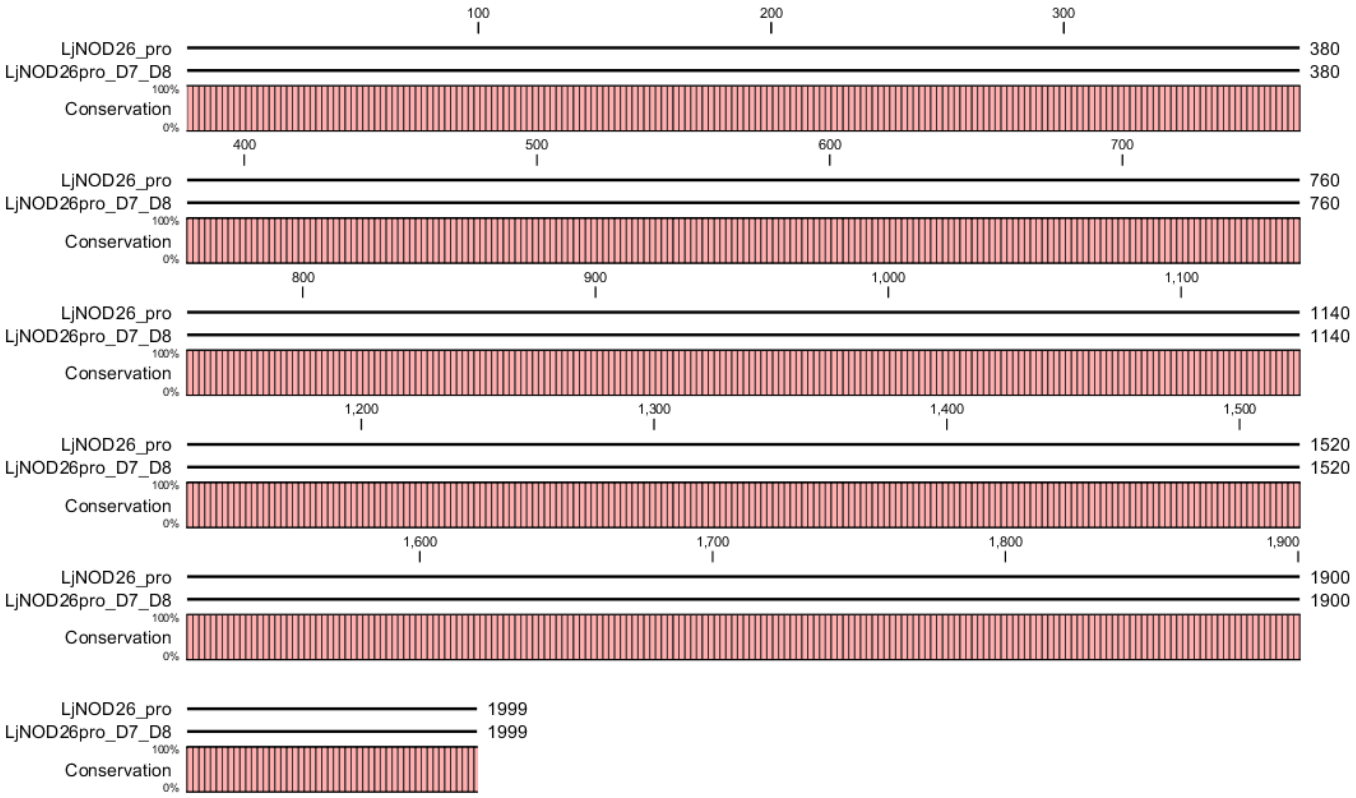

Figure A2 2. Alignment of cloned and publicly available 5' LjNOD26 regulatory element. Cloned sequence was sanger sequenced at AGRF while the publicly available sequence was obtained from LotusBase. Alignment was completed using CLC sequence viewer. No SNPs detected between the cloned and publicly available sequences.

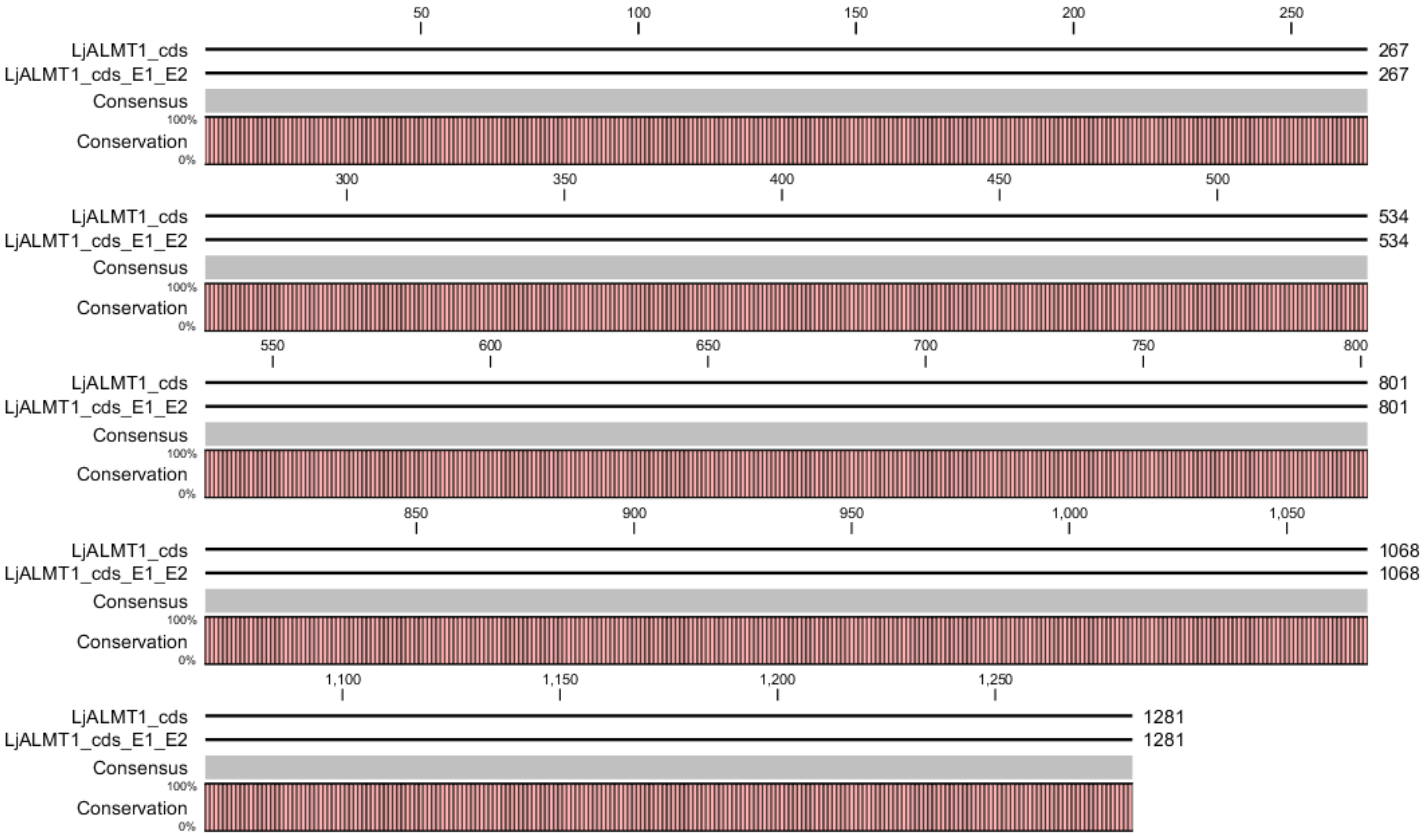

Figure A2 3. Alignment of cloned and publicly available LjALMT1 coding sequence. Cloned sequence was sanger sequenced at AGRF while the publicly available sequence was obtained from LotusBase. Alignment was completed using CLC sequence viewer. No SNPs detected between the cloned and publicly available sequences.

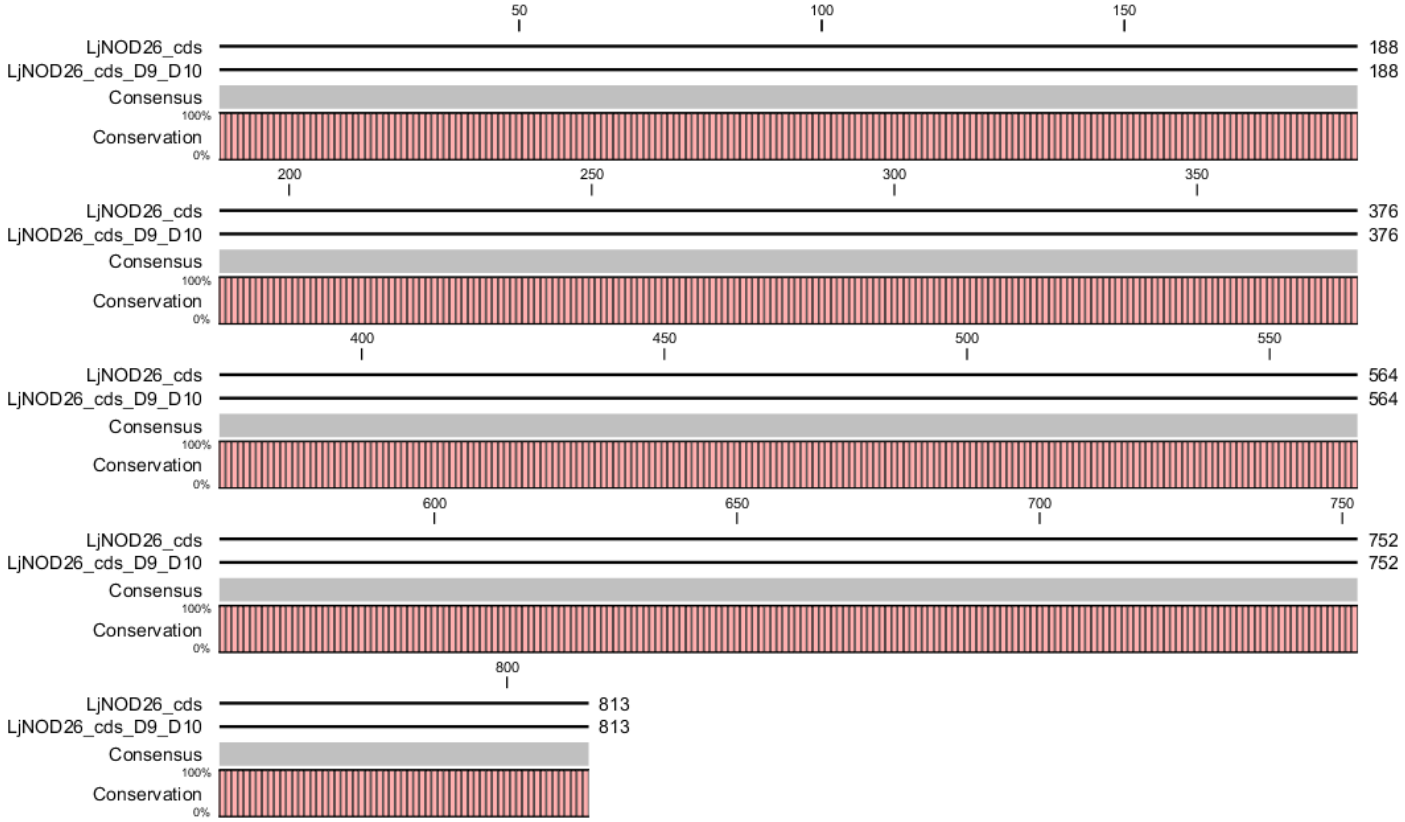

Figure A2 4. **Alignment of cloned and publicly available LjNOD26 coding sequence.** Cloned sequence was sanger sequenced at AGRF while the publicly available sequence was obtained from LotusBase. Alignment was completed using CLC sequence viewer. No SNPs detected between the cloned and publicly available sequences.

A3. Validation of DsRED expression using ChemiDoc XRS+ imaging system (Bio-Rad, USA)

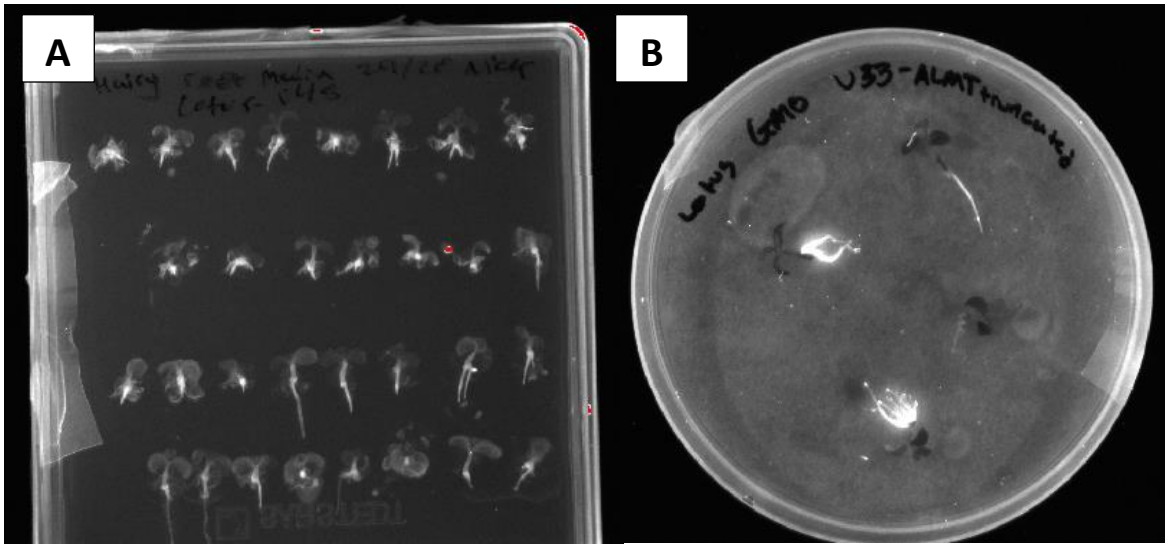

Figure A3 1. Validation of DsRED expression using ChemiDoc XRS+ imaging system (Bio-Rad, USA) under the 605/50 filter with Green Epi illumination. Images of *L. japonicus* transformants after 14 days of hairy root induction, A) plate image in root elongation media, B) selected plants removed from root elongation media. Red circles represent successful transformation while blue circles represent a null transformant.

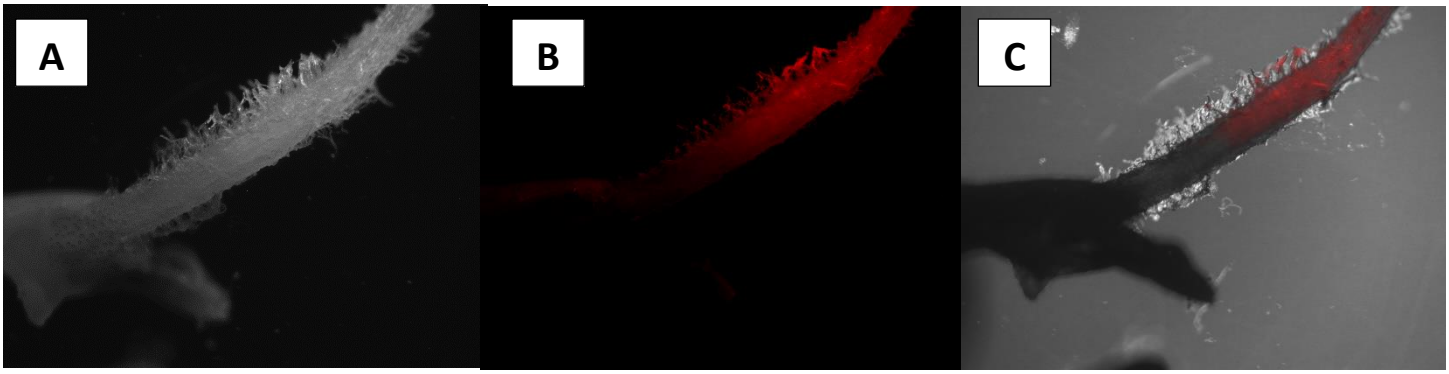

Figure A3 2. Validation of DsRED expression using EVOS® FL Auto Imaging System (Thermo Fisher Scientific, USA). Successful transformant selected using the ChemiDoc XRS+ imaging system (Bio-Rad, USA) was imaged for DsRED. *L. japonicus* root images using A) white light, B) DsRED filter (531/40 nm Excitation; 593/40 nm Emission), or C) merged image.

A4. Ponceau stain of *X. laevis* oocyte lysate

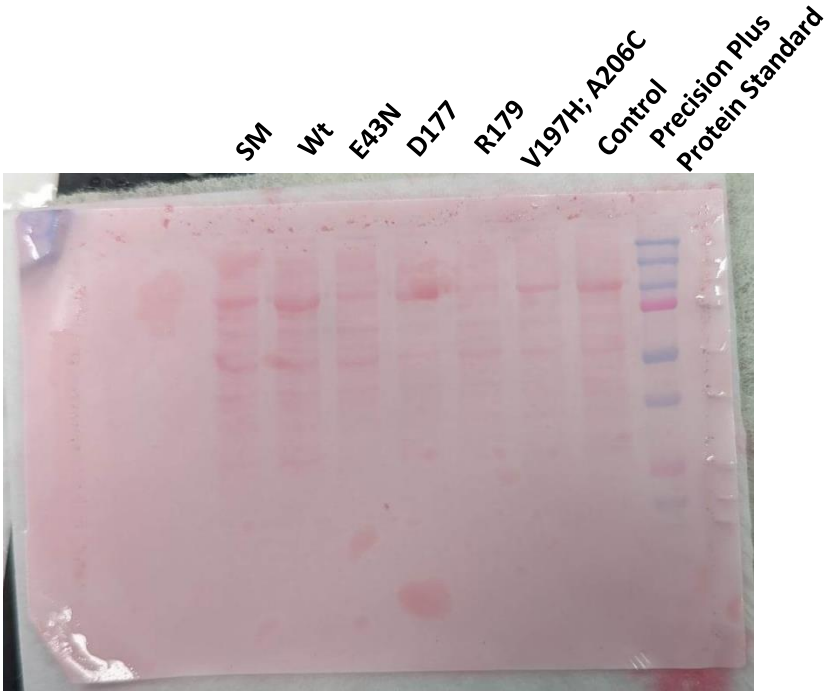

Figure A4 1. Total protein visualisation with Ponceau S stain (Thermo Fisher Scientific, USA). Homogenised oocyte lysate was separated through 12.5% (v/v) SDS-PAGE gel prior to transfer to nitrocellulose membrane. Following transfer, the membrane was washed three times in distilled MilliQ water and incubated in Ponceau S Staining Solution for five minutes with agitation. The membrane was briefly washed with distilled MilliQ water before imaging. It is clear that although lysate from a single oocyte was loaded onto the gel, there are discrepancies in the total protein loaded in each lane.

A5. Raw current-voltage curves of mutant GmNOD26-expressing *X. laevis* oocytes

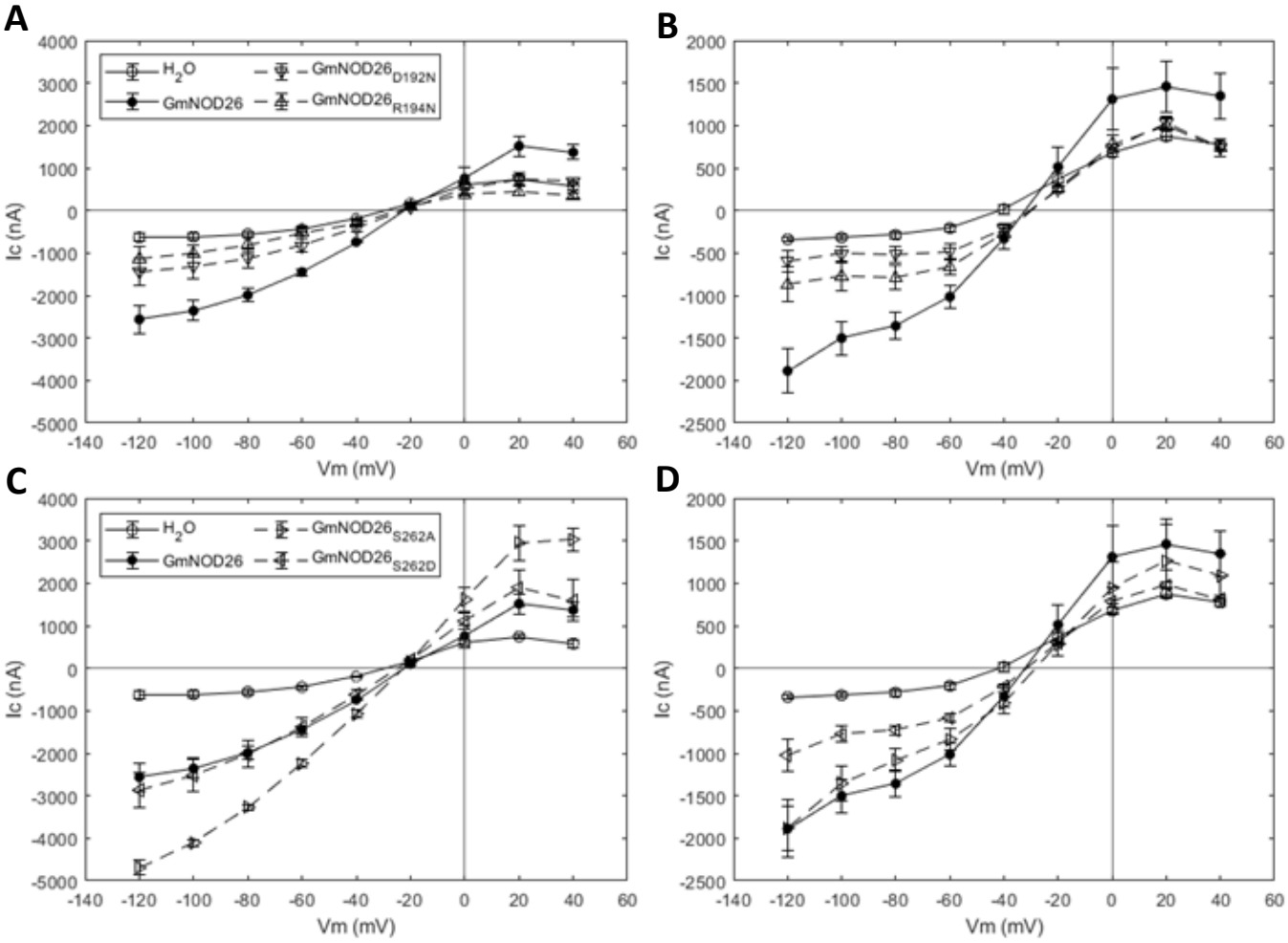

Figure A5 1 Raw current-voltage curves used in the calculation of relative plots shown in Figure 3.6d and 3.7d.

A) and B) averaged data from a single oocyte harvest of Control, Wt, D177N or R179N GmNOD26-expressing *X. laevis* oocytes (n=4). C) and D) averaged data from a single oocyte harvest of Control, Wt, S262A or S262D GmNOD26-expressing *X. laevis* oocytes (n=4). All curves depict the ungated current using 50 mM Na^+ as a chloride salt containing 50 µM Ca^{2+} buffered with HEPES and pH adjusted to 7.5 with TRIS base.

A6. Raw current-voltage curves of observed pH gating in phosphomimetic GmNOD26-expressing *X. laevis* oocytes

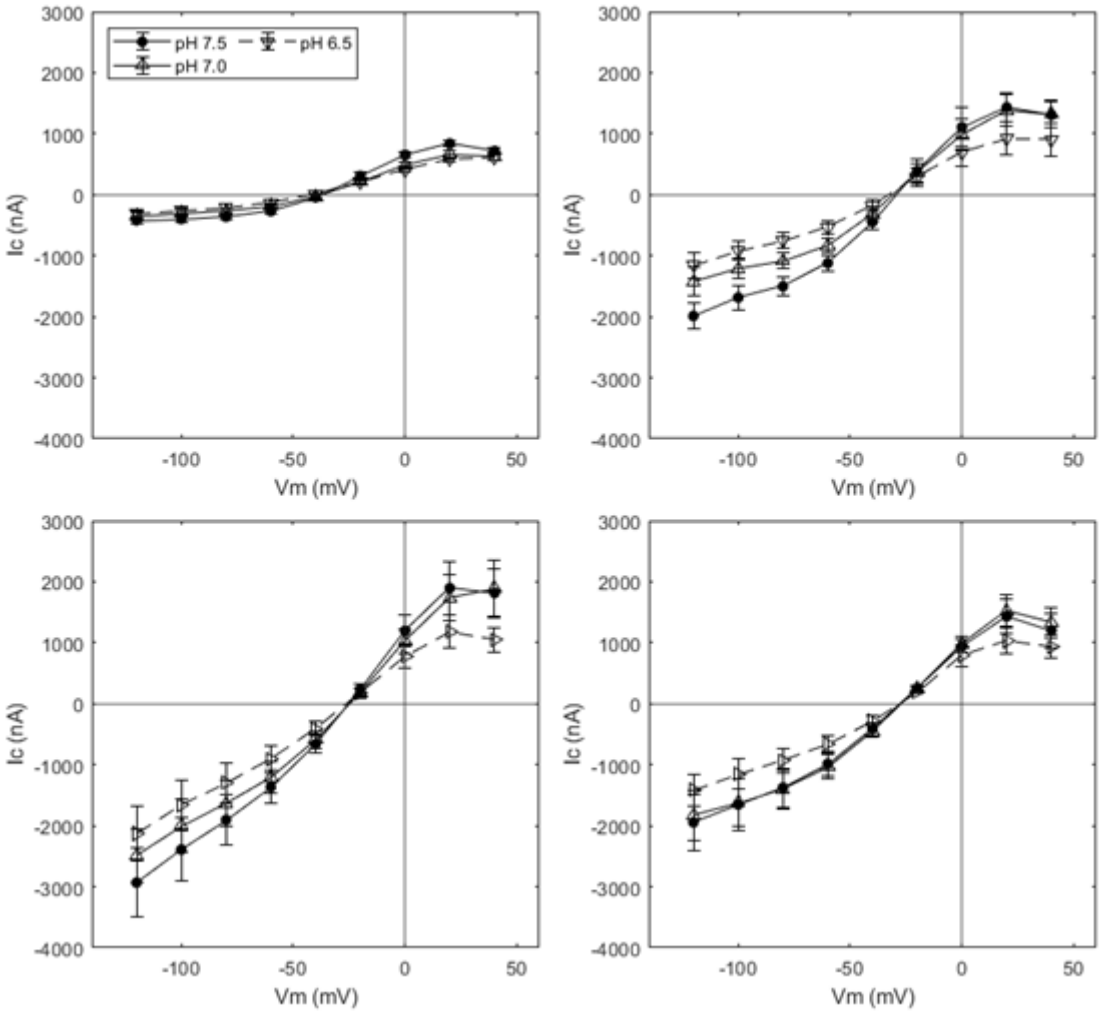

Figure A6 1. Dephosphorylation reduced external pH gating in GmNOD26 expressing *X. laevis* oocytes. A) Currents in control oocytes. B) Currents in GmNOD26 expressing oocytes. C) Currents in $GmNOD26_{S262A}$ expressing oocytes. D) Currents in $GmNOD26_{S262D}$ expressing oocytes. Testing solution contained 50 mM Na^+ as a chloride salt containing 50 µM Ca^{2+} buffered with HEPES and pH adjusted with TRIS base (n=8).

A7. Multiple sequence alignment of GmNOD26 with other aquaporin ion channels

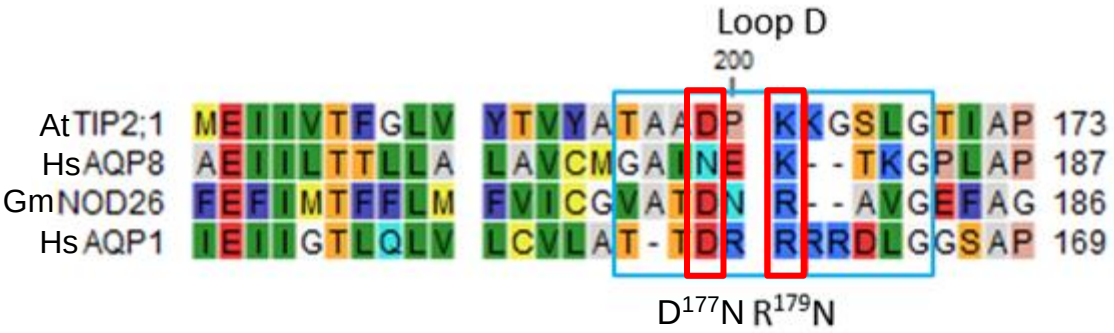

Figure A7 1. Multiple sequence alignment of aquaporin Loop D regions. In HsAQP1, mutations to the charged residues D158 and R160 impair the ion conductance of the channel, with no apparent effect on water transport (Yu et al. 2006; Kourghi et al. 2018a). Here, the corresponding sites were mutated to asparagine to remove the charge while maintaining polarity. Alignment was performed in CLC sequence viewer 6 and residues are coloured based on RasMol structure (Qiagen digital insights, USA).

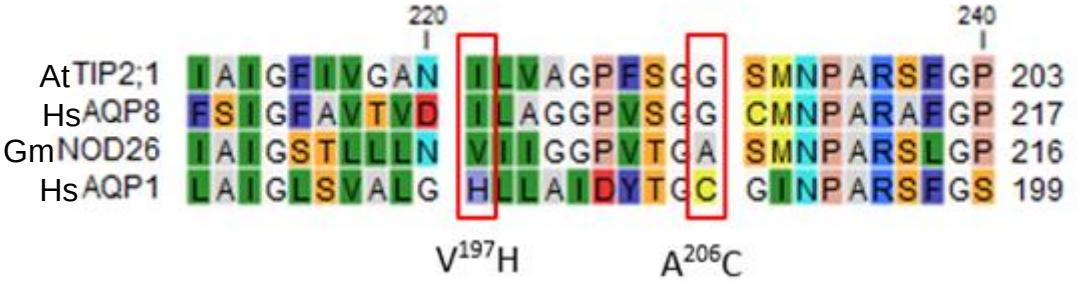

Figure A7 2. Multiple sequence alignment of the region used in the Tatip2;1 double mutant. In the Tatip2;1 mutant the sites were mutated to that of AQP1 (I184H, G193C) and the cation permeability was disrupted (Jahn et al. 2004). Here, the corresponding site in GmNOD26 have been mutated to that of the non-aquaammoniaporin HsAQP1. Alignment was performed in CLC sequence viewer 6 and residues are coloured based on RasMol structure (Qiagen digital insights, USA).

A8. 31019b cells appear to be permeable to ammonium

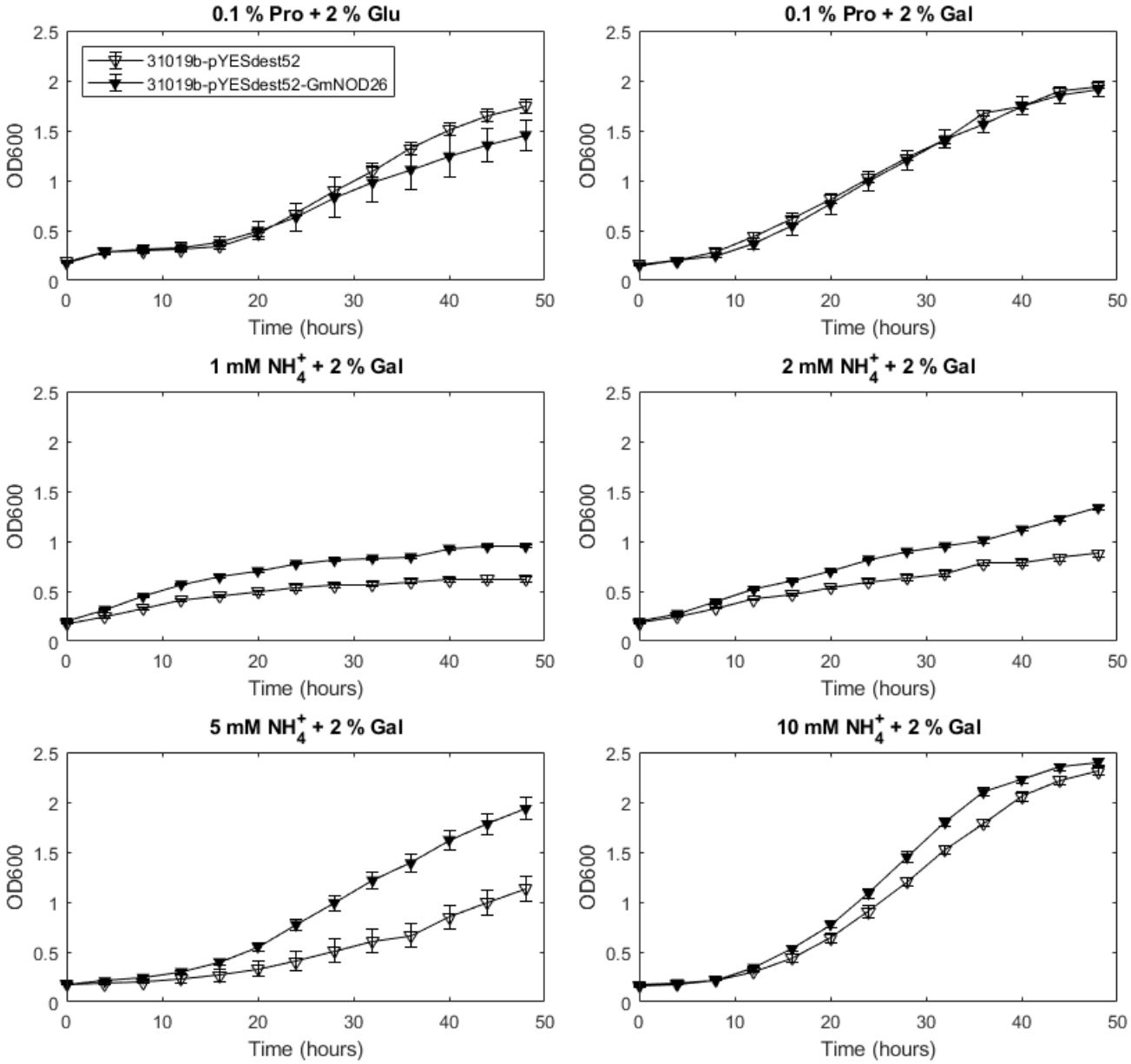

Figure A8 1 Optimising NH_4^+ concentration for GmNOD26 complementation of the ammonium transport deficient yeast strains 31019b. GmNOD26 and empty pYESdest52 vector 31019b transformants were grown in 200 µL of Medium M (pH 6.0) containing (A) 2% (w/v) Glucose (Glu) and 0.1% (w/v) Proline (Pro); or 2% (w/v) Galactose (Gal) and (B) 0.1% proline; (C) 1 mM NH_4^+, (D) 2 mM NH_4^+, (E) 5 mM NH_4^+, (F) 10 mM NH_4^+ for 48 hours at 28°C with 200 RPM shaking (n=4).

A9. Alanine transport by GmNOD26-expressing *X. laevis* oocytes

A9.1 Methods

A9.1.1 Oocyte alanine swelling

Relative change in oocyte volume was recorded as specified in section 2.7.3 with some modifications. Briefly, oocytes were maintained in low sodium ringers solution prior to incubation in an iso-osmotic solution containing 200 mM L-alanine, 2 mM KCl, 1 mM $MgSO_4$, 1.8 mM $CaSO_4$, 5 mM HEPES and pH was adjusted to 7.5 with TRIS base. Oocytes were then viewed with a Nikon SMZ800 light microscope (Nikon, Japan) and changes in volume captured every 30 seconds for 10 minutes prior to analysis using Image J software (National Institute of Health, USA). Post incubation oocytes were washed twice in ice-cold low sodium ringers solution and transferred to 80 µL of oocyte homogenization buffer.

A9.1.2 Alanine content measurements

Homogenised oocyte lysate (2.7.7) was assayed for NAD^+ reduction at 340 nm in the presence of alanine dehydrogenase using the following principle:

$$\text{L-alanine} + NAD^+ + H_2O \rightarrow \text{pyruvate} + NH_3 + NADH + H^+$$

Each reaction contained 60 µL homogenised oocyte lysate, 80 µL 2 mM EDTA and 0.1 M Tris-HCl (pH 10.1), 10 µL 20 mM NAD^+, 30 µl sterile MilliQ water and 20 µL alanine dehydrogenase (0.6 U/mg protein). The change in absorbance over 60 minutes at 25°C was recorded at 340 nm using a CLARIOstar Plate Reader (BMG LABTECH, Australia). Alanine content was calculated using the equation of the line of L-alanine standards 0 to 25 nmol/well and normalised to the percentage of homogenised oocyte lysate assayed (75%).

A9.2 Results and discussion

Initially water transport through GmNOD26-expressing *X. laveis* oocytes was investigated in hypo-osmotic Na^+ testing solution. It was found that GmNOD26 was expressing well, and water transport was comparable to previous assays (Figure A9.1a; Figure 3.6). It would be expected that if GmNOD26 was transporting alanine, an increase in oocyte volume would be observed due to an influx of water by the generated osmotic gradient, as has been previously demonstrated for boric acid uptake in AtNIP5;1 (Takano et al. 2006). However, for both control and GmNOD26-expressing *X. laveis* oocytes incubated in iso-osmotic alanine testing solution there was an observed decreased in relative volume (Figure A9.1b). The rate of 'shrinkage' was greater but not significant in GmNOD26-expressing oocytes, and after 10 minutes the relative volumes were equivalent. This may have been caused by minute variations in the osmotic conditions within the oocyte and the external testing solution and was likely enhanced by the water

permeability of GmNOD26. In the case of boric acid transport by AtNIP5;1 a significant swelling rate was observed but minute decreases in oocyte volumes were detected in control and the non-boric acid transporting PIP2;1-expressing oocytes in an iso-osmotic solution (Takano et al. 2006).

Following 10-minute incubation in iso-osmotic alanine, oocytes were homogenised for content analysis to further investigate alanine transport of GmNOD26-expressing oocytes. Taylor et al. (1996) previously determined the concentration of amino acids in within *X. laveis* oocytes, for alanine this was found to be 2.40 nmol following 24-hour incubation in media supplemented with 471 µM alanine. Firstly, the sensitivity of the alanine dehydrogenase assay was determined through 0 to 25 nmol/well standards, the assay was sufficient in detected alanine nmol quantities of alanine with a R^2 value of 0.9969 (Figure A9.2). The alanine content of control and GmNOD26-expressing oocytes was similar, 16.6 and 17.1 nmol/oocyte, respectively (Table A9.1). The reliability of the assay was also validated through spiking of oocyte lysate with 10 nmol of alanine, the recovery was varied from 92.6 to 103% (Table A9.1). The swelling and content data taken together suggest there was no enhanced transport of alanine by GmNOD26-expressing oocytes.

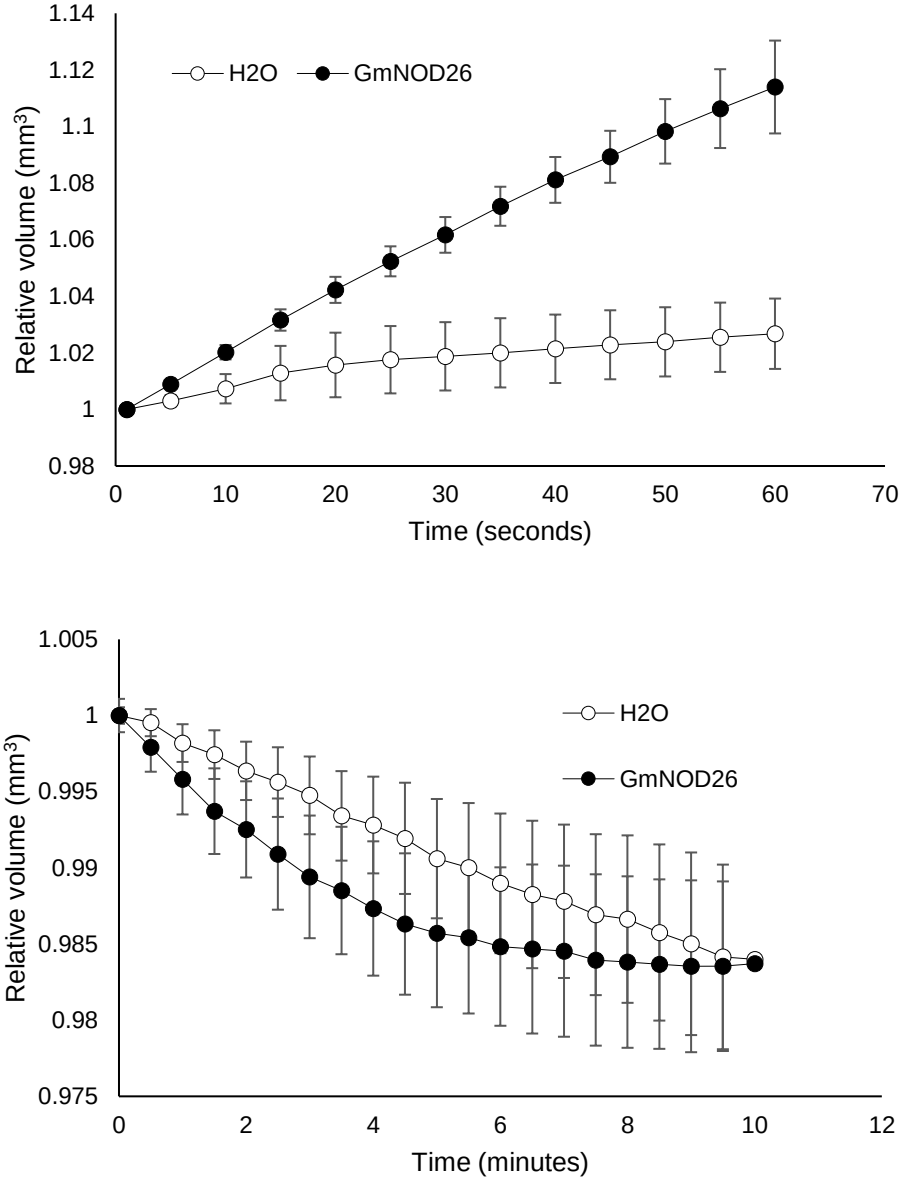

Figure A9 1. Osmotic swelling assays. A) Relative change in volume over 60 seconds in a hypo-osmotic Na^+ testing solution (44 mosmol kg−1). B) Relative change in volume over 10 minutes in iso-osmotic L-alanine testing solution (220 mosmol kg−1) (n= 3 for Na^+, n = 9 for alanine from a single oocyte harvest).

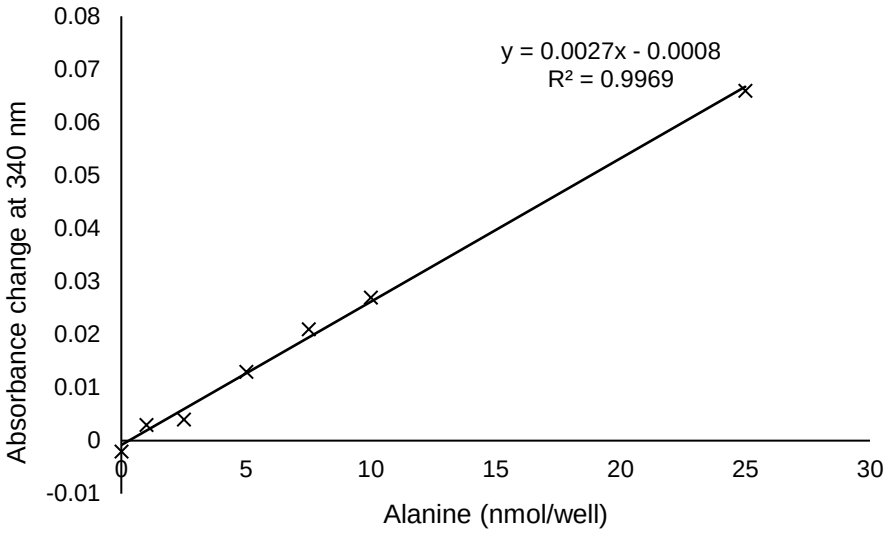

Figure A9 2. Figure A9.2. Alanine standard curve. The change absorbance of L-alanine standards 0 to 25 nmol/well were assayed for NAD^+ reduction at 340 nm in the presence of alanine dehydrogenase as specified in A1.1.2 (n=3).

Table A9 1. Alanine content of *X. laevis* oocytes. Relative change in volume over 10 minutes in iso-osmotic L-alanine testing solution (n = 6 for alanine, n = 3 for alanine spike from a single oocyte harvest).

	CONTROL	**GMNOD26**
ALANINE (NMOL PER OOCYTE)	16.6 ± 1.79	17.1 ± 1.76
10 NMOL ALANINE SPIKE (NMOL PER ASSAY)	24.6 ± 2.49	28.0 ± 0.96
SPIKE RECOVERY (%)	92.6	103

A10. Nodule laser-dissection of the *M. truncatula* ALMT family

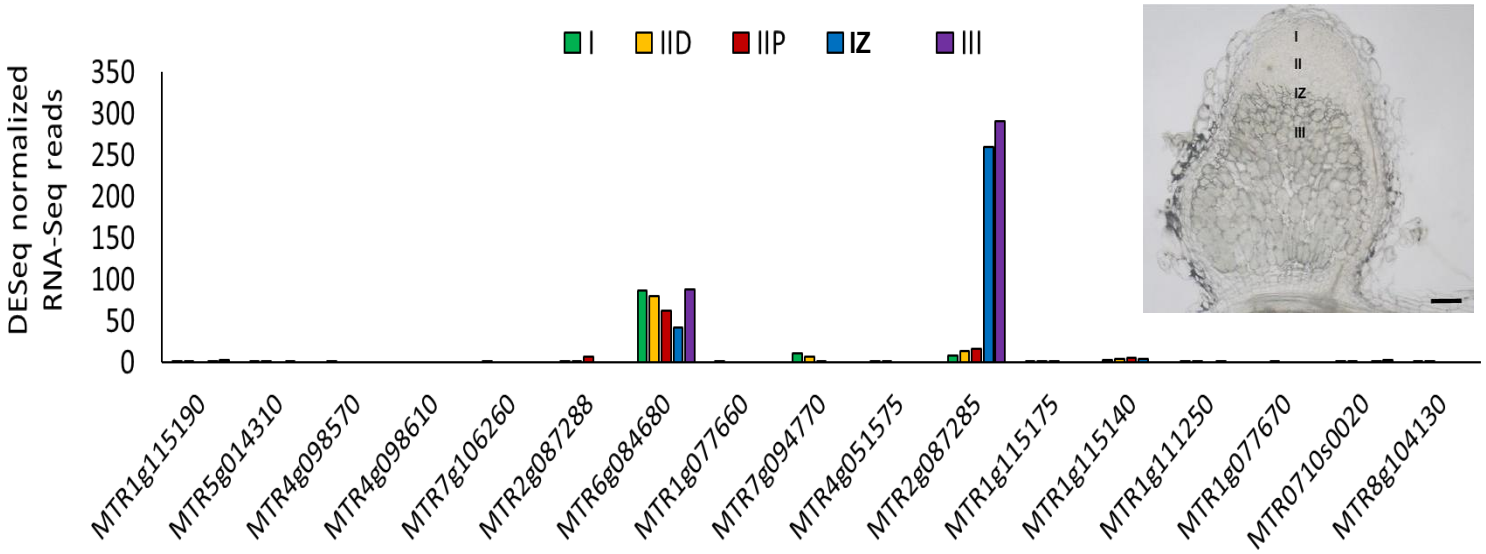

Figure A10 1 Nodule laser-dissection of the *M. truncatula* ALMT family. *M. truncatula* accession can be found in Table 6.1 and data was obtained from Symbimics. I = fraction I; IID = distal fraction II; IIP = proximal fraction II; IZ =interzone fraction; III nitrogen fixing fraction III.

A11. Radiolabeled malate efflux by GmNPF1.2 expressing oocytes

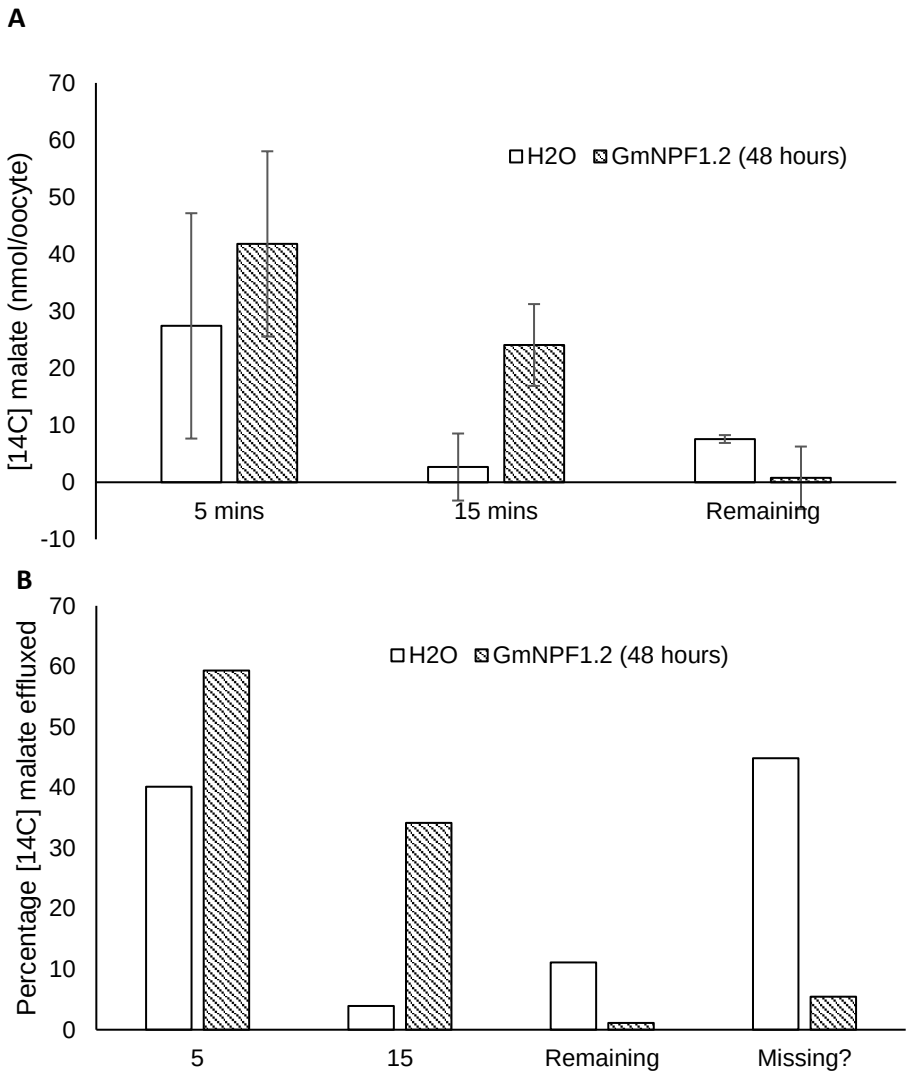

Figure A11 1. Radiolabeled malate efflux by GmNPF1.2 expressing oocytes. Control or GmNPF1.2 expressing oocytes were preincubated in [^{14}C] malate for 60 minutes prior to the radioactivity of the bathing solution being recorded. A) [^{14}C] malate (nmol/oocyte), B) percentage [^{14}C] malate effluxed from control and GmNPF1.2 oocytes assuming 2200 nmol [^{14}C] malate was taken up after 60 minutes of preincubation (as per Figure 6.8). Bathing solution contained 0.5 mM $CaCl_2$, buffered to pH 5.5 with BTP and osmolality adjusted to 220 mosmol kg^{-1} with D-mannitol (n = 6 from a single oocyte harvest).

A12. GUS staining of the 2-kb 5' regulatory sequence of GmNPF1.2 in soybean nodules

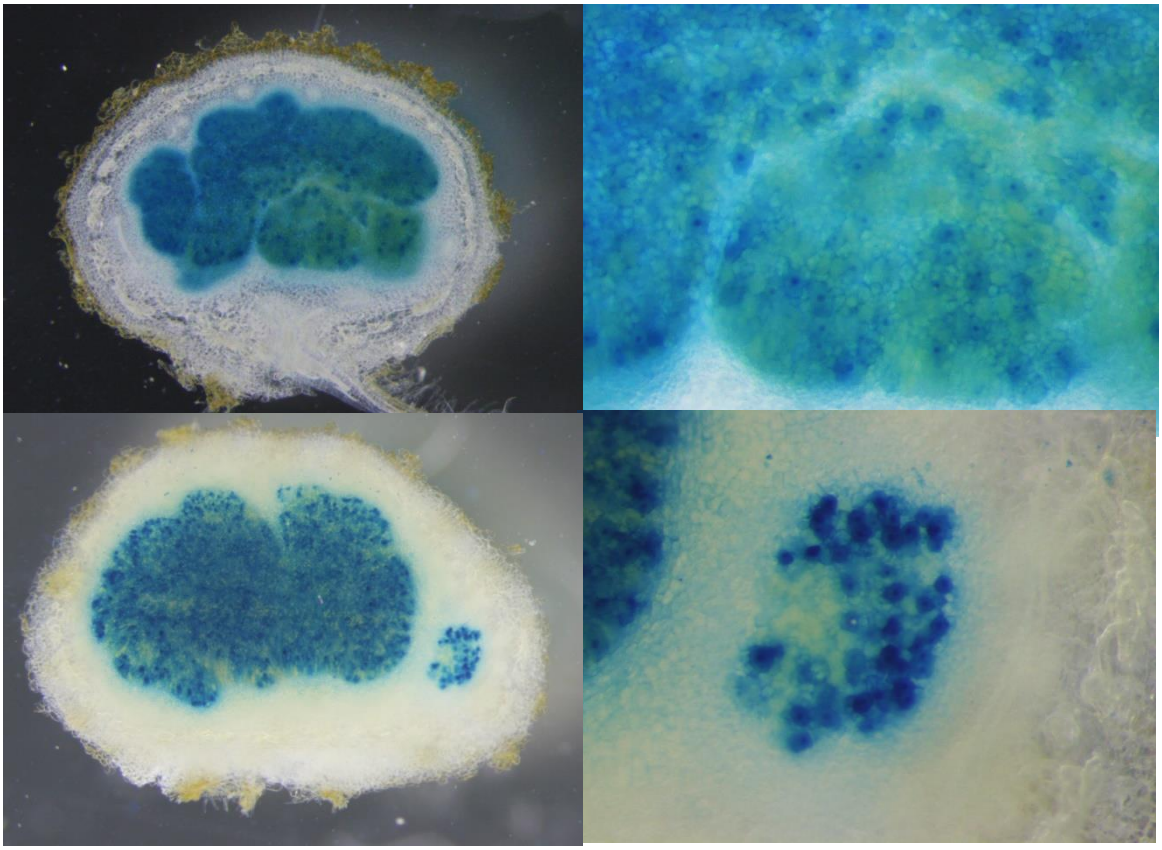

Figure A12 1. Spatial activity of the 2-kb 5' regulatory sequence of *GmNPF1.2* in soybean nodules 30 days after inoculation with *B. japonicum*. Expression of the GUS reporter gene was driven by the *GmNPF1.2* promoter in hairy root nodules. Blue staining highlights the spatial expression of the promoter post incubation with GUS staining buffer. All images were kindly provided by Penelope Smith (unpublished).

A13. GFP localization of GmNPF1.2 to the soybean symbiosome membrane

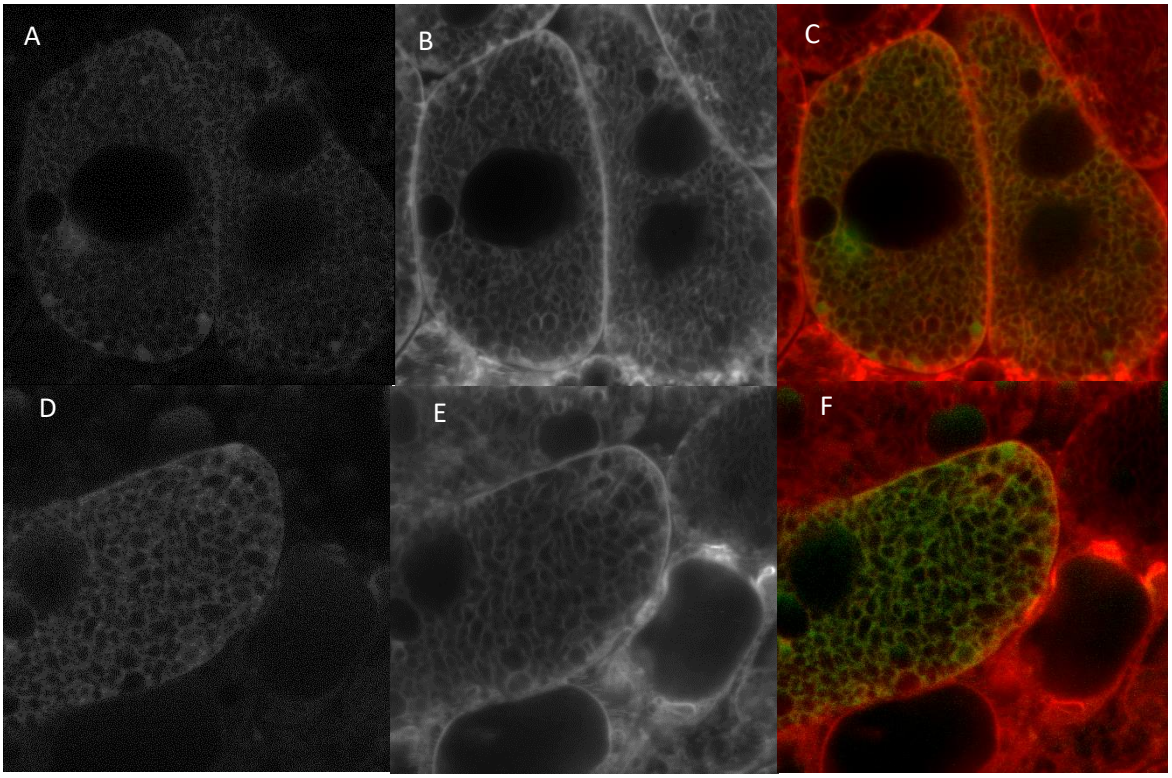

Figure A13 1. Localization of GmNPF1.2 to the soybean symbiosome membrane. GFP fused to the N-terminal of GmNPF1.2 and expressed in hairy root soybean nodules under the leghemoglobin promoter. Confocal images of: A and D, GFP signal; B and E, counterstaining of the SM with FM4–64; C and F, overlapping GFP and FM4–64 signals. All images were kindly provided by Penelope Smith (unpublished).

A14. GmNPF1.2 knockdown reduces nitrogen fixation rate

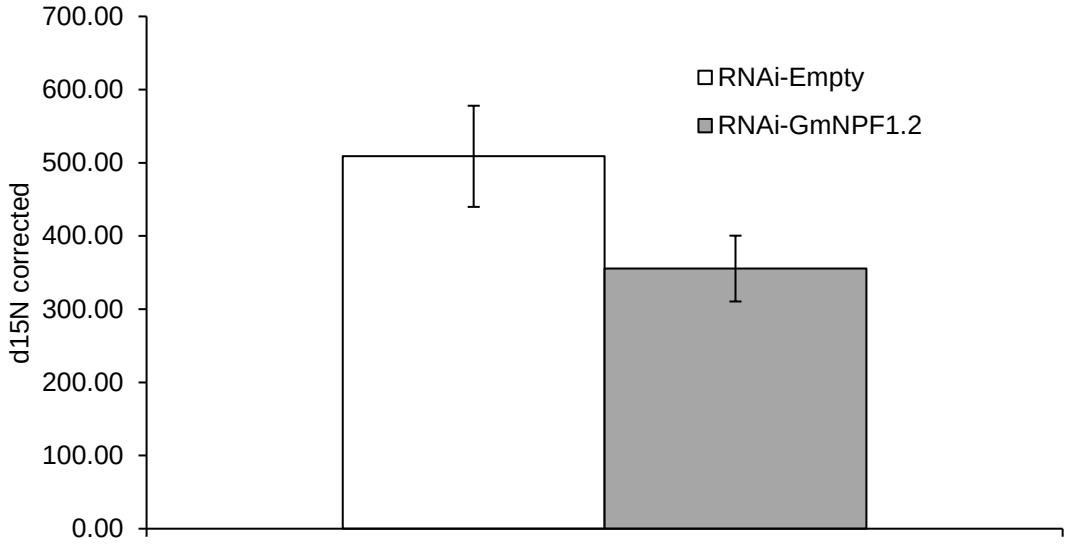

Figure A14 1. GmNPF1.2 knockdown reduces nitrogen fixation rate. Soybean nodule were transfected with an RNAi construct to knockdown GmNPF1.2 expression. Nitrogen fixation rates were estimated based on d15N. Data kindly provided by Penelope Smith (unpublished).